



University of HUDDERSFIELD

University of Huddersfield Repository

Haba, Usama A. M.

Information Extraction Based on the Analysis of Motor Supply and Structural Vibration for Machinery Condition Monitoring

Original Citation

Haba, Usama A. M. (2019) Information Extraction Based on the Analysis of Motor Supply and Structural Vibration for Machinery Condition Monitoring. Doctoral thesis, University of Huddersfield.

This version is available at <http://eprints.hud.ac.uk/id/eprint/35237/>

The University Repository is a digital collection of the research output of the University, available on Open Access. Copyright and Moral Rights for the items on this site are retained by the individual author and/or other copyright owners. Users may access full items free of charge; copies of full text items generally can be reproduced, displayed or performed and given to third parties in any format or medium for personal research or study, educational or not-for-profit purposes without prior permission or charge, provided:

- The authors, title and full bibliographic details is credited in any copy;
- A hyperlink and/or URL is included for the original metadata page; and
- The content is not changed in any way.

For more information, including our policy and submission procedure, please contact the Repository Team at: E.mailbox@hud.ac.uk.

<http://eprints.hud.ac.uk/>

**INFORMATION EXTRACTION BASED ON THE
ANALYSIS OF MOTOR SUPPLY AND STRUCTURAL
VIBRATION FOR MACHINERY CONDITION
MONITORING**

A THESIS SUBMITTED IN PARTIAL FULFILMENT OF THE REQUIREMENT FOR
THE DEGREE OF DOCTOR OF PHILOSOPHY AT THE UNIVERSITY OF
HUDDERSFIELD

By
USAMA A. M. HABA

School of Computing and Engineering
University of Huddersfield
UK

February 2019

ABSTRACT

Reciprocating compressors (RC) are one of the most widely used industrial machines due to their flexibility and reliability. Commonly exposed to harsh working environments, compressors experience various faults that affect their operational performance and functionality. Unfortunately, conventional condition monitoring methods such as vibration monitoring shows inefficiency sometimes in detecting multi-faults that occur in RCs even though it needs a high-cost system for monitoring equipment.

The AC motor driving the RC undertakes an oscillating torque which induces additional components in the measured current signals and changes with the presence of faults in either compressor or motor with consequent. Extensive investigations have shown that motor current signature analysis (MCSA) has the potential to be an accurate and cost-effective technique for the detection and diagnosis of common RC faults (i.e discharge valve leakage, intercooler leakage, broken rotor bars, stator winding asymmetry, and discharge valve leakage combined with stator winding asymmetry). However, a full study has not been found to consolidate this deduction. This research has adopted a model based simulation and experimental evaluation to verify and detail the use of MSCA for monitoring compressors under a wide range of load and fault conditions.

The study firstly develops an extended and comprehensive dynamic model of the compressor, which links the various effects including mechanical dynamics, electrodynamics and fluid dynamics and, thus allows the current signature variations, particularly the sideband patterns to be simulated, and studied under common faults and their combinations at different severity. The model was validated against measured current signatures. Moreover, an advanced and effective technique, modulation signal bispectrum (MSB) has been identified to be the accurate tool as it can accurately extract the effect of sidebands and suppresses inevitable noise influences.

Subsequently, a number of experiments were carried out based on a general purpose two-cylinder RC. Experimental results have shown that the seeded compressor faults caused observable changes in the motor current signature, inducing non-linear and modulation characteristics into the measured signal. The above-cited compressor faults generate different patterns and varying load on the motor, thereby inducing changes in modulation features in the current signal. Especially for the combined fault, an increase in sidebands

can be observed by MSB analysis due to its high performance of noise reduction and nonlinear feature extraction.

The MSB results in primary diagnostic features; sideband peaks at the first and second orders of compressor operating frequency has the ability to differentiate RC fault cases over a wide range of operating conditions, which allowed fault diagnosis without the need for additional measurements such as pressure, speed, or temperature. The successful detection and diagnosis of common compressor and motor faults through experiments and model developments confirm the capability of MSB based MCSA method.

With the successful diagnosis of RC and motor faults, this research study is progressed to validate the capability of MSB based methods to diagnose different common compressor faults relating to compressor leakages, motor faults, and combined fault. The results show that MSB signatures allow accurate differentiation between normal condition and abnormal change induced by these seeded faults compared to conventional analysis, confirming the efficiency of the signal processing technique proposed in this thesis.

ACKNOWLEDGEMENTS

Firstly and foremost, I would like to give all the praise and glory to **ALLAH** (God) the Almighty who has given me strength, blessing, knowledge, opportunity and good health to undertake and complete this research work.

Secondly, I would like to express my sincere thanks to my academic supervisors, **Prof Andrew Ball** and **Prof Fengshou Gu** for their encouragement, guidance, valuable suggestions and inspiration throughout all my study during my academic life in the University of Huddersfield. Their expertise and encouragement guided me to complete my research studies to the highest standard, in logic and consistent way. Special thanks for their constructive feedbacks, endless support and their help reviewing of this thesis.

I would like to give my grateful acknowledgements to the Ministry of Higher Education and Scientific Research (**MHESR**), Libya and Al-Jabal Al-Gharbi University for their financial support during my PhD studies.

Most of all I would like to dedicate this work to my family particularly: my father, my mother, my uncles and brothers and sisters back home for their best wishes and warm-hearted help in life support. A special and grateful thanks extended to my wife for her patience, love and care all through the years of my research and to my little three princesses: **Aisha, Jowairia** and **Sarah** who are priceless jewels of joy to me.

Also, very special thanks, gratitude and appreciation to all colleagues at the Centre for Efficiency and Performance Engineering (**CEPE**) research group for their continuous help and support during the unforgettable moments we spent together during the last four years.

DECLARATION

This research study is submitted for the degree of Doctor of Philosophy at the University of Huddersfield. I hereby declare that the work in this thesis was carried out in accordance with the Regulations of the University of Huddersfield.

No portion of the work presented in this dissertation has been or is being submitted for another degree, diploma, or other qualification of this or any other university or other institution of learning.

COPYRIGHT

- i. The author of this thesis (including any appendices and/or schedules to this thesis) owns any copyright in it (the “Copyright”) and s/he has given The University of Huddersfield the right to use such copyright for any administrative, promotional, educational and/or teaching purposes.
- ii. Copies of this thesis, either in full or in extracts, may be made only in accordance with the regulations of the University Library. Details of these regulations may be obtained from the Librarian. This page must form part of any such copies made.
- iii. The ownership of any patents, designs, trademarks and any and all other intellectual property rights except for the Copyright (the “Intellectual Property Rights”) and any reproductions of copyright works, for example graphs and tables (“Reproductions”), which may be described in this thesis, may not be owned by the author and may be owned by third parties. Such Intellectual Property Rights and Reproductions cannot and must not be made available for use without the prior written permission of the owner(s) of the relevant Intellectual Property Rights and/or Reproductions.

STATEMENT OF ORIGINALITY

I hereby certify that all of the work described within this thesis is the original work of the author. Any published (or unpublished) ideas and/or techniques from the work of others are fully acknowledged in accordance with the standard referencing practices.

(Usama A. M. Haba)

February 2019

LIST OF PUBLICATIONS

Journal Papers

1. Haba Usama, Feng Guojin, Shaeboub Abdulkarim, Peng Xinyu, Gu, Fengshou and Ball, Andrew (2017). Motor current signature analysis for the compound fault diagnosis of reciprocating compressors. *International Journal of Condition Monitoring and Diagnostic Engineering Management*.
2. Shaeboub Abdulkarim, Gu Fengshou, Lane, Mark, Haba, Usama, Wu, Zhifei and Ball, Andrew (2017). Modulation signal bispectrum analysis of electric signals for the detection and diagnosis of compound faults in induction motors with sensorless drives. *Systems Science & Control Engineering*, 5 (1). pp. 252267. ISSN 21642583.
3. Haba Usama, Brethee Khaldoun, Hassin Osama, Gu Fengshou and Ball Andrew (2018). An Investigation into Vibration Response for Condition Monitoring of Reciprocating Compressor based on Modulation Signal Spectrum Analysis. *International Journal of Condition Monitoring and Diagnostic Engineering Management (COMADEM)*, 21(3).

Conference Papers

4. Haba Usama, Feng Guojin, Shaeboub Abdulkarim, Peng Xinyu, Gu Fengshou and Ball Andrew (2016). Detection and diagnosis of compound faults in a reciprocating compressor based on motor current signatures. In: COMADEM 2016, the 29th International Congress on Condition Monitoring and Diagnostic Engineering Management, 20th-22nd August 2016, Empark Grand Hotel in Xi'an, China.
5. Shaeboub Abdulkarim, Lane Mark, Haba Usama, Gu Fengshou and Ball Andrew (2016). Detection and diagnosis of compound faults in induction motors using electric signals from variable speed drives. In: Proceedings 22nd International Conference on Automation and Computing (ICAC). IEEE. ISBN 9781862181328.
6. Haba Usama, Shaeboub Abdulkarim, Mones Zainab, Gu Fengshou and Ball Andrew (2017). Diagnosis of compound faults in reciprocating compressors based on modulation signal bispectrum of current signals. Proceedings of 2nd International

Conference on Maintenance Engineering, *IncoME-II 2017. The University of Manchester, UK*

7. Mones, Zainab, Feng, Guojin, Tang, Xiaoli, Haba Usama, Gu Fengshou and Ball Andrew (2017). A comparative study of gravitational acceleration cancellation from on-rotor MEMS accelerometers for condition monitoring. In *24th International Congress on Sound and Vibration*. International Institute of Acoustics and Vibration, IIAV.
8. Hassin Osama, Haba Usama, Gu Fengshou and Ball Andrew (2018). Monitoring Mis-Operating Conditions of Journal Bearings based on Modulation Signal Bispectrum Analysis of Vibration Signals.
9. Haba Usama, Brethee Khaldoon, Alabied Samir, Mondal Debanjan, Gu Fengshou and Ball Andrew (2018). Modelling and Simulation of a Two-Stage Reciprocating Compressor for Condition Monitoring Based on Motor Current Signature Analysis. *Condition Monitoring and Diagnostic Engineering Management*, 2.
10. Haba Usama, Brethee Khaldoon, Hassin Osama, Gu Fengshou and Ball Andrew (2017). Detection and Diagnosis of Reciprocating Compressor Faults Based on Modulation Signal Bispectrum Analysis of Vibrations. In: *COMADEM 2017, the 30th Conference on Condition Monitoring and Diagnostic Engineering Management, 10th-13th July 2017, University of Central Lancashire, UK*. ISBN: 9781909755109
11. Alabied Samir, Haba Usama, Daraz Alsadak, Gu Fengshou and Ball Andrew (2018). Empirical mode decomposition of motor current signatures for centrifugal pump diagnostics. 2018 *24th International Conference on Automation and Computing (ICAC), IEEE*.
12. Mondal Debanjan, Haba Usama, Gu Fengshou and Ball Andrew (2019). Airborne Acoustic Signature Analysis for Fault Diagnosis of Reciprocating Compressors Using Modulation Signal Bi-spectrum. *International Conference on Automation and Computing (ICAC'19)*.

Awards

- 1- Best Student Paper Presentation Award in the *30th International Conference on Condition Monitoring and Diagnostic Engineering Management (COMADEM) (2017)*.
 - Habab Usama, Brethee Khaldoon, Hassin Osama, Gu Fengshou and Ball Andrew (2017).

- 2- Best Student Paper Award 2nd Place in the *2nd International Conference on Maintenance Engineering (IncoME-II) 2017*.
 - Habab Usama, Shaeboub Abdulkarim, Mones Zainab, Gu Fengshou and Ball Andrew (2017).

TABLE OF CONTENTS

ABSTRACT	I
ACKNOWLEDGEMENTS	III
DECLARATION	IV
COPYRIGHT	V
STATEMENT OF ORIGINALITY.....	VI
LIST OF PUBLICATIONS.....	VII
TABLE OF CONTENTS	X
LIST OF FIGURES	XVII
LIST OF TABLES.....	XXIII
LIST OF ABBREVIATIONS	XXIV
LIST OF NOMENCLATURE	XXVI
CHAPTER 1: Introduction.....	1
1.1 Background.....	2
1.2 Research Application	3
1.3 The Importance of Maintenance	4
1.4 Research Scope	6
1.5 Research Motivation	7
1.6 Research Aim and Objective	8
1.6.1 Research Aim.....	8
1.6.2 Research Objectives	8
1.7 Thesis Organization.....	9
CHAPTER 2: Reciprocating Compressor Fundamentals, Their Faults and Conventional Condition Monitoring	12
2.1 Introduction.....	13
2.2 Principle of Operation	13

2.3 Compressor Types and Classifications.....	14
2.3.1 Continuous Flow, Dynamic Compressors	15
2.3.2 Positive Displacement Compressor (Intermittent Mode)	15
2.4 Reciprocating Compressors	16
2.5 Single-Stage Reciprocating Compressors (Single Action).....	18
2.5.1 P-V Diagram for an Ideal Single Stage (Single Acting) Compressor	18
2.6 Multi-Stage Reciprocating Compressors.....	19
2.6.1 P-V Diagram for An Ideal Multi-Stage Compressor (Two-Stage)	20
2.7 Reciprocating Compressor Faults	21
2.8 Induction Motor and Power Transmission	23
2.8.1 Induction Motor Construction.....	23
2.8.2 Induction Motor Operation Principles.....	25
2.9 Induction Motor Common Faults.....	28
2.9.1 Stator Failures (Stator Winding Asymmetry)	29
2.9.2 Rotor Faults.....	30
2.10 The Importance of Machine Condition Monitoring.....	30
2.11 Conventional Condition Monitoring Techniques	32
Visual Inspection.....	33
Dynamic Cylinder Pressure Monitoring.....	34
Instantaneous Angular Speed (IAS) Based Monitoring	34
Fault Detection and Diagnosis Using Vibro-acoustic Signals.....	35
Vibration Analysis For Fault Detection	35
Motor Current Signature Analysis For Diagnosis	37
2.12 Reciprocating Compressor Monitoring Techniques	41
2.13 Summary.....	43
CHAPTER 3: Reciprocating Compressor Fault Detection and Diagnosis Techniques	45

3.1 Introduction.....	46
3.2 Time Domain Analysis (Waveform).....	47
3.2.1 Peak Value (PV).....	48
3.2.2 Root Mean Square (RMS)	48
3.2.3 Crest Factor (CF).....	49
3.2.4 Kurtosis	49
3.3 Frequency Domain Analysis.....	50
3.3.1 Fast Fourier Transform (FFT).....	51
3.3.2 Shaft Frequency and IAS	52
3.3.3 Sideband Characteristics.....	52
3.3.4 Higher Order Spectra (HOS).....	53
3.4 Summary.....	56
CHAPTER 4: Reciprocating Compressor Experimental Test Rig.....	58
4.1 Test Rig Design.....	59
4.2 Test Rig Description.....	59
4.3 Seeding of Common Compressor Fault	60
4.3.1 Simulation of Valve Leakage.....	61
4.3.2 Simulation of Intercooler Leakage	62
4.3.3 Simulation of Stator Resistance	63
4.4 Measurement Transducers	64
4.4.1 Accelerometers.....	64
4.4.2 Cylinder Pressure Sensor	66
4.4.3 Static Pressure Transducer	67
4.4.4 Temperature Measurement	67
4.4.5 Shaft Encoder	68
4.4.6 Current Measurement	69

4.5 Data Acquisition System	70
4.5.1 Hardware: CED 1401 Plus.....	70
4.5.2 Software: Lab Windows TM/CVI Version 5.5	71
4.6 Data Management and Measurement Practice.....	72
4.7 Summary.....	74
CHAPTER 5: Mathematical Modelling and Fault Simulation	75
5.1 Introduction.....	76
5.2 Overview of the Compressor Model	76
5.2.1 Mathematical Model Objectives	77
5.2.2 Compressor Modelling (a Brief Review)	78
5.3 Electric Motor Model	81
5.3.1 Voltage and Flux Linkage Equations	81
5.3.2 Motor Torque Calculations	84
5.4 Compressor Dynamics	85
5.4.1 Crankshaft System.....	85
5.4.2 Piston Dynamic Model (Two-Stage Compressors).....	88
5.5 Cylinder Pressure Models	89
5.5.1 Cylinder Pressure	90
5.5.2 Cylinder Volume Equation	91
5.6 Valves Mass Flow Model.....	92
5.6.1 Inlet Valve Mass Flow Rate.....	92
5.6.2 Outlet Valve Mass Flow Rate	93
5.7 Valve Motion Modelling	93
5.7.1 Inlet Valve Motion	94
5.7.2 Outlet Valve Motion.....	95
5.8 Fault Simulation.....	96

5.8.1 Outlet Valve Seepage Simulation.....	97
5.8.2 Intercooler Seepage Simulation	97
5.8.3 Stator Short Circuit Simulation.....	98
5.9 Implementation Procedure.....	98
5.9.1 Compressor Parameters and Constants.....	102
5.10 Model Evaluation under Healthy Operation.....	104
5.10.1 Compressor Valve Operations	104
5.10.2 Comparison of Measured and Predicted Cylinder Pressures	105
5.10.3 Measured and Predicted Cylinder Pressure Comparison as a Function of Discharge Pressure.....	107
5.10.4 Discharge Valve Displacement as a Function of Discharge Pressure.....	108
5.10.5 Comparison of Measured and Predicted Motor Current Waveform	108
5.11 Model Evaluation Under Different Faulty Operations.....	111
5.11.1 Cylinder Pressure Comparisons	111
5.11.2 Motor Current Waveform Comparison	113
5.11.3 Comparative Spectral Analysis of Motor Currents	115
5.12 Diagnostic Feature Extraction Based on Simulated Data.....	117
5.12.1 Diagnostics of Mechanical Simulated Faults.....	118
5.12.2 Diagnostics of Electrical Simulated Faults.....	120
5.13 Summary.....	123
CHAPTER 6: Diagnosis of Combined Faults in Reciprocating Compressors based on Modulation Signal Bispectrum Analysis of Motor Current Signals.....	124
6.1 Introduction.....	125
6.2 Experimental Faults.....	126
6.2.1 Valve Leakage (DVL)	126
6.2.2 Inter-Cooler Leakage (ICL)	127

6.2.3 Stator Winding Asymmetry (SWA)	127
6.2.4 Test Procedure.....	127
6.3 Time Domain Analysis Under Healthy Operation.....	127
6.3.1 Changes in Cylinder Pressures.....	128
6.3.2 Changes in Current Waveforms	129
6.4 Data Analysis Under Healthy and Faulty Conditions	130
6.4.1 Changes in Cylinder Pressure Waveform.....	130
6.4.2 Changes in the Motor Current Waveform	131
6.4.3 Comparison of Motor Current Signal Spectra	133
6.5 MSB Magnitude Characteristics	135
6.6 Comparison between Spectrum and MSB Analysis	138
6.7 Summary.....	140
CHAPTER 7: Modulation Signal Bispectrum Diagnosis of Reciprocating Compressor Faults Based on Vibration Analysis.....	142
7.1 Introduction.....	143
7.2 Fault Simulation.....	144
7.3 Test Procedure	145
7.4 Time-Domain Analysis Under Healthy Conditions.....	145
7.4.1 Cylinder Pressure Waveform	145
7.4.2 Vibration Waveform Characteristics	146
7.5 Time Domain Analysis for Fault Conditions.....	148
7.6 Vibration Signal Spectrum Analysis.....	151
7.7 The Implementation of MSB Analysis.....	154
7.8 MSB Magnitude Characteristics	155
7.9 Averaged MSB Magnitude Comparisons.....	156
7.9.1 Comparison Between Spectrum and MSB	157

7.10 Summary.....	160
CHAPTER 8: Conclusions and Suggestions for Future Work.....	162
8.1 Objectives and Achievements.....	163
8.2 Conclusions.....	167
8.3 Contributions to the Knowledge	169
8.4 Recommendations for Future Work.....	170
Reference:.....	172

LIST OF FIGURES

Figure 1-1: Flowchart of the study work scheme	11
Figure 2-1 :The main categories of compressors [36]	14
Figure 2-2: Suction and compression steps of a compression cylinder.....	16
Figure 2-3: Photo of “exploded” multi-stage reciprocating compressor	17
Figure 2-4: Schematic of single-stage single-acting reciprocating compressor.....	18
Figure 2-5: An ideal Pressure-Volume diagram (P-V) [42].....	19
Figure 2-6: a) Two-stage compressor, b) Schematic diagram of a two-stage compressor .	20
Figure 2-7: An ideal P-V diagram for a multi-stage compressor (two stages) [24]	21
Figure 2-8: Reciprocating compressors failures rates [15]	23
Figure 2-9: A typical industrial induction motor.....	24
Figure 2-10: Squirrel cage rotor	25
Figure 2-11: Symmetrical induction motor simplified scheme [56]	26
Figure 2-12: Slip speed illustration [59]	27
Figure 2-13: Induction motor faults.....	28
Figure 2-14: Motor fault distribution [62].....	29
Figure 2-15: Three-Phase stator winding faults [52].....	30
Figure 2-16: Schematic of the compressor CM process.	31
Figure 2-17: Relative usage of common condition monitoring techniques [69].....	32
Figure 3-1 Raw vibration signals from the 2 nd stage of RC for baseline (healthy) and DVL – discharge valve leakage.....	48
Figure 3-2: Vibration spectrum of the second stage of a reciprocating compressor	50
Figure 3-3: The HOS classification map [117]	54
Figure 4-1: Broom-Wade TS9 reciprocating compressor.....	59
Figure 4-2: Second stage discharge valve components	62
Figure 4-3: Test rig schematic diagram and fault simulation.....	63

Figure 4-4: Photograph of external resistors bank and schematic diagram of stator winding asymmetry simulation (external resistors bank).....	64
Figure 4-5: Location of the accelerometer at top of the cylinder head.....	65
Figure 4-6: On-line vibration sensors output (raw-data)	65
Figure 4-7: In-cylinder pressure sensor	66
Figure 4-8: On-line dynamic pressure sensors output (raw-data)	66
Figure 4-9: Static pressure transducer mounted on the compressor tank.	67
Figure 4-10: Optical pulse high-resolution shaft encoder.....	68
Figure 4-11: On-line optical encoder raw-data	68
Figure 4-12: Three-phase current measuring unit	69
Figure 4-13: On-line motor current measurement raw-data.....	69
Figure 4-14: Pictorial diagram of CED 1401 Plus.....	71
Figure 4-15: Setup screen for data acquisition.	71
Figure 4-16: Data acquisition in progress	72
Figure 4-17: Schematic diagram of the compressor test system.	73
Figure 5-1: Crankshaft mechanisms of single cylinder compressor.....	77
Figure 5-2: Simplified schematic of asymmetrical induction motor [56].....	81
Figure 5-3: Two-Stage V-type reciprocating compressor [46]	85
Figure 5-4: Schematic of mass flow through a two cylinder RC [24].....	90
Figure 5-5: Mass flow model for inlet and outlet valves [141].....	92
Figure 5-6: Schema of a plate valve (motion is taken to be single-degree-of-freedom)	94
Figure 5-7: Compressor simulation model flowchart	101
Figure 5-8: The predicted motion of first stage valves of a healthy compressor for second stage discharge pressure of 120 psi.....	104
Figure 5-9: The predicted motion of second stage suction and discharge valves of a healthy compressor for second stage discharge pressure of 120 psi.....	105

Figure 5-10: First and second stages cylinder pressures for a healthy RC: (a) Measured values, (b) Predicted values.....	106
Figure 5-11: Measured and predicted second stage cylinder pressure for various discharge pressures, 60 psi, 90 psi and 120 psi.....	107
Figure 5-12: Second stage discharge valve displacement under various discharge pressures 60 psi, 90 psi and 120 psi.	108
Figure 5-13: Motor current waveform for induction motor driving a healthy compressor: (a) Measured, (b) Predicted	109
Figure 5-14: Motor current waveform for a healthy compressor under various discharge pressures 60 psi, 90 psi and 120 psi: (a) Measured, (b) Predicted	109
Figure 5-15: RMS values for the measured and predicted motor current of the healthy compressor as a function of discharge pressure	110
Figure 5-16: Predicted dynamic cylinder pressure in both stages under healthy (BL) and two faulty cases (ICL and DVL) at 120 psi discharge pressure.....	112
Figure 5-17: Measured dynamic cylinder pressure in both stages under healthy (BL) and two faulty cases (ICL and DVL) at 120 psi discharge pressure	113
Figure 5-18: Measured and predicted motor current waveforms under healthy (BL) and two faulty cases (ICL and DVL) at 120 psi discharge pressure.....	114
Figure 5-19: RMS values for measured and predicted motor current for compressor under healthy (BL) and two faulty cases (ICL and DVL) at three discharge pressures.....	114
Figure 5-20: Current spectrum for healthy (BL) and two faulty cases (ICL and DVL) at second stage discharge pressure 120 psi	115
Figure 5-21: Sidebands amplitudes for healthy (BL) and two faulty cases (ICL and DVL) at three discharge pressures. (a) Measured, (b) predicted.....	116
Figure 5-22: A typical MSB slice (at 50 Hz) through simulated current for healthy compressor and compressor with faulty discharge valve.....	117
Figure 5-23: A typical MSB slice through current for healthy compressor and motor with two simultaneous faults (Stator Winding Asymmetry, SWA, and Broken Rotor Bar, BRB)	118

Figure 5-24: Characteristics of feature extraction for both suction and discharge valve leakage.....	119
Figure 5-25: Characteristic feature extraction for intercooler leak and loose transmission belt	120
Figure 5-26: Feature characteristics for 1BRB and 2BRB faults	121
Figure 5-27: Characteristics features for stator winding asymmetry (SWA) and combined fault (SWA+1BRB)	122
Figure 6-1: Time domain representation of second stage cylinder pressure for the normal condition under various discharge pressures: 40 psi, 80 psi, and 120 psi.....	128
Figure 6-2: Time domain representation of the current signal for a healthy compressor under different discharge pressures 40 psi, 80 psi, and 120 psi.....	129
Figure 6-3: Time domain cylinder pressures for first and second stages, for second stage discharge pressure of 80 psi, for baseline condition and four faults.	130
Figure 6-4: Motor current waveform for healthy compressor and compressor with four seeded faults under 40 psi and 120 psi discharge pressure	132
Figure 6-5: RMS values of the motor current waveform for healthy and with seeded faults under a range of discharge pressures	133
Figure 6-6: Motor current spectrums for healthy and seeded faults under discharge pressures of 60 psi and 120 psi ($f_c=50\text{Hz}$ and $f_x =7.3\text{Hz}$)	134
Figure 6-7: Averaged sidebands amplitude for healthy and simulated faults under compressor discharge pressure	135
Figure 6-8: Characteristics of current MSB for (a) healthy compressor (BL) and (b) combined fault (DVL+SWA), both for 120 psi discharge pressure	136
Figure 6-9 :MSB characteristics of current signals for healthy and different fault conditions under the range of operating pressures	137
Figure 6-10: A typical MSB slice at 50.0 Hz for healthy and different fault conditions under the range of operating pressures	137
Figure 6-11: Comparison between MSB and spectral Analysis for the diagnosis of different faults.....	138

Figure 6-12: Percentage difference of BL and seeded faults under different compressor discharge pressures	140
Figure 7-1: Reciprocating compressor test rig and fault simulations	145
Figure 7-2: Time domain representation of (a): low stage, and (b) high stage in-cylinder pressures for a healthy condition for discharge pressures (60, 80, 100 and 120 psi)	146
Figure 7-3: Measured vibration and pressure signals for a healthy compressor under 100 psi discharge pressure.....	147
Figure 7-4: Time domain representation of a vibration signal for a healthy compressor under different discharge pressure (80, 100 and 120 psi).....	148
Figure 7-5: Time domain representation of vibration signal from second stage cylinder for (a) BL, (b) ICL and (c) DVL under 100 psi discharge pressure.....	149
Figure 7-6: RMS values for the time-domain waveform of the second cylinder vibration for healthy condition and two seeded faults for four discharge pressures	150
Figure 7-7: Kurtosis values for the time-domain waveform of the second cylinder vibration for healthy condition and two seeded faults for four discharge pressures	150
Figure 7-8: Low-frequency vibration spectra for the healthy compressor (BL) and compressor with two simulated faults (DVL and ICL) for discharge pressures 80, 100 and 120 psi	152
Figure 7-9: Envelope analysis of vibration signal for healthy (BL) and seeded faults (DVL and ICL) for discharge pressures 80, 100 and 120 psi.....	153
Figure 7-10: Magnitudes of the first (fr), second ($2fr$) and third harmonic ($3fr$) for healthy (BL) and seeded faults (DVL and ICL) for discharge pressures 60, 80, 100 and 120 psi.	154
Figure 7-11: MSB magnitudes for healthy (BL) and faulty conditions (DVL and ICL) for discharge pressures 60, 80, 100 and 120 psi. Modulator frequency f_x : 0 Hz \approx 30 Hz, carrier signal f_c : 3.0 kHz \approx 4.5 kHz.....	156
Figure 7-12: Average MSB magnitudes for healthy (BL) and faulty conditions (DVL and ICL) for discharge pressures 60, 80, 100 and 120 psi. Modulator frequency f_x : 0 Hz \approx 30 Hz, carrier signal f_c : 3.0 kHz \approx 4.5 kHz.....	157

Figure 7-13: Vibration signal based diagnosis comparison between MSB and Envelope spectrum for healthy (BL) and seeded faults (DVL and ICL) at four discharge pressures 158

Figure 7-14: Percentage difference between DVL and MSB, and ICL and MSB for four discharge pressures 159

LIST OF TABLES

Table 4-1: Broom-Wade TS9 specifications	60
Table 4-2: Experimental test conditions description	61
Table 4-3: Accelerometer technical specifications.....	65
Table 4-4: Pressure sensor technical specifications of the pressure sensor	67
Table 4-5: Technical specifications for the hall effect current transducer (RS 286-327)...	70
Table 4-6: Data acquisition CED 1401 plus channels	70
Table 5-1: Details of electrical motor parameters	102
Table 5-2: Broom-Wade TS 9-16 compressor parameters	102
Table 5-3: First / Second stage piston and cylinder parameters	103
Table 5-4: Compressor valve system parameters	103
Table 5-5: Difference of RMS values for healthy compressor	110
Table 6-1: Percentage difference between healthy compressor and compressor with seeded faults for discharge pressures 1, 40, 80 and 120 psi	139
Table 7-1: Differences between BL and seeded faults	160

LIST OF ABBREVIATIONS

AM	Amplitude Modulation
BDC	Bottom Dead Centre.
BL	Baseline
BRB	Broken Rotor Bar
CAM	Computer-Aided Modelling
CED	Cambridge Electronic Design
CF	Crest Factor
CM	Condition monitoring.
CT	Current Transducer
CWT	Continuous Wavelet Transforms
DAQ	Data Acquisition System.
DAQ	Data Acquisition System
DFT	Discrete Fourier Transform
DOF	Degree Of Freedom
DSP	Digital Signal Processing
DTW	Dynamic Time Wrapping
DVL	Discharge Valve Leakage
DWT	Discrete Wavelet Transforms
FFT	Fast Fourier Transforms
FM	Frequency Modulation
FT	Fourier Transforms
GUI	Graphical User Interface
HOS	Higher Order Spectra
Hz	Hertz
IAS	Instantaneous Angular Speed.
IC	Integrated Circuit.
ICL	Intercooler Leakage
IEEE	Institute of Electrical and Electronics

IFFT	Inverse Fast Fourier Transform.
K	Kurtosis
kW	Kilo-Watt
MCSA	Motor Current Signature Analysis
MSB	Modulation Signal Bispectrum
PCB	Printed Circuit Board
PPR	Pulses Per Revolution.
PS	Power Spectrum
PV	Peak Values
pV	Peak Value
P-V	Pressure-Volume
QPC	Quadratic Phase Coupling
RMS	Root Mean Square.
RPM	Revolution Per Minute
RVM	Relevance Vector Machines
STFT	Short Time Fourier Transform
SVL	Suction Valve Leakage
SVM	Support Vector Machine
SWA	Stator Winding Asymmetry
TDC	Top Dead Centre
WT	Wavelet Transform

LIST OF NOMENCLATURE

ω	IAS of the crankshaft [rad/sec]
$\phi(f)$	Phase of spectrum signal
θ	Crank angle [deg]
γ	Ratio of specific heats of the process gas (1.4 for air)
$x(t)$	Time waveform signal [V]
$X(f)$	Fourier spectrum signal
$X^*(f)$	The conjugate of X(f)
T_m	Motor driving torque [Nm]
s	Motor slip
p	Number of pole pairs
n_s	Synchronous speed
n_r	Rotor speed
N	Number of samples
m	Mass of air inside cylinder [g]
l	Connecting rod length [mm]
k	Valve spring stiffness [$\text{N} \cdot \text{m}^{-1}$]
J	Moment of inertia [kgs^2]
f_{vs}	Suction pressure force [N]
f_{vd}	Discharge pressure force [N]
f_{so}	Preset spring force of suction valve [N]
f_{sb}	Sideband frequency [Hz]
f_s	Fundamental supply frequency
f_r	Shaft frequency [Hz]
f_{gs}	Gravitation force for suction valve [N]
f_{gd}	Gravitation force for discharge valve [N]
f_{do}	Preset spring force of discharge valve [N]
f_c	Carrier frequency [Hz]
F	Cylinder air pressure force [N]
$E[B(f_1, f_2)]$	Magnitude of conventional bispectrum signal
D	Piston diameter [mm]

d	Cylinder bore length [mm]
cfs	Force coefficient of suction valve
cf _d	Force coefficient of discharge valve
C	Damping constant of valve chamber [N/ms ⁻¹]
$b_{MS^2}(f_1, f_2)$	Bicoherence of modulation signal bispectrum
$B_{MS}(f_1, f_2)$	Modulation signal bispectrum of two frequency components
$B(f_1, f_2)$	Conventional bispectrum of two frequency components
$ X(f) $	Magnitude of fourier transform
$ B_{MS}(f_1, f_2) $	Amplitude of modulation signal bispectrum
ω_s	The motor speed [rad/sec]
ρ_i	Density of the air in the plenum [kg/m ³]
ρ_c	Density of the air in the cylinder [kg/m ³]
x_v	Valve plate displacement [mm]
XS_{\max}	Suction valve max lift [mm]
x_p	Piston displacement [mm]
x_{\max}	Max valve plate displacement [mm]
Xd_{\max}	discharge valve max lift [mm]
v_c	Cylinder volume [m ³]
\dot{v}	Variable cylinders volume [m ³]
$T_{pmL,H}$	Torque produced by cylinder air pressure and piston mass [N. m]
T_m	Driving torque [N. m]
$T_{fl,H}$	Friction torque
m_v	Mass of the valve plate plus one-third of the spring mass [g]
m_{spring}	Mass of valve spring [g]
m_{rec}	Reciprocating inertial mass [g]
m_{plate}	Mass of valve plate [g]
m_p	Piston mass [g]
m_{cr}	Connecting rod mass [g]
m_{co}	Cylinder clearance volume [m ³]
$f_{pL,H}$	Force produced by the air pressure [N]
f_p	Force produced by the inertial force of reciprocating pressure [N]
$f_{mL,H}$	Force produced by the inertial force of reciprocating mass [N]

f_m	Force produced by the inertial force of reciprocating mass [N]
C_i	Speed of sound in the suction plenum [ms^{-1}]
$C_{di}(x)$	Variable suction coefficient
$C_{dd}(x)$	Variable discharge coefficient
C_d	DV Contact damping coefficients [$\text{N} \cdot \text{m}^{-1}$]
C_{cs}	SV Contact damping coefficients [$\text{N} \cdot \text{m}^{-1}$]
B_r	Transmission ratio [%]
A_L	Leakage valve size [mm^2]
A_{fl}	Maximum, flow area of the suction valve [mm^2]
A_{fd}	Maximum, flow area of the discharge valve [mm^2]
\dot{x}_v	Valve speed [ms^{-1}]
\ddot{x}_v	Valve acceleration [ms^{-2}]
\dot{x}_p	Vertical piston speed [ms^{-1}]
\ddot{x}_p	Vertical piston acceleration [$\text{m} \cdot \text{sec}^{-2}$]
\dot{m}_{vi}	Mass flow rate through the suction valve [kgs^{-1}]
\dot{m}_{vd}	Mass flow rate through the discharge valve [kgs^{-1}]
\dot{m}_{ls}	Mass flow rate of leakage suction valve [kgs^{-1}]

CHAPTER 1:

Introduction

Chapter one presents how fault detection, diagnosis, and machine condition monitoring is essential to maintain the smooth operations of any machinery in the industry. It starts with an introduction to the background of this study, motivation for pursuing the project, then states the aim and objectives. Finally, the chapter presents an outline of this thesis.

1.1 Background

Condition monitoring (CM) is considered essential in most industrial sectors; the monitoring of the physical parameters associated with machinery while in operation which provides information on the machine in order to determine its condition and potentially allow timely decision-making for effective maintenance [1]. Any change in the normal behaviour of a machine results in a change of signature of those parameters (large or small) that can act as an indicator of an abnormal operating condition and may indicate an incipient fault [2]. CM not only provides an early warning of potential failure and its nature but also allows any preventative strategies to be arranged. Thus, a suitable maintenance procedure can be scheduled to avoid the consequences of failure before it occurs, especially to prevent catastrophic machine failures and consequential losses [3, 4], or at least, eliminate unnecessary maintenance costs. CM plays an important role in modern organizations in the management of maintenance and operational activities. One of the main goals of machine CM is to optimize the plant operation by regularly evaluating the healthy conditions of machines and providing essential and accurate quantitative information regarding the machinery's operating condition in order to determine whether the machine's condition is normal or abnormal [5], thus enabling both preventive and corrective maintenance [2]. Incipient fault diagnosis and CM not only considerably improve the performance of the machine but could also have huge economic benefits by avoiding the consequences of unexpected failure and minimizing the number of unscheduled breakdowns [2, 3]. It is the interest of any industrial company to eliminate any unnecessary losses in production time or unexpected maintenance costs. This, in turn, will provide great opportunities for companies to significantly improve their machine availability [3].

Even though CM has been established since the 1960s, it is still developing in parallel with the advances in transducers and computer technology [6]. Today's monitoring strategies including advanced signal processing methods improve the accessibility to CM system by all industrial sectors, providing the ability to monitor machinery in order to avoid any system failure and reduce maintenance costs [6]. Any change in machine behaviour due to the presence of faults can be detected by monitoring the change of the machine parameters. However, the small variance between a machine's normal and abnormal operations might often be contaminated by background noise. Advanced signal

processing techniques along with modern transducers have the ability to distinguish any significant behaviour changes [7]. Additionally, analysis of the system parameters can assist in the prediction of certain failures and can provide valuable information to help in monitoring those faults [2].

The adoption of CM strategies within industrial plants has increased remarkably with more companies aiming to reduce the side effect of machine faults and develop alternative ways of using their resources. Some factors, for adopting CM are [2, 8-10]:

- ✓ To reduce maintenance cost and avoid unwarranted part replacement,
- ✓ To extend the life of the machine,
- ✓ To minimize unplanned maintenance,
- ✓ To enhance safety and reduce injuries to humans,
- ✓ To upgrade the quality of the production and reduce the cost,
- ✓ To improve productivity and profitability, and
- ✓ To improve machine availability.

1.2 Research Application

Reciprocating compressors and their three-phase induction motors (IM) are one of the most widely employed of all machines and play an essential role in various industrial sectors including petroleum refineries, petrochemical, recent renewable energy processes and so on. because they are simple yet powerful, flexible in use, relatively efficient and are highly reliable.

RC operates in a varied range of operation conditions, in which some of the compressor parts e.g. valve system, work in particularly harsh environments, including both high pressure and high temperature [11]. As a consequence, RC are susceptible to a range of different faults, which can occur in individually or combination, and which affect their operational performance and functioning. The occurrence of any failure within the compressor may alter the normal operating condition of the machine and usually leads to a total system failure. This failure not only increase maintenance cost and reduce compressor efficiency but can also be time-consuming and even life-threatening [12], and hence their condition needs to be monitored. The reciprocating motion, the pressure differences and the complexity of the interactions between compressor components lead to complicated signals contaminated with compressor background noise. Consequently,

effective CM techniques are essential for the detection and diagnoses of RC faults and its driving three-phase induction motor faults at an early stage to maximize system productivity by reducing maintenance costs and preventing any major failures [13, 14]. In this research, advanced signal processing techniques have been applied to characterise compressor behaviour under different working conditions to extract useful information in order to use the extracted features as a source for compressor CM.

1.3 The Importance of Maintenance

In industry, one of the main goals to reduce cost is considering the importance of maintenance costs. The cost of maintenance procedures in all manufacturing or production plants is a major contribution to the total operation costs [6]. Even small faults can contribute to shortening the life of machines, reduce efficiency and decrease machine productivity. In addition, in some cases, faults can cause secondary damage or even produce faults in other parts, which can lead to serious machine breakdowns [15]. Furthermore, these faults contribute to a plant's downtime that can be expensive and increase the maintenance and operating costs.

Monitoring the condition of any item of equipment involves both software and hardware tools. Usually, this procedure consists of three steps [16]: starting with parameter collection (data acquisition) from a machine using different sensors and transducers, then through signal processing techniques (data processing) to provide an evaluation of the condition of a system and its component, making the right maintenance decision (decision making), and to schedule any arrangement for maintenance procedure if necessary [17].

Nowadays, predictive maintenance requires the application of different techniques and tools to monitor the machine operation conditions, these include; thermal techniques, oil debris analysis, motor current signature, voltages signals, acoustic emission and vibration responses analysis which are used to monitor machine condition for the detection of any potential failure. Using time-domain, frequency-domain and joint time-frequency domain analysis to carry out machine fault detection will prevent failure and will reduce maintenance costs, reduce the operator's risk, help to avoid the progression of an abnormal event and decrease productivity losses [18].

CM provides the means by which to manage maintenance operations and reduce or eliminate unnecessary repairs and decrease the downside effect of maintenance operations on the production profitability [19]. The regular monitoring of the machine's condition can prevent or at least reduce any catastrophic failures within a plant. The early detection of incipient machine faults not only increases the life and the productivity of plant machinery but offers better reliability, maximises the interval between repairs; and will minimize the number and cost of unscheduled maintenance events and improve the overall availability of the machine [19]

Today, run-to-failure is considered as an unacceptable strategy for many processes and industrial operations. The more desirable alternative is CM performed to collect and analyse machine parameters to achieve early fault detection and diagnosis [2]. The advance of new microprocessors, computers, and software makes machine monitoring and data collection from plant equipment and systems easier. Efficient and effective CM methods are very essential for the detection and diagnoses of machine faults at an early stage in terms of accident prevention, decision-making, reduction of maintenance cost and maximizing the system productivity [13, 20]. Today, in the field of machine CM and fault diagnosis, there are large and growing variety of methods and techniques for CM applications in the industrial field, and each has its own advantages and disadvantages.

The periodic mechanical movements of compressor components, i.e. piston movements and valve flutter, provide vibration signatures which reflect the compressor's dynamic behaviour while in operation. These signatures will exhibit an immediate change when a fault occurs in the compressor. Vibration monitoring is the most effective and popular method, widely employed in RCs CM [12, 21-23]. However, vibration monitoring has limitations. One major problem is the background noise. Since the vibration data are obtained while the machine is in operation, the collected data will invariably be contaminated by this noise [24]. Yet, applying advanced signal processing techniques, i.e. modulation signal biospectrum, gives vibration analysis the capability to extract even very weak abnormal behaviour caused by an incipient fault from a noisy signal [25].

Motor current signature analysis (MCSA) has been proven a powerful approach for fault diagnosis and machine CM, it has been extensively utilized to determine the healthy operation of the three-phase induction motor and its downstream machines since the 1980s [26]. MCSA provides valuable and rich data regarding the machine conditions without

obstructing the operation of the monitored machine and can provide the same information as obtained by other monitoring tools without requiring access to the machine or using mechanical sensors [27-29]. MCSA measures the stator current of the motor to detect any abnormal changes, and when a fault occurs the signature of the stator current is different compared to the healthy condition [30].

Various studies using MCSA have been conducted to diagnosis different induction motor faults such as broken rotor bar and air-gap eccentricity and stator turn-to-turn faults [28, 29, 31-33]. The motor supply signature can also be used to detect abnormal conditions in downstream equipment such as air blowers, RCs, rolling mills as well as conditioning systems and pumps [34]. Furthermore, Alwodai et al. [31] have applied the modulation signal bispectrum (MSB) analysis to detect different severities of stator faults. They obtained more accurate diagnosis results compared to conventional analysis.

Fewer studies have been found in the literature studying the detection and diagnoses of RC faults based on three-phase induction motor current signals analysis, possibly because of the complexity of the RC and the varying load due to the compressor pressure changes while in operation, inducing noise in the measured stator current. This research considers the CM of an RC and focuses on the evaluation of acquired data from the compressor system including the induction motor to investigate non-linear and modulation effects on the measured signal. This will assist the development of an efficient data analysis tool based on advanced signal processing techniques for early detection and diagnosis of RC faults utilizing motor current and vibration analysis.

1.4 Research Scope

The project study provides the use of the information obtained from a three-phase induction motor current signal, and the structural vibration responses from an RC to detect and diagnose RC common faults. The experimental results were obtained through spectrum analysis of the stator current and vibration responses from the compressor experimental test rig; consisting of a two-stage RC driven by an induction motor.

Experimental studies were carried out on a single action, V-shaped two-stage RC system operated under different faulty operations, including a leaky discharge valve and leakage through intercooler pipe under various discharge pressures. The study also examined the

effect of the asymmetrical stator winding and combined faults (stator winding asymmetry and valve leakage) on the measured current signal. It examined the relative effectiveness of conventional diagnostic features in both motor current and structural vibration analysis based on the MSB and spectral analysis. Additionally, an extended dynamic model of the compressor has been developed to better understand the compressor behaviour and to examine the likely effects of different faults on the compressor performance.

1.5 Research Motivation

This project investigates a relatively new area of research where fewer studies have been carried out previously: to study the possibility of employing stator current analysis for detecting and diagnosing the condition of an RC .

Compressor faults i.e. leakage through the valve system or through intercooler pipe, produce repetitive impacts during the compressor cycle due to the movements of the piston inside the cylinder in a reciprocating motion. Additionally, the flutter of the valve plates upon their seats and dynamic load fluctuation will induce a modulation effect on the measured motor current signal. Consequently, the periodic and modulation effects induced by each fault need to be extracted in an effective way to implement reliable fault detection and diagnosis of the healthy running of the RC system

Additionally, few publications have been found which use a mathematical model to understand compressor interactions and the effect of different faults on the motor current signature of the compressor [35]. A model of a healthy compressor that can simulate different faults is needed to establish a baseline for the prediction of the effects of different simulated faults on the motor current signals. This will assist with determining which advanced signal processing methods could be utilized to detect and diagnose compressor fault.

For the development of accurate and advanced diagnosis, this research work has studied the application of CM on a two-stage RC . It has focused on the investigation of non-linear effects and modulation characteristics in the compressor dynamic behaviour induced by the compressor varying load and then used the model predictions to investigate the compressor operation under different conditions to develop effective signal processing tools to extract non-linear and modulation characteristics of the current signal for more accurate and reliable detection and diagnosis of the potential of RC faults at early stages.

1.6 Research Aim and Objective

1.6.1 Research Aim

The aim of this project is to develop a new effective method for the detection and diagnosis of common and compound faults in a two-stage RC system including the associated induction motor, based on the analysis of the motor current signatures, vibration responses in line with dynamic model predictions.

1.6.2 Research Objectives

In order to achieve the aim of this study, a number of main objectives are defined as follows:

Objective -1. To gain general knowledge on RC and associated three-phase induction motors, their working principles, operating mechanism and commonly occurring faults. To review different existing techniques for machine CM in order to evaluate the performance of these methods for early fault detection of RC.

Objective -2. To construct a compressor test facility and simulate different compressor faults in a realistic way to enable subsequent system behaviour to be characterised, then obtain experimental data to evaluate the compressor performance under these operating conditions.

Objective -3. To develop an extended model of compressor dynamics in a MATLAB environment to study compressor behaviour under a wide range of operating conditions including different faults. Also, to study the predicted changes in motor current signature - due to the presence of the seeded faults - on the AC induction motor, crankshaft dynamics, the mass flow rate through valves and cylinder pressure variation. To seek to establish effective and reliable diagnostic features.

Objective -4. To obtain an effective and stable analysis of the stator current signature of a two-stage RC under healthy and faulty operating conditions; in terms of both experimental tests and dynamic model responses. Also, compare experimental results and model predictions to evaluate the developed model to help implement a diagnostic approach for compressor fault feature extraction.

Objective -5. Investigate the capability of the induction motor current signals to detect and diagnose compressor and motor faults (individual or combined) and apply different signal processing methods to study the possibility of using motor current

for monitoring different compressor faults with a high degree of accuracy.

Objective -6. To study modulation effects and non-linear characteristics to extract weak signatures from vibration and current signals, then compare the performance of the current and vibration techniques for the development of more efficient and reliable signal processing tools and evaluate the performance of MSB for RC condition monitoring.

Objective -7. To provide useful information and recommendations for future research activity relating to this field.

1.7 Thesis Organization

This thesis is composed of eight chapters. A brief overview of each chapter as follows.

Chapter One. This chapter provides an introduction to the research work presented in this thesis including the research motivation, overall aim, research objectives and thesis outline.

Chapter Two. This chapter provides a brief overview of compressors types, operations, classification and common faults experienced in the industry. The chapter also presents a description of the three-phase induction motor, its construction and common faults. After that, the chapter presents an overview of CM, including common methods of fault detection used for RCs.

Chapter Three. This chapter presents an overview of the most widely conventional signal processing techniques applied for compressor CM and fault detection based on motor current and vibration measurements. Then a brief discussion is presented with suitable techniques in order to obtain diagnostic features to detect and identify various compressor faults more effectively. Finally, the chapter also describes HOS techniques such as modulation signal bispectrum, as a more accurate means of fault feature extraction for diagnosis of different simulated conditions in an RC.

Chapter Four. This chapter introduces the test facility and the simulation of common RC faults that were considered in this investigation. It starts with a detailed description of the test facility, seeded faults, measuring instruments, sensors, and a description of the data acquisition system used to carry out this investigation.

Chapter Five. This chapter presents a numerical two-stage RC dynamic model to study

the dynamic behaviour of the compressor under healthy and different fault conditions. It starts with a general concept of compressor operating mechanisms, then the piston-cylinder, the crankshaft arrangement and cylinder pressure are developed to show the mutual relationship between pressure and speed and their effects on the motor current. In addition, different common faults have been simulated to evaluate the model performance under these conditions. This chapter also presents a brief description of model parameter identification, then solving the model's equations in the MATLAB environment are followed. The chapter examines the RC responses from both experimental and numerical studies under both healthy and faulty conditions for model validation. Finally, the model is used for feature extraction based on different simulated motor and compressor faults occurring in isolation and combined for compressor fault diagnosis.

Chapter Six. This chapter investigates the capabilities of the motor current signature for RC condition monitoring. It examines the process of monitoring compressor operations under different common faults including the combined fault: discharge valve leakage, inter-cooler leakage, and stator winding asymmetry combined with discharge valve leakage. Both conventional spectrum and MSB analysis are used to characterise the current signatures corresponding to the modulation induced by the compressor varying loads. The results of the spectrum and MSB analysis are compared

Chapter Seven. This chapter presents the results of the MSB technique for the analysis of compressor performance under different conditions (discharge valve leakage and inter-cooler leakage) based on the compressor vibration responses. Both conventional spectrum analysis and MSB analysis were used to examine the effect of these abnormal conditions on the RC's vibration responses. Finally, the results of vibration analysis based on the spectrum and MSB analysis are compared

Chapter Eight. This chapter draws conclusions and summarizes the achievements based on the findings of this project. Also, suggestion and recommendations for future study are summarized.

Figure 1-1 illustrates the general structure and plan of the research project.

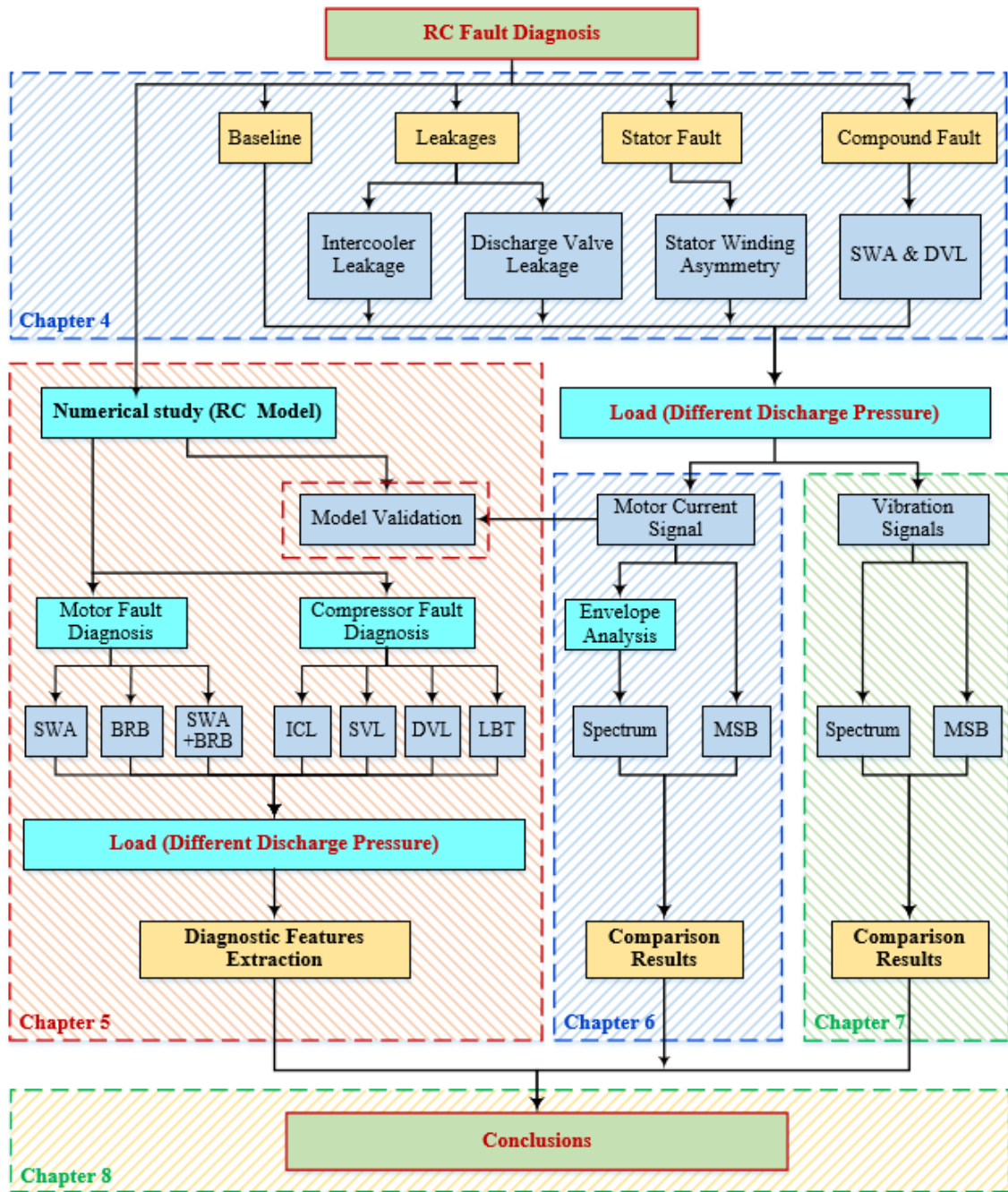


Figure 1-1: Flowchart of the study work scheme

CHAPTER 2:

Reciprocating Compressor Fundamentals, Their Faults and Conventional Condition Monitoring

This chapter starts by giving a brief overview of the different type of compressors. A detailed description of compressor operations and classification follows. It then gives general information about common compressor faults. Then, an introduction to the three-phase induction motor, its main components and common fault have been presented. Finally, the chapter reviews various common condition monitoring methods such as cylinder pressures, instantaneous angular speed analysis, vibration-based monitoring and motor current analysis which can be used for RC and the three-phase induction motor fault detection and diagnosis.

2.1 Introduction

As explained in Chapter 1, the RC plays an important role in numerous industrial systems, due to its efficiency, flexibility and reliability. This machine uses mechanical work to compress the gas inside its cylinder and increase its pressure to provide a useful power source for other machinery [24, 35, 36]. In general, compressors are categorised based on their compression mode: intermittent or continuous. Intermittent provides a high discharge pressure with less volume flow rate whereas the continuous mode provides a higher volume flow but lower discharge pressure [37].

2.2 Principle of Operation

Compressing the volume of the air or gas in the cylinder increases both its pressure and temperature. This may lead to problems since there are certain limits on the operational conditions that will depend on the specific application. To achieve the desired pressure, the compression process may be in more than one stage, such compressors are termed multi-stage. In general, there are four common approaches to compress the working gas [36]:

1. Trap an amount of gas in the cylinder, or any kind of enclosure, then reduce its volume which will cause an increase in pressure. After that, release the compressed gas from the cylinder, usually into a storage vessel.
2. Trap an amount of gas in a cylinder, or some kind of enclosure, move it without changing its volume to the outlet, then compress the air by backflow from the outlet system, and finally push it out of the cylinder (enclosure).
3. The third method is achieved by compressing the air by a mechanical movement such as a rotating impeller which increases the pressure of the flowing air by increasing its velocity.
4. Mix the gas with the same and different gas in the high-velocity jet to increase the air velocity and then convert this fast-flowing mixture into pressure in the cylinder.

The compressors that use the first and second methods are classified as positive displacement compressors whereas dynamic compressors use the third method, and ejectors the fourth. Ejectors usually operate with a suction pressure, i.e., below atmospheric pressure [36, 38].

2.3 Compressor Types and Classifications

In general, compressors are divided into two groups, as stated in the previous section: positive displacement compressors (*intermittent mode*) and dynamic compressors (*continuous flow*). Compressors can also be classified according to other characteristics including application, size, operating principles (dynamic, volumetric), and internal mechanical movement (linear, rotary). Additionally, different industrial applications require different compressor configurations. In this research, the concern is only on the positive displacement compressor, in particular, RC due to the widely spread of these compressors and the importance of these machines.

In positive displacement compressors, the increase in pressure is obtained by reducing the volume of gas contained within the compressor cylinder by means of mechanical action. While, in case of the dynamic compressor, the pressure is raised by increasing the velocity of the gas using a rotating element and converting the energy imparted to the gas into increased pressure [37, 39]. Figure 2-1 shows the main commonly used types of compressors in the process industries [40].

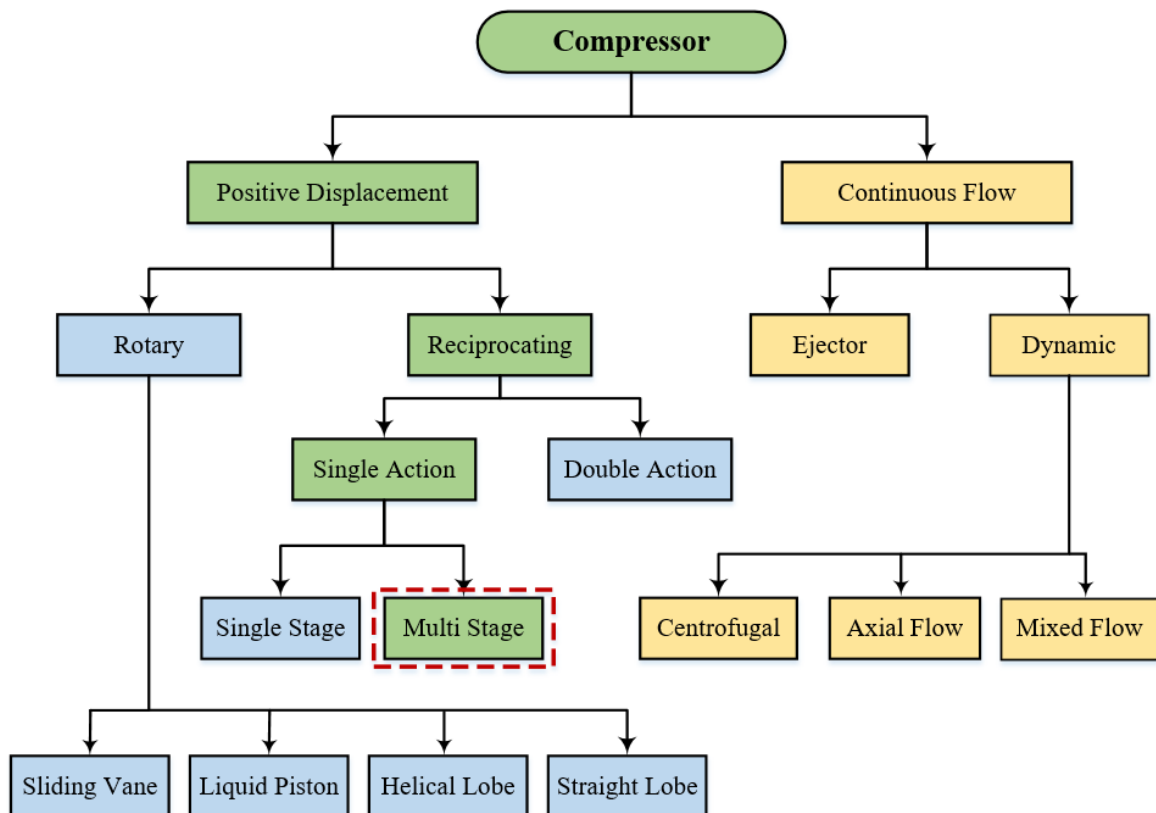


Figure 2-1 :The main categories of compressors [36]

2.3.1 Continuous Flow, Dynamic Compressors

The continuous compression-mode is widely used in chemical and petroleum plants; also they are used in some manufacturing industries such as the iron and steel industry [37]. These compressors are much smaller, in size, than positive displacement compressors and produce much less vibration. Continuous compressors can be categorised into two main categories: dynamic and ejector.

2.3.2 Positive Displacement Compressor (Intermittent Mode)

Compressors in this category can provide a fixed volume of air or gas at high pressure, for every stroke of the piston. Positive displacement compressors are cyclic in nature and can be categorized to different types, as illustrated in Figure 2-1 Rotary screw air compressors, vane compressors and RCs are the most common types of positive displacement compressors used in small and medium industries.

Their principle of operation is the compression of a volume of gas by the movement of a piston within a compression chamber. The rotational movement of the crankshaft is converted into linear movement via a connecting rod, see Figure 2-3, which moves the piston linearly inside the cylinder. The valves inside the compressor open and close automatically based on the pressure difference across them. Generally, the compressor cycle starts with the piston positioned at the highest point of the cylinder (top dead centre (TDC)). At TDC both the suction and discharge valves are closed as in position 1a, Figure 2-2. As the piston travels away from the cylinder head (“downward” movement), the small volume of trapped gas in the clearance volume expands but the continued downward movement of the piston reduces the pressure in the cylinder until the pressure is sufficiently below the atmospheric pressure that the pressure difference is sufficient to push it open against the action of the valve spring, and the gas enters the cylinder as shown in position 2 Figure 2-2 (suction). When the pressure difference between atmosphere and cylinder is no longer sufficient to overcome the force exerted by the suction valve spring, the valve closes. At this position, the piston has reached the lowest point of the cylinder (bottom dead centre (BDC)) and both valves are closed. As the piston travels “upward” towards TDC it compresses the accumulated gas inside the cylinder, increasing its pressure as shown in position 3 Figure 2-2. When the pressure inside the cylinder is sufficiently higher than the pressure in the gas receiver (tank) the discharge valve opens

against the force exerted by the spring of the valve, which allows the compressed gas to be pushed out into the receiver tank, see position 4 Figure 2-2. When the piston reaches TDC, the discharge valve is pushed shut by its spring leaving the clearance volume filled with compressed gas. At this point, the compressor has finished one cycle and starts another, driven by the revolution of the crankshaft.

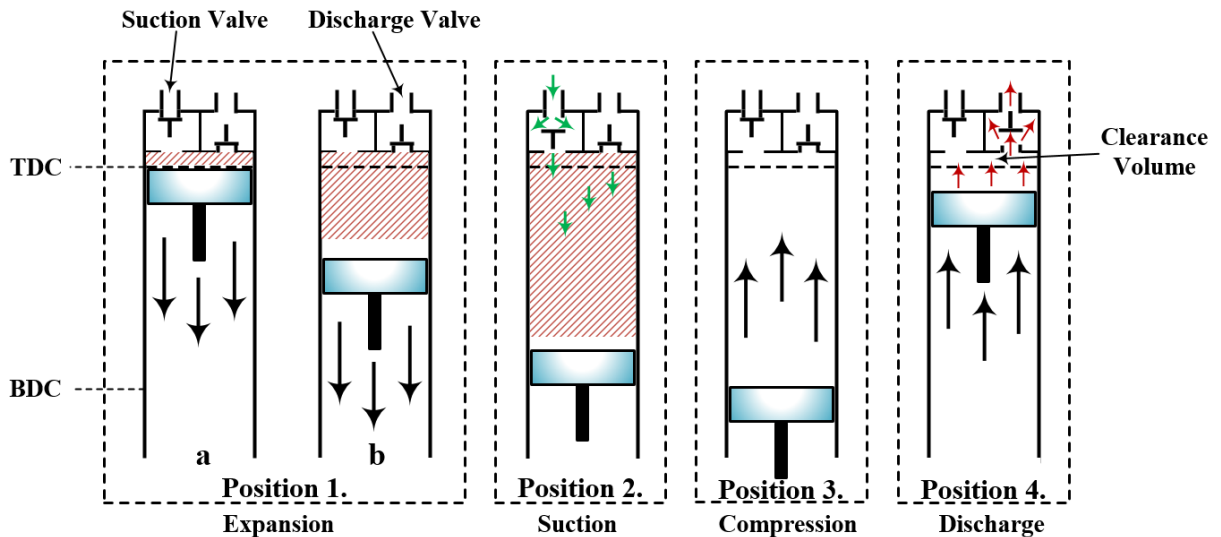


Figure 2-2: Suction and compression steps of a compression cylinder

2.4 Reciprocating Compressors

Reciprocating compressors (RC) are positive displacement compressors and are a useful power source for other machines by providing a continuous supply of compressed air or gas [36]. Modern RCs have a number of advantages due to their simple design and ease of installation, low power consumption, the capability of compressing gases to high pressures (particularly with multi-stage compressors), and having different capacities with different pressure ranges to meet almost all requirements. Today an oil-free model is available if required [24].

The prime driver, driving the compressor is likely to be an electric motor, internal combustion engine or steam turbine. RCs play an essential part in air and gas distribution plant, refrigeration services, and the oil and gas industry as an integral component of an offshore plant. The compression of the gas is obtained by a mechanical (reciprocating) movement of a piston inside a cylinder, created by a connecting crank-rod system [36, 41]. One cycle successively comprises expansion and suction during the backward stroke and compression and discharge during the forward stroke, see Figure 2-2. These machines

can be used in a wide range of harsh operating conditions and can be vulnerable to faults developed in the valve system. Thus, efficient and effective CM is necessary to detect and diagnose the faults at an early stage [13, 20, 35].

The RC can have a single-stage cylinder or multi-stage cylinders in different sizes, depending on the requirements, such as the need to meet a varying load with high-pressure levels. In each configuration, compression can be performed in single-acting or double-acting cylinders. In the single action compressors, the compression of air or gas is achieved using one side of the piston only, as described above and shown in Figure 2-2, whereas, in the double-acting compressor, the compression takes place on both sides of the piston [42].

One of the most common problems of single-stage compression is its high discharge temperature. Thus, when the required compression ratio is high, a multi-stage (two or more stages) compressor may be necessary for the application. Typically, the compressed air is cooled between stages to reduce its temperature before proceeding to the next stage [42]. Figure 2-3 shows a multi-stage RC designed for process applications.

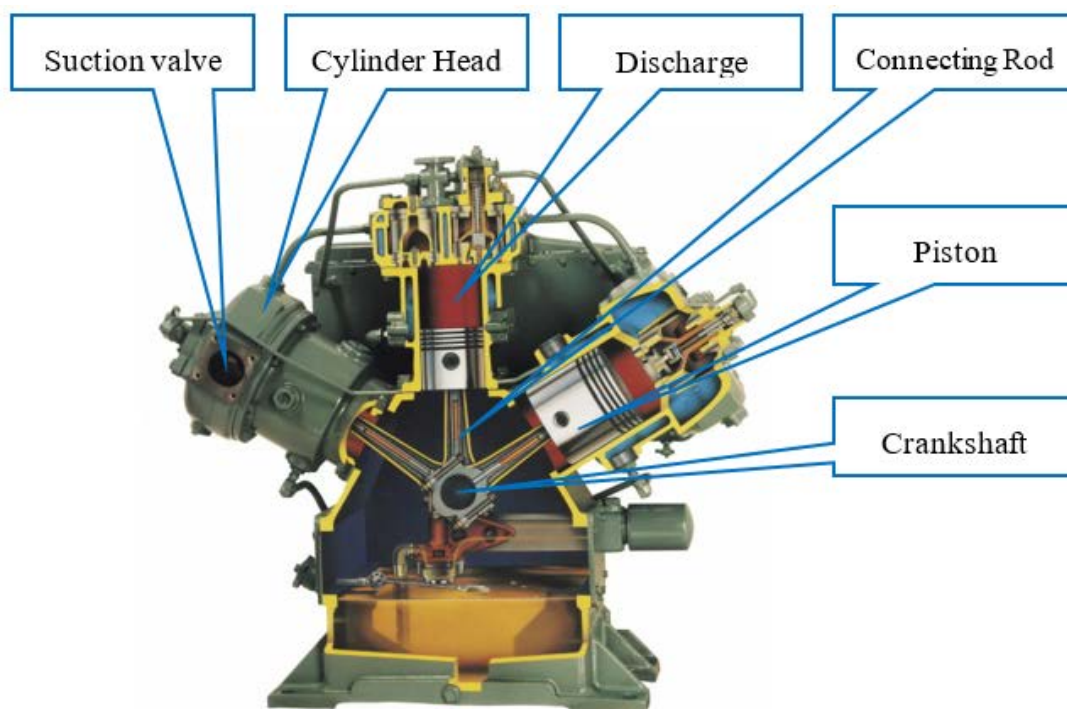


Figure 2-3: Photo of “exploded” multi-stage reciprocating compressor

2.5 Single-Stage Reciprocating Compressors (Single Action)

The most used RC and its simplest form is a single acting compressor (either single-stage or multi-stage) in which the compression cycle is achieved by compressing the gas using only one side of the piston [43]. In single-stage RCs, the compression cycle from initial to the final state is carried out in a single stage. In most cases, these compressors do not require any cooling system to reduce the gas temperature and can provide a compressed gas up to 100 psi [44]. Figure 2-4 shows the basic structure for a typical single-acting one-stage RC which generally consists of a single cylinder, cylinder head, piston, valves, crankshaft, and a connecting rod. Motion in these compressors is both rotation and linear, unlike rotary machinery in which only rotary motion takes place [24]. The compressor is powered by a prime mover (e.g., 3-phase induction motor) which drives the crankshaft which, in turn, moves the piston via a connecting rod [36].

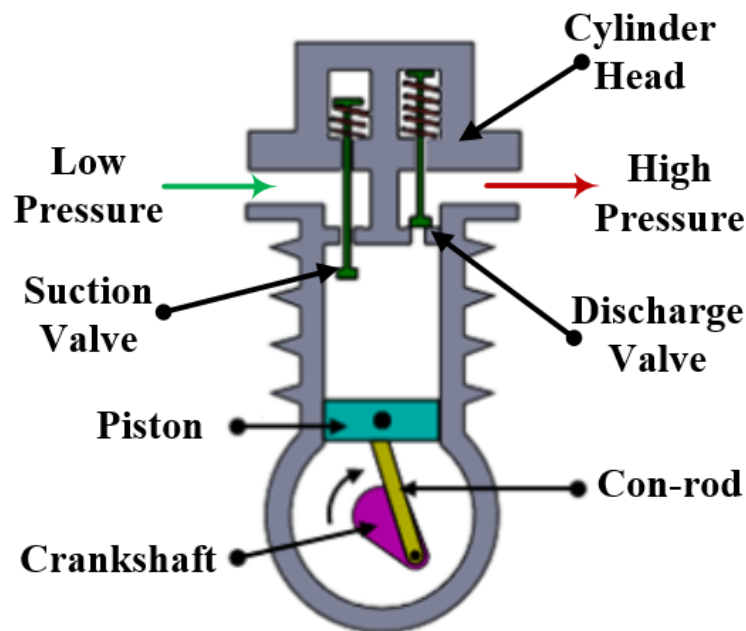


Figure 2-4: Schematic of single-stage single-acting reciprocating compressor

2.5.1 P-V Diagram for an Ideal Single Stage (Single Acting) Compressor

The compression cycle for the single stage compressor takes place in four basic steps as illustrated in Figure 2-5. As mentioned in Section 2.3.2, the cycle starts with the piston position at the top dead centre (TDC). Figure 2-5 shows an ideal Pressure-Volume diagram for a single-stage RC one complete cycle showing the main processes (expansion, suction, compression and discharge) [36, 42].

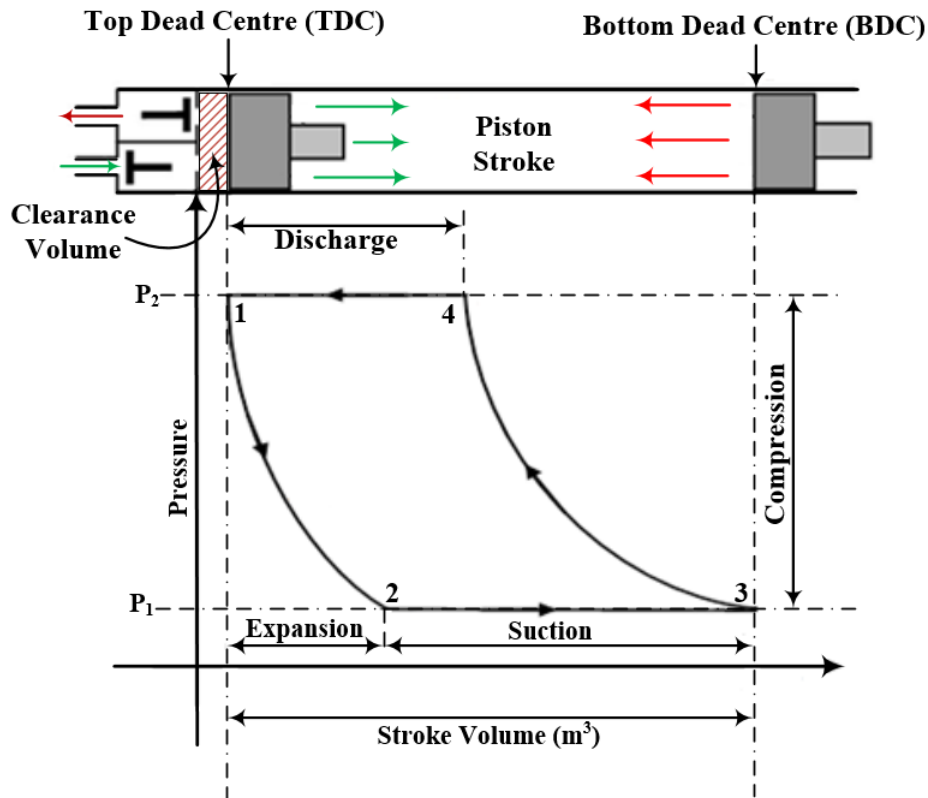


Figure 2-5: An ideal Pressure-Volume diagram (P-V) [42]

2.6 Multi-Stage Reciprocating Compressors

The single-stage compressor provides high-pressure air accompanied by a temperature increase, which affects the efficiency of the compressor. A multi-stage compressor can be used when the high pressure required exceeds the capability of a single-stage compressor and/or to minimise the increase in temperature that occurs during the compression process. Multi-stage compressors are able to produce pressures more than 300 kPa and are used widely in the industry [24]. Heat exchangers are used to remove excess heat from the compressed air between intermediate stages, see Figure 2-6 (b). These heat exchangers/intercoolers reduce the air temperature to be as close as possible to that at the inlet (suction) [45]. Figure 2-6 shows a photograph and a schematic diagram of multi-stage (two stages) RC [46]. In a small multi-stage compressor, the intercooler is air-cooled, i.e., the high-temperature air passes through the intercooler pipe and cooled using air movement generated by the flywheel or a suitable cooling fan. Larger multi-stage compressors require water-cooling to reduce the compressed air temperature to a satisfactory level.

At the low (first) stage the gas is compressed into an intermediate pressure, then it passes through the intercooler to extract the excess heat from the compressed air. The pressure is again increased in the next stage until it reaches the required pressure [24]. The benefit of having inter-cooling between compressor stages is to increase compressor efficiency and reduce input power requirements. Multi-stage compressors are considered as expensive because of high initial fitting costs, and relatively high maintenance costs but, nevertheless, are still considered to be amongst most efficient industrial air compressors. Both single and multi-stage compressors are usually driven by an induction motor. In some cases, a diesel engine is used to power very large compressors and the drive power is transmitted to the compressor via a belt or directly [35].

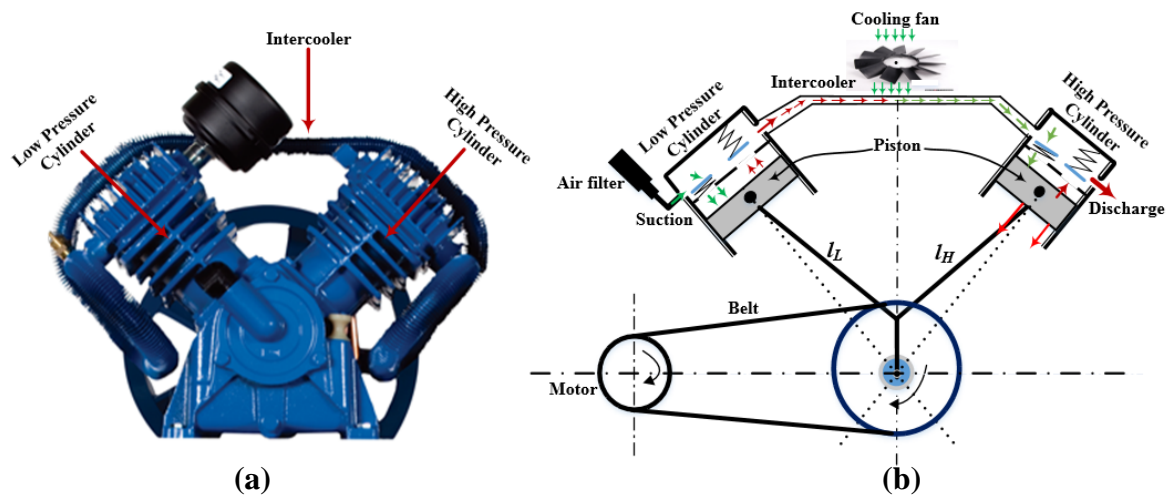


Figure 2-6: a) Two-stage compressor, b) Schematic diagram of a two-stage compressor

2.6.1 P-V Diagram for An Ideal Multi-Stage Compressor (Two-Stage)

The Pressure-Volume diagram (PV) is used to analyze the operation of the RC, and to study the compressor cycle [24]. In multi-stage RCs, the cross-section area of each stage is proportional according to the total compression ratio. The higher stage cylinders are smaller in size than the lower stage cylinders because the air has already been partially compressed and cooled in the intermediate levels, which means a smaller volume cylinder is required compared to the previous stage. The ideal cycle pressure of an RC with two stages is depicted in Figure 2-7. Similar to a single-stage compressor, the two-stage RC consists of the same four events that make up one compression cycle: expansion, suction, compression and discharge, but now there are four events for each stage [24]. The air expands into the compressor cylinder as the piston travel downward from point 1 for the

first stage, and from point 5 for the second-stage cylinders. Then the suction valves open and air enters the cylinders to a maximum from point 2 to 3 for the first stage, and from point 6 to 7 for the second stage. At point 3 (point 6) suction and discharge valve are both closed and the position of the piston is at BDC. From point 3 to 4 for the first stage, and from point 7 to 8 for the second stage, the piston travels upwards compressing the air above it until the pressure inside the cylinder pushes open the discharge valve. The piston continues its upward movement until it reaches TDC point 1 for the first stage and point 5 for the second stage. The two discharge valves close leaving the clearance volume filled with compressed air and another cycle commences [24, 36, 42].

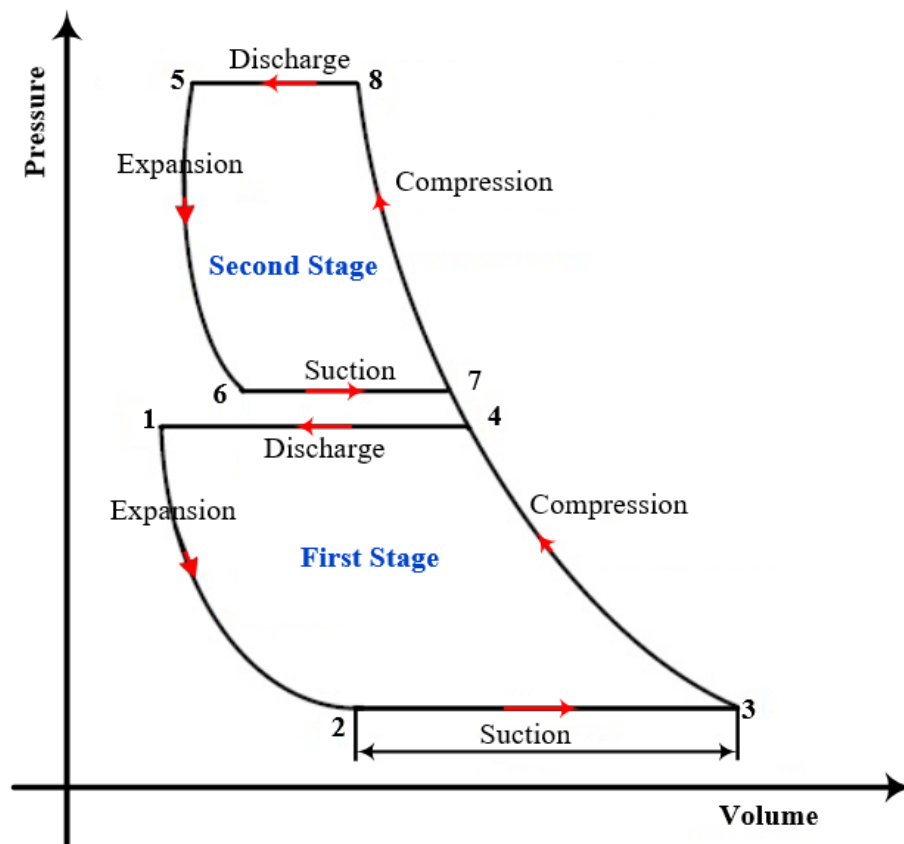


Figure 2-7: An ideal P-V diagram for a multi-stage compressor (two stages) [24]

2.7 Reciprocating Compressor Faults

RCs are considered the most widely used equipment in most industrial sectors including the petrochemical industries, oil refineries and refrigeration plants, etc. This is largely due to compressor simple construction yet powerful design, its flexibility and its reliability. Due to its working environment, many compressor parts work in adverse working

situations such as high-pressures and high-temperatures, which reduce compressor reliability and efficiency [11]. Consequently, RCs are subjected to numerous faults related to its functions and its operating conditions. Such faults not only degrade machine performance they also cause production losses and consume additional energy, which increases maintenance costs and even leads to severe damage in other parts, resulting in a reduction in machine availability [47].

Any failure occurring in the machine may alter the operating condition of the compressor and eventually lead to a total system failure. These faults occur for a variety of reasons including poor design and manufacturing error. In addition, some compressor components may fail due to the mechanical movement of its internal parts. Also, excessive vibration can result in friction and excessive heat and can adversely affect the valve system, belt, pistons, and piston rings. Furthermore, any lubrication failure will affect the crankshaft, con-rods, and bearings of the compressor. Moreover, wear to the piping system will result in leakages within the compressor [24].

Hence the condition of compressors needs to be monitored. Efficient CM methods are being actively examined for the detection and diagnosis of faults in RC and associated motors in the early phase to prevent compressor failures and decrease maintenance cost [13, 14]. The pie chart presented in Figure 2-8 gives an overview of the most common compressor faults are observed in the industrial practice [15]. Valves appear to be the most vulnerable component of the RC, thus, faults occur more often than in other components. Cracked or broken compressor valves, are considered as the major cause of machine failures and account for 31% of compressor failures [48]. In addition, valve faults reduce the compressor performance, might cause secondary compressor damage and can lead to unplanned breakdown [15, 24, 49]. Furthermore, deterioration over time of seals and connections to/from the intercooler cause leakage and this, in turn, will affect compressor efficiency.

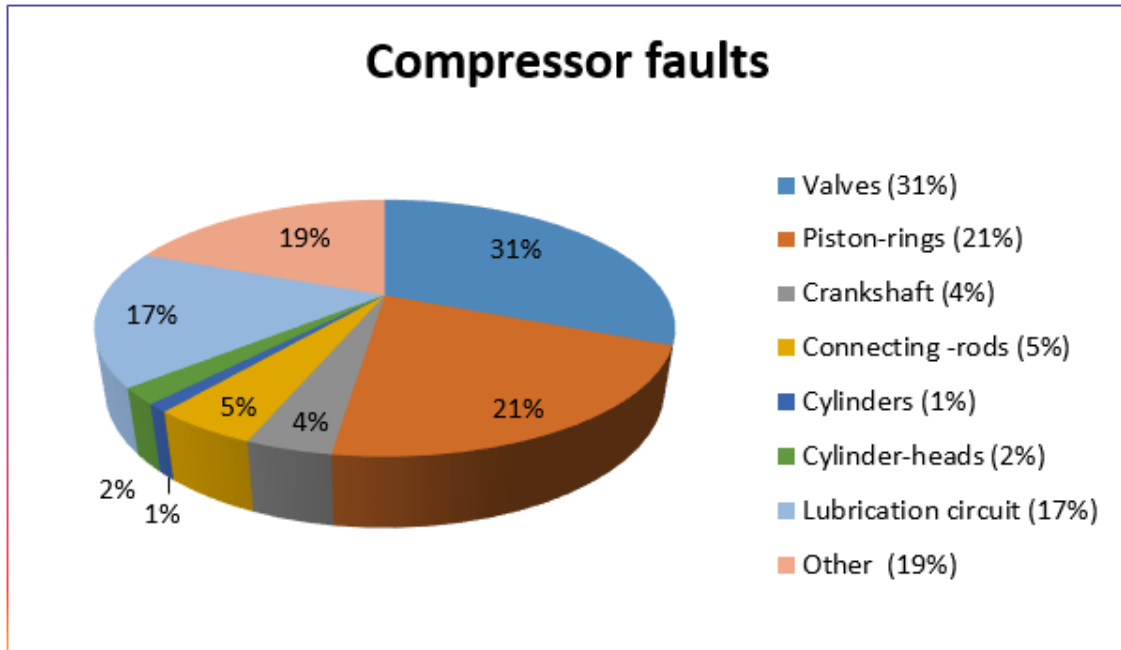


Figure 2-8: Reciprocating compressors failures rates [15]

2.8 Induction Motor and Power Transmission

Three-phase IM are the electrical devices used to convert electrical energy into mechanical energy (rotational motion) and are highly valued for their reliability [20, 50, 51]. Induction motors have different categories based on their physical configuration. The most popular is the squirrel cage induction motor because of its simple design, reliability, easy maintenance and relatively cheap cost [35, 50].

2.8.1 Induction Motor Construction

In general, induction motors consist of three main components. A stationary part, a rotating part, and the housing [48, 52]. Additional parts include a rotor shaft, bearings, and a cooling fan. The three-phase IMs are by far the backbone of modern industry and critical component extensively used in many industrial processes [28]. Figure 2-9 shows the typical components of an electrical induction motor.

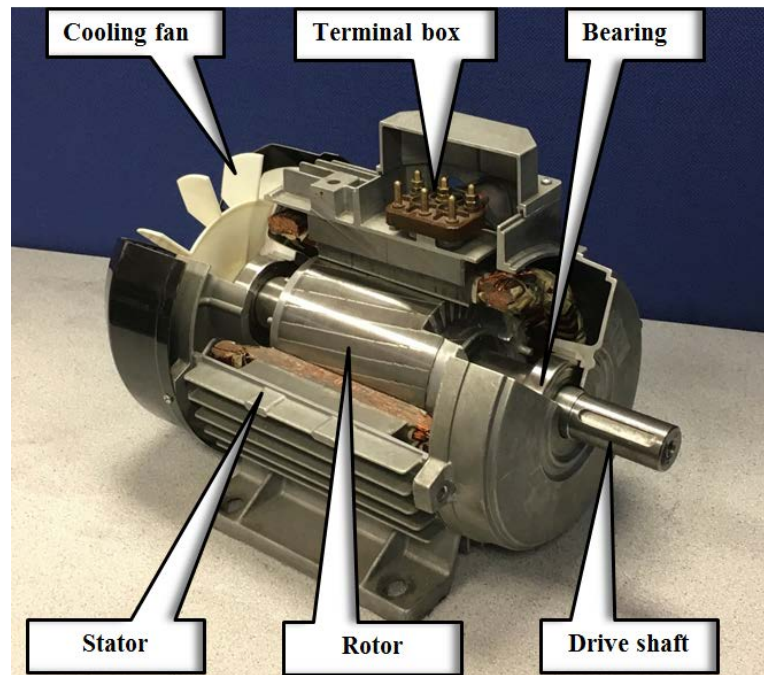


Figure 2-9: A typical industrial induction motor

The main component of an IM, as shown in Figure 2-9, are two main electromagnetic parts [52]:

- A stationary component named the *stator*.
- A rotating component named the *rotor*.

2.8.1.1 Stator

The stator is the outer stationary component of the motor; which composed of three parts [52]:

1. Stator frame: is the outer case made of steel, cast iron or aluminium alloy. The main function of the frame is to support the stator core, the winding, and the rotor shaft bearings.
2. Stator core (magnetic path): consisting of a set of laminated steel layers attached together to form the stator core.
3. Stator windings: composed of three coils. Each coil consists of a number of turns of copper insulated wire equally distributed and installed into insulated slots in the laminated magnetic path. These wires, carry the stator current and produce the magnetic field that causes the rotational motion of the rotor.

The orientation and the sequence of the stator windings determine the number of poles and shaft speed of the rotor [52]. In a three-phase induction motor, the windings are geometrically spaced 120° apart to produce a rotating magnetic field [53].

2.8.1.2 Rotor

The rotor is the rotating part of the motor and is composed of the main shaft and a squirrel cage which employ a number of aluminium bars that are connected to two shorting rings, one at each end, see Figure 2-10. These help the current to flow through these bars of the rotor squirrel cage [48, 53]. In addition, laminated iron core, which separate rotor bars, mechanically support the rotor shaft. The rotor slots are not parallel to the motor, they are slightly skewed to prevent the magnetic locking onto the teeth of the stator and rotor, which help the motor operate more smoothly and quietly [52]. Also, the bearings at each end of the rotor shaft allow for smooth rotation inside the stator. It is worth mentioning that there is an air gap between the rotor and the stator; due to induction, the energy is then transferred from the stator to the rotor. The generated torque causes the rotor to rotate with the load attached to it [54].

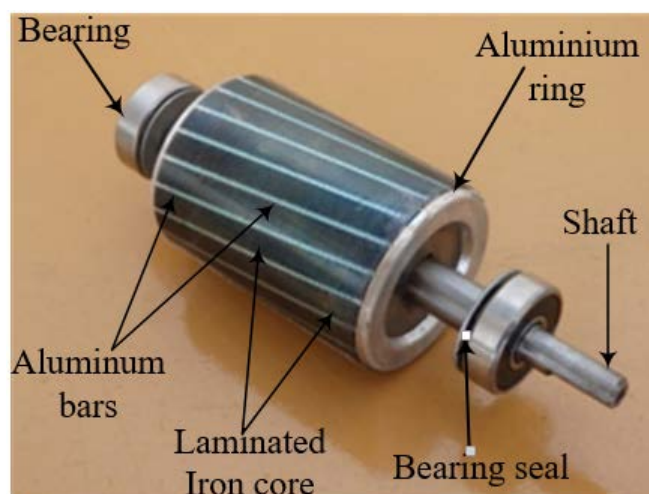


Figure 2-10: Squirrel cage rotor

2.8.2 Induction Motor Operation Principles

The main concept of the IM operation is depended on the rotation of the magnetic field [55]. As stated above, the stator is composed of three-phase windings (A, B, C) which are geometrically separated by 120° to create the formation of the poles as shown in Figure 2-11. In the simplest terms: the electric motor is called an induction motor because

the alternating current flowing through the stator will induce a current in the rotor; the interaction between the forces generated by these currents causes the rotational movement of the motor.

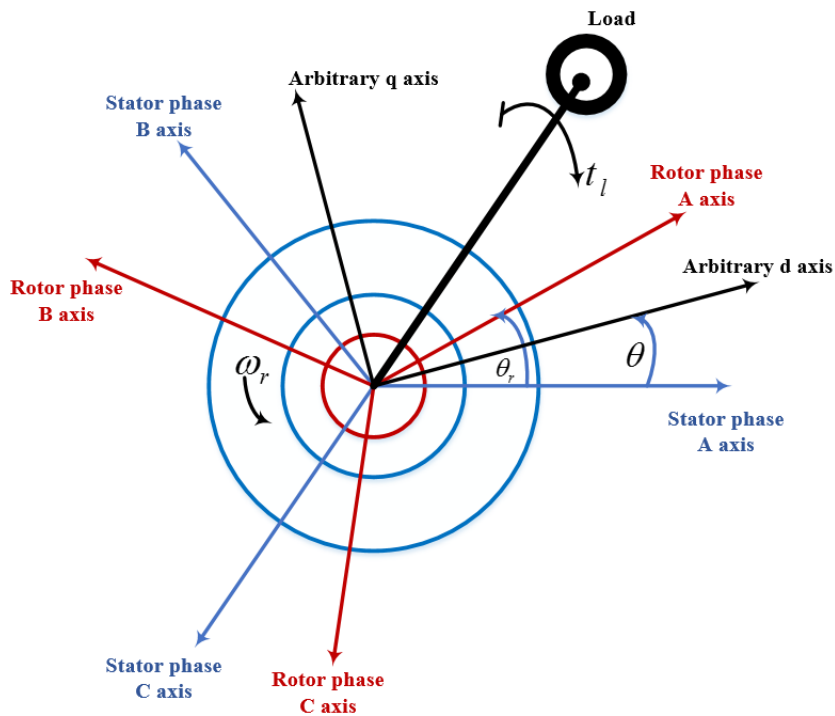


Figure 2-11: Symmetrical induction motor simplified scheme [56]

When three-phase current is fed to the stator phases, the current passes through the stator winding which generates a rotating magnetic field inside the stator. As the stator windings differ by 120° electric phase difference from their neighbours around the stator perimeter, their magnetic poles rotate in rotation motion around the stator [35, 52, 57]. This rotational speed is termed as the synchronous speed [52]. As described above, both the stator and rotor consist of three symmetrical phase windings with a constant 120° phase difference and equivalent turns (N_s, N_r) for the stator and rotor respectively. The three-phase stator and rotor windings are as illustrated in Figure 2-11; the subscripts A, B, C represent the stator three-phase supply and a, b, c represent the rotor three-phase windings. Initially, the rotor is stationary, the power supply generates an electromagnetic field in the windings of the stator, which cuts through the air gap to the rotor winding of the rotor inducing a voltage in the rotor and results in an induced current in the rotor bars as described by Lenz's law [35]. The interaction between the magnetic fields of the stator and the rotor generates a force and rotating torque, hence, the rotor is pushed into rotation around by the magnetic field of the stator [35, 52, 58]. The direction of rotation of the rotor is

governed by the stator winding (A, B, C) connection sequence, changing these connections will reverse the magnetic field direction and the rotor direction [52].

The induction motor synchronous speed (n_s , rpm) is the speed at which the stator magnetic field moves and it can be controlled by adjusting the supply frequency f_s or the number of poles p and is given by [48]:

$$n_s = \frac{120f_s}{p} \quad (\text{rpm}) \quad (2.1)$$

Where; n_s is the stator synchronous speed (rpm), f_s is the frequency of the power supply (Hz), and p is the number of poles which controls how fast the induced magnetic field will rotate around the inside of the motor housing at a given value of the frequency [7]. The rotor speed is usually slower than that of the stator magnetic field. In fact, if both speeds were the same, there would be no induced voltage and no torque would be produced. So, the rotor usually rotates at speed less than the rotating magnetic field and never catches up the synchronous speed [59]. The difference between the rotor speed (n_r) and the synchronous speed (n_s) is termed slip. It is normally referred to as the ratio of the slipping back of the rotor speed to the synchronous speed as illustrated in Figure 2-12 and defined as [54, 59]:

$$\text{Slip } s = \frac{(n_s - n_r)}{n_s} \quad (2.2)$$

Normally the slip is presented as a percentage of the synchronous speed [60].

$$s = \frac{(n_s - n_r)}{n_s} \times 100 \quad (2.3)$$

Where: s is the slip, n_s is the synchronous speed and n_r is the rotor speed.

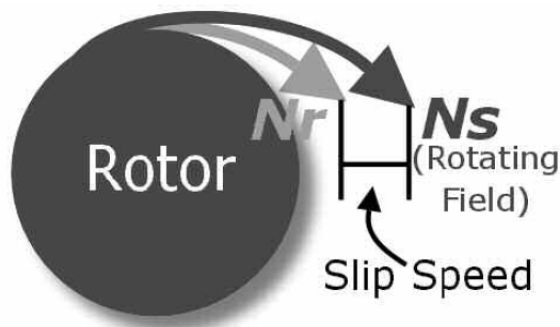


Figure 2-12: Slip speed illustration [59]

2.9 Induction Motor Common Faults

Induction motor (IM) are commonly considered as rugged, robust and reliable, and widely used as a power source for numerous industrial machines, including RCs, due to their simple design, low cost, flexibility in use and high level of reliability [50]. However, these machines are vulnerable to faults which reduce machine performance, consume excess energy, incur increased maintenance cost and can lead to sudden and unexpected system shut-down [12]. Again, an effective CM technique is needed to detect incipient faults in order to prevent machine failure, reduce maintenance cost and production downtime [20, 61]. The induction motors faults have been divided into two main categories based on their behaviour [61]: a) Electrical faults including stator and rotor winding faults, and broken rotor bar(s); b) Mechanical faults such as misalignment, bearing faults, etc., see Figure 2-13.

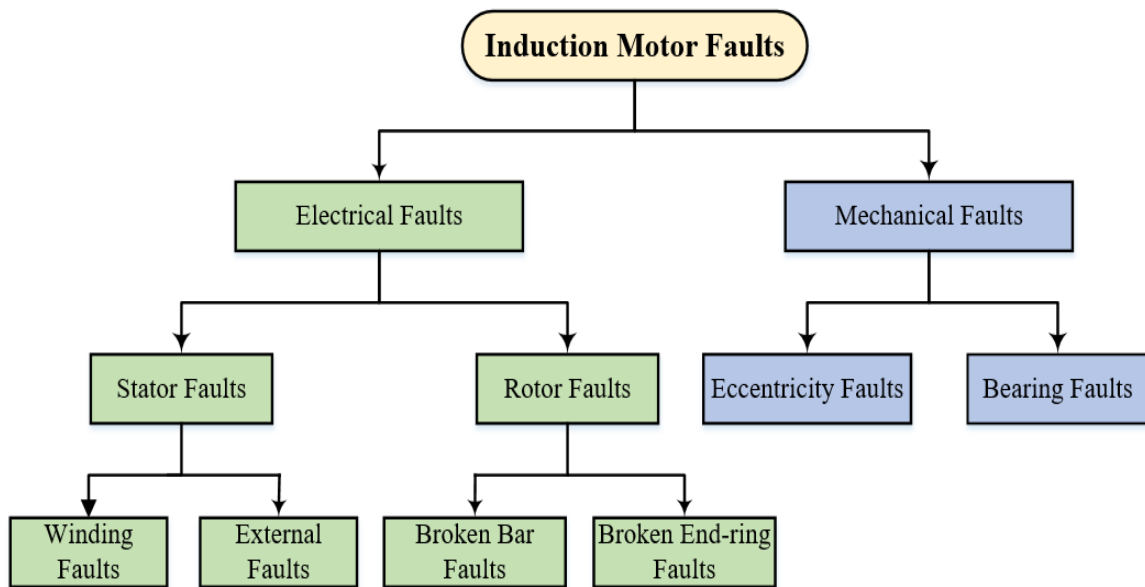


Figure 2-13: Induction motor faults

Due to its wide usage, IM has received considerable attention regarding fault detection and monitoring its operating condition. Because IM plays such an essential role as a power source for so many industrial machines, any flaw in this machine will have a significant impact on the industry, and further studies focused on detection of induction motor faults could be enormously useful. The pie chart (Figure 2-14) gives the occurrence probability of each individual motor fault in real industrial operations [62].

Bell, et al. [62] in an IEEE motor reliability study found the most frequent single fault causing the failure of three-phase induction motors was mechanical, bearing failure which accounted for 41% of total motor faults. However, stator and rotor faults combined contributed about 50% of all failures in three-phase induction motors. So, electrical faults should receive the greatest attention. This study considers only electrical faults in a three-phase IM and faults effects on the overall efficiency of the machine.

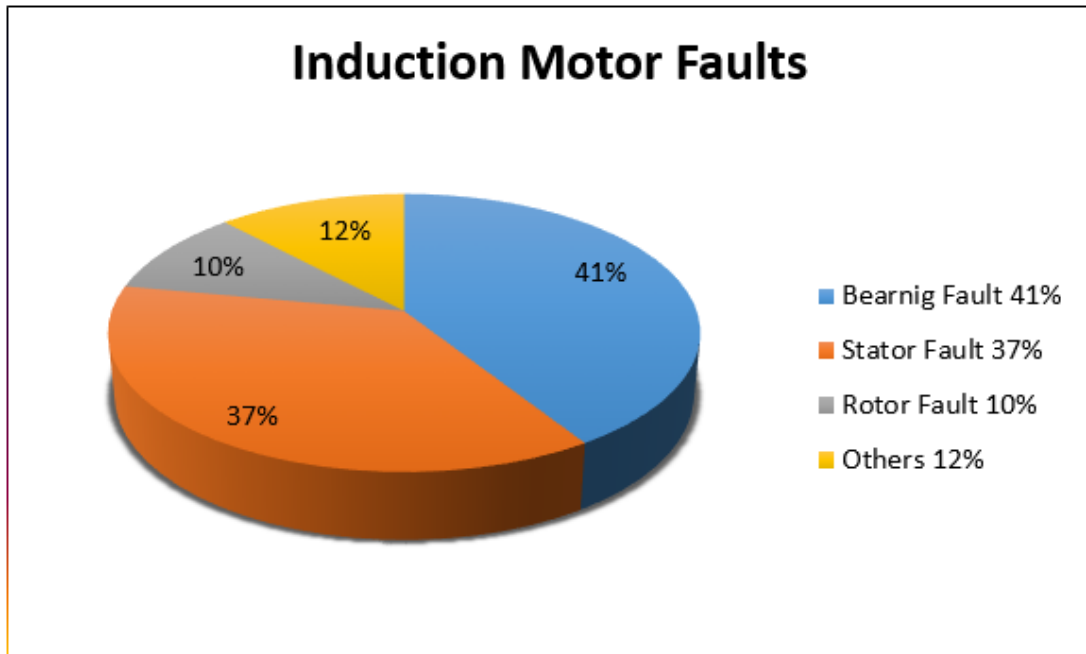


Figure 2-14: Motor fault distribution [62].

2.9.1 Stator Failures (Stator Winding Asymmetry)

By far, the most common electrical failure in an induction motor is stator winding failures [50], contributing almost 40% of motor faults, as discussed above. The increase in the stator resistance of the driving motor may result in voltage imbalances in the motor which reduces motor efficiency. Simultaneously, it will increase the temperature and introduce oscillatory operating conditions that can be responsible for other electrical or mechanical failures. Stator winding faults can be divided into several categories, see Figure 2-15 [52]

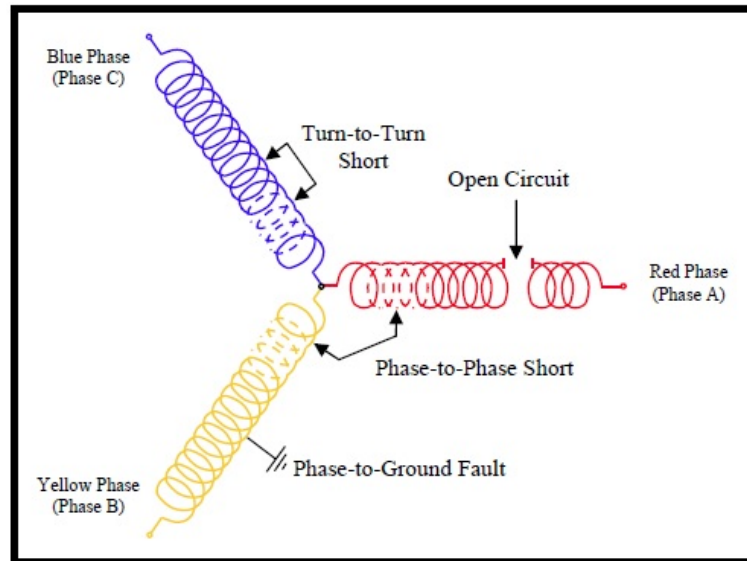


Figure 2-15: Three-Phase stator winding faults [52]

2.9.2 Rotor Faults

The electric current in squirrel cage rotor induced by the stator field produces the required torque which flows through the bars that are welded to the end-rings (see Figure 2-10) which in result generates an electromagnetic force. The problem arises when these bars get broken or separated from the end rings. The broken rotor bar (BRB) affects the current flow from one end to another and the motor performance is drastically reduced [63]. As there is an absence of the current flow, no magnetic field will be produced; no attraction force will be generated. The application of MSB in MCSA has been presented as an effective diagnostic tool for BRB in [32]. The study explains the differences in the characteristics of the current signals recorded for the healthy motor and motor with a broken rotor bar. They showed that the motor with a BRB compared to a healthy motor showed an additional current component in the form of a sinusoidal wave with frequency $2sf_s$ (where s is a slip and f_s is supplied frequency).

2.10 The Importance of Machine Condition Monitoring

Maintenance costs make an important contribution to the total operating cost of any plant. It has been measured as between 15% - 60% of the value of goods produced, depending on the industry [6]. Therefore, it is essential that CM techniques are efficient and effective in detecting and diagnosing machinery faults in the early phase [13, 20]. The topic of CM is growing rapidly, every year there are hundreds of publications; both theoretical and

practical, presented in academic journals and conference proceedings [16]. CM can be achieved by examining indicative physical parameters of the machines while it is in operation [2]. The purpose of adopting a CM strategy within a plant is to carry out a detection and diagnosis approach to examine the presence of any failure, its location and severity level in the early phase in its progression [2, 8-10]. The reliability of industrial processes will be enhanced with an appropriate CM programme with maintenance procedures scheduled at convenient times while avoiding potential catastrophic fault and preventing disastrous failures. [10].

Today's CM systems which include advanced signal processing tools extend the accessibility of such systems to all industrial sectors and provide the ability to monitor their machinery and diagnose faults [6]. CM is a procedure that recommends maintenance decisions based on ongoing data collection and analysis. Usually, this procedure consists of different steps as illustrated in Figure 2-16. It starts with collecting data (data acquisition) through different sensors and transducers mounted on the machine in order to obtain useful information. Then, data processing (information handling) is used to extract any useful features to define the operational behaviour of the machine. Finally, the machine condition is estimated based on the data analysis, any faults identified and quantified and then (decision-making) the scheduling of appropriate arrangements in the form of a maintenance plan [17].

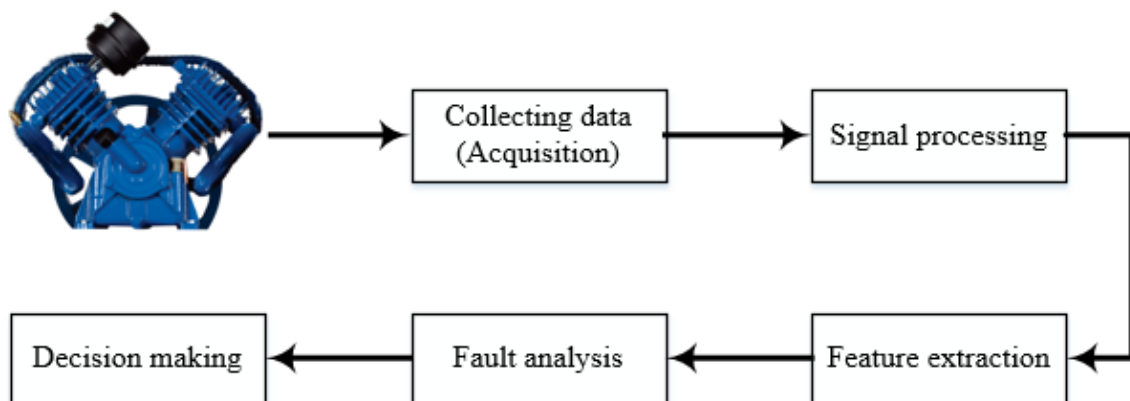


Figure 2-16: Schematic of the compressor CM process.

The CM of RCs is an important industrial activity in, for example, natural gas and oil plants which depend heavily on RCs to process natural gases which, in some cases, include corrosive gases at very low or very high temperatures [24]. These harsh conditions may lead to blockages in compressor valves causing faults within the valve system, which incur

high replacement costs and might lead to unexpected production losses. Thus detection and diagnosis of faults at early stages will not only improve the performance and availability of RCs but have huge economic benefits [35].

2.11 Conventional Condition Monitoring Techniques

For the best results, the CM system applied should be tailor to match the machine or system being monitored, and the goal of the maintenance procedure. For example, a simple system or machine might require only a visual inspection to monitor its condition. Whereas, for a complicated system, an advanced CM process might be required [50]. Nowadays, the increasing variety of machines, system components, and diversity of production procedures demand a selection of different CM methods for the detection and diagnosis of incipient faults, and there are various monitoring techniques which can be used for the detection of machine malfunctions [2, 60, 64-68]. According to [69], who surveyed CM systems used in industry, the most extensively used techniques as shown in Figure 2-17 are vibration analysis and oil analysis. Similar results were acquired by the 2002 Plant Maintenance Resource Centre (PMRC) survey on the use of CM technologies [70].

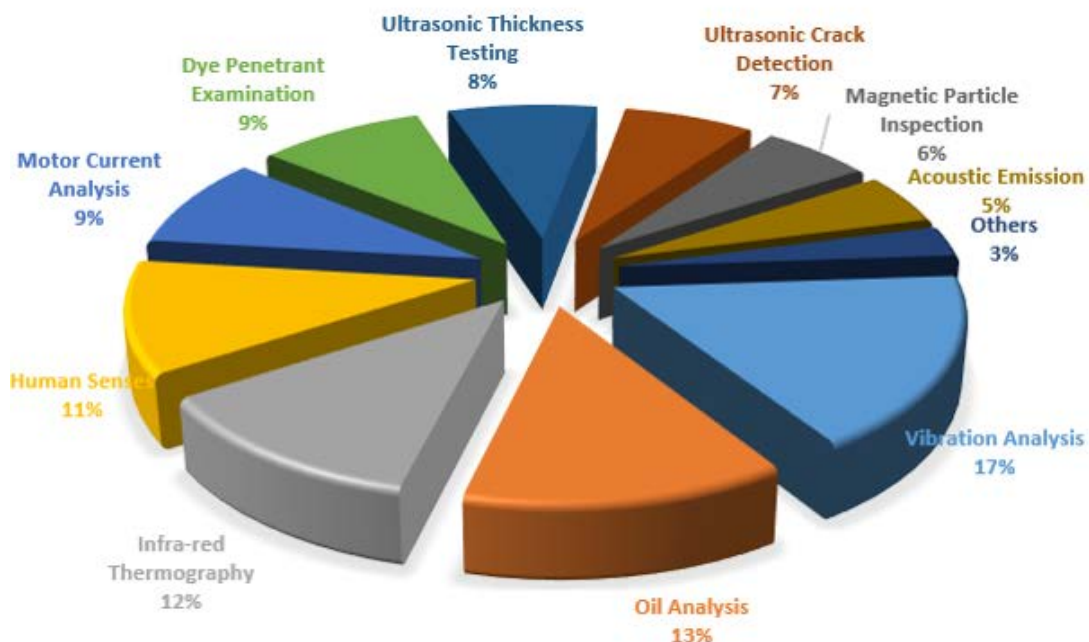


Figure 2-17: Relative usage of common condition monitoring techniques [69]

Each of the various CM techniques practised in industry for monitoring different types of machines has its own capabilities and limitations, especially when monitoring the early

changes in machine parameters and trends. The majority of generally used applications for monitoring machinery are outlined below.

Visual Inspection

Visual inspection (Human sense) is the most cost-effective and the simplest method for machinery CM [2]. However, “visual inspection” while commonly used is not an adequate description of the process, according to [6], “visual inspection” uses not only sight but also hearing, smell, and touch and inspection may, for example, be the direct observation of oil leaks, touching a machine to sense an unwarranted high temperature, hearing a loose drive belt or smelling an overheating motor [71]. This technique can be performed daily as a regular routine. Also, it is the primary method used for predictive maintenance [6] and does not require highly experienced inspectors, in fact, it may require only a normal level of skills or experience, with some simple specialist training. Human senses are usually limited to detecting large changes or differences in machine noise or performance and thus any small changes cannot be readily detected. Additionally, different inspectors may come to different conclusions for the same inspection due to the difference in their personal experience [35]. Yet this technique is still popularly applied for machine CM. Some of the advantages of this technique include being an easy method to employ, cheap and unsophisticated [2, 35]. The drawbacks of this technique include: it's being limited to stationery items of equipment at the time of inspection; it requires direct access but no further quantitative analysis. Visual inspection can be improved by using portable devices including thermographs and microphones to enhance the monitoring process and improve the consistency of different operators' results [24].

- **Portable Instruments**

Because of the limitation of human senses, which include the inability to access small spaces, especially when the machines are in operation, portable test instruments such as microphones, stroboscopes and thermographs [50] are available to collect machine data and transmit it to external devices to indicate the machine's condition. These portable instruments are used to increase the consistency of the outcomes of different inspection operators [24].

Dynamic Cylinder Pressure Monitoring

Monitoring dynamic cylinder pressure is a convenient diagnostic method to detect any changes of RC machine characteristics; for instance detection of changes in cylinder pressure caused by a leaky valve, which is considered the most common fault that occurs in RCs [24, 50]. Dynamic pressure tracing provides valuable information about the condition and efficiency of RCs, diesel engines, etc. [72]

Elhaj [24] studied the use of dynamic cylinder pressure to detect RC valve faults which included a leaky valve and a valve with weakened spring. The study compared the measurements of the pressure inside the cylinder in normal and abnormal conditions, which showed a clear deviation from the normal condition due to the presence of the valve fault. Results presented in [24] show that the dynamic cylinder pressure could be used for the diagnosis of RC valve faults.

Pressure transducers were used to monitor and collect the cylinder pressure signals for tracing any changes caused by the valve faults. Yet, it was not possible to mount these sensors directly inside the cylinder because of the harsh environment (high temperature and high pressure) [51]. Faults such as valve wear, sticking valve rings, can also be detected by monitoring the pressure inside the cylinder.

Instantaneous Angular Speed (IAS) Based Monitoring

Despite the assumption that machines such as RCs rotate at a constant speed, in reality, the angular speed varies, for example, due to fluctuations in the load during the machine's operation [50]. Theoretically, any change in the machine condition should affect the Instantaneous Angular Speed (IAS) [73]. Examining and analysing the IAS can offer useful information about the machine's operation. Changes of the IAS generated by the presence of a fault could be used to detect and identify the fault [74, 75]. Gu, et al., [76] examined the use of IAS for detection and diagnosis of faults in diesel engines and compressors. This technique requires transducers (encoders) to measure the IAS, these are usually fitted onto the crankshaft of the machine's flywheel.

Ben Sasi and Ball [50] studied the speed variations of IM by extracting the IAS waveform from an encoder mounted on the motor shaft. The results confirmed the capabilities of IAS for diagnosing motor faults such as a broken rotor bar. The key finding of this study

was the visibility of the sideband components of the pole pass speed at high loads around the rotor speed, which can be a good indication for the diagnosis of this fault. The main downside of the technique is that the implementation of this is very complex, but it could be used to confirm the identification of faults detected by other methods [35].

Fault Detection and Diagnosis Using Vibro-acoustic Signals

One of the most common CM methods is to use the noise (sound) generated while the machines are in operation. This technique analyses the sound generated from different sources within the machine during its operation, the level and characteristics of the sound will depend on the machine's design and construction. Vibro-acoustic has been found a useful technique especially when faults generate high noise and vibration levels, such as cracking, cleavage and fretting [77, 78]. Microphones, in general, used to detect the audio signals, these sensors are very sensitive with a wide frequency range and ability to provide useful and valuable information on the machine's operation. Hence, this technique is used in many applications such as gearboxes, bearings, diesel engines and machinery used underwater [64]. One of the advantages of this method is costs; the sound sensors (transducers) are relatively cheap and easy to install. However, acoustic signals are often contaminated with substantial levels of background noise [77, 79]. In which, it is very difficult to extract useful information from acoustic signals. Elhaj [24] explored the use of the acoustic signals to detect faults occurring in the RC. His study showed that simple acoustic analysis which included time and frequency may not provide sufficiently useful information to detect compressor faults. Advanced signal analysis was required to get more valuable information to detect compressor fault.

Vibration Analysis For Fault Detection

All industrial machines operate in either rotating or reciprocating motion while in operation. Due to their motion, these machines (even healthy equipment) produce a vibration signature or profile which contains valuable information, sufficient to identify their operating condition [6]. Industrial machines including RC are naturally noisy and have a vibrating body while in use, and RC vulnerable to failures, for example, fatigue and wear. These faults may lead, for example, shaft misalignment and rotor unbalance which in turn increases the vibration responses produced while the machine is in operation. Each part of the machine produces a distinct vibration signature that has its own

waveform which distinguishes it from other machine components and identifies the condition of its health. A high level of vibration can be an indication of the potential failure of a machine. The idea of vibration signature analysis is to study the change of the vibration signal produced by the machine to detect the occurrence of a machine fault or damage. Vibration analysis has been considered one of the most effective and widely used method to monitor machine operation and fault detection, including RC machines [2]. This technique can measure and/or record the vibration profile to predict the machine's malfunction, without interrupting the normal machine operation, and this is what makes the technique so powerful. Thus, it is widely used as a primary tool for machinery CM, for early detection and diagnoses of faults for avoiding the consequences of failure before it occurs or, at least, to prevent catastrophic machine failures [2, 3].

Many industrial plants have found that vibration-based practice to be one of the best ways for machine CM. Deterioration or defects in machine parts, e.g. broken gears, defective bearings, etc., can be detected through the analysis of the machine vibration [10]. In practice vibration is often measured using accelerometers; these transducers transform a vibration waveform into an electrical signal that represents the machine behaviour. The analysis of these signals can lead to the detection of incipient faults.

A large amount of research has been conducted on the detection of faults occurring in machinery. For example, Gu and Ball [21] presented a new method based on the use of a smooth pseudo-Wigner–Ville distribution for interpretation of machinery vibration data to diagnose various RC valve faults. Lin, et al., [80] combined an artificial neural network and time-frequency analysis of vibration data to differentiate between new and worn valves. Ahmed, et al., [47] developed a method to diagnose RC faults based on features extracted from the envelope spectrum of compressor vibration signals. Hassin, et al., [81] studied the condition of journal bearings under different lubricated regimes using vibration measurements. These studies confirmed that abnormal levels of lubricant can be detected via vibration monitoring.

CM systems based on the analysis of the compressor vibration have been used to monitor various RC faults, e.g. leakage through valve system and intercooler pipe and been found to be robust and reliable [25]. Vibration signals produced by a reciprocating machine are described as a sequence of periodic events, e.g. piston movements, and the impact of valve plates during the opening and closing events; additional, unbalanced dynamic loadings

due to the presence of a fault will generate additional vibration signals and may lead to machine breakdown [36]. Generally, valve parts generate transient vibrations during the opening and closing events due to the impact of its components, which can be described as non-linear and non-stationary signals [25]. Moreover, another vibration source is generated by the airflow fluctuation during the compressor process which produces sound. Thus, the compressor vibration responses are complex and have a wide frequency range [24]. The waveforms of the vibration signal are analysed and processed using a variety of techniques, for instance, time and frequency domain [6]. One of the most common measures based on analysis of these waveforms are statistical parameters; e.g., Root Mean Square (RMS), etc. [82]. Frequency domain data are acquired by converting the time domain data by means a mathematical technique referred to as a Fourier Transform (FT). Other analytic techniques to study the vibration waveforms include higher order spectral analysis and wavelet analysis [6].

However, one of the major difficulties with vibration analysis is that the signal acquired from the machine is a summation of different components which create a complex signal. Additionally, vibration generated by internal components travels to the machine surface through transmission paths which influence the acquired signal [24]. Another drawback of this technique is the implementation cost of this system. Different type of machines produces different vibration signatures, for instance, RCs, as mentioned earlier, real-life produce a complex vibration signal. Nevertheless, vibration analysis with a suitable signal processing approach can provide useful information related to specific faults and their locations [35].

Motor Current Signature Analysis For Diagnosis

As explained above there are many different techniques and tools available for monitoring and diagnosing industrial machine faults, most of which have some restrictions limiting their application. They might require expensive transducers, they might require access to the machine being monitored, either to mount the transducers and/or to collect samples [83].

Various researchers have suggested that monitoring machines could be done using the signature of the motor current to provide useful and rich information on the machine's operating conditions. The current fed to the motor can be measured at any convenient

point even far from the machine, which gives current analysis an advantage over other monitoring techniques, especially when the monitored machine is physically inaccessible or in a hazardous environment because it is not necessary to fix any sensors directly on the machine [84]. Normally, the motor runs at a constant speed and when a fault occurs the frequency of the current changes compared to the healthy condition [30]. Thus, any small variation in the motor current may indicate the presence of an incipient fault.

In recent years, motor current signature analysis (MCSA) has proven to be an effective and efficient monitoring technique capable of detecting or quantifying defects and degradations and has already been applied successfully to various motor systems, including industrial and consumer equipment for fault diagnosis that includes air-gap eccentricity and a broken rotor bar [28, 29], deterioration of a gearbox bearing [83] and a stator turn-to-turn fault [85]. Haynes and Kryter [34] showed that the signature of the current signal could also be used as a mean for detecting abnormal operations in downstream machines such as RC, pumps and air conditioning systems. Benbouzid [28] showed that the rotor disturbances due to mechanical problems can be detected by the analysis of induction stator current. Gu, et al, [86] examined the use of motor current signature to detect and diagnose individual faults that commonly occur in compressors. As a non-intrusive technique, MCSA has become more and more widely accepted and is increasingly used to determine the conditions of the induction motor and its downstream machines [26, 28, 29].

MCSA does not obstruct the operation of the monitored equipment, it only requires access to the current supply lines, which can save time as well as reducing cost, and can provide the same information as other monitoring tools [27-29]. A number of other publications have mentioned the advantage of using MCSA compared to other monitoring techniques for early fault detection [3, 35].

In summation the relative advantages of MCSA cited in the above research publications are:

- ✓ Reducing maintenance cost.
- ✓ Improved safety (no risk in the data collection process).
- ✓ No requirement for expensive sensors.
- ✓ Lower noise levels on the measured signal.

- ✓ The ability to use this technique while the machine in operation.
- ✓ The ability to monitor machines in unreachable environments, for instance, oil wells.

MCSA can be used as a means to diagnose the condition of a machine and predict the likely remaining working life of an electric motor using conventional analysis methods [35]. It can offer a clear indication of current harmonics and sideband components, using commonly available frequency analysis methods. Benbouzid, et al., [87] examined the effectiveness of applying MCSA to the diagnosis of induction motor faults. Applying high-resolution spectral analysis allowed the identification of signature of asymmetrical motor fault frequencies and proved very sensitive to the effects of motor faults on the spectral components.

Jung, et al., [88] studied induction motor CM under different operating conditions using MCSA. The study proposed advanced signal-and-data-processing algorithms to achieve accurate diagnosis based on MCSA. The method was verified by experimental results. It was concluded that with more advanced signal processing techniques being developed for machine fault diagnosis, MCSA would be able to differentiate between different motor faults.

Mehala [9] investigated the effect of different common induction motor faults including both electrical and mechanical faults based on MCSA. This study applied spectral analysis and advanced signal processing techniques including the Short Time Fourier Transform (STFT) and Wavelet Transform (WT). The study concluded that applying MCSA for induction motor CM provides an inexpensive technique which does not require any additional expensive sensors.

Messaoudi and Sbita [89] investigated the use of MCSA to study the operation of an induction motor operating with electrical and mechanical faults. The study showed that these faults could be clearly identified by the harmonic modulations around the supply frequency. Additionally, the experimental results showed the ability of MCSA to discriminate between the healthy and different faulty operations.

Gu, et al., [86] examined the performance of high order spectral analysis of the motor current signal to diagnose RC faults and demonstrated how compressor load influenced

the induction motor speed by causing speed fluctuations so that the motor current signal exhibited amplitude modulation. Different faults caused different degrees of modulation. The study results showed that conventional spectrum analysis is not effective for analysing this motor current modulation, a proposed method based on higher-order spectral analysis was used to obtain more accurate results. The developed method was able to differentiate between different compressor faults and able to quantify compressor faults.

Alwodai, et al., [31] investigated the use of an advanced signal processing technique - Modulation signal bispectrum (MSB) - to detect common stator faults of different severities. Their results, after comparing the performance of MSB with the conventional spectrum analysis, showed that the MSB provided a more accurate fault diagnostics performance

Zhen, et al., [90] proposed a new method for fault diagnosis of an induction motor and the equipment and/or machinery driven by the motor, based on the MCSA using the Dynamic Time Wrapping (DTW) technique. This method overcame the limitations of the Fourier Transform (FT) which include spectral leakage and aliasing. Zhen, et al., studied compressor operations under different fault conditions and different loads, then applied DTW to analyse the motor current signature, highlighting the sideband component characteristics related to the different compressor faults. This led to a more accurate fault diagnosis compared to FT analysis.

Zhang, et al., [91] monitored a gear transmission system using MCSA to study gear wear progression. This study proposed a novel monitoring method for gear wear using the MSB to analyse the modulation phenomena induced in the induction motor current due to different wear severities. The study showed that the MSB was able to identify faulty gears and classify them according to the severity of the wear. Based on the results, the developed method confirms that MSB-MCSA is a reliable and accurate method for monitoring deterioration of gears due to wear.

To sum up, many studies have been carried on MCSA and numerous signal processing techniques have been applied. Yet, necessity work is still needed to assess this method and test its capability to real situations applications. To obtain more useful information from the acquired signal, and develop an accurate and effective monitoring technique, further studies are required.

2.12 Reciprocating Compressor Monitoring Techniques

Considerable attention has been paid to compressor fault diagnosis, in which, numerous publications and numerous researches have been conducted in which, different signal processing techniques and methods have been proposed for the detection of commonly occurring faults in a compressor.

Gu and Ball [21] propose a method applying a smooth pseudo-Wigner–Ville distribution to better understand the machine’s vibration behaviour as induced due to various compressor faults. This study successfully analysed compressor vibration to diagnose different compressor valve faults.

Yang, et al., [92] presented a new scheme for the detection and diagnosis of refrigerator compressor faults. The study developed a new classification method based on the analysis of vibration and noise data using a wavelet transform, then different classifiers were applied including artificial neural networks and a support vector machine (SVM). The study results showed that the developed method was able to differentiate between healthy and faulty operations with high accuracy, but this work was limited to small refrigerator compressors.

Cui, et al., [93] developed a method to identify compressor valve condition by studying the vibration signal from the compressor. The study used information entropy and SVM to study the non-linear fault features and then applied the SVM to identify these patterns. The study showed that the proposed method was a good generalization of non-linear pattern recognition with a small sample number. The study, however, did highlight the effect of valve failure on RC operation but did not examine other common compressor faults.

Lin, et al., [80] combined an artificial neural network and time-frequency analysis to develop an automated system for RC condition classification. The time-frequency representation of the vibration signal was performed by applying a pseudo-Wigner-Ville distribution to extract vibration characteristics in which three indices were defined (time, frequency and amplitude). Then the neural network was applied on combinations of these indices to develop automated condition classification using pattern recognition. The authors claimed that the proposed method can provide a good classification for

compressor CM, but only if a suitable index combination and time-frequency band are chosen.

Elhaj, et al., [22] have applied IAS and dynamic cylinder pressure to develop an accurate and effective monitoring technique for the detection and diagnosis of valve leakage faults in an RC. The study produced a Truth Table for each technique and then combined both tables to produce a Decision Table. The developed table lists each fault signature which can be used for the detection and diagnosis of compressor valve leakage. However, this study applied only time domain analysis to monitor the compressor conditions.

Pichler, et al., [94] a data-driven approach was presented for the detection of a broken compressor valve based on analysis of the P-V diagram for feature extraction and classification using Support Vector Machines (SVM). A very high degree of accuracy was obtained under conditions of varying compressor load and pressure.

Ahmed, et al., [47] developed a procedure of diagnosing RC faults based on feature extraction from the envelope spectrum of the vibration signals based on Relevance Vector Machines (RVM). They achieved RVMs higher accuracy rates (96.87%). Wang, et al., [95] proposed a method using acoustic emission signals for diagnosing faults in RC valves where the authors were able to distinguish between normal valve operation, valve flutter and valve delayed closing. Pichler, et al., [23] proposed an automated method for compressor valve fault detection under different load condition based on the time-frequency representation of vibration signals.

Even though the previous methods gave a clear indication to detect and diagnose different faults. Yet, nearly all of these methods analysis acquired data statistically driven by learning theory data-driven methods from wideband data, that might contain irrelevant information leading to an unstable diagnosis of incipient faults.

Many studies have been carried out in this area based on MCSA. Various signal processing techniques including a combination of neural networks and neural fuzzy inference system logic [96], induction MCSA [60, 86] and high-resolution spectral analysis [97] have been used for detection and diagnosis of different RC faults. Furthermore, a study by [31] investigated the use of MSB to detect different severity of stator faults. The results showed that the MSB provides better diagnostic performance compared to conventional analysis. However, most of these theoretical frameworks focus on the fault detection of the induction motor and have not been extended to investigate the potential of using the

current signal as a means of assessing the condition of downstream driven equipment such as RCs.

From the brief review above, it is clear that researchers pay most attention to diagnosing rotating machine faults using vibration and current signature analysis. The analysis of machine vibration has the ability to provide a quick and economical monitoring technique in an industrial environment. Vibration analysis has been applied for RC fault diagnosis and can be considered as an approach tool to monitor the RC condition. However, vibration monitoring cannot provide all the information required for a condition-based maintenance program, not least because of its limitations related either to the complexity of RC behaviour or measurement practice and data analysis[24].

On the other hand, motor current signature changes with the change of compressor load and when the compressor operates under abnormal conditions. Thus, the motor current signature contains useful and adequate information on the compressor's operating condition. It does not require any additional transducers and there is no need to get direct access to the monitored machine either to mount transducers and/or to collect samples. These factors give this technique many advantages over other compressor CM methods.

2.13 Summary

This chapter provides an overview of different types of compressors, compressor operations, classification and most common faults that occur in a rotating compressor and its driving motor. These include valve leakage and stator winding asymmetry. These faults not only reduce compressor performance but also lead to machine breakdown. Any failures occurring in either the compressor or its motor will affect the operating condition and eventually, lead to system malfunction.

Different techniques utilized to obtain information regarding the compressor and its motor have been reviewed. Various diagnostic methods can be applied to monitor the compressor condition and extract useful information about its health. Motor current signature analysis has previously received attention and is a technique that is readily available and does not require access to the motor. MCSA contains valuable information by which to determine compressor conditions, it has been used to monitor compressors subject to a single fault, and also to investigate the presence of combined faults. However, no previous work has

been found that detects the presence of, and analyses the effect of, simultaneous mechanical and electrical faults on a compressor and its induction motor.

CHAPTER 3:

Reciprocating Compressor Fault Detection and Diagnosis Techniques

This chapter provides a review of the most widely signal processing techniques which have been used for compressor fault detection and condition monitoring, based on the analysis of current and vibration measurements. Then there is a brief discussion of suitable techniques to obtain reliable diagnostic features to detect and identify various compressor faults. Finally, the chapter presents the modulation signal bispectrum (MSB), which is more potential to lead to more accurate extraction of fault features for diagnosis of different fault conditions in a reciprocating compressor.

3.1 Introduction

In any mechanical rotating equipment such as an RC, the moving parts are subject to varying forces that generate vibration in the machine, with each part of these machines generating its own vibration signature which differs from the signatures of other parts [98]. When an incipient fault occurs in a component part, its vibration signature will change, providing useful information about the presence of a fault, and can be used to identify the part and diagnose the fault before it becomes severe [99]. Because of the complex nature of the signal acquired from an RC which has a number of rotating and reciprocating components, more research is necessary to find a reliable monitoring strategy [23, 35, 46, 49, 86]. Various fault detection techniques enable extracting useful information through the analysis of vibration signal which enables the associated faulty rotating parts to be identified.[100, 101].

In order to detect and correctly diagnose an incipient fault, suitable techniques are required to analyse and assess any abnormal operating condition of the machine. This is often achieved by evaluating some useful statistical parameters highly correlated with a particular fault. However, as a consequence of the presence of background noise in the acquired signal, it is a great challenge to extract the characteristic fault features, thus an effective signal processing method is required to extract useful information to diagnose the machine condition [102].

In general, RC faults e.g., valve leakage, a loose belt, intercooler leakage, etc. produce repetitive impulses, which in turn lead to modulation phenomena in the acquired signals. Due to this effect, sidebands will be present around the mains supply frequency. Hence, demodulation is necessary in order to extract the frequencies responsible for the modulation effect and this is considered to be an important part in the monitoring and fault diagnosis of RCs. There are different techniques to suitably analyse the acquired signal, among these techniques are: Waveform analysis, Fourier Transform (FFT), Spectral analysis, and Higher Order Analysis (HOA) [102]. The frequency domain analysis usually gives a better insight into the signal. However, this technique has the drawback that it is not suitable for non-stationary signal analysis and alternative methods are required. Time-frequency analysis has proved to be a powerful technique in CM and fault diagnostic. One

of the advantages of time-frequency analysis in comparison to FFT, it is two-dimensional representations (time-frequency scale).

With the use of a proper feature extraction method, the specific vibration signature for a particular machine component can be identified and the location of the fault can be detected [102]. For reliable extraction of the fault features, it is very important to increase the signal to noise ratio by reducing or even eliminating the amount of random noise present in the acquired signal. Different signal processing techniques based on vibration signals have been developed and a significant amount of attention has been paid to the development of useful methods to detect and diagnose various faults in order to establish an effective, efficient CM technique for RCs [12, 24, 103].

The widely used signal processing methods utilized on RCs for the purpose of fault diagnosis are discussed below:

3.2 Time Domain Analysis (Waveform)

The most general and simplest CM technique for the analyses of the acquired signal is the time-domain. This widely used technique for machine fault diagnosis uses statistical parameters to examine machine signals [6]. The traditional time-domain analysis calculates characteristic features that have previously been found to be useful in determining the presence of faults in the machine. Some of the most commonly used statistical parameters to diagnose compressor faults are the root mean square (RMS) and peak value (PV) [24, 35, 104].

The time-domain vibration signal is a graphical depiction of the magnitude of the measured acceleration, containing all frequency components [6]. The procedure involves analysing a signal either by visual inspection or by determining relevant statistical parameters which can show the existence of faults. The presence of a fault might be indicated by a periodic impulse of high amplitude; the duration of the peak may be short but its frequency content will extend over a broad range of frequencies. But that alone would not provide the location of the fault.

3.2.1 Peak Value (PV)

Figure 3-1 shows a typical time domain vibration waveform for the second stage of an RC, at different discharge pressures, 80 psi and 120 psi. The time domain signal shows a variation between the normal (BL) and abnormal conditions (discharge valve leakage - DVL-). From the figure, it can be seen that the presence of the faults caused observable changes in the amplitude of the vibration signal.

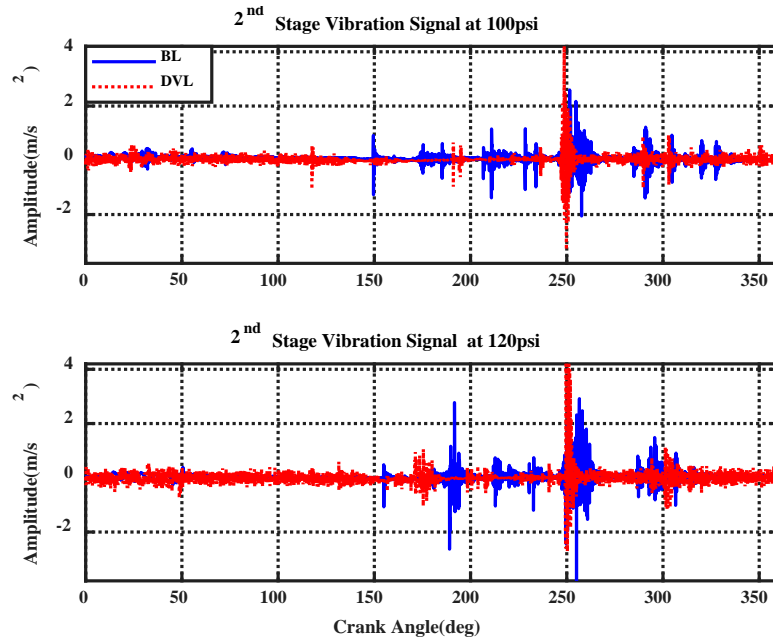


Figure 3-1 Raw vibration signals from the 2nd stage of RC for baseline (healthy) and DVL – discharge valve leakage.

The signals show that the compressor valve opening/closing events are affected by the faults introduced into the compressor, resulting in the unambiguous increase of amplitudes of the periodic impulses. However, it can be difficult to assist the detection of these faults simply by observing the vibration waveform if the change in amplitude of the signal is small. Therefore, it becomes necessary to use statistical parameters to evaluate the time-domain signal, but even then the particular fault probably not predicted accurately.

3.2.2 Root Mean Square (RMS)

This statistical parameter measures the overall energy content of the vibration signal. The most common approach to assess the presence of machine defects using the time domain signal is the RMS. It has been shown to be effective in tracking the unbalance in a rotating machine, however, will not be sensitive enough to detect any early failures, and does not

provide information that can lead to the diagnosis of the particular fault present in the machine [102].

The RMS is the normalized second central moment of the signal and is calculated as [82]:

$$RMS = \sqrt{\frac{1}{N} \sum_{n=1}^N [x(n)^2]} \quad (3.1)$$

Where N is the number of data points in the acquired signal and $x(n)$ is the signal amplitude for the n^{th} sample.

In general, the acquired signal RMS is certainly a good indicator of the general machine condition. Thus, by trending observed RMS values and noting any change, the overall machine condition can be easily monitored. However, the RMS value changes with the operational condition, making it less reliable in term of repeatability.

3.2.3 Crest Factor (CF)

The CF is the ratio of the peak level of the acquired signal to the value of the RMS [102], this is also referred to as the peak-to-RMS ratio. This particular statistical parameter has been found to be useful in early stage detection of faults in machines [105], the higher the value of the peak level, the larger the crest factor, thus, any increase of the CF is an indication of an abnormal condition. The mathematical formula for the CF is [106]:

$$Crest \ Factor = \frac{Peak \ level}{RMS} \quad (3.2)$$

$$Peak \ level = Max(|x(t)|) \quad (3.3)$$

Where $x(t)$ the time domain signal.

3.2.4 Kurtosis

Kurtosis simply described, is the normalized method of the 4th moment of a distribution of a signal. The 4th power usage enables Kurtosis to be very sensitive to the peakness of the signal and it will provide the measurement of the impulsive nature of the acquired time domain waveform. The higher the kurtosis value, the sharper peaks and longer the tails of the acquired signal [36]. It is a reliable and sensitive parameter only in the absence of

significant impulsiveness [107]. For a distribution $x(t)$, its normalized kurtosis is provided by the sample values: x_1, \dots, x_n , measured at times and can be defined as [106]:

$$Kurtosis = \frac{\frac{1}{n} \sum_{i=1}^N (x_i - \bar{x})^4}{RMS} \quad (3.4)$$

There will be more than one source or signal present while the machine in operation; which add together, to represent the total displacement and it is not easy to identify the contribution of a particular signal [6]. Therefore, there will be hidden features in the time domain signal. In order to extract more information from the acquired data, the signal needs to be transformed into the frequency domain using, for example, the Fourier Transform to reveal significant parameters to be able to assess the machine condition [64].

3.3 Frequency Domain Analysis

This analysis domain is an extremely effective signal processing method for machinery CM; to detect and diagnose a fault occurring in the machine, since there are usually more useful features observable in the frequency spectrum of these signals compared to waveform analysis [108], [109]. The energy of the signal is represented as a function of the frequency. Frequency domain analysis has the advantage over the time domain analysis in the sense that it has the ability to identify and isolate certain frequency components of interest. For example, repetitive impulsive peaks in the time domain will clearly show as a form of harmonics in the frequency spectrum [110]. Figure 3-2 shows the vibration characteristics of the second stage of an RC, and the compressor fundamental frequency (working frequency of the compressor, 7.3 Hz) and a number of the rotation frequency's harmonics are very clear.

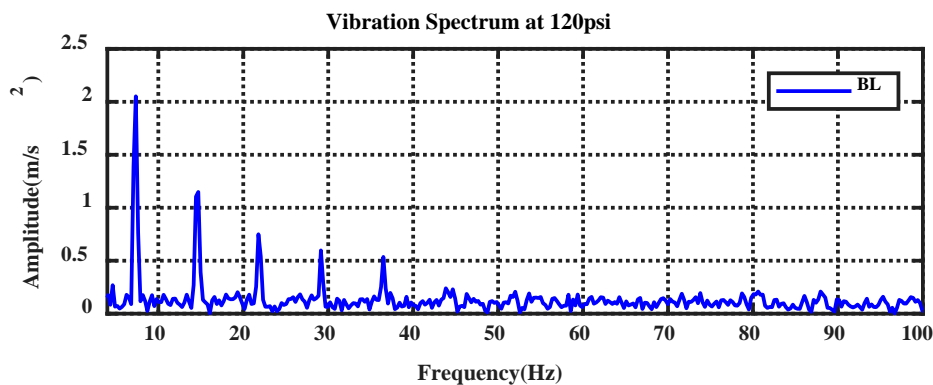


Figure 3-2: Vibration spectrum of the second stage of a reciprocating compressor

The principle idea of spectrum analysis is to focus on and identify the components of a particular frequency in order to extract the characteristic pattern from the acquired data for the detection and diagnosis of potential faults effectively [111]. There are several transformations that can be used to convert the time domain representation to its frequency domain representation but mostly the widely used approach is the Fast Fourier Transform (FFT) [6, 108].

3.3.1 Fast Fourier Transform (FFT)

The Fast Fourier Transform (FFT) transforms the signal from the time domain into the frequency domain, so further valuable information could be obtained from the measured signal [109]. Consider $x(t)$ is the continuous time series, which contains valuable information regarding the operation condition of the machine, the FT is obtained by the following equation [108, 109].

$$X(f) = \int_{-\infty}^{\infty} x(t)e^{-2j\pi ft} dt \quad (3.5)$$

Where $x(t)$ is the periodic time-domain signal, f is the frequency, and $X(f)$ is the frequency spectrum of $x(t)$. Today, with the ready availability of fast, cheap and sophisticated laptops, the Discrete Fourier Transform (DFT) is by far the most commonly used method of deriving the frequency spectrum from the time domain signal.

Let $x(t)$ be the continuous signal from which extracting N samples: $x(0), x(1) \dots x(N-1)$. The DFT:

$$DFFT = \sum_{x=0}^{x=N-1} xne^{-2j\pi ft} \quad (3.6)$$

Use of the frequency domain helps to isolate certain part linked to a particular machine component or faults, and the impulsive repetitive character of the vibration signal can be clearly distinguished in the frequency spectrum [16]. Various methods based on spectral analysis are discussed in greater detail in [25].

Yet, despite the wide use of this popular method it is unable to extract information from a non-stationary signal and, in general, real-life signals from a machine and any fault associated with it will always have some sort of non-stationarity present, and which will

contain significant information about the machines' faults [112]. Hence, it is necessary to process non-stationary signals for the purposes of fault detection and diagnosis.

3.3.2 Shaft Frequency and IAS

In general, the vibration of the shaft and its coupling occur at the rotational frequency of the machine shaft. These dominant vibration amplitudes are invariably a function of the angular speed. Usually, various kinds of faults, e.g., misalignment, shaft bending and unbalance could be identified by studying the amplitude and phase response from the shaft speed components [113, 114].

For an RC which is operated at a notional constant speed, the change of shaft frequency (7.33 Hz) occurs because of load fluctuations and change of cylinder pressures during the compressor cycle. However, this change in the rotational frequency is often assumed to be negligible. The shaft frequency ($f_{r_{com}}$) of the compressor can be formulated as a function of the rotational speeds (ω_{com}) and can be expressed as follows:

$$f_{r_{com}} = \frac{\omega_{com}}{60} \quad (3.7)$$

3.3.3 Sideband Characteristics

As the gas in the cylinder of the RC is compressed it takes more effort to compress it further, increasing the load and requiring additional power. This situation results in a periodical varying load to the induction motor, consequently, the motor speed will vary, which means the current through induction motor will change, and exhibit modulation phenomena [60]. As a result, families of sidebands appear around the supply frequency. Therefore, if a fault such as a valve leakage occurs within the compressor, it will lead to further fluctuation in the load and enhance the degree of current amplitude modulation [24] and enhance the sidebands around the supply frequency. Study the sideband amplitudes provides information regards the nature of the compressor fault which can be used to monitor the condition of the compressor.

The sidebands (f_{sb}) are formed according to:

$$f_{sb} = f_s \pm mf_{r_{com}} \quad (3.8)$$

Where f_s denotes the supply frequency, $f_{r_{com}}$ is the working frequency of the compressor and $m = 1, 2, 3, \dots$

3.3.4 Higher Order Spectra (HOS)

To obtain a reliable fault diagnosis using spectral analysis, efficient signal processing methods have been developed with the aim to enhance the signal-to-noise ratio (SNR) to provide more effective fault diagnosis. Higher Order Spectral (HOS) analysis can be a useful signal processing tool in this case for analysing the data [115]. The main advantage of using HOS is that, unlike the Fourier transform, it can preserve both the phase and magnitude response of a signal.

Generally, the HOS functions [116] can contain different information about the signals, Figure 3-3 demonstrates the classification map of the high order spectrums [117]. The HOS functions are defined as a form of cumulants. The spectrum of the n^{th} order, $C_n(f_1, f_2, \dots, f_{n-1})$ for a time domain signal $x(t)$, is calculated by the FT of its n^{th} order cumulant order $C_n(\tau_1, \tau_2, \dots, \tau_{n-1})$ [116]. The HOS consist of cumulant spectra and higher-order moment spectra. The cumulant spectra are very effective in the analysis of stochastic random processes, whereas the higher order moment spectra are more suitable for analysing the transient or periodic response. The main objectives of using the HOS are [116]:

1. To enhance SNR by suppressing the Gaussian noise from background sources.
2. To simultaneously restore the magnitude and phase response of the signal.
3. To identify and characterize the non-linear properties in a given signal.

The bi-spectrum analysis comes under the family of (HOS) and has been broadly applied since the early 1980s by a large number of researchers [118]. The advantage of HOS includes: it is suitable for detecting deviations from Gaussian and characterising non-linearity as well as extracting phase information.

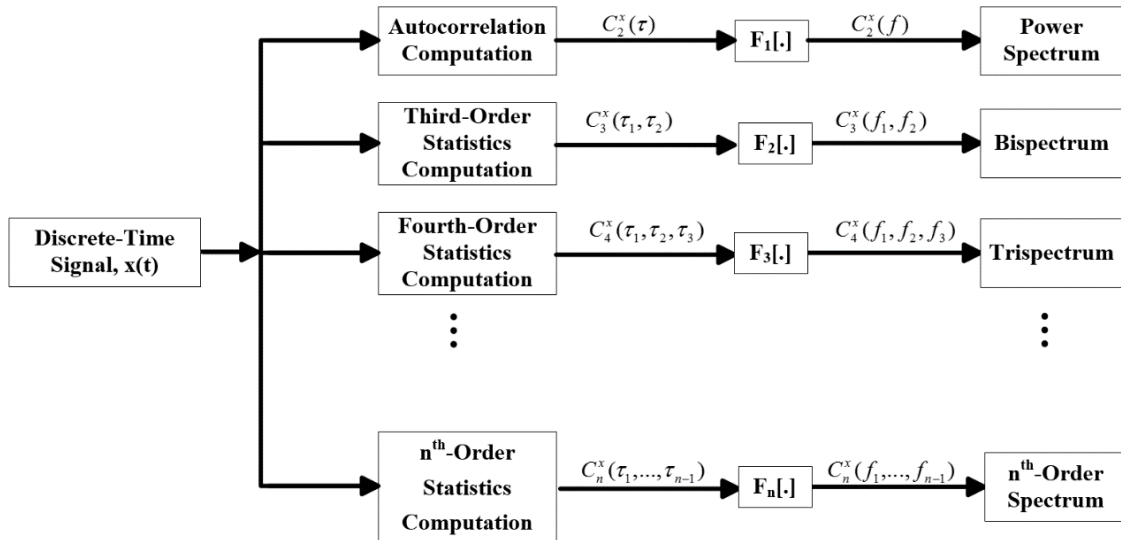


Figure 3-3: The HOS classification map [117]

3.3.4.1 Power Spectrum (PS)

The PS of a signal is a second order measurement of the harmonic power which is a real, positive quantity. It can be explained in term of its order spectrum with an order of $n=2$. For a discrete current signal, $x(t)$, it's Digital Fourier Transform (DFT), Eq. (3.6), the PS $P(f)$ of the time-varying series $X(n)$ is computed according to [60, 119]:

$$P(f) = E[X(f)X^*(f)] \quad (3.9)$$

Where $X^*(f)$ is the conjugate of $X(f)$, the FT of the time domain current signal $x(t)$ and $E[\]$ is the statistical expectation.

From the discussion, it can be shown that statistical averaging is important in order to obtain the power spectrum and the calculation does not include phase estimation which is necessary for identification of system nonlinearities.

3.3.4.2 Conventional Bi-spectrum Analysis (CB)

The conventional bi-spectrum analysis is a HOS analysis with order 3 that can be used effectively for suppressing noise and identifying nonlinearities present in the signals. The method is very useful to extract the phase information as well as the magnitude of the original signal [120].

CB $B(f_1, f_2)$ could mathematically be depicted by the DFT of a time domain data in order to calculate the mean product of 3-Fourier components:

$$B(f_1, f_2) = E[X(f_1)X(f_2)X^*(f_1 + f_2)] \quad (3.10)$$

Let the three frequency components obtained from the analysis be f_1, f_2 and $(f_1 + f_2)$ in which the last frequency component is achieved by summing the other two frequencies based on the Fourier series integral [20, 32].

In contrast to PS, the 3rd order analysis has a number of unique properties, for instance, non-linear system identification. The 3rd order determines a complicated quantity which has phase information and magnitude for the acquired signal $x(t)$. The bi-spectrum has the capability to detect the presence of Quadratic Phase Coupling (QPC) which occurs when the sum of the phases of the frequencies f_1, f_2 is equal to the phase at $(f_1 + f_s)$ and can be an indication on second-order non-linearities.

In case of frequencies at f_1, f_2 and $(f_1 + f_2)$ are independent components, thus, each individual frequency is going to be classified by statistical independent random phases distributed over the range $(-\pi, \pi)$. The random noise eliminations, in this case, can be achieved by implementing statistical averaging denoted earlier in Eq. (3.10). As a result, the bi-spectrum will tend to zero because of the phase mixing phenomenon and the noise will be considerably eliminated [86].

3.3.4.3 Modulation Signal Bispectrum (MSB)

The conventional bi-spectrum discussed in the previous subsection, shown in Eq. (3.10) can show the presence of QPC due to the non-linear effects from the components f_1, f_2 , and $(f_1 + f_2)$ that are harmonically related. However, it fails to include the frequency component $(f_1 - f_2)$ that might be present because of the non-linear interaction between the f_1 and f_2 . Thus the conventional bi-spectrum is not adequate to highlight the amplitude modulation effect in the current signals [60].

In order to meet the requirement and to overcome the limitation of conventional bi-spectrum to characterise the current signal, a modified version of CB, termed the modulated signal bi-spectrum (MSB) was proposed in [31, 32, 60, 86].

$$B_{MS}(f_1, f_2) = E[X(f_2 + f_1)X(f_2 - f_1)X^*(f_2)X^*(f_2)] \quad (3.11)$$

Unlike the conventional bi-spectrum in Eq. (3.10), both $(f_1 + f_2)$ and $(f_1 - f_2)$ are now considered simultaneously in Eq. (3.11) for measuring the non-linear effects of modulated signals. If both $(f_1 + f_2)$ and $(f_1 - f_2)$ appear because of non-linear effects between f_1 and f_2 , then a peak of a bi-spectral will appear at bi-frequency $B_{MS}(f_1, f_2)$. According to [121], this way is more accurately to represent the sidebands of the modulated signal.

Like the conventional bi-coherence, an advanced normalised MSB method is used to calculate the coupling degree among these components [121]

$$b_{MS}^2(f_1, f_2) = \frac{|B_{MS}(f_1, f_2)|^2}{E[|X(f_2)X(f_2)X^*(f_2)X^*(f_2)|^2]E[|X(f_2 + f_1)X(f_2 - f_1)|^2]} \quad (3.12)$$

Furthermore, the MSB is the PS if $f_1 = 0$, and Eq. (3.11) and could be re-written as:

$$B_{MS}(0, f_2) = E[X(f_2)X^*(f_2)X(f_2)X^*(f_2)] \quad (3.13)$$

Which is quite similar to Eq. (3.9):

$$PS(f) = \sqrt{B_{MS}(0, f_2)} = E[X(f_2)X^*(f_2)] \quad (3.14)$$

3.4 Summary

This chapter has presented various signal processing methods that can be useful for extracting diagnostic information on the RC in order to monitor its condition.

Time domain representation is definitely the easiest and commonly used signal processing approach to acquire useful information from the raw signal, usually using statistical analysis. Typically, the machine faults produce non-stationary responses in the acquired data that can provide essential information about the machine's condition.

Spectral analysis is by far the most popular signal processing procedure for the CM of machines, but the process is unsuitable for non-stationary signal analysis. Most compressor defects cause a dynamic load fluctuation, which results in modulation of the current signal. For instance, if a fault such as a leaky valve occurs within the compressor,

it will increase the load fluctuation, which will enhance the amplitude modulation in the measured current signal. MSB analysis effectively suppresses background noise and non-periodic components within the recorded signal. On the other hand, the nonlinear components that have a modulation effect present in the signal are usually decomposed and revealed with clarity in MSB analysis.

CHAPTER 4:

Reciprocating Compressor Experimental Test Rig

This chapter introduces the test facility and the simulation of the common RC faults that were considered in this investigation. The chapter was started by providing a brief description of the test rig, seeded faults and the measurement instruments. Finally, the chapter describes the data-acquisition procedures used for the analysis was presented at the end.

4.1 Test Rig Design

To evaluate the condition of a machine and assess the effectiveness of using current signatures for compressor CM, the experimental study was carried out on a laboratory RC test rig. a test rig was designed in a manner so that different types of common industrial faults could be introduced to the test rig. It provided a testbed for CM and the obtained test data from this rig were used to identify the different seeded faults to the RC. So the design of this test rig allows different faults to be introduced into the compressor. Then the compressor behaviour with and without these faults will provide experimental data to carry out the analysis of the compressor condition.

4.2 Test Rig Description

In industry, several kinds of compressors are utilized with regards to the various working condition and principles. One of the most widely used machines to compress air/gas in industries is the RC. Therefore, the experimental tests were performed on a single action, two-stages Broom-Wade TS9 RC Model TS9. This test rig comprises of three main components, a mover (induction motor), a two-cylinder V-shaped unit and air/gas tank [46]. The selected compressor, As shown in Figure 4-1, has the ability to compress the air/gas up to 120 psi. The compressor is driven by a three-phase, Brook Crompton induction motor type KX-C184 with a 2.5kW with rated speed 1420 rpm. A belt pulley system was used to transferee the induction motor power to the flywheel with a transmission ratio of 3.2:1. the compressor rated speed is about 440 rpm.

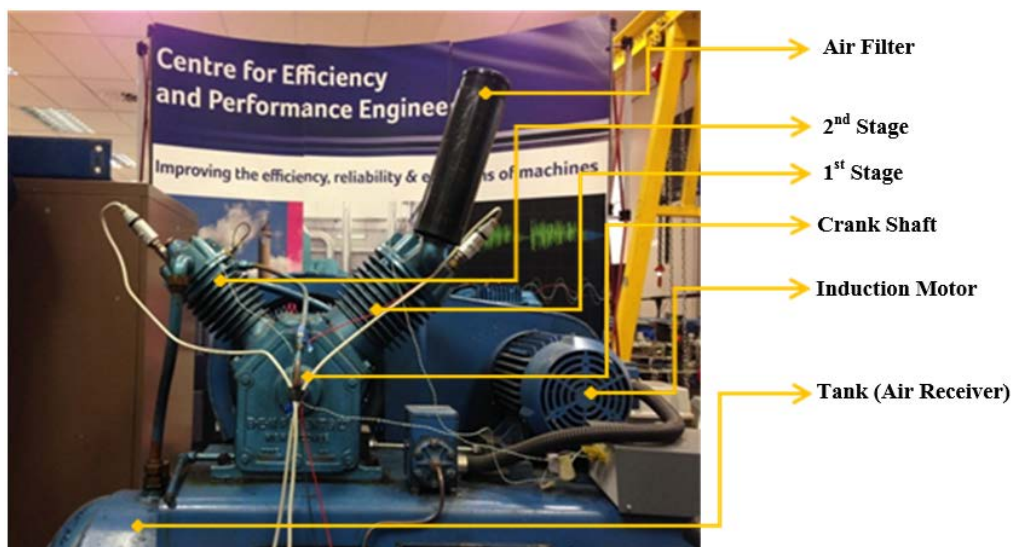


Figure 4-1: Broom-Wade TS9 reciprocating compressor

The Broom-Wade TS9 RC basic specifications are presented in Table 4-1[[122](#), [123](#)].

Table 4-1: Broom-Wade TS9 specifications

Broom Wade TS9 Compressor	
Max working pressure	1.38 MPa
Number of Cylinders	2 (90° Opposed)
Piston Stroke [mm]	76.2 mm
Compressor Speed [rpm]	440 rpm
Motor power [Kw]	2.5 (3 HP)
Voltage	380/420 V
Motor Speed [rpm]	1420 rpm
Current	4.1/4.8 A
Piston Diameter [Low Pressure Cylinder]	93.6 mm
Piston Diameter [High Pressure Cylinder]	55.6 mm

The compressor starts by compressing the gas from the first-stage cylinder, then cools the compressed gas by the help of intercooler placed between the two cylinders before it passes to the second stage cylinder, which is comparatively smaller in size than the first stage cylinder. After that, the compressed gas is injected into the receiver (air storage). A safety valve installed on the receiver to protect it against excessive pressure and motor from overload [[24](#)]. Splash lubrication is used for the smooth running of the moving parts involved in the compressor working.

4.3 Seeding of Common Compressor Fault

To assess the RC performance, vibration and motor current signals have been studied in this work. The data sets were collected from the compressor for five working conditions performed one by one. Two common compressor faults were separately seeded into the compressor. These faults are a leaky second stage discharge valve and a leak in the

intercooler. Also, another fault to the three-phase induction motor was also introduced (Stator Winding Asymmetry). The sequence of experimental tests as follows:

1. A healthy compressor with both stages operating normally.
2. A leak in a high-pressure cylinder discharge valve.
3. A leak in the intercooler.
4. Stator Winding Asymmetry.
5. Combined discharge valve leakage with stator winding asymmetry.

In order to define the healthy state of the compressor, a reference or a baseline is required. This baseline was obtained while the compressor operates normally as a healthy condition. After that, the compressor was operated with each fault isolated and one combined fault, then the signal deviations from the baseline were measured. Table 4-2 lists the different conducted conditions performed on the test rig to monitor the effect of these faults on the compressor performance.

Table 4-2: Experimental test conditions description

#	Test case	Description
1	BL	Healthy Compressor
2	ICL	Intercooler Leakage
3	DVL	Discharge Valve Leakage at 2 nd stage
4	SWA	Stator Winding Asymmetry
5	DVL+SWA	Discharge Valve Leakage & Stator Winding Asymmetry

4.3.1 Simulation of Valve Leakage

Compressor valves considered the most fragile component of the compressor. The valve works in a severe environment and exposed to a number of impacts per second during the compressor cycle causing non-uniform wear to the valve components which may lead to a leaky valve. In general, there are various valve types installed in the different compressor, which include, reed valve, poppet valve, ring valve and plate valve. The test rig used in this research fitted with plate valve as illustrated in Figure 4-2.

The leaky valve was introduced to the discharge valve of the second-stage. A small hole was drilled into the valve plate to simulate the leakage through the valve. Figure 4-3 (a) depicts a compressor schematic diagram with the valve plate after introducing this fault respectively. The size of the hole was 2mm in diameter which is measured as the 2% of the cross-section for the air flow.

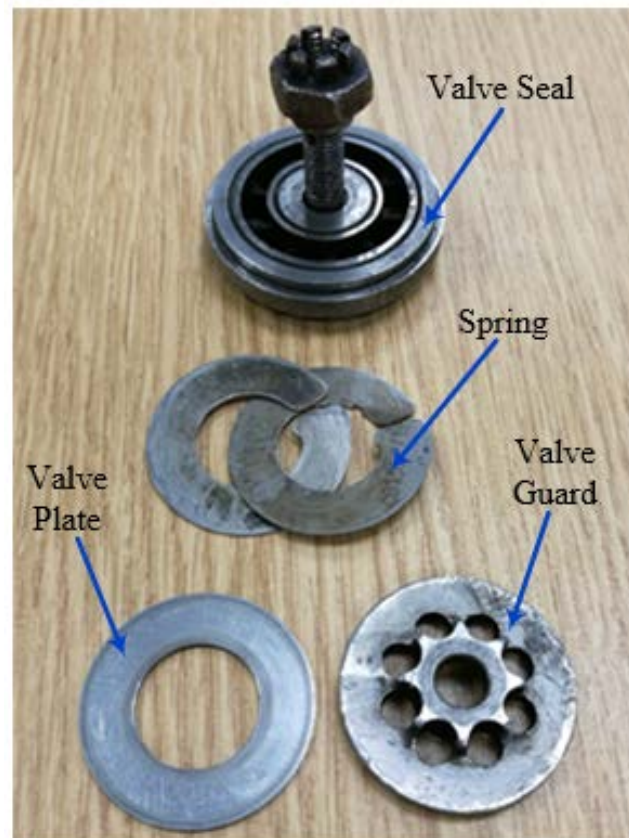


Figure 4-2: Second stage discharge valve components

4.3.2 Simulation of Intercooler Leakage

The compressed gas transferred by means of the intercooler pipe from the low-pressure cylinder into the higher pressure cylinder. A common fault is a leakage through the joints of this pipe. In order to seed this fault, the pipe joint was loosened to simulate a small leak in intercooler by turning it only one turn as shown in Figure 4-3 (b). Unfortunately, while this represents a practical fault; it was not feasible to measure the leakage as a percentage of the air-flow cross-section area.

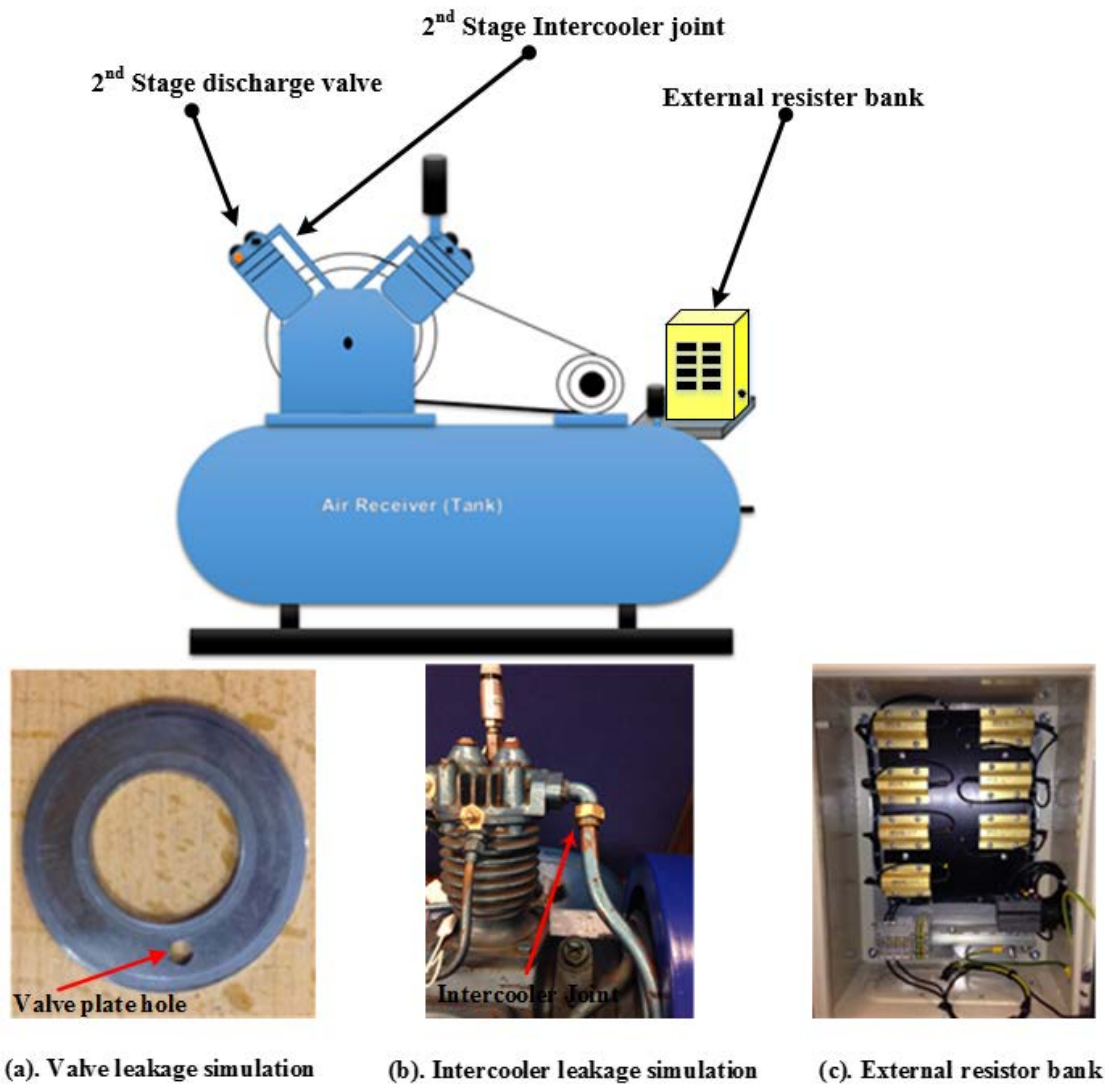


Figure 4-3: Test rig schematic diagram and fault simulation

4.3.3 Simulation of Stator Resistance

The third fault seeded to the test rig was the phase imbalance. Faults occurred in the induction motor not only can decrease machine production but also might cause a catastrophic incident resulting in an increase in repairs costs and machine downtime. Moreover, the increment of the induction motor stator resistance may result in another fault such as voltage imbalances, which in term causes the reduction of motor efficiency. Ideally, the three-phase balanced power supply for the induction motor can be represented by three magnitude voltages equally spaced by 120° [52]. However, this is not the case in practice. There are numerous causes of unbalance in the supply, e.g., the generator's terminal voltages, etc., see [124]. Yet, this fault may stay undiscovered due to the motor will still operate normally under these conditions, with less efficiency. This fault was

simulated by increasing the stator winding resistance by 1.0Ω to the three-phase motor as depicts in Figure 4-4.

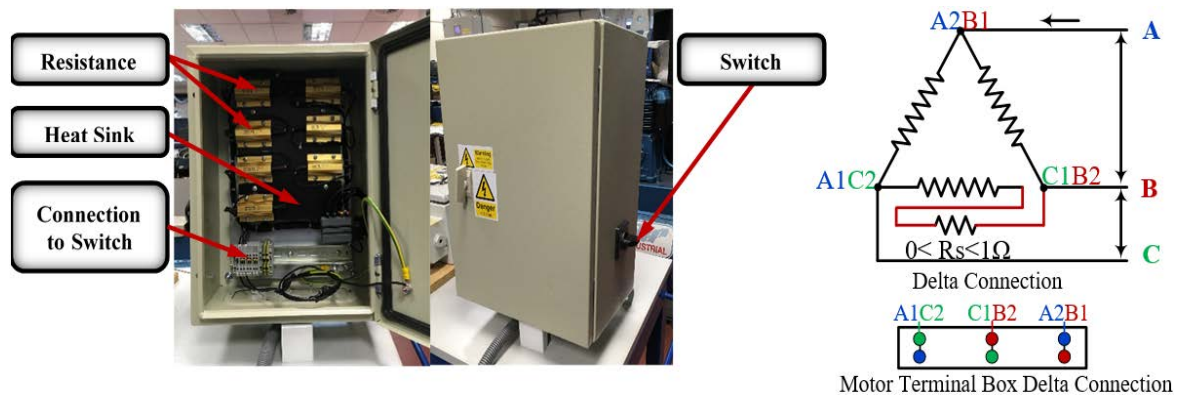


Figure 4-4: Photograph of external resistors bank and schematic diagram of stator winding asymmetry simulation (external resistors bank)

4.4 Measurement Transducers

The test rig has been previously used for a number of researches for the CM purposes at the University of Huddersfield. Therefore, there are a variety of different sensors that were already installed on the test rig: static and dynamic pressure transducers, vibration accelerometers, encoder and thermocouples. These senses were connected to the data acquisition system to collect data from the compressor and the coaxial BNC cables were used for this purpose to reduce signal noise.

4.4.1 Accelerometers

Two accelerometers were used for acquiring the vibration signal from the compressor; Bruel and Kjaer type YD-3 with a frequency range 0-40kHz. These accelerometers can withstand the temperature up to 150°C and they were installed on the top of each cylinder near the suction and discharge valves. Pictorial view of the accelerometer, its output raw data and specifications are given in Figure 4-5, Table 4-3 and Figure 4-6 respectively. These accelerometers were mounted on the cylinder heads via screw threaded brass studs to the cylinder casing using ceramic cement that helped to avoid the overheating of the sensors.



Figure 4-5: Location of the accelerometer at top of the cylinder head

Table 4-3: Accelerometer technical specifications

Features	Specifications
Type	TD-5-2
Frequency range	0-15 kHz
Acceleration	2000 ms ⁻²
Temperature range	Up to 150°C
Sensitivity	45 mv/ms ²

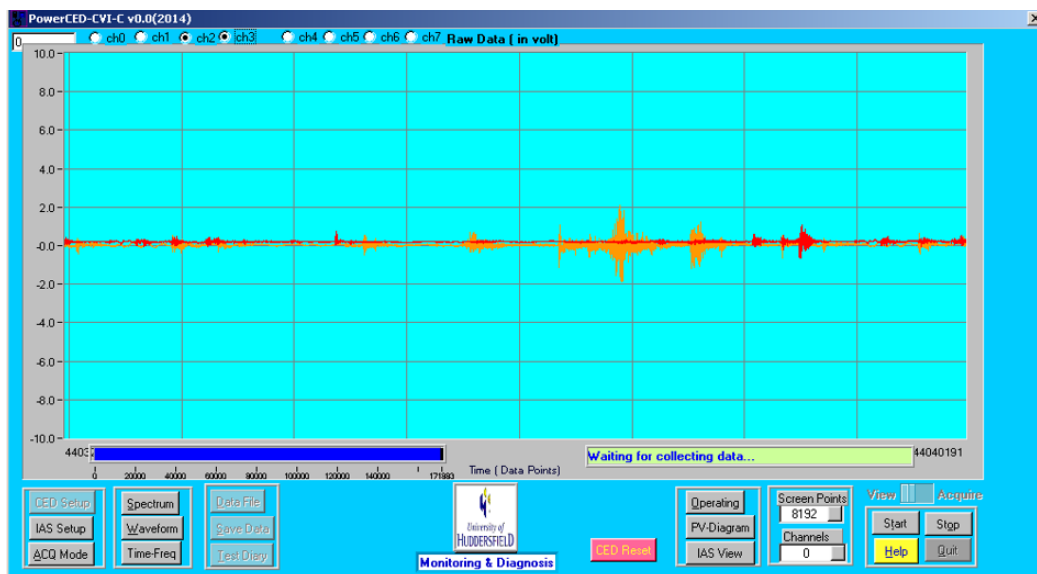


Figure 4-6: On-line vibration sensors output (raw-data)

4.4.2 Cylinder Pressure Sensor

An analogue pressure sensor was used to collect dynamic pressure data from each cylinder. Each transducer was installed through a hole at the top of the cylinder as illustrated in Figure 4-7. The dynamic pressure transducers were GEMS 2200 strain gauge pressure sensors and they had the maximum pressure limit up to 4MPa (600psi) and upper-frequency limit of about 4 kHz. Table 4-4 illustrates the sensor technical specifications. The output signal through the DAQ is illustrated in Figure 4-8. It shows a recorded of the first and second stage cylinder typical dynamic pressure.



Figure 4-7: In-cylinder pressure sensor

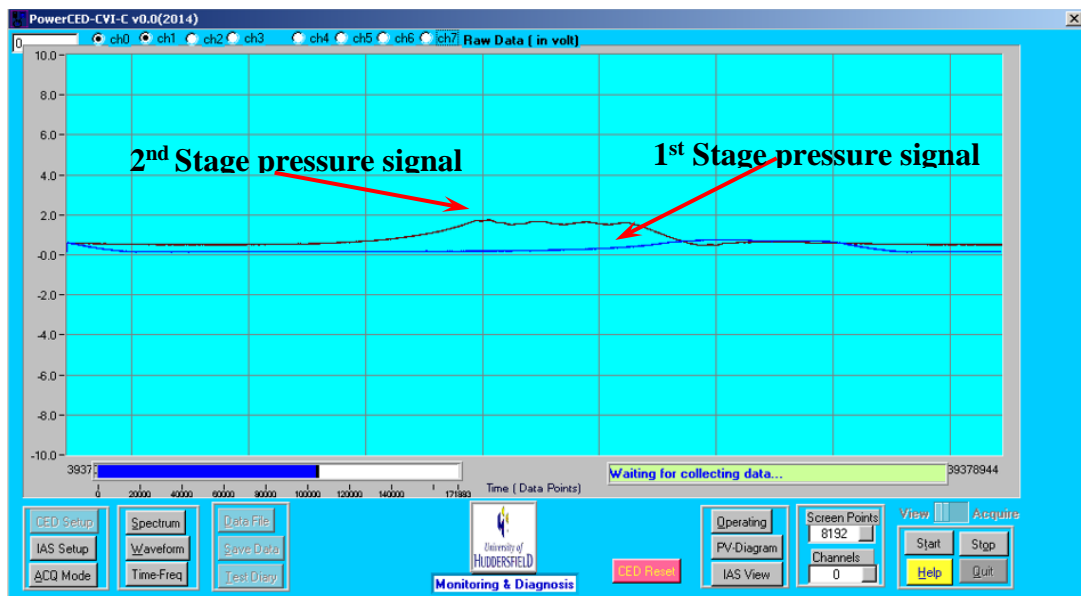


Figure 4-8: On-line dynamic pressure sensors output (raw-data)

Table 4-4: Pressure sensor technical specifications of the pressure sensor

Features	Specifications
Type	GEMS type 2200 strain gauge
Output	100 mV
Power supply	10 Vdc
Pressure range	4 Mpa (600 psi)
Frequency limit	4 kHz

4.4.3 Static Pressure Transducer

A Gem type PS20000 static pressure transducer was fitted on the compressor tank (gas storage) as illustrated in Figure 4-9. This sensor with a range of 0-200psi (1.35MPa), a maximum output 100 mV and a wide temperature range of -20°C to $+105^{\circ}\text{C}$. The transducer monitor and measure the tank pressure and triggering the data-collection process automatically once the pressure inside the tank reached to 0 psi, 20 psi, 30 psi, ..., 120psi.



Figure 4-9: Static pressure transducer mounted on the compressor tank.

4.4.4 Temperature Measurement

The thermocouples used for this experimental study was a *K-type* sensor which has a temperature range of -20°C to 220°C to monitor the compressor temperature. Measuring compressor temperature is necessary not only to monitor the machine operation but also

to protect the pressure sensors and other measurement equipment and ensure the safe operating conditions of the test rig.

4.4.5 Shaft Encoder

The optical encoder is a device that determines the angular position of the shaft and can measure the instantaneous angular speed (IAS) of the compressor drive shaft. An incremental RI32 shaft-encoder mounted on the compressor flywheel as shown in Figure 4-10 and was connected to the PC directly via the DAQ system. The response from a shaft encoder is a squared pulse output every one complete cycle referred to the index signal [24].



Figure 4-10: Optical pulse high-resolution shaft encoder.

The output online raw signal of the encoder is illustrated in Figure 4-11 Through the DAQ software, the encoder measurements show two different pulses, the electrical pulse trains (100 for each complete shaft revolution) and index signal.

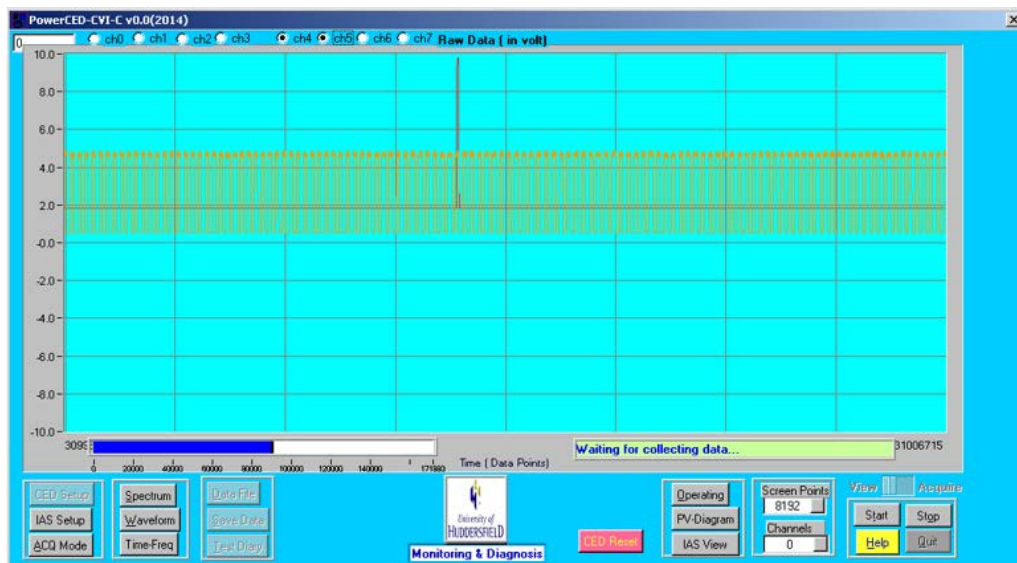


Figure 4-11: On-line optical encoder raw-data

4.4.6 Current Measurement

The measurement unit for measuring motor current already existed with the compressor test rig. To study the current characteristics, the measurement of the three-phase induction motor stator current was achieved using a Hall Effect current transducer (CT) mounted on a printed circuit board (PCB) to measure the circuit current without connecting the sensor directly into the circuit. Pictorial view of this unit, online current signal output (raw data) and its specification are given in Figure 4-12, Figure 4-13 and Table 4-5 respectively.



Figure 4-12: Three-phase current measuring unit

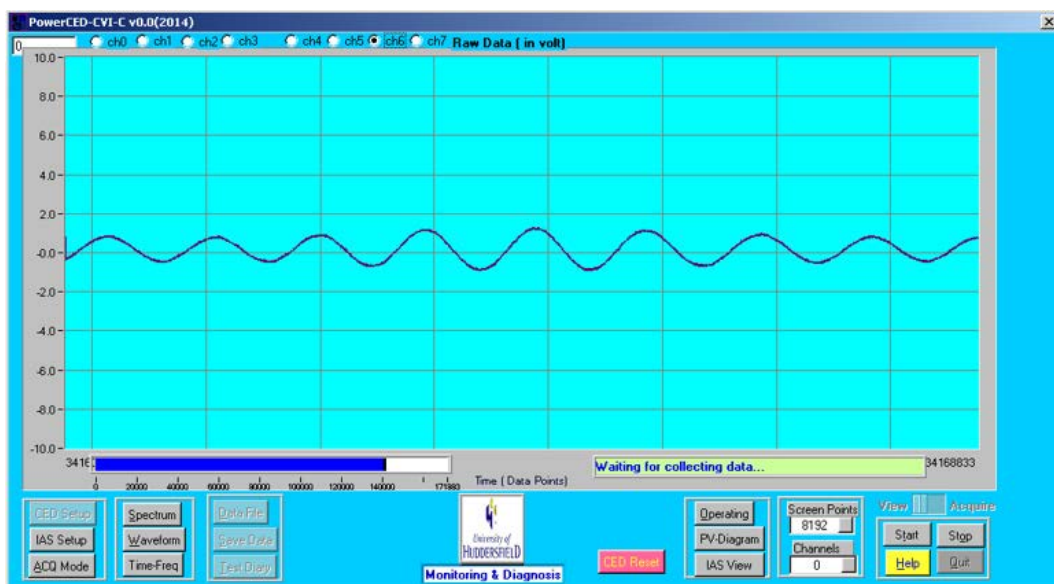


Figure 4-13: On-line motor current measurement raw-data

Table 4-5: Technical specifications for the hall effect current transducer (RS 286-327).

Features	Specifications
Response time (Inst.)	<1 μ sec.
Supply voltage	± 15 V dc, ($\pm 5\%$)
Operating temperature	0 $^{\circ}$ C to +70 $^{\circ}$ C
Bandwidth	DC to 100 kHz
Analogue output voltage	5 V

4.5 Data Acquisition System

4.5.1 Hardware: CED 1401 Plus

The hardware system used in this experiment was the Power 1401 Plus CED from Cambridge Electronic Design that converts an analogue voltage to digital values. It has the ability to record the raw data, events and marker information at 400 kHz and with sixteen-bit resolution [35]. Another feature of this DAQ device is that, has the ability to generate waveform and digital output in real time concurrently. Built-in 16 channels to collect machine data among which. In this experimental study, seven channels have been utilized as illustrated in Table 4-6. Figure 4-14 shows the CED Power 1401 Plus DAQ system.

Table 4-6: Data acquisition CED 1401 plus channels

Channel number	Data Type
Channel one	Collected pressure data from first stage (low pressure) cylinder
Channel two	Collected pressure data from second stage (high pressure) cylinder
Channel three	Acquired vibration data from first stage
Channel four	Acquired vibration data from second stage.
Channel five	Recorded the data from the shaft encoder
Channel six	Data to measure the angular position mark for piston TDC position
Channel seven	Measured motor current data from the current transducer



Figure 4-14: Pictorial diagram of CED 1401 Plus

4.5.2 Software: Lab Windows TM/CVI Version 5.5

The DAQ was written in the C programming language, this package contains large pre-installed facilities, e.g., run-time libraries to control system instruments, effective data acquisition facilities [6]. It contains a Graphical User Interface (GUI) editor thus the data acquisition process can be easily controlled by the DAQ software. Different channels of different data can be obtained with the various sampling rate and data length (e.g. vibration, pressure data, acceleration, sound and IAS). This package has set-up interface which provides a user-friendly guide to modifying the experimental parameters, for instance, the sample data length. Figure 4-15 shows a screenshot of the set-up panel.

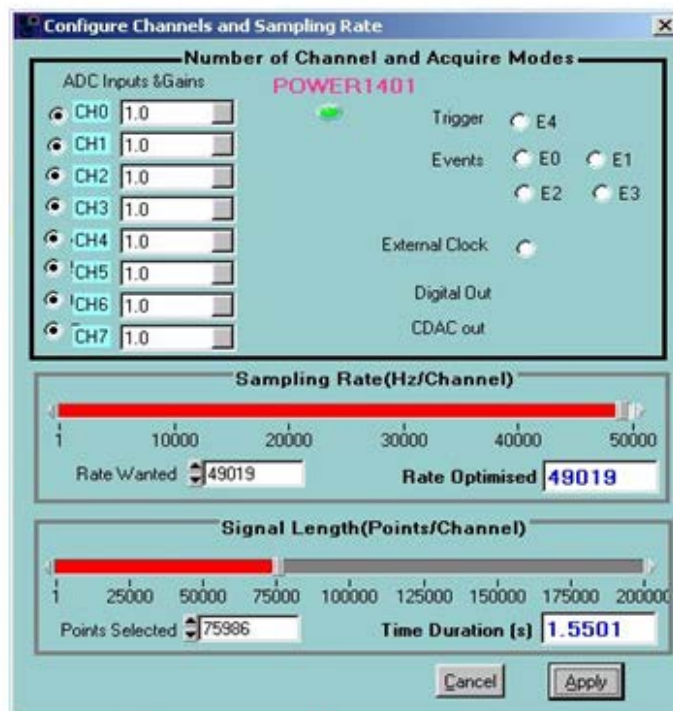


Figure 4-15: Setup screen for data acquisition.

In this experimental the data were recorded at the sampling frequency of 49.019 kHz, the data length was of 75986 sample points. Thus the acquired data time duration was 1.55 sec (Data points time duration = number of samples ÷ sampling frequency).

Each channel from the DAQ system shows different parameters: in-cylinder pressure from both cylinders, vibration responses from the first and second stage, motor current signal and encoder signal. When the piston is at TDC, then a trigger signal initiates the data collection process and each pulse is recorded at the same crank angle to make sure the accuracy of the time domain averaging. Running averages of four consecutive data segments were used to obtain a ‘clean’ signal. Figure 4-16 depicts the panel displaying all sensors data acquired from the compressor.

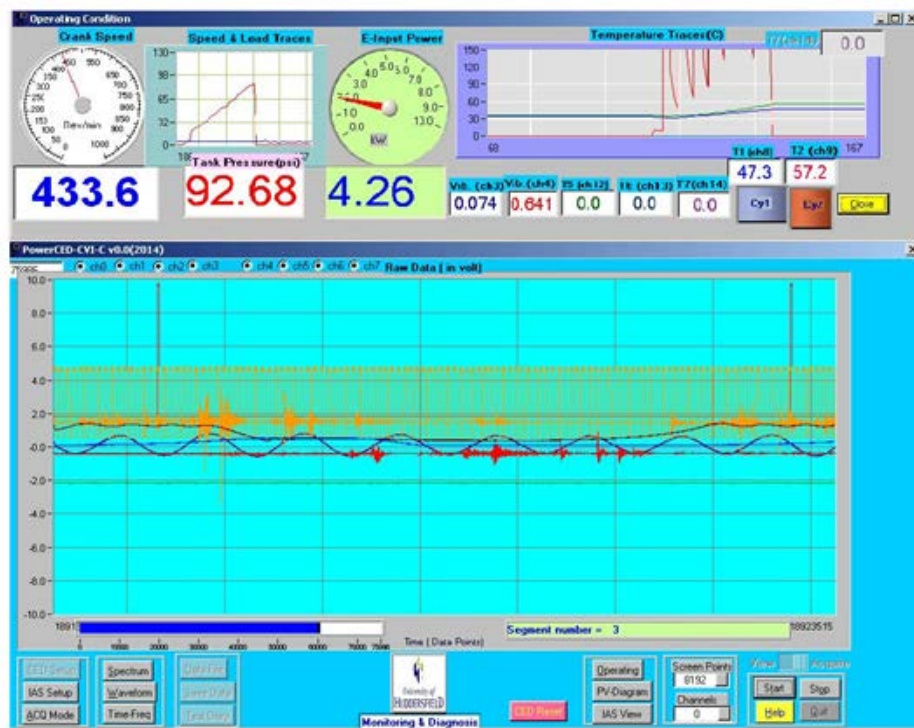


Figure 4-16: Data acquisition in progress

4.6 Data Management and Measurement Practice

Figure 4-17 illustrates the experimental test schematic diagram which shows a number of various sensors and their placements. To ensure good practice, a normal test approach was implemented as following: all sensors and accelerometers were connected to the DAQ system and checked by the GUI on the computer, all the required parameters have been entered to the DAQ such as a number of samples as shown in Figure 4-15. Each individual

machine condition was performed and data-set was stored with the length of 1.55 second with 49 kHz (sampling rate). For more reliable analysis, four sets of data were collected for each individual condition.

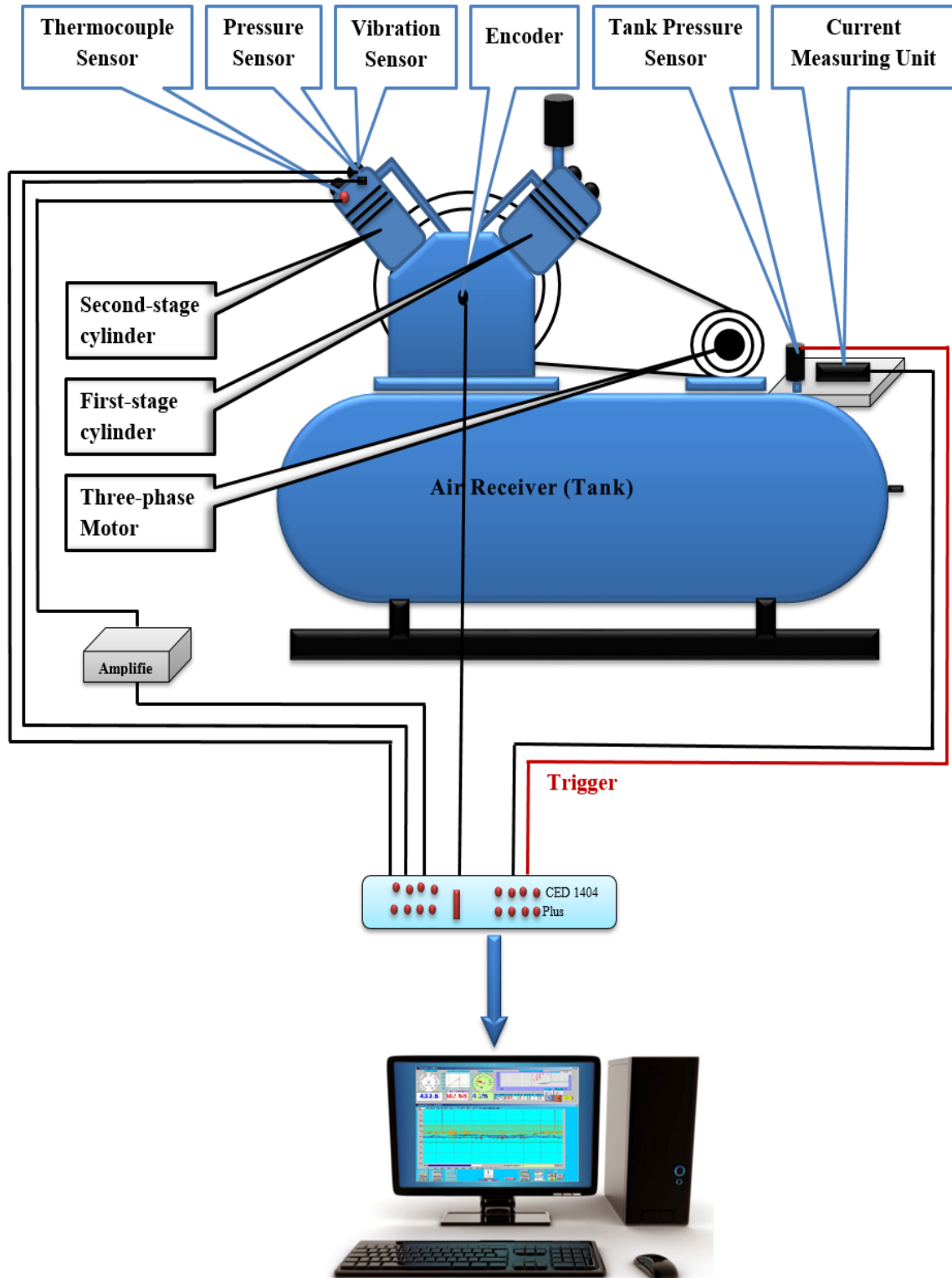


Figure 4-17: Schematic diagram of the compressor test system.

To evaluate the performance of diagnostics over wide range operating conditions and ensure the repeatability of test conditions, data acquisitions were carried out at successive discharge pressures up to 120 psi, which were set up automatically by the acquisition system. The acquired data sets were stored under a data directory specifically for this study. The specific test, compressor load, different fault conditions, and related file numbers were identified by a structured filename which was established for this purpose for further analysis using MATLAB.

4.7 Summary

The test facility was used to carry out the investigation of the RC condition monitoring. The chapter has shown the test rig development including the necessary measuring equipment and senses including the data acquisition system used to acquire data from the test rig. All test rig cables, DAQ channels and fault types were uniquely labelled. To examine the compressor performance under different operating condition, different faults were seeded to replicate compressor faults in industry real scenario. The safety check was carried out including checking all cables and covering any moving parts with safety grid before operating the test rig and acquiring data. Then, the compressor was operated under each fault and data acquired for this particular condition. Acquired data were organized including test number, date, time and test condition and stored for further analysis via MATLAB environment. The obtained result showed that the test-rig well-constructed and could be used for monitoring the compressor performance under the different condition and a wide range of compressor pressure.

CHAPTER 5:

Mathematical Modelling and Fault Simulation

To assist the condition monitoring and accurate diagnosis of compressor faults, a mathematical model of a compressor is presented in this chapter in order to gain a more in-depth understanding of the dynamic behaviour of two-stage RCs. Such a model can be used for predicting and characterising compressor behaviour including various dynamic parameters such as motor current signatures under different simulated faults.

The development of the extended model starts with a general concept of compressor operating mechanisms. Then, the piston-cylinder and the crankshaft arrangement are discussed. After that, cylinder pressure and angular speed equations are developed to demonstrate the mutual relationship between pressure and rotational speed and their effects on the motor current signal. Then, the mathematical equations were solved in a MATLAB environment to predict the current signatures for both a healthy compressor and compressor with specified common fault conditions (both single and combined faults). Good agreement between the predicted and measured results was found which suggests that the model is sufficiently precise to be used to simulate both simple and combined faults within the compressor and induction motor. It is concluded that the faults produced current signatures which can be differentiated by the analysis techniques used.

5.1 Introduction

Mathematical modelling is one way to study and gain a better knowledge of the behaviour of any machine and the relationships between its components. Computer-aided modelling (CAM) has enabled significant development in a large number of engineering disciplines, particularly prediction of machine performance and hence improved the diagnostics of machine malfunction. CAM assists the developments of effective data analysis approaches to characterize complex and weak signatures affected by various noise levels. Additionally, it can be used to predict fault signatures in the RC system. Modelling the compressor and simulating different faults can hugely benefit facilitating machine diagnostic and improving the monitoring system [73], which should help increase machine reliability.

5.2 Overview of the Compressor Model

RC is usually powered by an electric motor which converts electric energy into rotating motion and then into reciprocating, linear motion using a connection which translates shaft rotation into reciprocating linear motion of a piston, see Figure 5-1.

The RC normal operation is described in Chapter 2, Section 2.2. Briefly, with downward piston movement, in-cylinder pressure falls, the inlet valve opens and “air” enters the cylinder. As the piston starts to move upward, it compresses the “air” trapped above it, increasing the pressure until the “air” is forced into the outlet manifold via the discharge valve [36]. After which the cycle repeats itself. The working principle of a compressor can be described by three different processes: firstly, an electromagnetic process whereby electrical torque is generated and transmitted to a crankshaft, the second is the dynamic movement of the crankshaft which represents the mechanical processes including piston and valve motion, and finally, the fluid flows into and out of the cylinder through the inlet and outlet valves, generated by movement of the piston. The two-stage RC model is focused on these main processes.

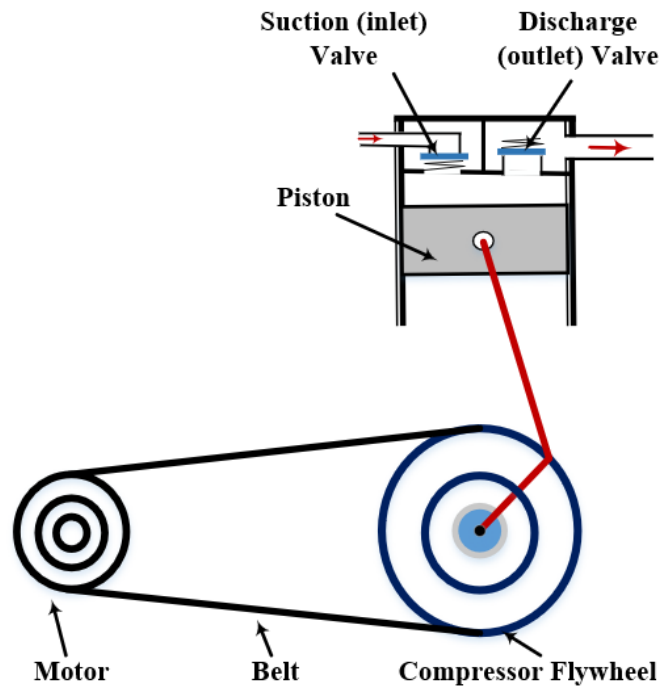


Figure 5-1: Crankshaft mechanisms of single cylinder compressor

5.2.1 Mathematical Model Objectives

The main objective of this chapter is to study and analyse the dynamic responses of a compressor in the context of compressor CM, using a mathematical model of an RC and induction motor to simulate different operating conditions.

Reciprocating compressors are complex and expensive items of equipment, and it would be difficult and time-consuming to attempt to experimentally seed all common faults into such a compressor in order to study their effects on its operation. Therefore, modelling the RC should be cost-effective and time-saving in the investigation of the consequences of faults that may develop within the machine [125]. Quantified and known faults can be introduced into the simulation and the numerical results used to develop a model-based CM method for the RC [24].

The mathematical study and numerical simulation of a machine offers a number of advantages: the model could provide useful fault signatures to look for, particularly for faults which cannot be seeded easily into a real compressor and studied experimentally; and secondly, it would allow researchers to study compressor performance under different working and fault conditions [46].

The model describes the compressor's working principles, valve movements, crankshaft motion and pressures in the first and second stages. The simulation considers both healthy and faulty conditions and specifically includes seepage through valve and intercooler pipe, and how such electrical defects in the prime mover as stator asymmetry and broken rotor bars affect compressor performance. In addition, in-cylinder pressure and motor current signals are analysed to identify the fault features. Finally, to validate the performance of the model, the chapter presents a comparison of measured and predicted in-cylinder pressure and motor current signals.

5.2.2 Compressor Modelling (a Brief Review)

The early compressor model was developed by [126] to review the dynamics of a RC fitted with a reed valve. In that study, the torsional vibration of a helical gear was considered with a one-degree of freedom (1 DOF) system representing valve motion.

Wambsganss [127] studied the performance of a hermetic refrigeration compressor equipped with self-acting reed valves. He studied the movement of both valves and the pressure differences across them. In that model different degrees-of-freedom were considered for valve dynamics. Also, model results were compared with the experimental results.

Singh et al., [128] introduced a dynamic model for analysing valve displacement by studying the influence of backflows on the discharge system, and monitored the resulting pressure fluctuations, taking into consideration the cylinder and valve mechanisms. The compressor capacity, energy consumption, and unsteady gas flow in the valve chamber were considered. The obtained results from the theoretical and experimental studies were in excellent agreement.

Sun and Ren [129] applied a new method to study factors that influence the compressor working processes, including heat transfer and valve motion, for the prediction of compressor performance. The model only considered a ring valve and the movement of the valve plate, so a 1 DOF model of valve motion was developed. An experimental examination was performed to validate the model findings, the volume displacement for both experiment and simulation were compared.

The majority of former research has centred on compressor operation and behaviour, studying how to improve the compressor design by predicting its performance. The

researchers did not take into account compressor faults such as seepage past the closed discharge valve (also known as leakage) - which has a great impact on compressor performance.

Manepatil et al., [130] simulated compressor performance as affected by faulty valves and piston ring seepage. The model studied in-cylinder pressure to predict the compressor performance, with dynamic pressure measurements used for RC condition monitoring.

Winandy et al., [131] observed the compressor working process to study factors that affected the mass flow rate, including the clearance volume and the heat generated during compression. Then, they developed a model based on their observations to estimate the performance of the compressor and to compute the mass flow rate and temperature of the compressor discharge. The model was able to determine discharge temperature accurately.

Elhaj, et al., [46] developed a numerical simulation for compressor CM. In that model, different operating conditions were investigated. Also, the model included the effect of changes in load due to valve seepages. An experimental study was conducted to validate the model's predictions. In-cylinder pressure and the speed-fluctuations of the crankshaft were used as featured tools for detection of different faults. Model and experimental results were in good agreement.

Ndiaye and Bernier [132] introduced a hermetic RC model to determine the inlet and outlet mass flow rates of the compressor. They investigated the compressor during on-off cycling operations and electrical power used by the prime mover. Both steady-state and transient conditions were validated by an experimental study. The comparison of results showed that the model was relatively accurate but there were some discrepancies with the experimental results due to the unavailability of certain manufacturer's data. In that study, oil effects on the refrigerant flow rate and the compressor were neglected as was the influence of the superheat of the refrigerant on the electrical consumption.

Link and Deschamps [133] used analytical methods to examine the effect of the compressor start-up and shutdown on energy consumption, noise levels and compressor reliability. Also, the minimum voltage required during the compressor start-up was estimated using the model, it also showed that the dynamics of both inlet and outlet valves suffered from impacts during the start-up and shutdown processes which, in turn, had an effect on the compressor performance. Experimental data and model results were

compared to verify the developed model during start-up, and good agreement was observed.

Yang, et al., [134] developed a semi-hermetic CO₂ RC model to study the effect of the ratio of stroke-bore on the compressor's performance. The model included the compressor valve, the compression event, seepage past the piston ring and frictional power loss. The model predicted the compressor mass flow rate and input power, then compared the predicted results with the experimental findings and showed good agreement between model and experimental results.

Dutra and Deschamps [135] simulated a hermetic RC model for prediction of compressor performance. They also proposed a single-phase motor model for calculating the motor slip and to estimate the speed of the compressor for different operating conditions, to study the compressor power and the motor efficiency relationship. A deviation of 1.5% of the motor efficiency from the measured values was estimated by the model, good agreement was obtained between model prediction and experimental data.

Silva and Deschamps [136] studied the effect of gas seepage through the reed-type valves of a small RC and its effect on performance, using a one-dimensional valve model. They studied the valve dynamics and predicted seepage due to sealing defects for both inlet and outlet valves. They concluded that the compressor efficiency was reduced significantly due to the valve seepage, with outlet valve seepage having a greater impact than inlet valve seepage.

As reviewed above, several models now exist to simulate RC behaviour and to determine the key factors affecting compressor performance. However, relatively few researchers have modelled an RC with the aim of diagnosing different compressor faults and/or their effects on compressor performance, and there has been virtually nothing on using motor current signatures for this purpose. In fact, none of the RC models reviewed included the influences of electrical faults such as faults in the stator winding and/or broken rotor bars, on compressor performance. A few attempted to show the potential of utilizing induction motor current as a means of assessing the condition of downstream driven equipment such as RCs. However, it is clear that a more accurate, effective, and flexible model needs to be developed to inspect how different electromechanical faults affect the RC.

5.3 Electric Motor Model

A three-phase induction motor comprises two main parts: a rotor and a stator. Both rotor and stator comprise three identical and symmetrically positioned windings, with N_r and N_s turns respectively. The stator is stationary and composed of the windings, the rotor is on the “inside” and rotates, driven by Faradays laws. The phase shift, or electrical angle, between adjacent windings is 120° and this provides the electromagnetic forces which cause the rotor to rotate. The stator and rotor phase axes shown are separated an angle of θ_r . Figure 5-2 illustrates a simplified schematic of the asymmetrical induction motor.

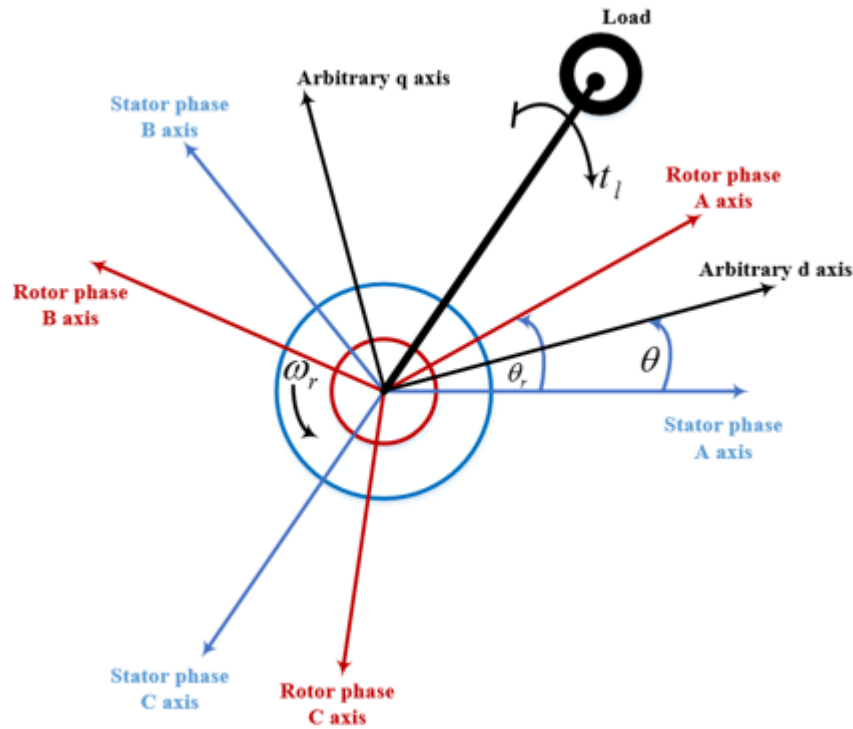


Figure 5-2: Simplified schematic of asymmetrical induction motor [56]

5.3.1 Voltage and Flux Linkage Equations

The voltage equations for the stator and rotor are usually developed in relation to self and mutual inductances, because of the variations in the angle between the stator axis and rotor, as well as the change of the mutual inductances of the stator and rotor coils. The equations of stator voltage for the three stator phases in the abc reference frame are as follows [56, 137]:

$$u_s^a = r_s \cdot i_s^a + \frac{d\lambda_s^a}{dt} \quad (5.1)$$

$$u_s^b = r_s \cdot i_s^b + \frac{d\lambda_s^b}{dt} \quad (5.2)$$

$$u_s^c = r_s \cdot i_s^c + \frac{d\lambda_s^c}{dt} \quad (5.3)$$

In the ideal induction motor, the resistances are equal: $r_{sa} = r_{sb} = r_{sc} = r_s$.

The rotor voltage equations for the three rotor phases are:

$$u_r^a = r_r \cdot i_r^a + \frac{d\lambda_r^a}{dt} \quad (5.4)$$

$$u_r^b = r_r \cdot i_r^b + \frac{d\lambda_r^b}{dt} \quad (5.5)$$

$$u_r^c = r_r \cdot i_r^c + \frac{d\lambda_r^c}{dt} \quad (5.6)$$

Where the subscripts s and r are for stator and rotor respectively, and superscripts a , b and c the motor's three-phases. u_s^{abc} & u_r^{abc} are column vectors representing the voltages, i_s^{abc} & i_r^{abc} denotes the stator and rotor currents respectively, and λ_s^{abc} & λ_r^{abc} represents the respective phase flux linkages. The motor flux linkages in the stator are as follows:

$$\lambda_s^a = L_{ss}^a \cdot i_s^a + L_{sr}^a \cdot i_r^a \quad (5.7)$$

$$\lambda_s^b = L_{ss}^b \cdot i_s^b + L_{sr}^b \cdot i_r^b \quad (5.8)$$

$$\lambda_s^c = L_{ss}^c \cdot i_s^c + L_{sr}^c \cdot i_r^c \quad (5.9)$$

The flux linkages equations in the rotor are:

$$\lambda_r^a = L_{rr}^a \cdot i_r^a + L_{rs}^a \cdot i_s^a \quad (5.10)$$

$$\lambda_r^b = L_{rr}^b \cdot i_r^b + L_{rs}^b \cdot i_s^b \quad (5.11)$$

$$\lambda_r^c = L_{rr}^c \cdot i_r^c + L_{rs}^c \cdot i_s^c \quad (5.12)$$

Where the self-inductances L_{rr}^{abc} and L_{ss}^{abc} are for rotor and stator respectively. The mutual inductance, L_{rs}^{abc} and L_{sr}^{abc} , are for rotor-to-stator and stator-to-rotor, respectively. All inductances are in the form of symmetrical matrices. To have all the motor equations in the same reference frame, the original abc variables has to be transformed into d, q variables, here this reserch use $dq0$, an arbitrary frame of reference [137]. If θ is the angle between the q-axis and a-axis of the two reference frames, then the matrix which transforms the variables from the abc to $dq0$ reference frame is defined as [137]:

$$T_{dq0}(\theta) = \frac{2}{3} \begin{bmatrix} \cos \theta & \cos(\theta - \frac{2\pi}{3}) & \cos(\theta + \frac{2\pi}{3}) \\ \sin \theta & \sin(\theta - \frac{2\pi}{3}) & \sin(\theta + \frac{2\pi}{3}) \\ \frac{1}{2} & \frac{1}{2} & \frac{1}{2} \end{bmatrix} \quad (5.13)$$

Transforming Eqs. (5.64) - (5.75) to the $dq\theta$ frame of reference

$$u_s^{qd0} = r_s^{qd0} \cdot i_s^{qd0} + E_s^{qd0} + \frac{d\lambda_s^{qd0}}{dt} \quad (5.14)$$

$$u_r^{qd0} = r_r^{qd0} \cdot i_r^{qd0} + E_r^{qd0} + \frac{d\lambda_r^{qd0}}{dt} \quad (5.15)$$

Where:

$$E_s^{qd0} = \omega \begin{bmatrix} 0 & 1 & 0 \\ -1 & 0 & 0 \\ 0 & 0 & 0 \end{bmatrix} \cdot \lambda_s^{qd0} \quad (5.16)$$

$$E_r^{qd0} = (\omega - \omega_r) \begin{bmatrix} 0 & 1 & 0 \\ -1 & 0 & 0 \\ 0 & 0 & 0 \end{bmatrix} \cdot \lambda_r^{qd0} \quad (5.17)$$

$$\omega = \frac{d\theta}{dt} \quad (5.18)$$

$$\omega_r = \frac{d(\theta_r)}{dt} \quad (5.19)$$

Resistance matrices in the $dq0$ frame of reference are:

$$r_s^{qd0} = r_s \begin{bmatrix} 1 & 0 & 0 \\ 0 & 1 & 0 \\ 0 & 0 & 1 \end{bmatrix} \quad (5.20)$$

$$r_r^{qd0} = r_r \begin{bmatrix} 1 & 0 & 0 \\ 0 & 1 & 0 \\ 0 & 0 & 1 \end{bmatrix} \quad (5.21)$$

The matrices for the flux linkage are:

$$\begin{bmatrix} \lambda_s^{qd0} \\ \lambda_r^{qd0} \end{bmatrix} = \begin{bmatrix} L_{ls} + L_m & 0 & 0 & L_m & 0 & 0 \\ 0 & L_{ls} + L_m & 0 & 0 & L_m & 0 \\ 0 & 0 & L_{ls} & 0 & 0 & 0 \\ L_m & 0 & 0 & L_{lr} + L_m & 0 & 0 \\ 0 & L_m & 0 & 0 & L_{lr} + L_m & 0 \\ 0 & 0 & 0 & 0 & 0 & L_{lr} \end{bmatrix} \begin{bmatrix} i_s^{qd0} \\ i_r^{qd0} \end{bmatrix} \quad (5.22)$$

Where L_{ls} & L_{lr} are, respectively, the stator and rotor winding leakage inductance per phase. L_m is the mutual inductance.

5.3.2 Motor Torque Calculations

During the compressor cycle (suction and compression), the change of discharge pressure causes fluctuation of the crankshaft speed which inturn would affect the capability of the motor torque T_{em} to provide the required speed. The motor current (i) compensates for the effect of changes in motor torque which correlate with the current as [138]:

$$T_{em} = \frac{3}{2} \frac{P}{2} L_m (\lambda_{dr} i_{qs} - \lambda_{qr} i_{ds}) \quad (5.23)$$

Where L_m , P , λ_{dr} , i_{qs} , λ_{qr} and i_{ds} represent the mutual inductance, number of pole pairs, the rotor flux d-axis, stator current q-axis, the rotor flux q-axis, stator current d-axis, respectively. Selecting a particular model of the motor fixes these parameters. The load change will affect the current statically or dynamically according to the load-variation characteristics due to the change of pressure.

5.4 Compressor Dynamics

Figure 5-3 illustrates a two-stage RC piston and crank arrangement. A motor (mover) with angular speed, ω rotates the crankshaft with radius r converts the rotation motion from the mover (electric motor) into linear movements through the connecting rod of length l which moves the piston in a reciprocating motion [24]. The compressor cycle consists of two basic working processes: suction and discharge which takes low-pressure “air” into one cylinder and delivers high-pressure “air” from a second cylinder. It commences at TDC where $\Theta = 0^\circ$ and ends when $\Theta = 360^\circ$, a revolution of the crankshaft. This procedure is the foundation of the model to simulate motor current signal, in-cylinder pressure, and angular speed. The model comprises coupled non-linear differential equations which correspond to the motor torque variation, crankshaft mechanism, cylinder pressure, and valves behaviour in both stages.

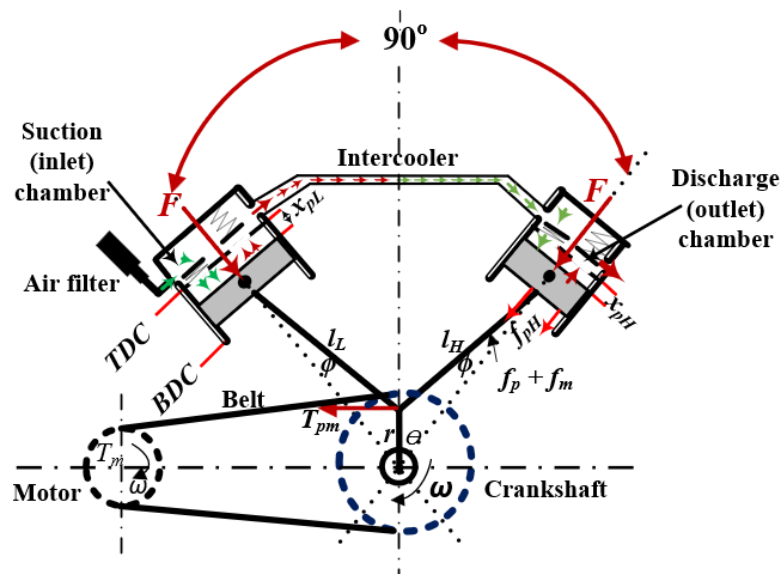


Figure 5-3: Two-Stage V-type reciprocating compressor [46]

5.4.1 Crankshaft System

As shown in Figure 5-3, a typical crank system of the RC could be considered as a two-degree-of-freedom (2 DOF) system. The movement of the piston is considered as the first DOF and the crankshaft rotation can be regarded as the second DOF. The fluctuations of the RC angular speed will be linked to the fluctuations of the torque acting on the compressor shaft. This torque will be influenced by the “air” pressure inside the cylinder,

vertical unbalanced inertia forces and the load of the motor. As per Newton's second law, the torque balance equation can be written as follows:

$$J\dot{\omega} = T_{im}(t) - T_{pmL,H}(t) - T_{fL,H}(t) \quad (5.24)$$

Where shaft speed ω is a function of time (t), J is the corresponding total inertial-moment of the compressor which consists of the movement of both reciprocating and rotating components of the RC, the electrical drive and power transmission. $T_{im}(t)$ is the induction motor torque, $T_{pmL,H}(t)$ is the torque resulting from cylinder pressure, and the unbalanced inertial force of the piston and con-rod of both lower and higher cylinders. $T_{fL,H}(t)$ is the frictional torque of both cylinders.

In-cylinder pressures produce torques T_{pmL} and T_{pmH} which can be found from the inertia forces of the compressor piston $f_{pL,H}$ and con-rod mass $f_{mL,H}$ for the first and second stages [46] as:

$$T_{pmL} = (f_{pL} + f_{mL})R_{eL} \quad (5.25)$$

$$T_{pmH} = (f_{pH} + f_{mH})R_{eH} \quad (5.26)$$

Where $f_{pL,H}$ are the forces produced by the "air" pressure in the low and high-pressure cylinders respectively.

The masses of the pistons, produce reciprocating inertial forces, $f_{mL,H}$, for the low- and high-pressure cylinders respectively. $R_{eL,H}$ are the effective radii of the crankshafts, for the low and high-pressure cylinders respectively and their values can be calculated as:

$$\begin{aligned} R_{eL} &= r \frac{\sin(\theta + \phi)}{\cos\phi} \\ &= r \frac{\sin\theta \cos\phi + \cos\theta \sin\phi}{\cos\phi} \\ &= r \sin\theta + r \frac{\cos\theta \sin\phi}{\cos\phi} \end{aligned} \quad (5.27)$$

The effective radii $Re_{L,H}$ of the crankshaft in the low and high pressure cylinders respectively become,

$$Re_L = r \sin\theta + \frac{r \cos\theta \sin\theta}{l \cos\phi} \quad (5.28)$$

$$= r \sin\theta + \frac{r}{2l} \sin 2\theta / \sqrt{1 - \frac{r^2}{l^2} \sin^2(\theta)}$$

$$Re_H = r \sin\left(\theta + \frac{\pi}{2}\right) + \frac{r}{2l} \sin 2\left(\theta + \frac{\pi}{2}\right) / \sqrt{1 - \frac{r^2}{l^2} \sin^2\left(\theta + \frac{\pi}{2}\right)} \quad (5.29)$$

Additionally, the “air” pressures in the low and high stage cylinders induce forces acting on both pistons, f_{pL} and f_{pH} , which can be calculated as:

$$f_{pL} = P_{cL} s_{cL} \quad (5.30)$$

$$f_{pH} = P_{cH} s_{cH} \quad (5.31)$$

Where P_{cL} and P_{cH} are the “air” pressures and, s_{cL} and s_{cH} are the cross-sectional areas of the low and high-pressure cylinders respectively:

$$s_{cL} = 0.25\pi d_L^2 \quad (5.32)$$

$$s_{cH} = 0.25\pi d_H^2$$

Where d_L and d_H are the bore diameters of the low and high-pressure cylinders respectively.

The inertial forces produced by the vertical reciprocating masses of both cylinders are:

$$f_{mL} = -m_{recL} \ddot{x}_{pL} \quad (5.33)$$

$$f_{mH} = -m_{recH} \ddot{x}_{pH}$$

Where \ddot{x}_{pL} and \ddot{x}_{pH} are the piston accelerations, and m_{recL} m_{recH} are the reciprocating inertia masses for both stages and can be calculated as:

$$m_{recL} = m_{pL} + 0.5m_{crL} \quad (5.34)$$

$$m_{recH} = m_{pH} + 0.5m_{crH}$$

Where m_{pL} and m_{pH} are the piston masses for both stages, m_{crL} and m_{crH} are the masses of the connecting-rods for each cylinder.

5.4.2 Piston Dynamic Model (Two-Stage Compressors)

Figure 5-3 demonstrates the displacement of the compressor piston from TDC indicated as x_p for a crank angle rotation of θ . The assumption is that the crankshaft rotates at constant angular speed, ω . Thus, the piston location can be calculated in terms of the crank angle θ [46]. For the two-stage RC test rig (Broom Wade TS-9) used in the study the piston of the low cylinder lags the high cylinder displacement by a phase of $\pi/2$ because of the V-shaped 90° arrangement. This was taken into consideration when developing the model. The lower stage cylinder was used as the reference and the displacements of the low and high pressure pistons, subscripts L and H respectively, are:

$$x_{pL} = r(1 - r \cos(\theta)) + l \left[1 - \sqrt{1 - \frac{r^2}{l^2} \sin^2(\theta)} \right] \quad (5.35)$$

$$x_{pH} = r \left(1 - r \cos \left(\theta + \frac{\pi}{2} \right) \right) + l \left[1 - \sqrt{1 - \frac{r^2}{l^2} \sin^2 \left(\theta + \frac{\pi}{2} \right)} \right] \quad (5.36)$$

The piston velocity can be calculated by obtaining the first derivative with respect to time of the piston displacement as shown in Eq.(5.35):

$$\begin{aligned} \dot{x}_{pL} &= \omega r \sin(\theta) + l \left(\frac{1}{2} \left(1 - \frac{r^2}{l^2} \sin^2(\theta) \right)^{-1/2} \cdot \left(-\frac{r^2}{l^2} 2\omega \cos(\theta) \sin(\theta) \right) \right) \\ &= \omega r \sin(\theta) - \frac{1}{2} l \left(\frac{-2r^2/l^2 \omega \sin(\theta) \cos(\theta)}{\sqrt{1 - \frac{r^2}{l^2} \sin^2(\theta)}} \right) \end{aligned} \quad (5.37)$$

The piston velocity $\dot{x}_{pL,H}$ will be as follows:

$$\dot{x}_{pL} = \omega r \sin \theta \left(1 + \frac{r}{l} \cos \theta \right) / \left(\sqrt{1 - \frac{r^2}{l^2} \sin^2 \theta} \right) \quad (5.38)$$

$$\dot{x}_{pH} = \omega r \sin \left(\theta + \frac{\pi}{2} \right) \left(1 + \frac{r}{l} \cos \left(\theta + \frac{\pi}{2} \right) \right) / \left(\sqrt{1 - \frac{r^2}{l^2} \sin^2 \left(\theta + \frac{\pi}{2} \right)} \right) \quad (5.39)$$

The ratio of the lengths of the crankshaft and con-rod is 1:4. Thus, the term r/l is less than 1, as is $\sin(\theta)$ (except momentarily at $\theta = 90^\circ$ and 270°), consequently, the term $r^2 \sin^2(\theta)/l^2$ in Eqs. (5.38 and 5.39) is sufficiently small to be ignored without introducing substantial error and Eqs. (5.38 and 5.39) can be re-written as [24]:

$$\dot{x}_{pL} = \omega r \sin(\theta) \left(1 + \frac{r}{l} \cos(\theta)\right) \quad (5.40)$$

The piston acceleration can be obtained by differentiating the piston velocity Eq. (5.40) with respect to time as follows:

$$\begin{aligned} \dot{x}_p &= \omega r \sin(\theta) + \frac{\omega r^2}{l} \sin(\theta) \cos(\theta) \\ \ddot{x}_p &= \omega^2 r \cos(\theta) + \left(\frac{\omega r^2}{l} \sin(\theta)\right) (-\omega \sin(\theta)) + (\cos(\theta)) \left(\frac{\omega^2 r^2}{l} \cos(\theta)\right) \\ &= \omega^2 r \cos(\theta) - \frac{\omega^2 r^2}{l} \sin^2(\theta) + \frac{\omega^2 r^2}{l} \cos^2(\theta) \\ &= \omega^2 r \cos(\theta) + \frac{\omega^2 r^2}{l} (\cos^2(\theta) - \sin^2(\theta)) \\ &= \omega^2 r \cos(\theta) + \frac{\omega^2 r^2}{l} \cos(2\theta) \end{aligned} \quad (5.41)$$

Then the piston acceleration $\ddot{x}_{pL,H}$ will be:

$$\ddot{x}_{pL} = \omega^2 r \left(\cos\theta + \frac{r}{l} \cos 2\theta \right) \quad (5.42)$$

$$\ddot{x}_{pH} = \omega^2 r \left(\cos\left(\theta + \frac{\pi}{2}\right) + \frac{r}{l} \cos 2\left(\theta + \frac{\pi}{2}\right) \right) \quad (5.43)$$

5.5 Cylinder Pressure Models

Figure 5-4 shows the airflow associated with a two-stage RC. The “air” enters through the intake port and moves through the “air” filter and then it passes through the first stage inlet/suction valve into the low-pressure cylinder to be compressed. After that, the compressed “air” passes through the outlet/discharge valve and enters the intercooler where it is cooled before it goes to the second stage. Then the cycle repeats itself for the second

stage where finally the compressed “air” passes through the outlet valve and is stored in the receiver (storage tank).

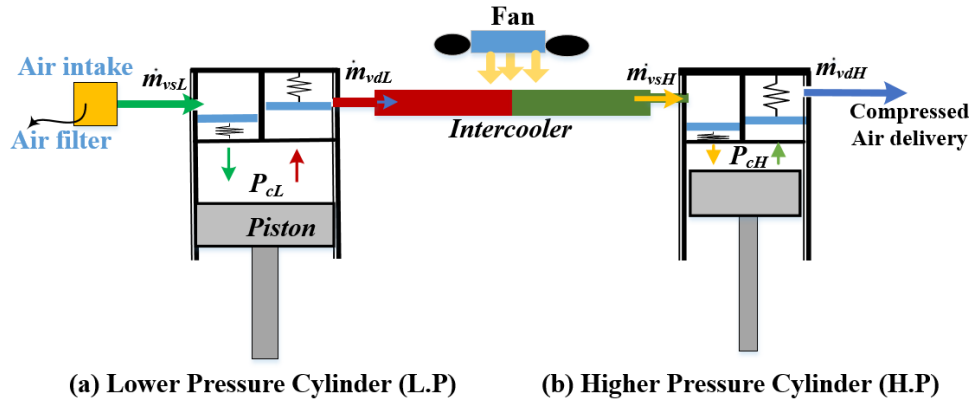


Figure 5-4: Schematic of mass flow through a two cylinder RC [24].

5.5.1 Cylinder Pressure

The assumption for modelling the cylinder pressure is that the “air” is an ideal gas and the process is isentropic, then the pressure in the cylinder is found from application of fundamental gas laws [139]:

$$\dot{P}_{cL} = \frac{1}{v_{cL}} \left[c_{sL}^2 \dot{m}_{vsL} - c_{cL}^2 \dot{m}_{vdL} - \gamma P_{cL} \dot{v}_{cL} \right] \quad (5.44)$$

$$\dot{P}_{cH} = \frac{1}{v_{cH}} \left[c_{sH}^2 \dot{m}_{vsH} - c_{cH}^2 \dot{m}_{vdH} - \gamma P_{cH} \dot{v}_{cH} \right] \quad (5.45)$$

Where \dot{m}_{vsL} , \dot{m}_{vsH} and \dot{m}_{vdL} , \dot{m}_{vdH} are the mass flow rates via the inlet and outlet valves for the lower and higher pressure stages respectively. The ratio of specific heats for the “air” is taken to be, $\gamma = 1.4$, the symbol c represents local velocity of sound, and subscripts sL and sH are for the suction chambers of both stages, and cL and cH are for each cylinder.

These are related as:

$$c_{s(L,H)}^2 = \gamma R T_{s(L,H)} \quad (5.46)$$

$$c_{c(L,H)}^2 = \gamma R T_{c(L,H)} \quad (5.47)$$

Where $R = 287 \text{ m}^2 \text{ s}^{-2} \text{ K}^{-1}$ is the universal gas constant, $T_{cL,H}$ is the average absolute temperatures of “air” in both cylinders, these can be calculated as

$$T_{C(L,H)} = T_{s(L,H)} \left(\frac{P_{c(L,H)}}{P_{s(L,H)}} \right)^{\gamma-1/\gamma} \quad (5.48)$$

Where $P_{cL,H}$ is the pressure inside each cylinder, and $P_{sL,H}$ is the suction pressure, for the low and high cylinders respectively $T_{iL,H}$ is the average “air” temperature, in Kelvin, at the inlets of the low and high cylinders respectively.

5.5.2 Cylinder Volume Equation

For the RC, the cylinder wall, its head and the cross-sectional area at the piston are viewed as the boundaries of the control volume. According to Elhaj [24], the instantaneous cylinder volumes $v_{cy.(L,H)}$ for the first and second stages are given by:

$$v_{cy.L} = v_c + S_{p.L} x_{pL} \quad (5.49)$$

$$v_{cy.H} = v_c + S_{p.H} x_{pH} \quad (5.50)$$

Where v_c is the volume of “air” remaining above the cylinder at TDC, $S_{p.(L,H)} = \pi/4 d_{L,H}^2$ are cross-section areas of the pistons, $d_{L,H}$ are the respective piston diameters, and x_{pL} and x_{pH} are the respective distances of the pistons from their reference points. By substituting the values from Eq. (5.35) and Eq. (5.36) into Eq. (5.49) and Eq. (5.50), $v_{cy.(L,H)}$ cylinder volume above the piston in the lower and higher pressure cylinders is:

$$v_{cy.L}(t) = v_{cL} + S_{p.L} \left\{ r(1 - \cos(\theta)) + l \left(1 - \sqrt{1 - \frac{r^2}{l^2} \sin^2(\theta)} \right) \right\} \quad (5.51)$$

$$v_{cy.H}(t) = v_{cH} + S_{p.H} \left\{ r \left(1 - \cos \left(\theta + \frac{\pi}{2} \right) \right) + l \left(1 - \sqrt{1 - \frac{r^2}{l^2} \sin^2 \left(\theta + \frac{\pi}{2} \right)} \right) \right\} \quad (5.52)$$

The $\dot{v}_{c(L,H)}$ cylinder volume change rate is obtained as:

$$\dot{v}_{cy.L} = S_{pL} \times \dot{x}_{pL} \quad (5.53)$$

$$\dot{v}_{cy.H} = S_{pH} \times \dot{x}_{pH} \quad (5.54)$$

Where $\dot{x}_{p(L,H)}$ is the velocity of the first and second stage pistons, respectively.

5.6 Valves Mass Flow Model

Figure 5-5 depicts the $\dot{m}_{vsL,H}$ inlet mass flow rates and $\dot{m}_{vdL,H}$ the outlet valves mass flow rates at the cylinder pressures given by Eq. (5.44) and Eq. (5.45). The expressions for the mass flow rates can be obtained according to [140] and divided into inlet and discharge mass-flow models.

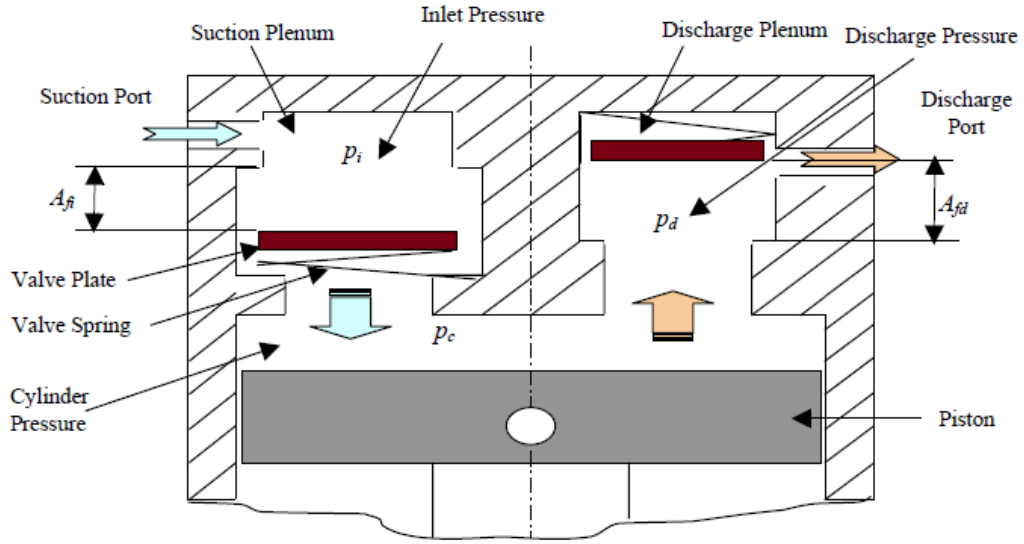


Figure 5-5: Mass flow model for inlet and outlet valves [141].

5.6.1 Inlet Valve Mass Flow Rate

The $\dot{m}_{viL,H}$ inlet mass-flow rate for the first and second stages respectively is modelled as follows [46]:

$$\dot{m}_{viL,H} = \beta_{iL,H} c_{diL,H}(x) \cdot A_{fiL,H} \sqrt{2\rho_{cL,H} |p_{iL,H}^e - p_{cL,H}|} \quad (5.55)$$

$$\beta_{iL,H} = \text{sign}(p_{iL,H}^e - p_{cL,H}) \quad (5.56)$$

$$c_{diL,H}(x) = 0.42 \frac{x_{L,H}}{x_{\max L,H}} \quad (5.57)$$

$$A_{fiL,H} = 2.\pi.r_{L,H}.d_{iff} \quad (5.58)$$

Where $\beta_{iL,H}$ is the direction of the flow, this is +1 for forward flow and -1 for backflow, $c_{diL,H}(x)$ is the variable suction coefficient, and $A_{fiL,H}$ is the area of flow surrounding the inlet valve plate as indicated in Figure 5-5. $p_{iL,H}^e$ is the suction plenum pressure.

$p_{cL,H}$ is the in-cylinder pressure of both stages and $\rho_{cL,H}$ is the “air” density inside the lower and higher cylinders and is expressed as:

$$\rho_{cL,H} = \rho_{iL,H} \left(\frac{p_{cL,H}}{p_{iL,H}} \right)^{1/\gamma} \quad (5.59)$$

$\rho_{iL,H}$ is the “air” density and is taken to be 1.177 kgm^{-3} .

5.6.2 Outlet Valve Mass Flow Rate

The rate of flow of “air” through the discharge valve for the first and second stages, $\dot{m}_{vdL,H}$, is modelled as:

$$\dot{m}_{vdL,H} = \beta_{dL,H} c_{ddL,H}(x) . A_{fdL,H} \sqrt{2\rho_{cL,H} |p_{cL,H} - p_{dL,H}^e|} \quad (5.60)$$

$$\beta_{dL,H} = \text{sign}(p_{cL,H} - p_{dL,H}^e) \quad (5.61)$$

$$c_{ddL,H}(x) = 0.35 \frac{x_{L,H}}{x_{\max L,H}} \quad (5.62)$$

$$A_{fdL,H} = 2.\pi.r_{L,H}.d_{dff} \quad (5.63)$$

Where $\beta_{dL,H}$, $c_{ddL,H}(x)$, $A_{fdL,H}$, $p_{dL,H}^e$ and $p_{cL,H}$ are as described above, see Section 5.5.1.

5.7 Valve Motion Modelling

Reciprocating compressor valves normally open and close once in each cycle and the movement of its plate, from fully closed to fully open is driven by the differences of the pressure across the valve plate while the piston travels upwards increasing the in-cylinder pressure [104, 142]. Thus, the valve plate movements are non-linear processes [15, 143]

which involves a number of events: a linear movement of the plate, the impact of the valve plate upon its seat, and the rapid opening of the valve [144, 145].

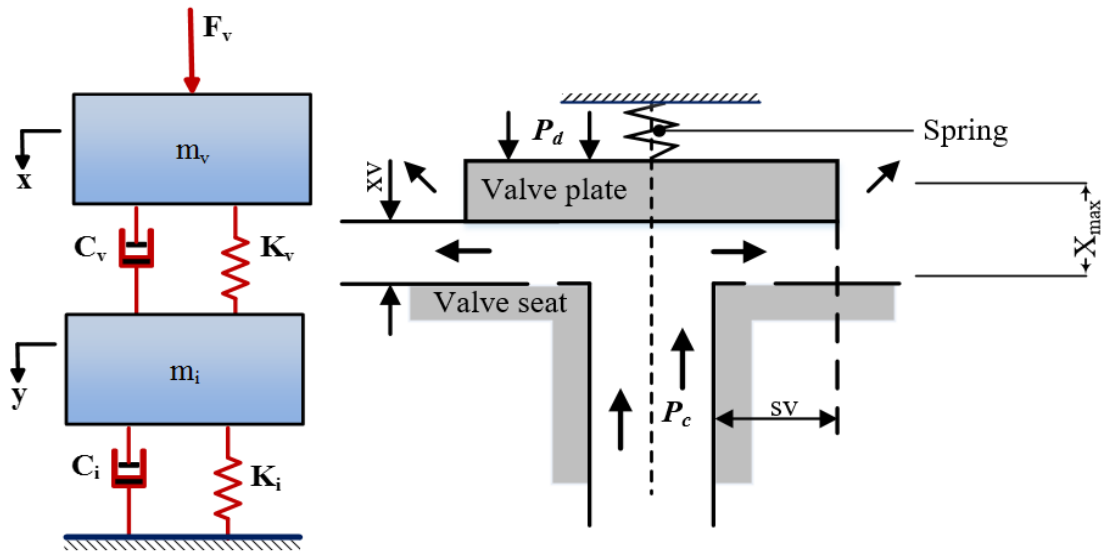


Figure 5-6: Schema of a plate valve (motion is taken to be single-degree-of-freedom)

Generally, RC inlet and outlet valves have the same design, see Figure 4-2, in which each valve is constructed with a spring and a valve plate in a similar chamber. Forces acting on the valve plate drive the plate either upwards or downwards. This movement results from three contributing factors: firstly, the pressure variation throughout the valve, secondly, the force exerted by the spring, and finally, resistance forces existing in the early stages of the opening of the valve [46]. The valve plate motion prior to impact is assumed linear and considered as a single DOF system as illustrated in Figure 5-6. The valve is modelled as a mass, spring and damper system.

5.7.1 Inlet Valve Motion

The equation of motion (EOM) for the inlet valve and force of the “air” acting on the plate during the opening and closing process is described according to Newton’s second law, as follows:

$$m_{vsL,H}\ddot{x}_{vsL,H} + c_{sL,H}\dot{x}_{vsL,H} + k_{vsL,H}x_{vsL,H} = \sum f_{vsL,H} \quad (5.64)$$

When the valve is totally open or totally closed, then the EOM of the suction valve becomes:

$$m_{vsL,H}\ddot{x}_{vsL,H} + c_{csL,H}\dot{x}_{vsL,H} + k_{cvsL,H}x_{vsL,H} = \sum f_{vsL,H} \quad (5.65)$$

$$m_{sL,H} = m_{plate} + \frac{1}{3}m_{spring} \quad (5.66)$$

Where $m_{sL,H}$ is the corresponding inlet valve mass, m_{plate} is the valve plate mass and m_{spring} is the spring mass. $c_{sL,H}$ the damping coefficient $k_{vsL,H}$ is spring stiffness which is assumed non-linear, $c_{csL,H}$ is the contact damping coefficient, $k_{cvsL,H}$ is the stiffness of the valve plates and valve seat while in contact, for both cylinders. $\ddot{x}_{vsL,H}$, $\dot{x}_{vsL,H}$ and $x_{vsL,H}$: are acceleration, velocity and displacement of the valve, respectively.

The $\sum f_{vsL,H}$ can be obtained as follows:

$$\sum f_{svL,H} = fvs_{L,H} - fgs_{L,H} - fso_{L,H} \quad (5.67)$$

Where $fvs_{L,H}$ is the pressure force on the inlet valve for both stages and can be calculated as:

$$fvs_{L,H} = cfs_{L,H}sv_{L,H}(pi_{L,H} - pc_{L,H}) \quad (5.68)$$

Where $cfs_{L,H}$ is the force coefficient, $sv_{L,H}$ is the area across which the force acts, $pi_{L,H}$ the inlet plenum pressure, $pc_{L,H}$ is the pressure inside the cylinder.

$fgs_{L,H} = -mg_{L,H}$ is the gravitational force acting on the inlet valve in the first and second stages respectively, and $fso_{L,H}$ is the pre-set spring force [140].

5.7.2 Outlet Valve Motion

The EOM of the discharge valve during the opening and closing process is described using the Newtonian law: Force = mass x acceleration,

$$m_{vdL,H}\ddot{x}_{vdL,H} + c_{cdL,H}\dot{x}_{vdL,H} + k_{cvdL,H}x_{vdL,H} = \sum f_{vdL,H} \quad (5.69)$$

When totally open or totally closed, the EOM of the discharge valve is:

$$m_{vdL,H}\ddot{x}_{vdL,H} + c_{cdL,H}\dot{x}_{vdL,H} + k_{cvdL,H}x_{vdL,H} = \sum f_{vdL,H} \quad (5.70)$$

Where $m_{vdL,H}$ is the discharge valve corresponding mass and can be obtained as described earlier for the inlet valve, see Eq. (5.66), $c_{dL,H}$ is the coefficient of damping, $k_{vdL,H}$ is the stiffness of the spring, $C_{cdL,H}$ is the contact damping coefficient, $k_{cvdL,H}$ is the discharge valve plate and valve seat stiffness while in contact, $\ddot{x}_{vdL,H}$, $\dot{x}_{vdL,H}$ & $x_{vdL,H}$: acceleration, velocity and displacement of discharge valve.

For the outlet valve, the total force on the plate $\sum f_{vdL,H}$ can be obtained as:

$$\sum f_{dvL,H} = fvd_{L,H} - fgd_{L,H} - fdo_{L,H} \quad (5.71)$$

Where $fvd_{L,H}$ is the force due to the pressure for both discharge valves:

$$fvd_{L,H} = cfd_{L,H} Sv_{L,H} (pc_{L,H} - pd_{L,H}) \quad (5.72)$$

Where $cfd_{L,H}$ is the force coefficient, $sv_{L,H}$ is the area across which the force acts, $pc_{L,H}$ is the pressure inside the cylinder, $pd_{L,H}$ is the discharge plenum pressure. $fgd_{L,H} = -mg_{L,H}$ is the weight of the outlet valve for both cylinders, $fso_{L,H}$ is the pre-set spring force [140].

5.8 Fault Simulation

According to [15], the most frequent source of compressor failure is valve damage. Seepage from the intercooler is another common fault that may occur in a compressor. Therefore, this research focuses on the simulation of discharge valve seepage, intercooler seepage and will examine their effects on compressor performance. The simulation provides the prediction of each fault signature, then comparison of these signatures with experimental results for model validation. The simulation results should also provide helpful guidance in examining the experimental data. After that, the model should be able to predict different fault signatures with different severities. In addition, any faults of the prime mover such as an electrical motor can also affect the efficiency of the RC. Different types of faults may occur in the induction motor, e.g., stator asymmetry, broken rotor bar, etc. The following subsections explain the simulation of the seepages through the valve and intercooler pipe.

5.8.1 Outlet Valve Seepage Simulation

Valve seepage occurs when there is damage to the valve plate or valve seat, usually caused by the high temperature, the rapid movement and impacts of the valves. The operating environment of the discharge valve is harsher than that of the suction valve (higher temperatures and pressures), so seepage is much more common in discharge valves than inlet valves [146].

It has been decided, see Section 4.3.1, to simulate seepage through the discharge valve as a hole of 0.2 mm diameter drilled in the valve plate. The simulation considered the seepage as a simple orifice in parallel to the normal valve flow. The pressure inside the second stage cylinder in Eq. (5.45) was modified to include an additional mass flow term (\dot{m}_{vdH}) to allow for the seepage via the discharge valve of the higher cylinder

$$\dot{p}_{cH} = \frac{1}{V_{cH}} [c_{iH}^2 \dot{m}_{viH} - c_{cH}^2 \dot{m}_{vdH} - \gamma p_{cH} \dot{v}_{cH} - c_{cH}^2 \dot{m}_{vdH}] \quad (5.73)$$

The rate at which mass flows through the outlet valve via the orifice can be obtained based on Eq. (5.60) as:

$$\dot{m}_{vdH} = \beta_{dlH} c_{ddH}(x) A_{dl} \sqrt{2\rho_{cH} |p_{dH}^e - p_{cH}|} \quad (5.74)$$

Where, $\beta_{dlH} = \text{sign}(P_{dH} - P_{cH})$ represents the direction of the flow, see above, $c_{ddH}(x)$ represents a variable coefficient of discharge, A_{dl} is the seepage area for the second stage discharge, p_{dH}^e is the pressure in the discharge plenum, p_{cH} is the in-cylinder pressure of the second stage cylinder, ρ_{cH} is the “air” density and is taken to be 1.177 kgm^{-3} .

5.8.2 Intercooler Seepage Simulation

The assumption is made that the intercooler pipe of the RC was leaking. The simulation considered the seepage as a simple orifice in parallel to the normal flow through the intercooler pipe. An additional mass flow term (\dot{m}_{in}) to allow seepage via the intercooler, can be represented by the following expressions [35]:

$$\dot{p}_{in} = \frac{1}{V_{in}} [c_{cL}^2 \dot{m}_{vdL} - c_{iH}^2 \dot{m}_{viH} - c_{in}^2 \dot{m}_{in}] \quad (5.75)$$

$$\dot{m}_{in} = \beta_{in} c_{in}(x) A_{in} \sqrt{2\rho_{in} |p_{in} - p_o|} \quad (5.76)$$

Where $\beta_{in} = \text{sign}(p_{in} - p_o)$, as above, represents the direction of the flow and $A_{in} = 2\pi r x$ is the flow area of the leak which allows the “air” to flow out from the pipe.

5.8.3 Stator Short Circuit Simulation

Stator fault is simply modelled by increasing the resistance towards infinity during the simulation. Resistance and flux linkage matrices in the $qd0$ reference frame for the healthy motor as defined in Eqs. (5.20 and 5.21) [56]. For the simplicity, the assumption is that the stator fault occurs only in phase a in the stator. Resistance matrix of the stator with shorted turns in the $qd0$ reference frame can be derived as [138]:

$$r_{sf}^{qd0} = r_s \begin{bmatrix} r_{s(11)} & 0 & r_{s(13)} \\ 0 & r_{s(22)} & 0 \\ r_{s(31)} & 0 & r_{s(33)} \end{bmatrix} \quad (5.77)$$

where r_{sf}^{qd0} is the matrix for the faulty motor stator winding resistance. Taking g_{as} to be the percentage of the remaining un-shortened winding in stator phase a , then the non-zero elements of the matrix r_{sf}^{qd0} Eq. (5.77) can be defined as [56, 138]:

$$\begin{aligned} r_{s(11)} &= \frac{1}{3}(2g_{as} + 1) \\ r_{s(13)} &= \frac{2}{3}(g_{as} - 1) \\ r_{s(22)} &= 1 \\ r_{s(31)} &= \frac{1}{3}(g_{as} - 1) \\ r_{s(33)} &= \frac{1}{3}(g_{as} + 1) \end{aligned} \quad (5.78)$$

5.9 Implementation Procedure

To implement the model, a MATLAB code was compiled and used to simulate compressor operation. The model equations were solved using the “fourth order Runge-

Kutta algorithm” [24, 35, 140] known for its efficiency and stability. A MATLAB platform was used to solve the differential equations representing non-stiff systems. The movements of the valves on impact contain transients, so there some stiffness in the resulting movement of the valve. If the transient step size is too large then inaccurate solutions will result, but if the step size is too small the solution will take too long a time to compute [35]. Taking these considerations into account a suitably size of step was chosen for the simulation process to give repeatable and stable solutions for the motion of the valve.

The simulation describes the crankshaft mechanism, valve mass flow and cylinder pressure. Figure 5-7 shows the flowchart of the process. The required parameters that serve as input data for the simulation of the RC test rig are listed in Section 5.9.1, Tables 5.1 to 5.4. The model implementation predicts the values of the cylinder pressure, cylinder volume and valve movement. The simulation began with the piston in the first stage at TDC ($\theta = 0^\circ$). At this point in the cycle both valves, inlet and outlet, are closed and the pressure in the cylinder is low. The piston in the second stage leads the first by 90° . Thus, initially, the second stage piston is at the mid-point of its suction, or downward, stroke with a pressure that is higher than that in the first-stage. The cycle finishes at TDC ($\theta = 360^\circ$).

The volume enclosed above the piston when it is at TDC is taken to be the initial volume of the cylinder [35, 46]. The temperature and pressure of this “air” trapped above the piston are considered equal those of the discharge. The crankshaft instantaneous angular speed was obtained by computing Eq. (5.24). Then, computing pressure, Eqs. (5.44 and 5.45) and mass flow, Eqs. (5.55 and 5.60) for the inlet and outlet valves respectively, the mass and pressure of the “air” above the piston were found based on the conservation of energy [24, 35, 104].

the time derivative of the volume above the piston $\dot{v}_{c(L,H)}$, was found by means of Eqs. (5.51 and 5.52) for both cylinders. Four equations of valve motion, Eqs. (5.64, 5.65, 5.69 and 5.70) describe how the valve dynamics were used to determine lift for both inlet and outlet valves for both stages [24, 104]. The equation of state, Eq. (5.35), was used to calculate the average absolute temperatures of the “air” in both cylinders $T_{c(L,H)}$.

To determine the conditions in the first cylinder the simulation began by assuming a value for the cylinder pressure. Eq. (5.44), for cylinder pressure, and Eqs. (5.55 and 5.60) for the inlet/outlet valve mass flow rate equations, were used to find the in-cylinder mass flow and pressure. This was repeated until the initial assumed, and calculated cylinder pressures were sufficiently close [24, 35]. Then the temperature in the cylinder was computed using Eq. (5.48). The expansion process (suction) continued until the inlet valve opened. When the piston reaches BDC, the inlet valve closes. Then, the compression stage starts, where the pressure in the cylinder, inlet/outlet mass flow rates and temperature of the “air” in the cylinder were found following steps parallel to those implemented during the expansion stage.

After the completion of the compression process, the outlet valve opens and discharge commences, the values of temperature and pressure within the cylinder were found by following a process parallel to that of the expansion [104]. Discharge begins immediately with the opening of the outlet valve. Throughout the discharge process, the temperature and pressure in the cylinder were determined following a process parallel to suction. When the piston reaches TDC, the outlet valve closes and discharge is completed, the computed values of the pressure and temperature in the cylinder were then assessed against the assumed values input at the beginning of the computation process, any noteworthy difference between them meant the calculation process was carried out again, taking these values as inputs for the next calculation. This process was reiterated until an acceptable level of similarity was obtained for the values at the start, and the final, computed values [24, 104].

To simulate compressor performance and operation, cylinder pressure, mass flows through the inlet and outlet valves along with other parameters were calculated in order to predict the volumetric flow rates and performance ratio. Figure 5-7 depicts the RC simulation flowchart.

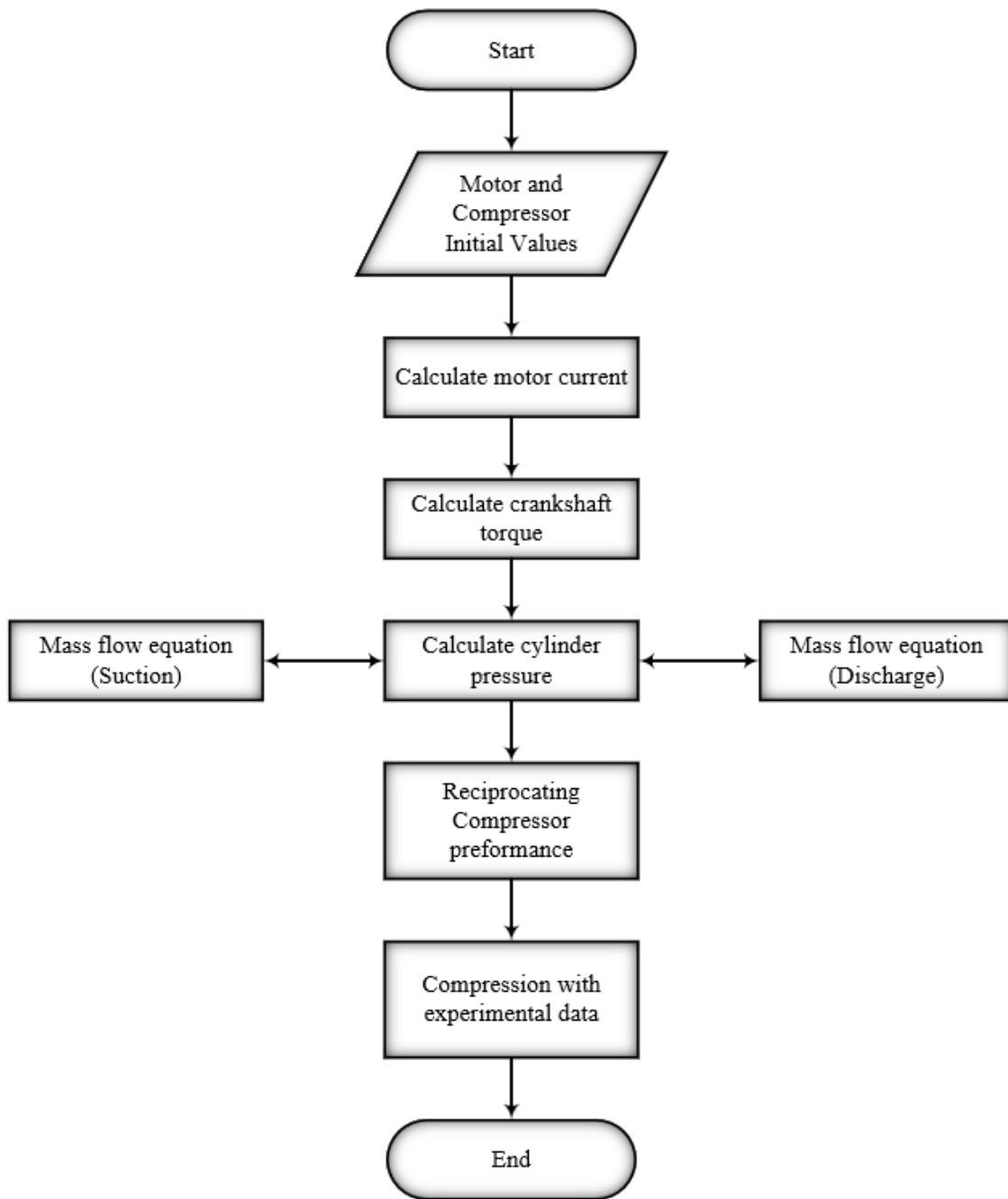


Figure 5-7: Compressor simulation model flowchart

To carry out the compressor modelling of the two-stage, healthy “air” RC, it was assumed that the “air” flow into the first stage inlet valve was at atmospheric pressure, 101.3 kPa (14.7 psi). Because the settings on the compressor were in psi, these are the values given here. The headings on the graphs below are in psi for the same reason. The outlet pressure of the first stage was 0.27 MPa (40 psi). When simulating the compressor cycle, it was accepted that the outlet of the lower pressure cylinder was directly coupled to the higher pressure cylinder inlet via the intercooler, and the inlet pressure to the second stage was assumed to be 0.20 MPa (30 psi), with the highest outlet pressure from the second stage

cylinder 0.82 MPa (120 psi). The outlet valve of the second stage was coupled to the storage “air” tank through the exhaust pipe. In order to study the effect of various discharge pressures on compressor performance, the “air” tank relief regulator was fixed at different pressures.

5.9.1 Compressor Parameters and Constants

The important compressor system parameters for cylinder, piston, valve and the associated driving motor which used to perform the experiment study have been obtained from the manufacturer. The parameters required as input data for simulating the RC are presented in tables: 5-1 to 5-4 [[122](#), [123](#)].

Table 5-1: Details of electrical motor parameters

Motor Parameters	
Motor Speed [rpm]	1420
Motor Power [Kw]	2.2

Table 5-2: Broom-Wade TS 9-16 compressor parameters

Compressor Parameters	
Number of Cylinders	2 (90° Opposed)
Compressor Speed [rpm]	425
Flywheel Ratio	3:1
Diameters of the motor pulley [cm]	12
Diameters of the compressor pulley [cm]	36
Tank Capacity [litres]	272
Piston Stroke [mm]	76.2
Connection Rod Length [mm]	171.6
Crank Radius [mm]	38.1

Table 5-3: First / Second stage piston and cylinder parameters

	Low Pressure Cylinder	High Pressure Cylinder
Piston Mass [kg]	1.78	0.89
Piston Head Diameter [mm]	93.6	55.6
Cylinder Bore [mm]	101.6	63.5
Inlet Pressure [kPa/psi]	100/14.7	270/39.2
Discharge Pressure [kPa/psi]	270/39.7	816/120
Suction temperature [°C]	21	41
Discharge temperature [°C]	50	80

Table 5-4: Compressor valve system parameters

Compressor Valve System	
Maximum Suction Valve lift [mm]	2.2
Maximum discharge Valve lift [mm]	2.6
Mass of Valve Plate, Low-Pressure Cylinder [g]	2.3
Mass of Valve Plate, High-Pressure Cylinder [g]	2.1
Mass of Valve Spring, Low-Pressure Cylinder [g]	1.0
Mass of Valve Spring, High-Pressure Cylinder [g]	2.0
Outer Radius Valve Plate, Low Pressure Cylinder [mm]	21.0
Outer Radius Valve Plate, High-Pressure Cylinder [mm]	14.0
Inner Radius Valve Plate, Low-Pressure Cylinder [mm]	12.5
Inner Radius Valve Plate, High-Pressure Cylinder [mm]	10.5

5.10 Model Evaluation under Healthy Operation

The RC model was tested under three second stage discharge pressures 60 psi, 90 psi and 120 psi in order to obtain characteristic features for the CM of RC and fault diagnosis. Here the model simulated the dynamic responses under healthy operating conditions.

5.10.1 Compressor Valve Operations

Generally, compressor valves open and close once in each compressor cycle. The pressure difference between that inside the cylinder and the relevant plenum controls the opening and closing time of the valves.

Operations of Compressor Valves

Figure 5-8 illustrates the predicted displacements of the first stage valves and their corresponding crank angles. For discharge pressure 120 psi, it can be clearly seen that the inlet valve is predicted to open (SVO_L) at a crankshaft angle of 41.6°, and the discharge valve is predicted to open (DVO_L) at an angle of 299.4°. The closing of the suction and discharge valves are predicted as SVC_L = 193.7° and DVC_L = 357°.

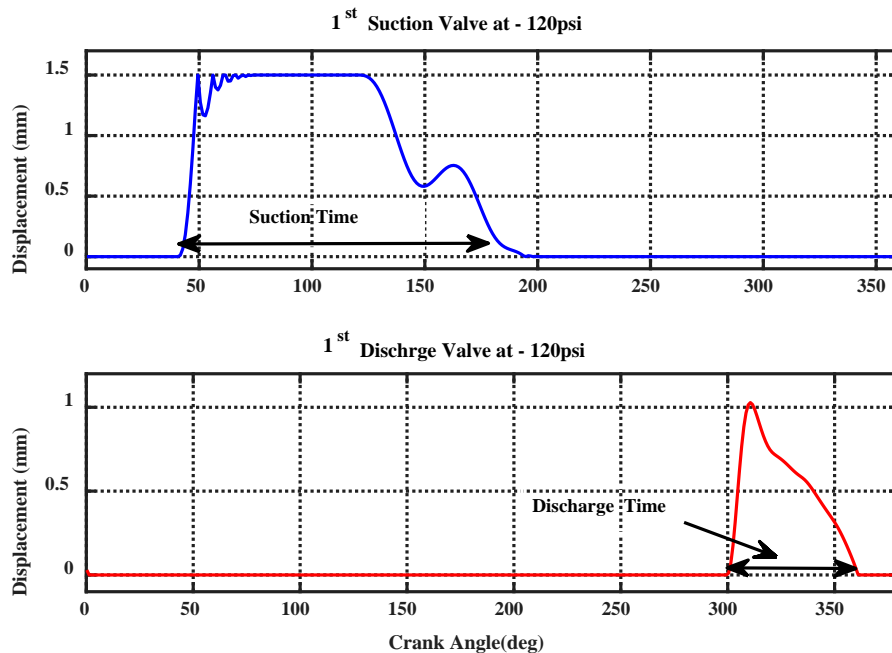


Figure 5-8: The predicted motion of first stage valves of a healthy compressor for second stage discharge pressure of 120 psi.

The second stage piston (the higher-pressure cylinder) leads the first stage by 90°, thus when the first stage piston is at TDC, the inlet valve of the second stage will be open and

the discharge valve will be closed. Figure 5-9 shows the predicted inlet and discharge valve displacement at 120 psi discharge pressure. It is obvious that the precise timing of the discharge opening and closing depend on the discharge pressure. The higher the discharge pressure, the later the valve will open. In Figure 5-9, the crankshaft angles at which the timing of opening and closing of suction and discharge valves are clear, and it can be seen that the inlet and discharge valves are predicted to open at crankshaft angles of 302.5° and 188.5° respectively. The closing of the suction and discharge valves are predicted at crankshaft angle of 103.1° and 274.9° respectively.

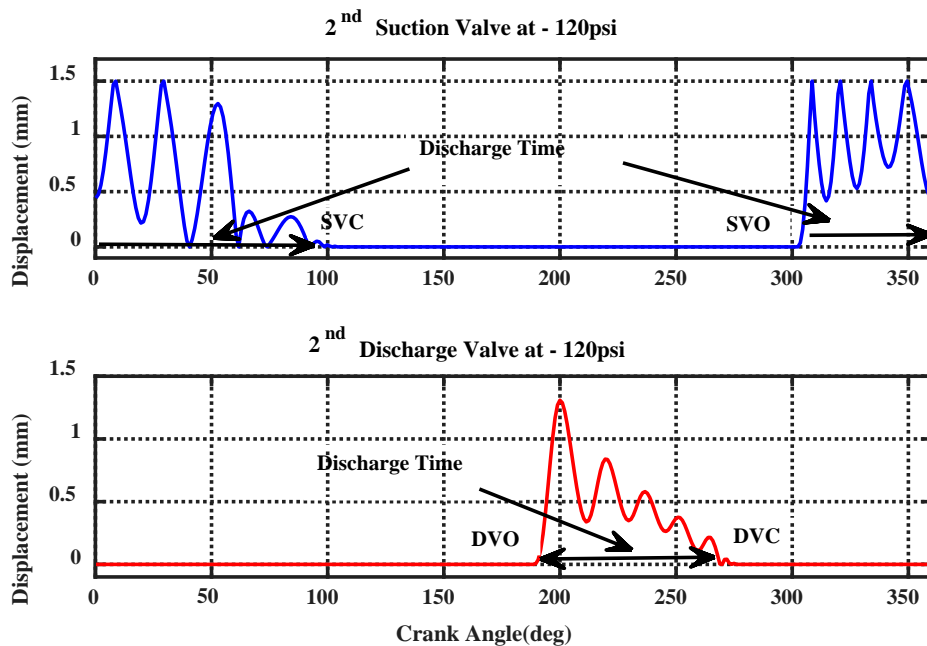


Figure 5-9: The predicted motion of second stage suction and discharge valves of a healthy compressor for second stage discharge pressure of 120 psi.

5.10.2 Comparison of Measured and Predicted Cylinder Pressures

Figure 5-10 presents both simulated and measured values of in-cylinder pressures for both cylinders. The solid blue line in this figure clearly shows the four working processes (expansion, suction, compression and discharge) of the first stage cylinder. The figure shows the downward movement of the piston, expansion of the “air”, produces a speedy fall in in-cylinder pressure for crank angles in the range 0° to 40°. Once the pressure in the cylinder falls far enough, sufficiently below that in the inlet manifold, so the pressure exerted on the valve plate will cause the inlet valve to open against the action of the valve spring, and allow “air” to enter the cylinder, and the piston moves towards BDC. This lasts from 40° to about 194°. When the pressure difference between atmospheric and

cylinder is no longer sufficient to overcome the force exerted by the inlet valve spring, the valve closes and the piston starts to move upwards, compressing the trapped “air”, and the pressure increases gradually to a maximum which occurs from about 170° to about 270°. The discharge valve opens against the force exerted by the valve spring, and the compressed “air” is pushed out.

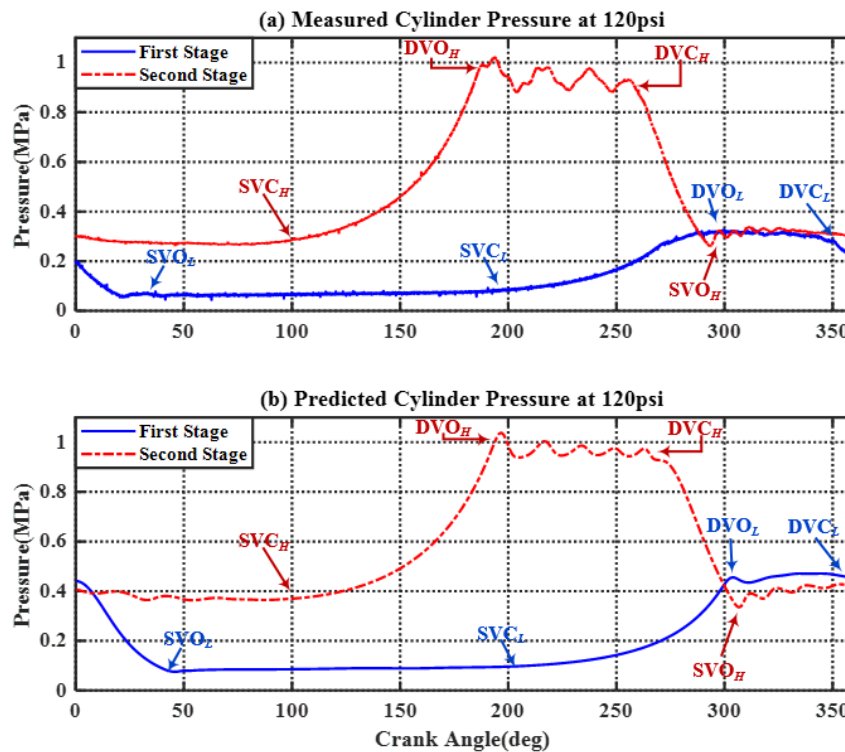


Figure 5-10: First and second stages cylinder pressures for a healthy RC: (a) Measured values, (b) Predicted values.

For the second stage, cylinder, pressures are represented by the dotted red lines in Figure 5-10. As explained earlier the second stage pressure profile leads the first stage by 90°. Thus, the second stage inlet process occurs simultaneously with the discharge process of the first stage cylinder. Comparing both waveforms, the experimental and the predicted model they show a good agreement for both cylinders and each shows the same trend demonstrating the reliability of this pressure simulation. The measured and predicted results show a slight oscillation especially in the second stage during the discharge process and this is likely caused by valve flutter.

5.10.3 Measured and Predicted Cylinder Pressure Comparison as a Function of Discharge Pressure

Figure 5-11 depicts the cylinder pressure curves of the higher cylinder for healthy compressor operation under various discharge pressures: 60 psi, 90 psi and 120 psi, respectively. Figure 5-11 (a) illustrates the experimental measurements and Figure 5-11 (b) model predictions for the compressor cycle. The cylinder pressure values in Figure 5-11 show a clear periodicity over two cycles of the compressor crankshaft.

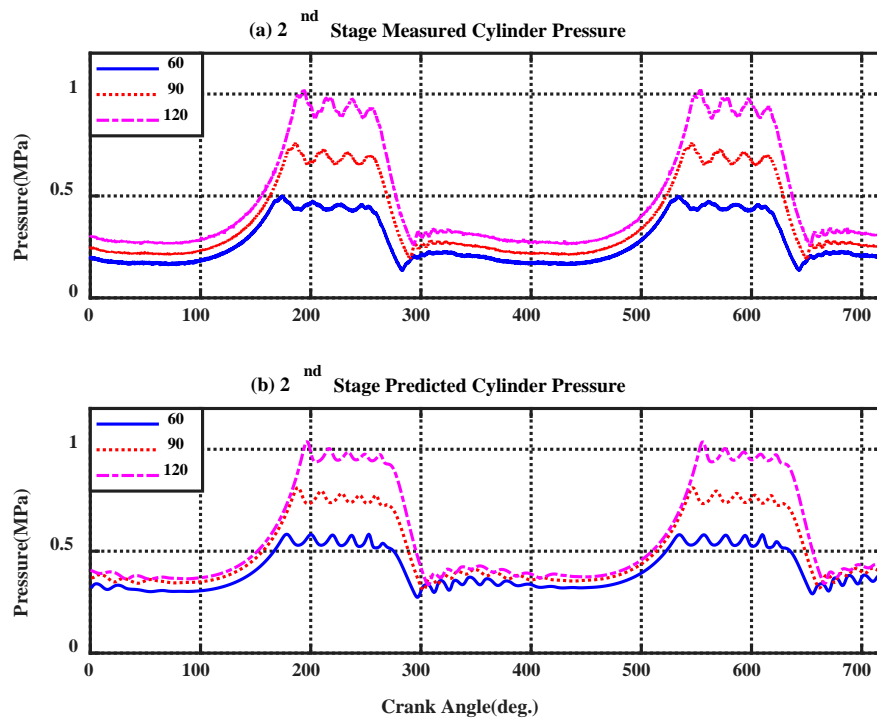


Figure 5-11: Measured and predicted second stage cylinder pressure for various discharge pressures, 60 psi, 90 psi and 120 psi.

From the figure, it can be seen that the opening of the discharge valve is delayed as the pressure increases. Similarly, the discharge valve closes earlier when the discharge pressure increases. However, the plot also shows that the higher the discharge pressure the sooner the plot of the pressure rises and the later it returns to its suction value. The waveform comparison of the experimental and the model demonstrations a good agreement for the higher cylinder pressure and have the same trend which confirms that the pressure model is reliable. The model prediction values are confirmed both quantitatively and qualitatively.

5.10.4 Discharge Valve Displacement as a Function of Discharge Pressure

Figure 5-12 illustrates the displacement of the discharge valve under various discharge pressures (different loads). As can be seen, changing the discharge pressure affected valve displacement. More importantly, the displacement amplitude has higher values as the discharge pressure increases. It can be noticed that the increases in discharge pressure delayed the opening of the valve. This change in valve displacement with the change of discharge pressure explains the rising and falling slopes of the cylinder pressure. Thus, the cylinder rising slope reflects the compression process and the delayed opening of the discharge valve, whereas, the falling slope of the cylinder pressure indicates the discharge valve closing earlier, and the commencement of the expansion process [141].

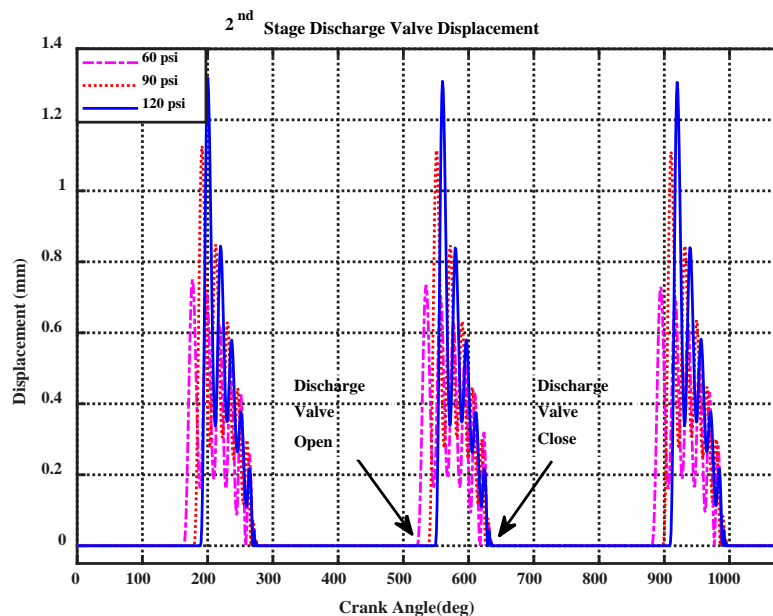


Figure 5-12: Second stage discharge valve displacement under various discharge pressures 60 psi, 90 psi and 120 psi.

5.10.5 Comparison of Measured and Predicted Motor Current Waveform

The predicted and experimentally measured current waveforms of the motor for a healthy compressor are presented in Figure 5-13 for more than three cycles. After studying the figure, it can be seen clearly that the current waveform exhibits a clear amplitude modulation (AM) effect. The compressor is under a dynamic load fluctuation during its working cycle which leads to a motor current modulation at 7.3 Hz (the working frequency of the compressor). A direct waveform comparison of experimental and model prediction shows that both waveforms exhibit a clear amplitude modulation. A good agreement can

be observed between experimental measurements and model prediction trends which confirms that the motor current model is reliable.

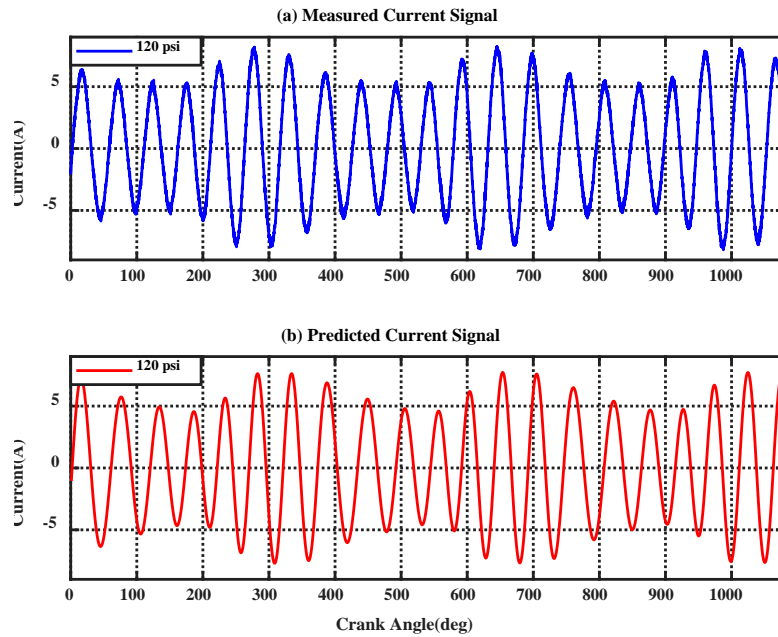


Figure 5-13: Motor current waveform for induction motor driving a healthy compressor:

(a) Measured, (b) Predicted

The motor current waveform presented in Figure 5-14 shows that current waveform amplitude from 250° – 350° crankshaft angle is higher than that from 100° – 200° crankshaft angle due to the increasing pressure required during the compression stroke.

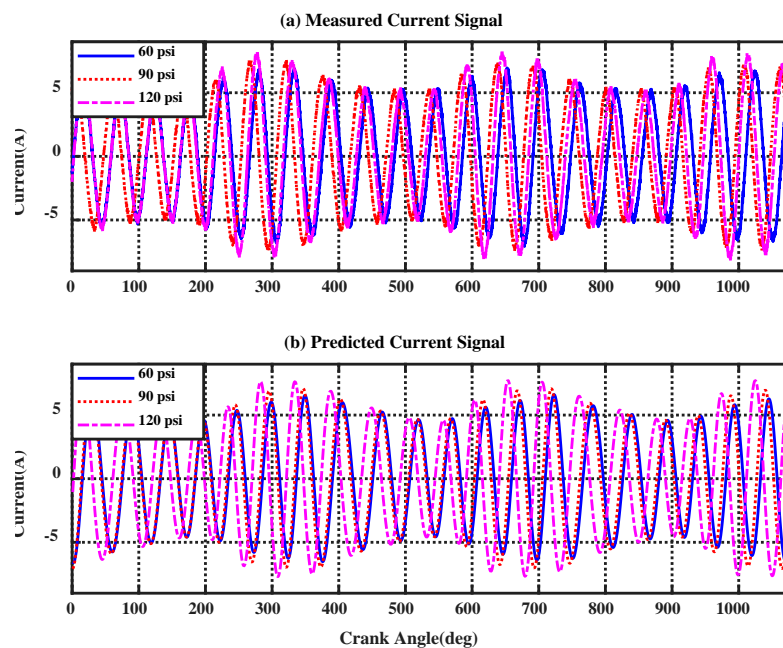


Figure 5-14: Motor current waveform for a healthy compressor under various discharge pressures 60 psi, 90 psi and 120 psi: (a) Measured, (b) Predicted

For a better understanding, the current RMS values were calculated for a broad range of compressor discharge pressures. As illustrated in Figure 5-15 the relationship between measured and predicted RMS values under different discharge pressures. The first observation from the figure is that the RMS values have the same rising trend as discharge pressure increases. Additionally, Figure 5-15 shows that motor current amplitude increases as the discharge pressure increases. Thus, the current signals could be used to attain useful information in regards to the operating condition of RC. A comparison between the experiment measurement and model prediction of the current signals demonstrates that the basic features are the same and have good consistency over a range of compressor discharge pressures. This confirms that the model is valid for different discharge pressures and it can be used for fault simulation studies.

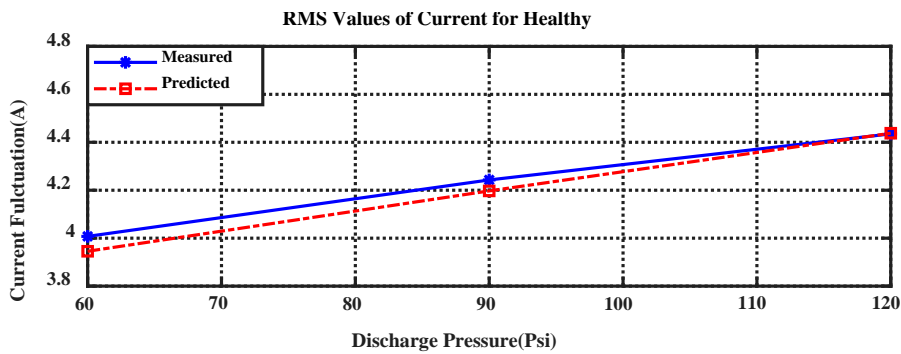


Figure 5-15: RMS values for the measured and predicted motor current of the healthy compressor as a function of discharge pressure

The comparison of the measured and predicted RMS values shows a good agreement and their values have the same trend as discharge pressure increases. However, a small divergence can be seen, especially when discharge pressure is 60 psi. This is ascribed to insufficient data on compressor and motor parameters from the manufacturer. Yet, the difference is only about 1.75% between the measured and predicted values. Table 5-5 illustrates the actual and percentage-difference between the measured and predicted RMS values of the current.

Table 5-5: Difference of RMS values for healthy compressor

	60 psi	90 psi	120 psi
Difference (Amps)	0.062	0.037	0.003
Percentage difference	1.75%	0.88%	0.07%

5.11 Model Evaluation Under Different Faulty Operations

Valve leakage as mentioned early is one of the most common faults in RCs and was simulated as an additional flow via an orifice in parallel to the normal valve flow (see Section 5.7.1). Additionally, a loose connection to the intercooler pipeline was simulated during the experimental study by loosening the nut close to the inlet valve of the higher stage, by one complete turn (see Section 4.3.2).

The developed model considers the leakages through the discharge valve and intercooler to be compared with measured results for model validation under faulty conditions. Simulation is used in each case to predict the signatures of each fault, then comparing prediction fault signature with the experimental results Figure 5-16 and Figure 5-17.

5.11.1 Cylinder Pressure Comparisons

Figure 5-16 and Figure 5-17 show model predictions and experimental results for the first and second stages under a discharge pressure of 120 psi for various operating conditions (healthy, discharge valve leakage and intercooler leakage). It can be seen from Figure 5-17, that the discharge valve leakage causes a significant effect on the pressure waveform for both stages. For the second stage cylinder pressure illustrated in Figure 5-16 (b) and Figure 5-17 (b), a noticeable deviation of the pressure waveform for valve leakage is visible during the expansion and suction strokes due to a high-pressure backflow via the discharge valve which raises the in-cylinder pressure above the normal conditions, and hence the discharge valve opens earlier in compression to the healthy operation. Another observation is that the cylinder pressure for discharge valve leakage is almost higher than that for the healthy operation.

Figure 5-16 (a) and Figure 5-17 (a) shows first stage cylinder pressure. It can be seen that leakage through the second stage discharge valve affects the discharge pressure for the first stage. The first stage cylinder pressure during discharge for leaky valve is substantially higher than the healthy condition, as a result, the valve needs more time to overcome the higher cylinder pressure and consequently, the first stage discharge valve closes late.

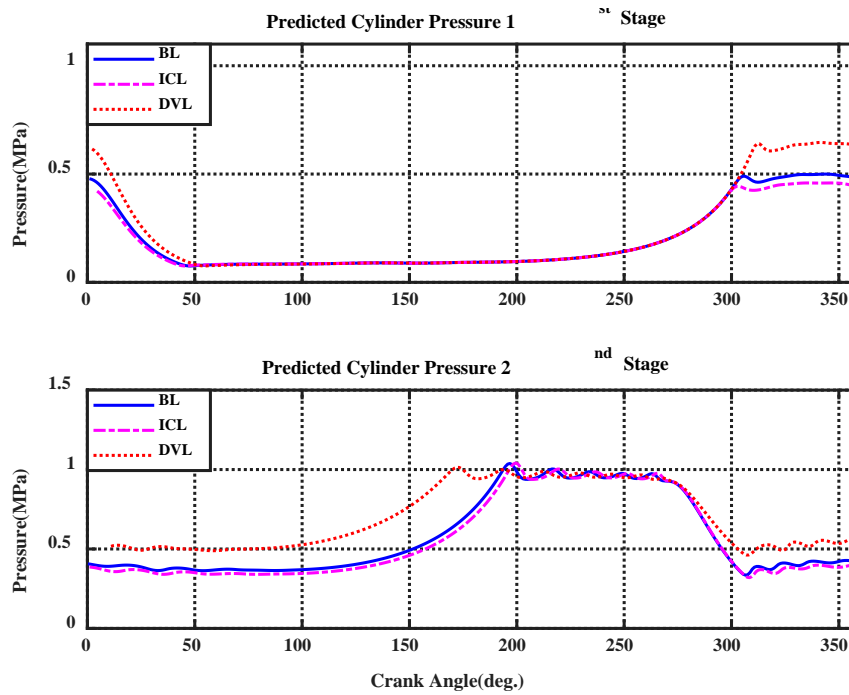


Figure 5-16: Predicted dynamic cylinder pressure in both stages under healthy (BL) and two faulty cases (ICL and DVL) at 120 psi discharge pressure

The intercooler leakage shows as a small decrement of in-cylinder pressure for both stages due to the fact that air escapes through the intercooler leak. The cylinder pressure variation is mostly seen in the higher-pressure cylinder during the suction and compression processes. Both inlet and outlet valves of the second stage opened late due to the low cylinder pressure caused by the leakage through the intercooler and this in turns reduced the compressor discharge efficiency. For the first stage cylinder, the effect of intercooler leakage is more obvious during the discharge process. This leak reduces the pressure inside the intercooler leading to the reduction of the force that keeps the discharge valve closed, so the discharge valve opens earlier than that for healthy operation. The simulated faults cause clear cylinder pressure variations in both stages and tracing the change of pressures provide the possibility of monitoring these faults. Comparison of both the measured and predicted cylinder pressures shows good qualitative agreement and this agreement is considered to be acceptable quantitatively. Hence the model is proved to be adequate for further study.

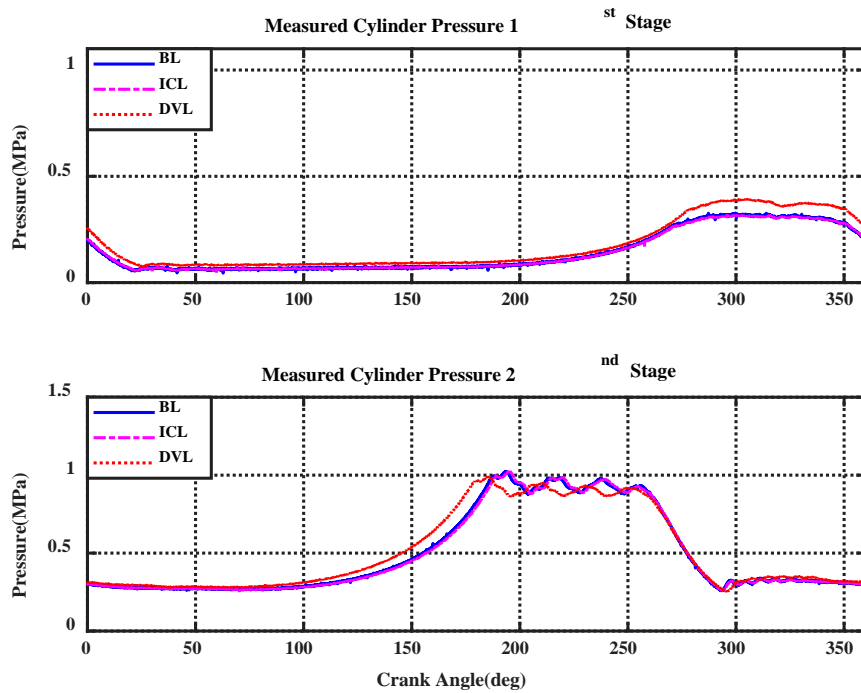


Figure 5-17: Measured dynamic cylinder pressure in both stages under healthy (BL) and two faulty cases (ICL and DVL) at 120 psi discharge pressure

5.11.2 Motor Current Waveform Comparison

The model prediction and the experimental results of the motor current at 120 psi for different operating conditions as mentioned early are illustrated in Figure 5-18. It can be seen that the predicted and measured current signals exhibit amplitude modulation due to the varying load during compressor operations. From the figure, it can be seen that different faults cause a significant change to the motor current waveform and amplitude. The motor current amplitude with discharge valve leakage is slightly higher than that for the healthy operation, this is because the leakage reduces compressor efficiency. Thus, the motor requires more power to overcome the consequence of the leakage to produce the required pressure, or a smaller flow rate would be delivered for the same motor input power. Additionally, the impact of intercooler leakage on the motor current consumption is that the current waveform amplitude is clearly less than that for the healthy condition, which means the motor requires lower power as the compressor does less work due to the lower effective cylinder pressure into the second stage compared to the healthy operation.

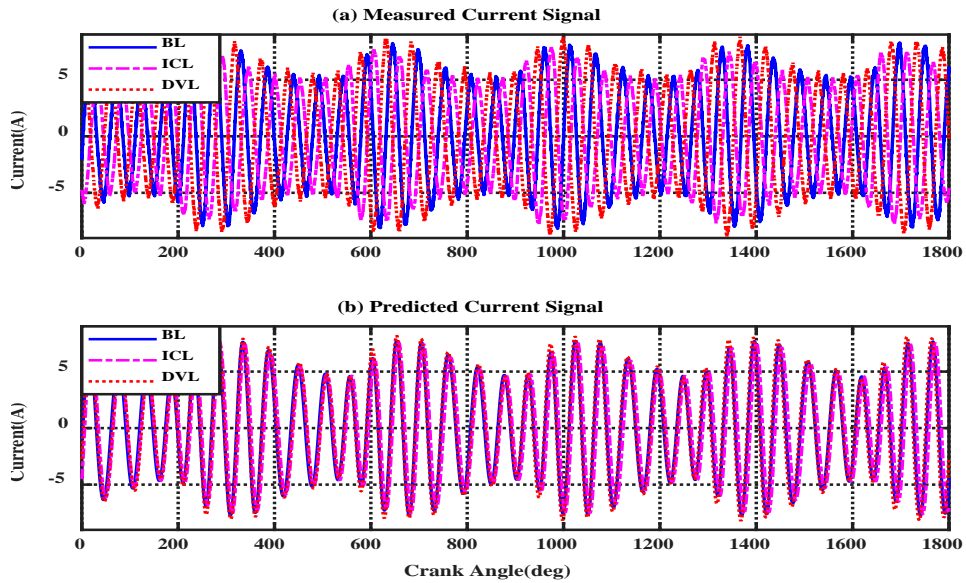


Figure 5-18: Measured and predicted motor current waveforms under healthy (BL) and two faulty cases (ICL and DVL) at 120 psi discharge pressure

Figure 5-19 shows the motor current RMS values for different operating conditions under various discharge pressures. It is very clear that the occurrence of faults causes a change in the current drawn by the motor. From Figure 5-19 the measured RMS values confirm these observations, but indicate that the predicted values correspond more closely to the measured at higher pressures.

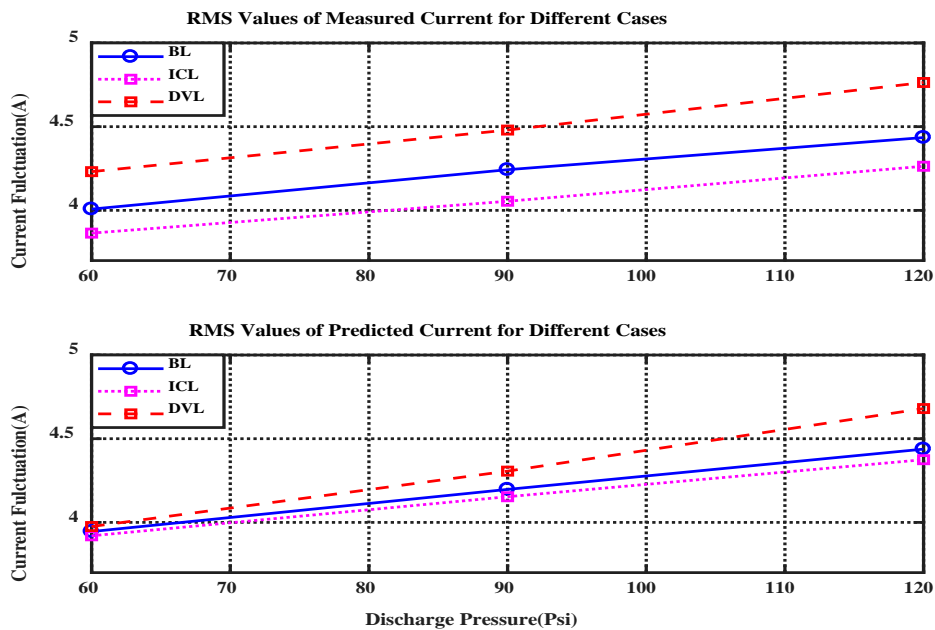


Figure 5-19: RMS values for measured and predicted motor current for compressor under healthy (BL) and two faulty cases (ICL and DVL) at three discharge pressures.

5.11.3 Comparative Spectral Analysis of Motor Currents

Normally, the motor current for a healthy motor should exhibit only one frequency component at the supply frequency of 50 Hz in the current spectrum. However, in practice, this is not the case due to such factors as motor manufacturer's errors that cause asymmetry between the motor phases, imbalance of the power supply, and fluctuation of the operating load (pressure). The measured and the predicted current spectra for both normal and abnormal conditions at 120 psi discharge pressure are depicted in Figure 5-20. As anticipated, the current spectra exhibit a clear amplitude modulation for both measured and predicted signals. The modulation effect is noticed due to the fluctuation of the compressor load and possible faults. In Figure 5-20 both healthy and faulty cases show that the supply frequency component 50 Hz has much the greatest amplitude, but is accompanied by a number of sidebands. The first pair of sideband components is at 50 ± 7.3 Hz (working frequency of the compressor) due to compressor load fluctuation. Interestingly both measured and predicted curves show a change in the magnitude of these sidebands in the occurrence of a fault, and even more interesting the direction of the changes are predicted correctly. Finally, It can be noted that the peak at $50 - 7.3$ Hz is greater than the peak at $50 + 7.3$ Hz in both measured and predicted signals.

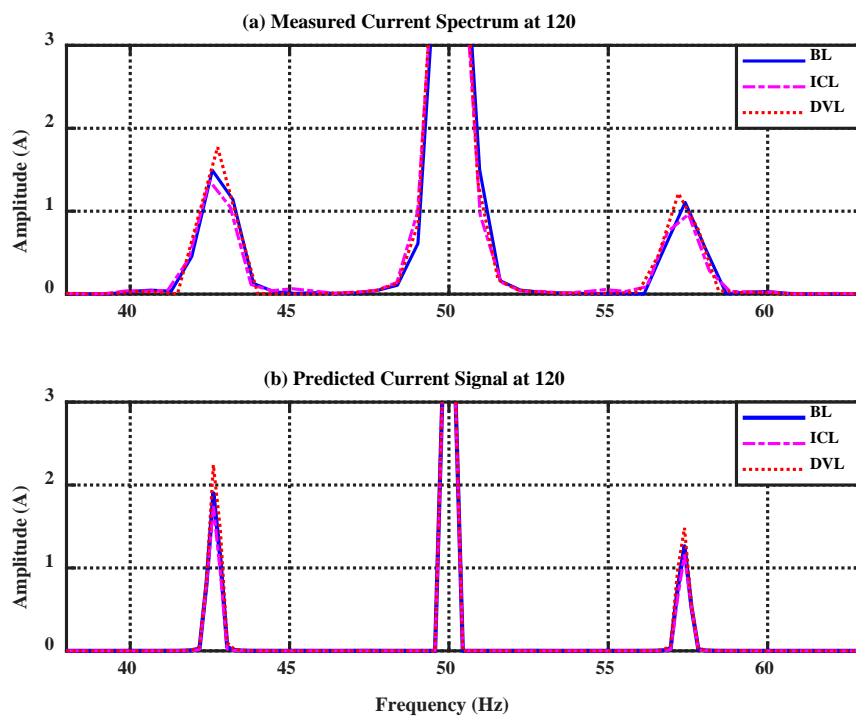


Figure 5-20: Current spectrum for healthy (BL) and two faulty cases (ICL and DVL) at second stage discharge pressure 120 psi

Figure 5-21 depicts the average amplitude of upper and lower sideband components. It can be observed that the measured sideband amplitude of the motor current increases as the compressor discharge pressure increases. The amplitudes of the sideband change according to the fault and the second stage discharge pressure. It can be seen that a clear trend, that the sideband amplitude for discharge valve leakage is greater than for the normal condition, whereas for intercooler leakage it is lower. The amplitudes of the sidebands increase monotonically with compressor discharge pressure, and this particular representation could be used to differentiate between ICL and DVL compressor faults, and hence could be used as an effective method of fault detection. Consequently, the current signals provide useful information for compressor fault detection and diagnosis.

Comparing the sideband amplitudes of both measured and predicted results, it can be concluded that both results have the same trend, see Figure 5-21 which shows good consistency over a wide range of RC discharge pressure. It is considered that the results obtained under normal and abnormal operating conditions for in-cylinder pressures and the current signals from the electrical motor have been validated by a comparative study and the experimental and simulated results show good agreement.

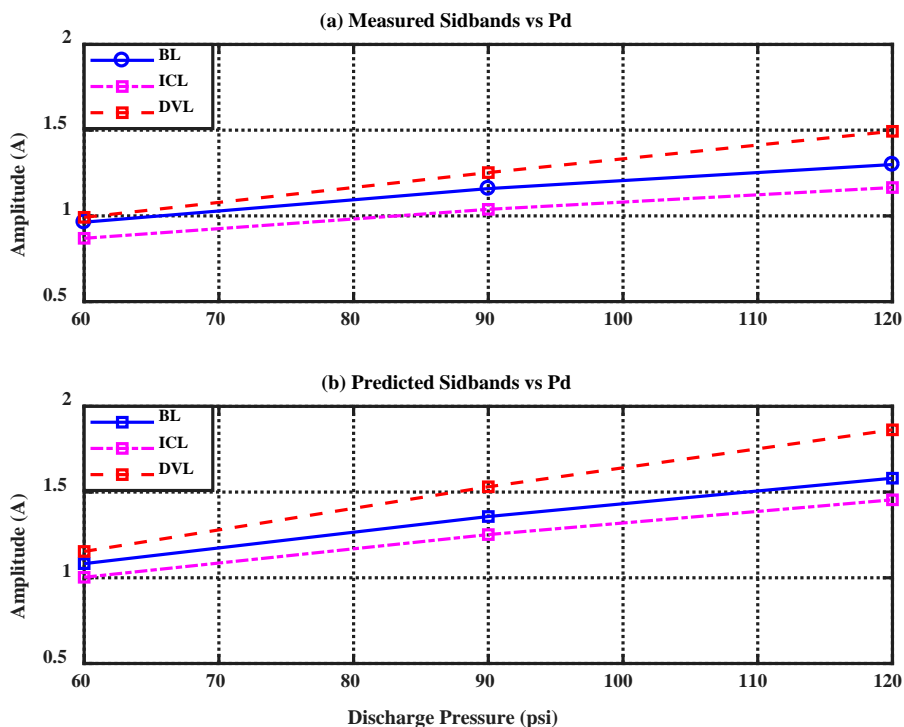


Figure 5-21: Sidebands amplitudes for healthy (BL) and two faulty cases (ICL and DVL) at three discharge pressures. (a) Measured, (b) predicted

5.12 Diagnostic Feature Extraction Based on Simulated Data

In order to help develop accurate fault detection and diagnostic approach for early-stage faults, a comprehensive compressor model has been extended to study the effect of various faults on compressor dynamic response and to predict the performance of the RC under a wide range of compressor discharge pressure. The developed model utilised the current response of the induction motor driving the RC for the purpose of CM.

Advanced signal processing technique, the modulation signal bi-spectrum (MSB) was utilized to analyse the simulated current signals in order to obtain a reliable diagnostic tool for feature extraction. Unique properties of the MSB are its sensitivity to the presence of sidebands and its ability to remove background, Gaussian noise. A typical MSB slice at the supply frequency 50 Hz for the healthy motor with healthy compressor, and then with a compressor with a faulty second stage discharge valve is shown in Figure 5-23. A number of MSB peaks appear at different orders of the first sideband, of frequency $f_r = 7.3\text{Hz}$, can be clearly seen. Another clear observation is that the amplitude of the MSB peak increases with the presence of the DVL fault. These features will allow compressor fault diagnostics to be implemented without the need for additional measurements such as pressure, temperature, etc.

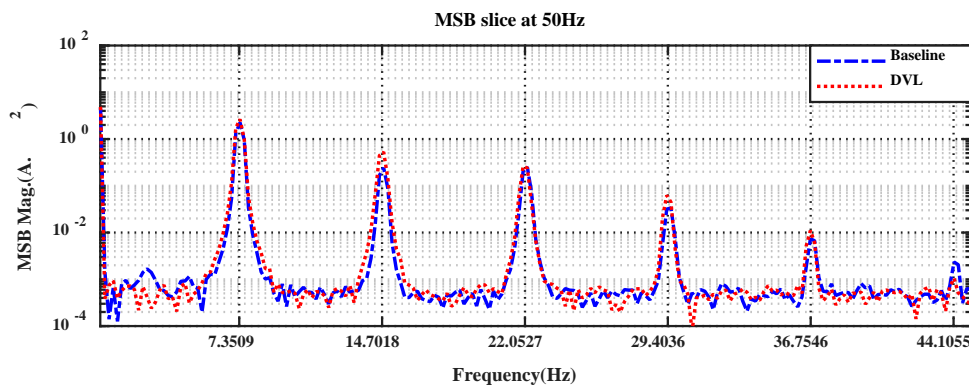


Figure 5-22: A typical MSB slice (at 50 Hz) through simulated current for healthy compressor and compressor with faulty discharge valve

Different faults have their unique characteristics which cause changes in the motor current signatures and this has been demonstrated for leakages through discharge valve and intercooler faults in the compressor itself, now the study investigates whether motor faults such as broken rotor bars and stator winding asymmetries can be simulated by the model, leading to the establishment of effective and reliable diagnostic features. A typical MSB

slice at the $f_c 50$ Hz for healthy motor and motor with both stator winding asymmetry (SWA) and a broken rotor bar (BRB) is depicted in Figure 5-23.

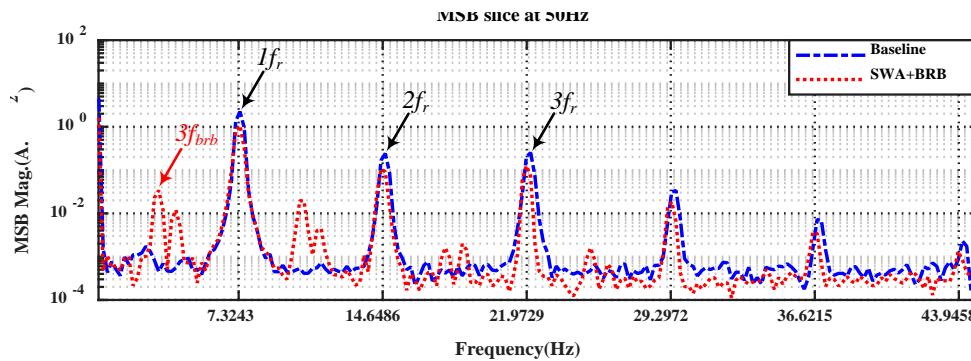


Figure 5-23: A typical MSB slice through current for healthy compressor and motor with two simultaneous faults (Stator Winding Asymmetry, SWA, and Broken Rotor Bar, BRB)

The compound fault (SWA+BRB) causes a small but noticeable decrease of the MSB peaks at multiples of compared to the healthy operation. Furthermore, an additional frequency component can be observed among the MSB peak at the twice slip frequency: $f_{brb} = 2sf_s = 3.2\text{ Hz}$. This is due to the presence of the simulated broken rotor bar fault.

Based on these analytical observations from the MSB slice of the induction motor current, four primary diagnostic features can be implemented for the feature extraction of the compressor based on the mathematical modelling:

- 1- The speed normalised by rated speed.
- 2- Current amplitude normalised by the rated current of AC motor.
- 3- Two MSB peaks (f_{brb}) are extracted from the MSB slice to differentiate different fault cases.

5.12.1 Diagnostics of Mechanical Simulated Faults

Faults occurring in either the compressor or its driving motor will induce a load fluctuation characteristic which differs from the healthy condition as can be seen in Figure 5-23. As a result, the speed pattern and the amplitudes of the MSB peak at $1f_r$ and $2f_r$ will also change. Based on this analysis, these simulated faults can be detected by studying the motor speed and the MSB peaks for any given fault. Figure 5-24 and Figure 5-25 show

the relationships between the motor current and its operating speed. It represents a way for monitoring the changes in the consumed current with the change of operating speed for different operating conditions, which may be used to identify the signature of a particular fault effectively.

Figure 5-24 illustrates the feature characteristics for simulated suction valve leakage (SVL) and discharge valve leakage (DVL) for the second stage cylinder. From the figure representation, it can be seen that SVL fault induces a small change in the cylinder pressure which affects the torque dynamics and small deviations from the healthy condition can be seen in the current signal, Figure 5-24 (a3) at the MSB peak corresponding to the second harmonic $2f_r$. The amplitudes of the difference from the baseline case are small but sufficient to differentiate suction valve leakage from the healthy operation. The presence of a DVL, on the other hand, induces a much larger change in the pressure, and this causes a much greater deviation in the MSB peak at $2f_r$ from the baseline, though small deviations can also be noted at the first MSB peak at $1f_r$. It is worth mentioning that both SVL and DVL cause a significant change in the normalised current values which can be used as a feature to separate it from other faults.

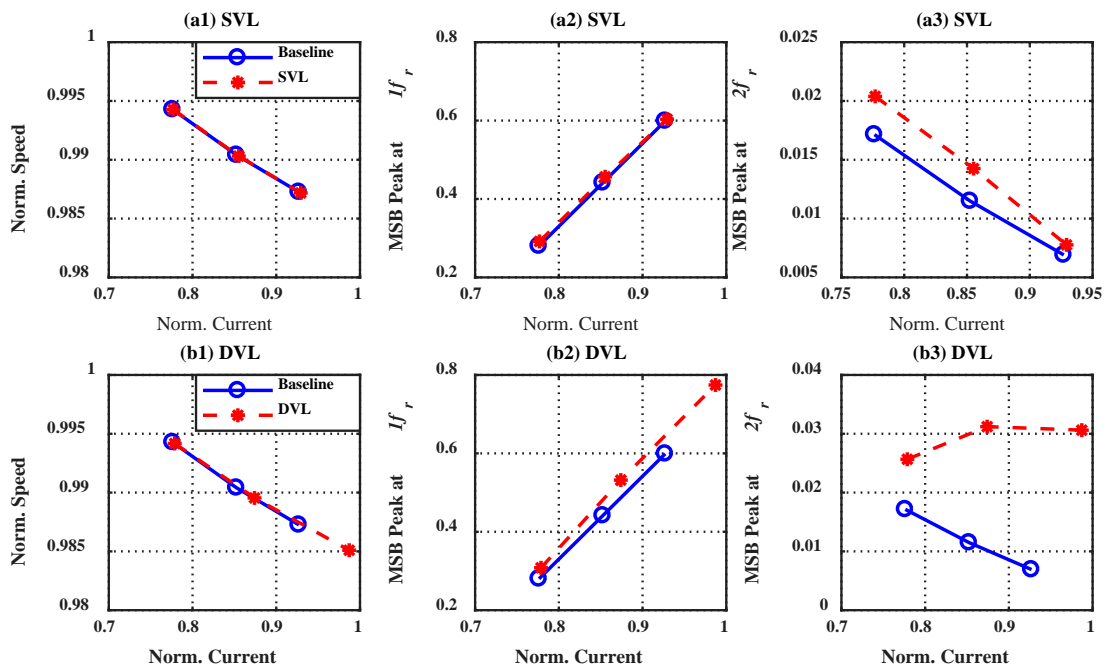


Figure 5-24: Characteristics of feature extraction for both suction and discharge valve leakage

Figure 5-25 depicts the extracted feature with MSB peaks at $1f_r$ and $2f_r$ for the simulated intercooler leakage (ICL) and loose transmission belt (LBT), respectively. From the result presented in this figure, it can be seen that ICL produces a very noticeable change from the baseline condition as the fault affects the in-cylinder pressures for both stages, which in turn has an effect on the torque dynamics. These extracted features can be useful for differentiating the ICL fault from others.

Figure 5-25 (b1-b3) illustrates the effect of the simulated LBT on the speed pattern and current signature. A small but significant deviation from the healthy speed pattern is seen in Figure 5-25 (b1). The difference from the baseline can be used to differentiate it from other faults (DVL, ICL and SVL). Even though the difference values are smaller compared with the speed patterns for other compressor faults, using the results for higher order harmonic MSB (peak at $2f_r$) for those simulated faults will ensure diagnostic accuracy.

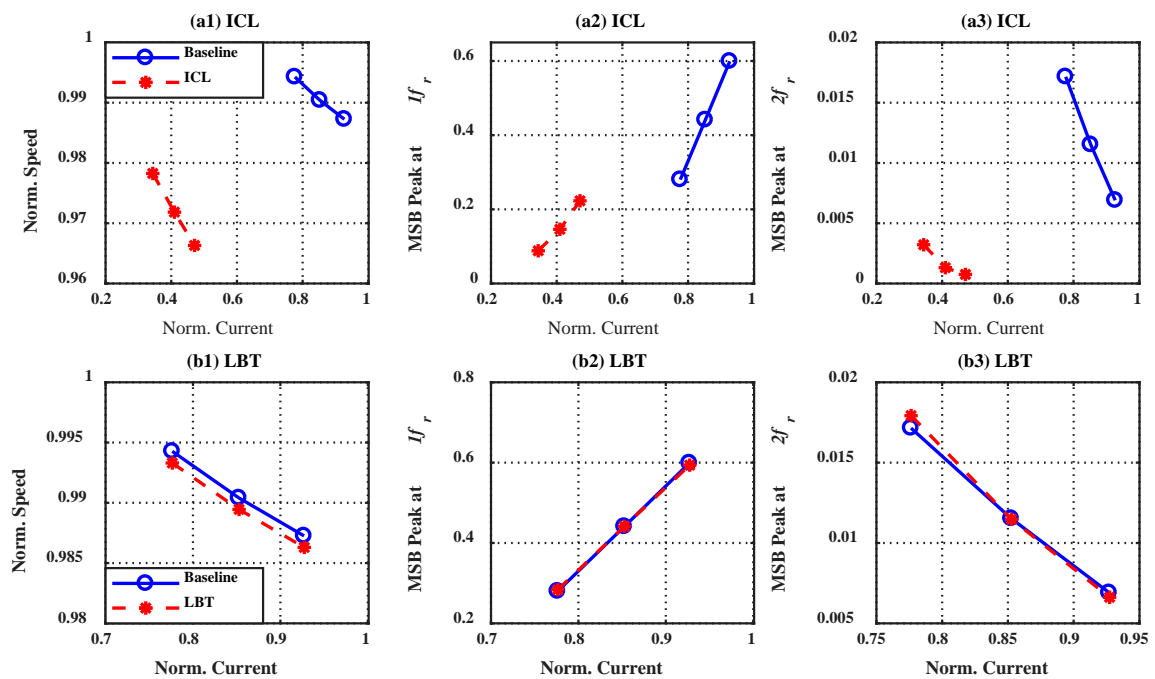


Figure 5-25: Characteristic feature extraction for intercooler leak and loose transmission belt

5.12.2 Diagnostics of Electrical Simulated Faults

Figure 5-26 represents the relationship between the consumed current and the motor speed fluctuation for simulated broken rotor bars (BRB) with different fault severities (1BRB and 2BRB). As stated above, this fault produces an additional frequency component in the

MSB peaks at twice of the slip frequency as illustrated in Figure 5-23. Thus, this fault can be monitored by studying the effect on the speed pattern and consumed current for MSB peaks at $1f_r$ and at f_{brb} . From the figure, it can be seen that there is a small deviation of the MSB peak at $1f_r$ from the healthy operation shown in Figure 5-26 (a2 and b2), whereas, a significant difference can be noticed for BRB fault at f_{brb} shown in Figure 5-26 (a3 and b3). Thus, the BRB fault with different degree of severities can be separated using this unique feature (MSB peak at f_{brb})

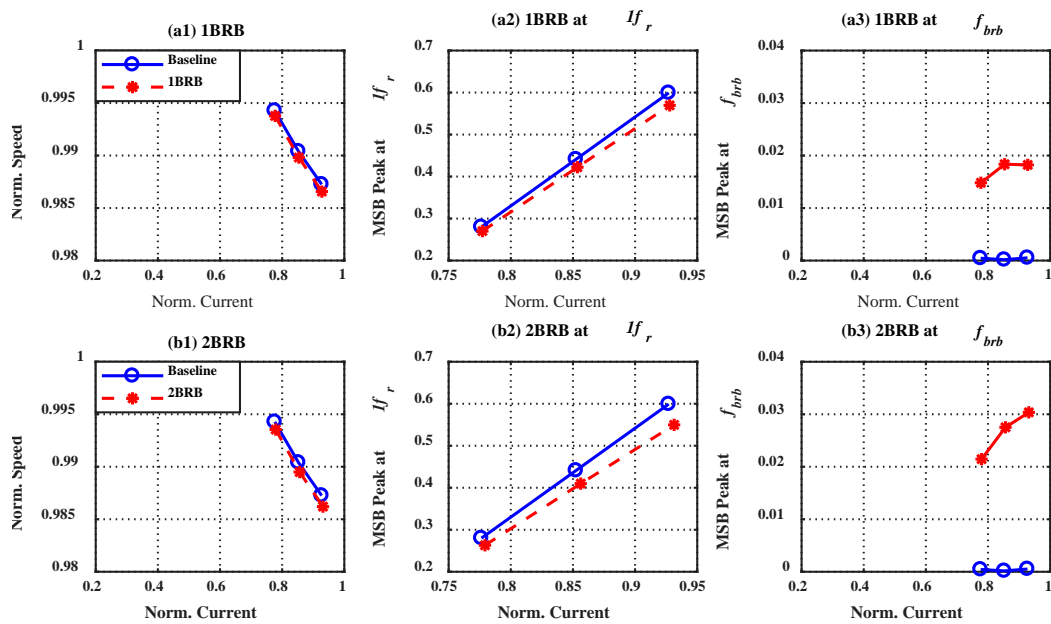


Figure 5-26: Feature characteristics for 1BRB and 2BRB faults

On the other hand, the presence of SWA increased stator phase resistance by 10%, and in Figure 5-27 (a1-a3) a clear deviations in both speed and in the MSB peak at $1f_r$. It's worth mentioning that the deviation of SWA from the baseline is significant and differs from the ICL features as shown in Figure 5-25 (a1 and a2). Thus, SWA can be easily identified.

The simulation also considers the combined fault (SWA + 1BRB) as shown in Figure 5-27 (b1-b3). A clear deviation from the baseline for the speed pattern can be noted from Figure 5-27(a) similarly for the MSB peak values. Thus, these features can be used to differentiate this fault clearly from others. Even though both the SWA and the compound fault SWA+1BRB have similar values for the speed pattern and MSB at $1f_r$ as shown in Figure 5-27 (a1 and a2) and (b1-b2) respectively, these faults can be easily separated

because of MSB peaks at f_{brb} are very different for those faults, as can be seen in Figure 5-27 (a3 and b3).

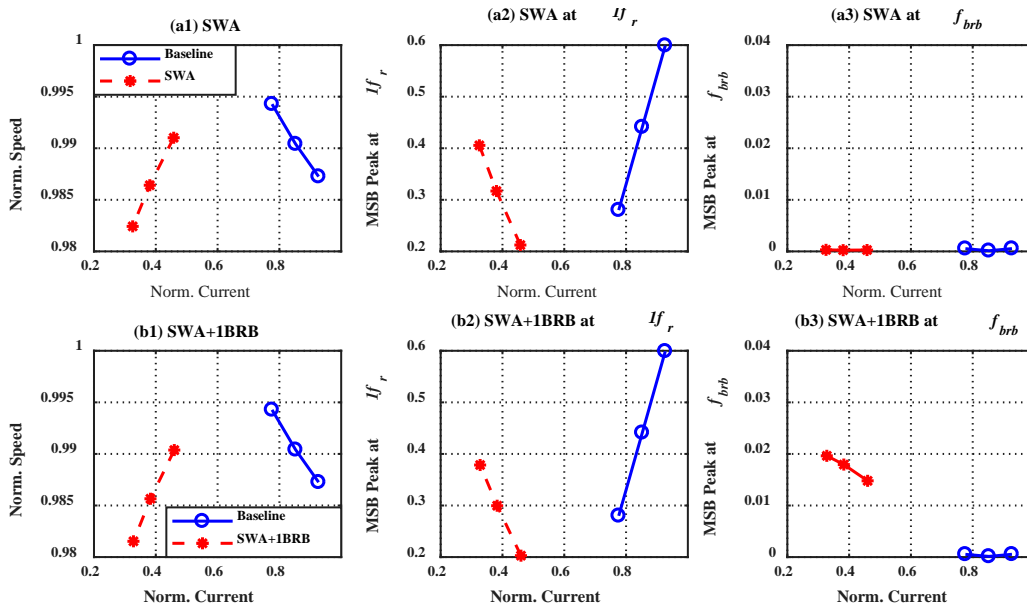


Figure 5-27: Characteristics features for stator winding asymmetry (SWA) and combined fault (SWA+1BRB)

To sum up, this comparative study has demonstrated that the fluctuations in both in-cylinder pressure and motor current waveform generated by the faults described, can be utilized for the detection and diagnosis of the faults. Consequently, fault feature extraction has contributed to applicable diagnostic approaches. The simulated results represent the changes in consumed current due to the changes in working conditions for each of the given faults and can be effectively used to identify the signatures of the faults. Additionally, MSB peaks at various harmonics offer an effective way to differentiate these fault signatures one from another.

For simulated mechanical faults: SVL and DVL can be distinguished by the MSB amplitude at $2f_r$ (Figure 5-24: a3 and b3). Whereas speed pattern and MSB peak at $1f_r$ and $2f_r$ can be used to separate ICL from other faults (Figure 5-25: a1-a3). For the LBT, the speed pattern (Figure 5-25: b1) is sufficient to diagnose this fault. For simulated faults in the motor: 1 BRB and 2 BRB Figure 5-26, a clear feature can be obtained by considering the MSB peak at f_{brb} (Figure 5-26: a3 and b3). SWA and the combined fault are diagnosed by their MSB peak values at f_{brb} (Figure 5-27: a3 and b3).

5.13 Summary

In this chapter, an extended numerical model of a two-stage RC has been developed to simulate a healthy compressor's working cycle, to study its behaviour and to predict the signatures of different faults seeded into the compressor. There are only a few models available for fault detection and diagnosis of RC because of the complexity of construction of compressors and most of these models did not take into consideration the effect of motor faults on RC efficiency, especially important where the motor is the prime mover of the compressor. The model of the induction motor describes both flux linkage and voltage equations. Additionally, the equations required for mechanical dynamic system modelling were deduced so that the mathematical model for the RC is considered to have been developed. The motor current contains distinctive features which could be implemented to detect failure modes of the compressor under different loads, based on the cylinder pressure changes during the compressor cycle.

The evaluation of the developed model has been carried out for healthy operation and two compressor faults. The predicted results will be compared with the experimental ones obtained during tests. The model predictions show a good agreement with the measured results and thereby the model can be used for understanding the behaviours of different variables, thus leading to effective diagnostic features.

The sidebands around the supply frequency show a clear difference with the presence of fault compared with the healthy condition, which can be considered as an effective diagnostic feature for various compressor faults. After that, a number of characteristic features were extracted to identify the faults and demonstrate that the current signature is very useful to monitor the compressor's condition. It was found that features extracted for different simulated faults could provide accurate diagnoses. The model was also utilized to predict the signatures of other faults including faults in the motor (SWA, BRB and SWA+BRB), based on analysis of the MSB peak values at different harmonics.

Finally, the simulated faults produced different current signature which can be used as a basis for diagnosing these faults in terms of not only differentiating but also explaining between faults.

CHAPTER 6:

Diagnosis of Combined Faults in Reciprocating Compressors based on Modulation Signal Bispectrum Analysis of Motor Current Signals

This chapter studies reciprocating compressor fault detection and diagnosis based on the motor current signature analysis. It starts with an introduction to the four faults to be seeded into the two-stage RC (second stage discharge valve leakage, intercooler leakage, stator winding asymmetry and combined fault of discharge valve leakage with winding asymmetry). The motor current signal was acquired for the compressor for the healthy condition and with these faults present, for a range of discharge pressures. Time domain and frequency domain were performed to identify the motor current signatures that correlate with compressor performance and provide the basis for offline condition monitoring. Then, modulation signal bispectrum analysis is utilized to process the current signature to obtain an accurate characterisation of the modulation induced by the compressor's varying load. The results of the motor current signature based on spectrum and MSB analysis are shown to achieve early detection and diagnosis of the condition of the reciprocating compressor. The MSB results were better at extracting fault features than spectral analysis and provided a more consistent and accurate diagnosis of compressor faults.

6.1 Introduction

The availability and the efficiency of an RC are subject to the condition of its components, thus valve deterioration or leakage in the intercooler which causes a drop in the compressor pressure also reduce compressor efficiency [11, 143, 147]. Furthermore, any failures occurring within its driving induction motors, such as broken rotor bars or resistance imbalance will also affect the performance of the compressor. Thus efficient and effective CM methods are being actively developed for the detection and diagnosis of faults in compressor systems at ever earlier stages in order to avoid the development of faults which might cause a major failure of the machine [13, 14].

MCSA has already proved to be an effective and efficient monitoring tool, able to detect induction motor faults including a broken rotor bar, stator turn-to-turn fault, and air gap eccentricity [28, 148] without disturbing motor operation [149]. MCSA uses frequency analysis techniques to study current harmonics and sideband components at frequencies that distinctively identify faults.

Sharifi and Ebrahimi [85] proposed a new MCSA technique to detect IM stator faults, this used current spectra to overcome the problem of supply voltage unbalance. The study results showed the effectiveness of the proposed method for the detection of such a fault.

The detection of combined faults in IM represents a major challenge because it makes the fault characteristic more difficult to identify and interpret, and the fault diagnosis much more challenging. Ballal et al. [96] used neural fuzzy inference system logic for the detection and identifying of combined stator inter-turn insulation and bearing wear faults in a single-phase IM. The application of high-resolution spectral analysis to identify multiple combined faults in IMs has been used by [97]. It has been shown that motor current asymmetry combined with other faults such as a BRB, significantly increased the motor's temperature and reduced the efficiency of the machine [124].

Benbouzid [28] has shown that rotor disturbances caused by mechanical problems can be detected using changes in the induction motor stator current. A study by [31] showed that MSB provides better diagnostic performance compared to conventional analysis to detect different severities of stator faults. Shaeboub et al. [33] used MCSA to examine the effect of the stator winding asymmetry combined with other induction motor faults and showed that the presence of the combined fault increased the amplitude of the current sidebands.

However, all of these focused on fault detection within the induction motor and did not extend to investigate the potential of using MCSA as a means of assessing the condition of downstream driven equipment such as RCs. Few studies have been found where MCSA were used as a mean to monitor the condition of downstream driven equipment, including RCs [86].

This chapter presents the use of MCSA combined with an advanced signal processing method to detect the presence of common faults in the compressor in their early stages including leaky discharge valve (DVL), Stator Winding Asymmetry (SWA), inter-cooler leakage (ICL) and the combined fault (SWA with DVL). The variation in compressor load, both during healthy working and due to the presence of faults produces oscillations in the speed of the drive shaft which, in turn, induces harmonic components in the measured motor current signals. Here, an investigation of the changes in the motor current signal was carried out using different techniques, starting with a common time domain analysis of the acquired data, then spectral features in the frequency domain, and finally by detecting and identifying features in the modulated signal by means of the MSB. The signals to be analysed were obtained from the test rig described in Chapter 5, following the procedure described in the previous chapter.

6.2 Experimental Faults

Different faults were seeded into the test rig to study the current signature of each individual fault: in the compressor, discharge valve leakage in the high-pressure cylinder and intercooler leakage, and in the induction motor stator winding asymmetry. A combination of discharge valve leakage with stator winding symmetry was the final fault studied.

6.2.1 Valve Leakage (DVL)

Leakage through the compressor discharge valve causes a backflow of high-temperature gas into the cylinder through the valve which accelerates valve system deterioration and considerably reduces compressor performance and efficiency [150]. Second stage valve leakage was selected because it has a larger impact on the compressor performance than faults in first stage valves. A small hole was drilled into the valve plate to simulate the leakage through the discharge valve (see Chapter 4, Section 4.3.1)

6.2.2 Inter-Cooler Leakage (ICL)

Vibration and thermal stress cause leakage in pipeline systems, as stated in Chapter 4, Section 4.3.2, the inter-cooler leak was seeded by loosening by one complete turn the nut holding the intercooler pipe onto the second stage inlet valve. This was considered as representing a practical leakage but it was not possible to measure the leakage as a proportion of the cross-section area of the airflow through the intercooler joint.

6.2.3 Stator Winding Asymmetry (SWA)

Stator asymmetry is a possible fault that could occur in the 3-phase electric motor driving the compressor. Even though it is a non-critical fault it could lead to a reduction in motor efficiency. Figure 4-4 shows a photograph of the resistance bank used to increase the stator resistance, the motor terminal box connection and schematic diagram of induction motor delta connection respectively. This fault was seeded into the motor by increase the stator winding resistance by 1.0Ω to the three-phase motor. Finally, the compressor was operated under a combination of discharge valve leakage and stator winding asymmetry (DVL+SWA).

6.2.4 Test Procedure

To benchmark, the motor current signature five sets of current data were acquired from the test rig under healthy (baseline, BL) conditions. Similarly, for each of the four different failure scenarios (DVL, ICL, SWA and DVL+SWA), five sets of motor current data were also collected. The current signal was collected using the current unit connected onto the motor terminals. Figure 4-4 illustrates a schematic diagram of the test rig, highlighting the location of the discharge valve leak, the intercooler joint and the resistor bank used to increase the motor resistance.

6.3 Time Domain Analysis Under Healthy Operation

The time domain data contain valuable information on the machine's operation and its condition. Normal time domain analysis obtains characteristic features from time waveform signals as statistical measures of the waveform.

In this section, the change of the pressure inside compressor cylinders and the stator current measurements for a healthy (baseline -BL-) RC and compressor with different

seeded faults are analysed in the time domain to review compressor behaviour under different discharge pressures.

6.3.1 Changes in Cylinder Pressures

Figure 6-1 depicts the baseline waveforms of the second stage cylinder pressure under different values of discharge pressure 40 psi, 80 psi, and 120 psi. During expansion, as the piston moves downwards inside the cylinder for crank angles between about 255° to about 280°, the pressure drops rapidly. Once the cylinder pressure falls adequately below that of the inlet manifold, the inlet valve opens allowing air to enter the cylinder, a process which continues while the piston moves towards BDC, and lasts from a crank angle of about 280° to about 100°. Then the piston starts to move upwards compressing the trapped air from about 100° to about 190°. The pressure increases gradually to the maximum at about 190°, the discharge valve opens and the compressed air is pushed out into the air tank through the valve. It should be noted that the valve opening and closing times are given as “about” because they vary slightly with discharge pressure. From the figure, it can be seen clearly that, the second stage cylinder pressure is increased over the entire cycle as the compressor discharge pressure increase.

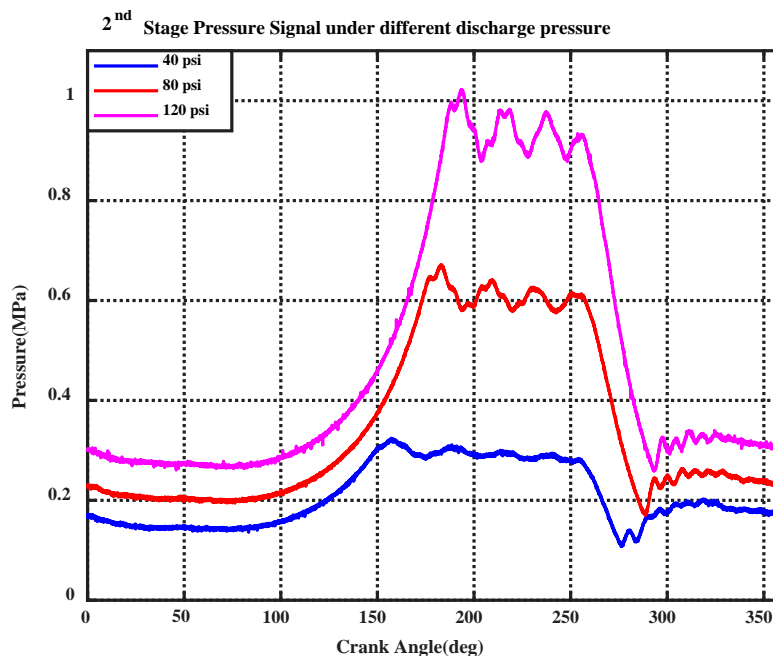


Figure 6-1: Time domain representation of second stage cylinder pressure for the normal condition under various discharge pressures: 40 psi, 80 psi, and 120 psi

6.3.2 Changes in Current Waveforms

The baseline waveforms of the current signal under different discharge pressures 40 psi, 80 psi, and 120 psi are shown in Figure 6-2. The existence of the motor current modulation and appearance of sidebands at about 7.3 Hz is explained in Section 5.10.5. In Figure 6-2 it can be observed that the amplitude of the current waveform for the crank angle between 240° to 360° is higher than that from 80° to 200°. This is due to load fluctuation during the compression process. Additionally, the figure shows that the amplitude of the motor waveform increased as the compressor discharge pressure increased and it can be concluded that the three-phase current signal can provide useful information about compressor performance. The force or torque exerted by the motor is indicated by the magnitude of the current, and the corresponding values of the IAS. Consequently, it can link current values to the speed and acceleration, or deceleration, of the IAS.

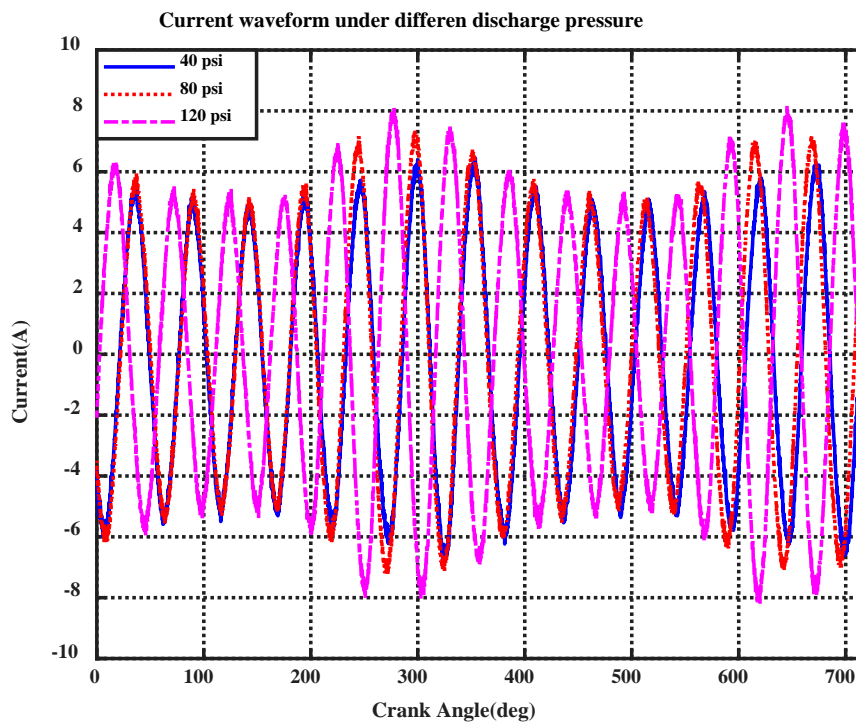


Figure 6-2: Time domain representation of the current signal for a healthy compressor under different discharge pressures 40 psi, 80 psi, and 120 psi

6.4 Data Analysis Under Healthy and Faulty Conditions

6.4.1 Changes in Cylinder Pressure Waveform

The effect of different faults on the cylinder pressure waveform for the low and high-pressure cylinders for a compressor discharge pressure of 80 psi is illustrated in Figure 6-3. It can be noted that the seeded faults have caused noticeable changes in the performance of the compressor.

The DVL allows a backflow of high pressure compressed air through the seeded hole which raised the pressure inside the first stage cylinder above the normal condition and the combined fault (DVL+SWA) had an even larger influence on the pressure of the first stage Figure 6-3(a). For the high-pressure cylinder, the pressure began to increase earlier and reached its peak value earlier than normal, so the discharge valve opening even earlier, as highlighted in Figure 6-3(b). The larger the leakage the higher-pressure air will leak back into the cylinder and the earlier the discharge valve will open. The discharge valve may close earlier with either DVL or DVL+SWA, but this effect is not nearly as significant as the early opening. Figure 6-3(b) shows the overall cylinder pressure for the second stage for DVL and DVL+SWA faults is slightly higher than healthy.

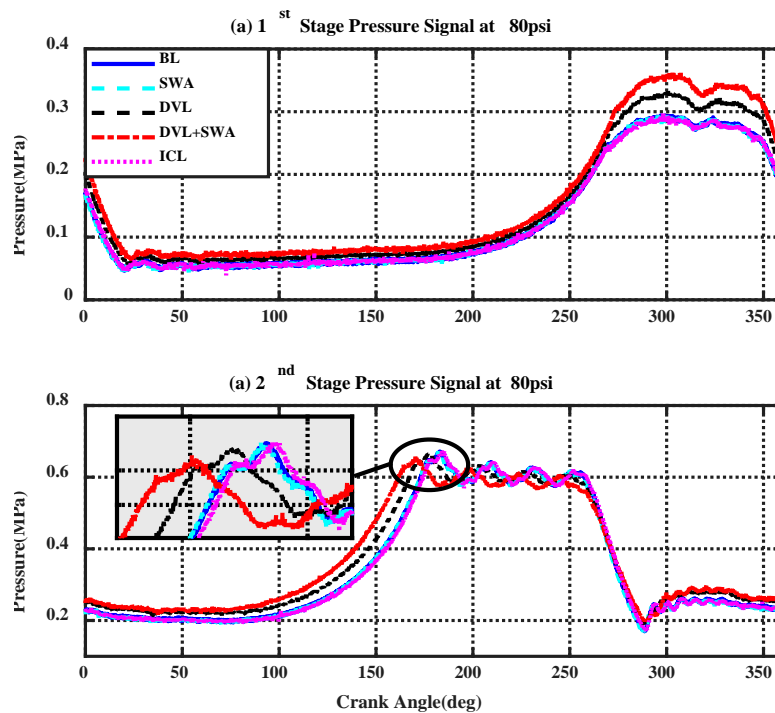


Figure 6-3: Time domain cylinder pressures for first and second stages, for second stage discharge pressure of 80 psi, for baseline condition and four faults.

From Figure 6-3(a) it can be seen that the DVL and DVL+SWA faults both lead to a noticeable increase of the first stage cylinder pressure during the discharge process, with the combined fault producing the maximum value. This increase in the cylinder pressure delays the opening of the first stage suction valve slightly and, consequently, the first stage discharge valve closes late. So, both seeded faults (DVL and DVL+SWA) caused a change to the cylinder pressure in both stages which can be used to detect their presence.

Introducing the intercooler leakage (ICL) caused a change in the pressure waveform for both stages. This change is clearly seen as a decrease in maximum pressure in the low-pressure cylinder. In the high-pressure cylinder, the presence of the ICL caused a noticeable delay in the discharge valve opening. This delay occurred because of the cylinder pressure is lower than normal during the compression and suction procedures compared to healthy operations. This change in the pressure waveform can be explained from the machine's working mechanism. When the intercooler leak occurs, the in-cylinder pressure for the first stage is lower than for healthy condition which causes a reduction in the force acting to close the discharge valve of the low-pressure cylinder. Thus, the discharge valve opens earlier than in healthy operation. This, in turn, causes a pressure reduction compared to the healthy condition. As for the second stage, the intercooler leakage causes a small but significant change in cylinder pressure; the in-cylinder pressure is lower than for healthy operation. This will result in a reduction in discharge efficiency. The drop in the cylinder pressure causes a delay in the opening of both discharge and suction valves. This fault causes a small variation in cylinder pressure; which offers a possibility of monitoring for a leak in the intercooler. Whereas, the SWA fault has a small but not significant effect on the cylinder pressure

6.4.2 Changes in the Motor Current Waveform

The motor current waveform under 40 psi and 120 psi compressor discharge pressure is presented in Figure 6-4. As mentioned earlier (see Section 6.3.2), the three-phase induction motor has a load fluctuation at 7.3 Hz (working frequency of the RC) which leads to a modulated current waveform [35] which can be clearly observed in Figure 6-4. Another observation is that the current amplitude with the DVL and DVL+SWA seeded faults is slightly larger than for healthy (BL) operation. The amplitude modulation becomes clearer as the discharge pressure increases. However, the figure shows no useful information by which to detect the other two faults seeded into the system (ICL and SWA).

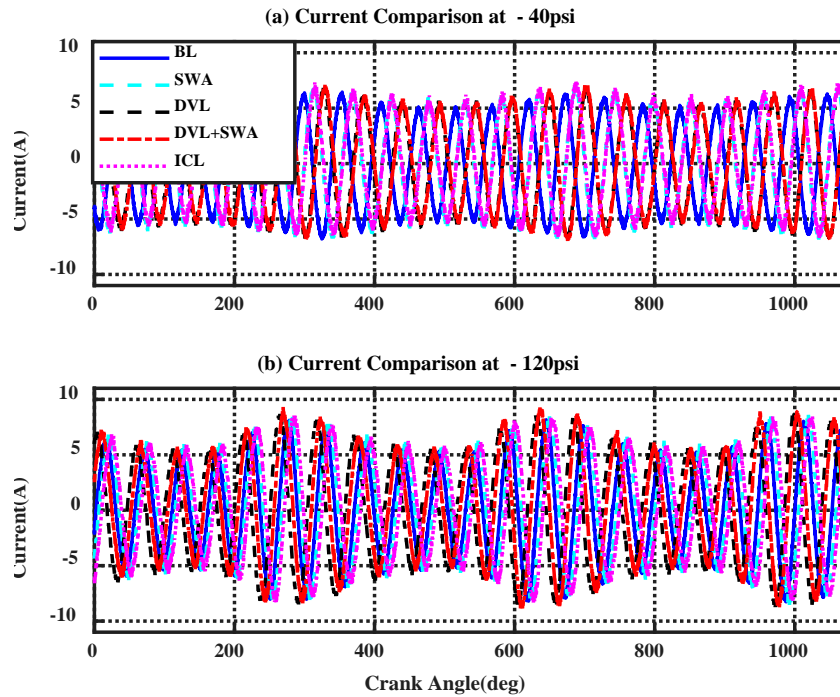


Figure 6-4: Motor current waveform for healthy compressor and compressor with four seeded faults under 40 psi and 120 psi discharge pressure

Figure 6-5 illustrates the RMS relationship between the current waveform and compressor discharge pressure. The first observation is that the RMS current increases monotonically with discharge pressure for both healthy (BL) and seeded faults. Additionally, the RMS values show a substantial difference between healthy compressor and compressor with any of the four seeded faults: higher in the case of DVL, SWA and DVL+SWA, but lower in the case of ICL. These amplitude difference can be interpreted as the compressor needing more or less power to deliver the same discharge pressure, affecting compressor operation and decreasing its efficiency.

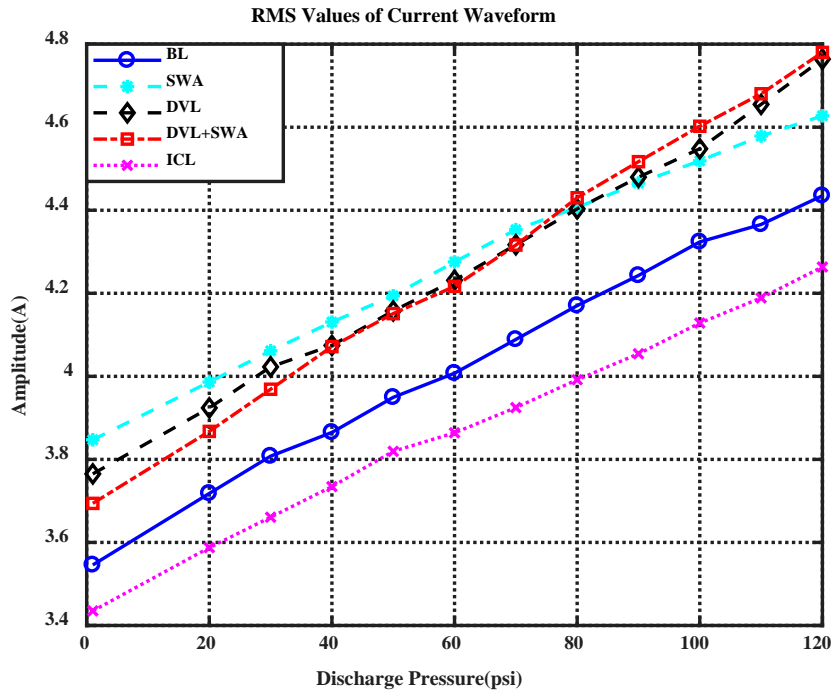


Figure 6-5: RMS values of the motor current waveform for healthy and with seeded faults under a range of discharge pressures

6.4.3 Comparison of Motor Current Signal Spectra

The time domain data acquired from the compressor was converted to the frequency domain to obtain the motor current spectrum by means of the DFFT. The frequency spectrum shows more useful information about the monitored machine. Current drawn by a normal motor ideally should exhibit the main frequency component at 50 Hz [28] which is the electrical supply frequency, supplemented by a pair of sidebands at 50 ± 7.3 Hz, where 7.3 Hz is the working frequency of the RC. The seeding of the four faults into the system is expected, see Section 5.10.5, to generate asymmetry between the three current phases and power supply imbalance, which cause load fluctuation of the machine operation, each of which indicates the presence of a seeded fault.

Figure 6-6 shows the current spectra for normal operation (BL) and the four seeded faults under compressor discharge pressures of 60 psi and 120 psi. It can be observed that the spectrum exhibits a high degree of AM. As expected, the peak at the supply frequency, 50 Hz, has by far the greatest amplitude, and pairs of sidebands around the f_c are clearly visible for the seeded faults. Note that the increase of the sidebands component amplitude induced by the combined fault (DVL+SWA) is the highest at the first sideband components, followed by the discharge valve leakage in comparison to the healthy

condition. In addition, as the compressor pressure increases, the amplitude of the sidebands increases.

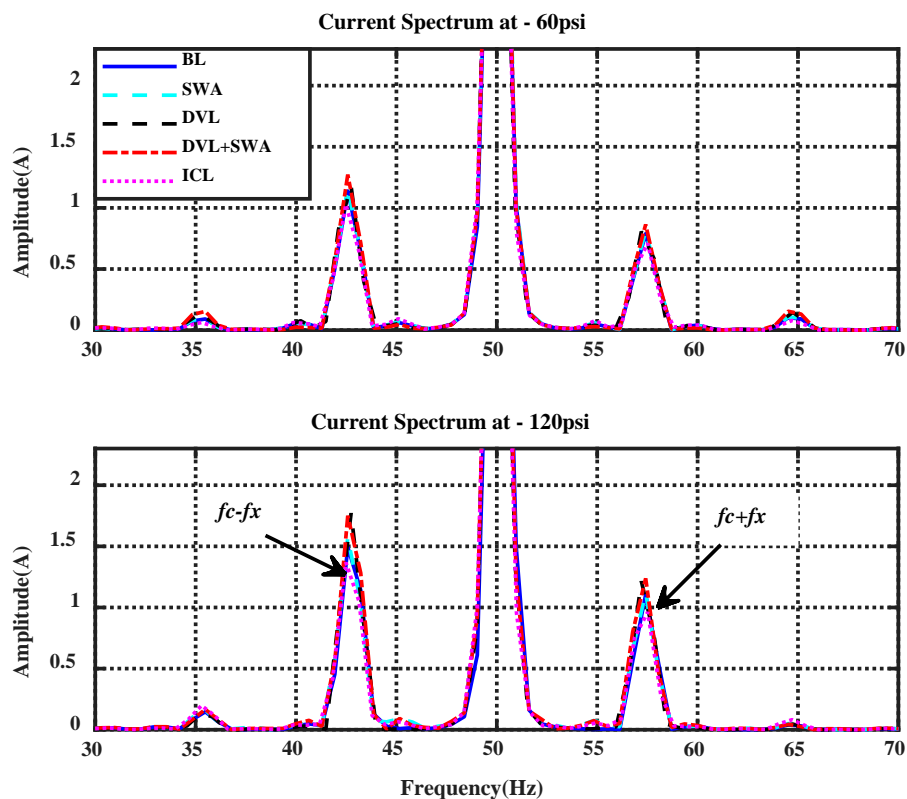


Figure 6-6: Motor current spectrums for healthy and seeded faults under discharge pressures of 60 psi and 120 psi ($f_c=50\text{Hz}$ and $f_x = 7.3\text{Hz}$)

To show the variation in the sideband amplitude between healthy and different faulty conditions more accurately, Figure 6-7 illustrates the variation in amplitudes of the averaged sideband at $50-7.3\text{ Hz}$ and $50+7.3\text{ Hz}$ for a range of discharge pressures under healthy and seeded fault conditions. It can be seen that the amplitudes of both sidebands increase monotonically with an increase in pressure for every operating condition. Note that the major difference in the amplitude of the sidebands occurred when the combined fault was introduced, which is consistent with the changes in the pressure graph Figure 6-3. In Figure 6-7, the amplitudes of the sideband for the examined conditions can be differentiated as the combined fault has the greatest amplitude, then the discharge valve leakage, followed by the healthy condition and finally the inter-cooler leakage being the lowest. Again, it is worth mentioning that, in the low-pressure range (up to 50 psi) it is difficult to distinguish between the healthy condition, valve leakage and combined fault (DVL+SWA). Close to the maximum pressure of 120 psi, it becomes difficult to differentiate between the combined fault (DVL+SWA) and valve leakage (DVL),

especially for the lower sideband, suggesting that at high pressures valve leakage is the dominant mechanism.

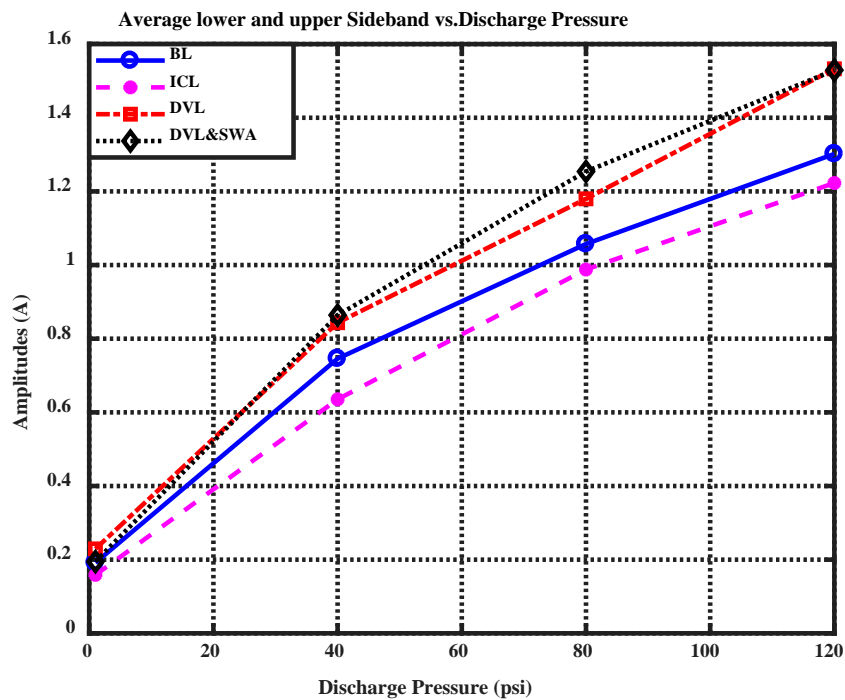


Figure 6-7: Averaged sidebands amplitude for healthy and simulated faults under compressor discharge pressure

6.5 MSB Magnitude Characteristics

The compressor normally provides a wide range of discharge pressures which cause variations to the motor current signals and can hide small changes caused by incipient faults. This makes it challenging to identify and quantify various types of faults. Thus, advanced signal processing techniques need to be utilized to study not only amplitude changes but also phase and nonlinear interaction in the current signal to enhance the changes required to separate various types of compressor and motor faults.

For a more accurate and effective diagnosis, the MSB was applied to the stator current signal to analyse these nonlinear and modulated characteristics and to extract useful features for CM under the different operating conditions, with three different simulated faults seeded into the compressor. Figure 6-8 illustrates the results obtained for MSB analysis of current signals for a healthy compressor and compressor with the combined fault (DVL+SWA) under 120 psi compressor discharge pressure (load).

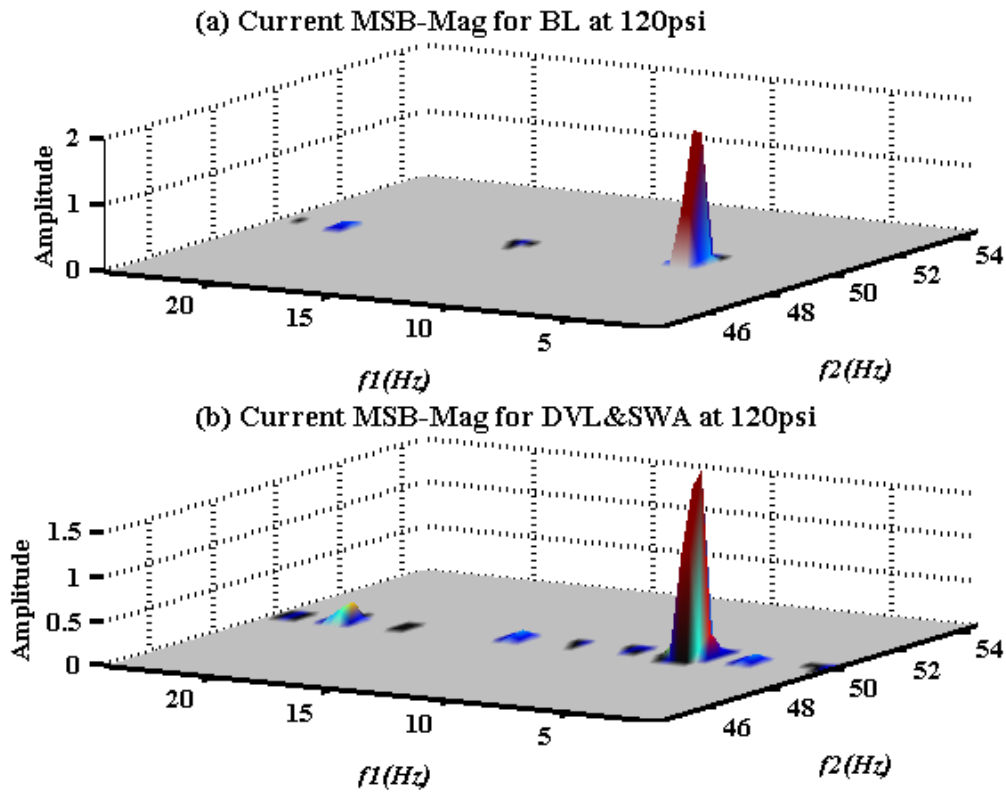


Figure 6-8: Characteristics of current MSB for (a) healthy compressor (BL) and (b) combined fault (DVL+SWA), both for 120 psi discharge pressure

From the figure representation, it can be seen that the MSB result shows the most distinctive peak at (7.3, 50.0) Hz in the bispectrum domain. Clearly, the peak represents the sidebands component and the supply frequency at $50+7.3$ Hz. This shows the interaction of two independent components 50 Hz, the supply frequency, and 7.3 Hz, the compressor working frequency. Importantly, the peak amplitude at (7.3, 50.0) Hz for the compound fault is more than 35% higher than for the healthy condition and can be used directly as a feature indicating the presence of a fault, and can be relied on for the detection of the presence of compressor faults.

Figure 6-9 shows the MSB magnitude results under a wide range of compressor discharge pressures (1, 40, 80 and 120 psi) for healthy compressor and compressor with different seeded faults including the combined fault (DVL, ICL and DVL+SWA). As with Figure 6-8, the MSB representation exhibits two distinctive peaks, with the major peak at bifrequency (7.3, 50.0) Hz. The amplitude of this peak increases with the increase of compressor discharge pressure.

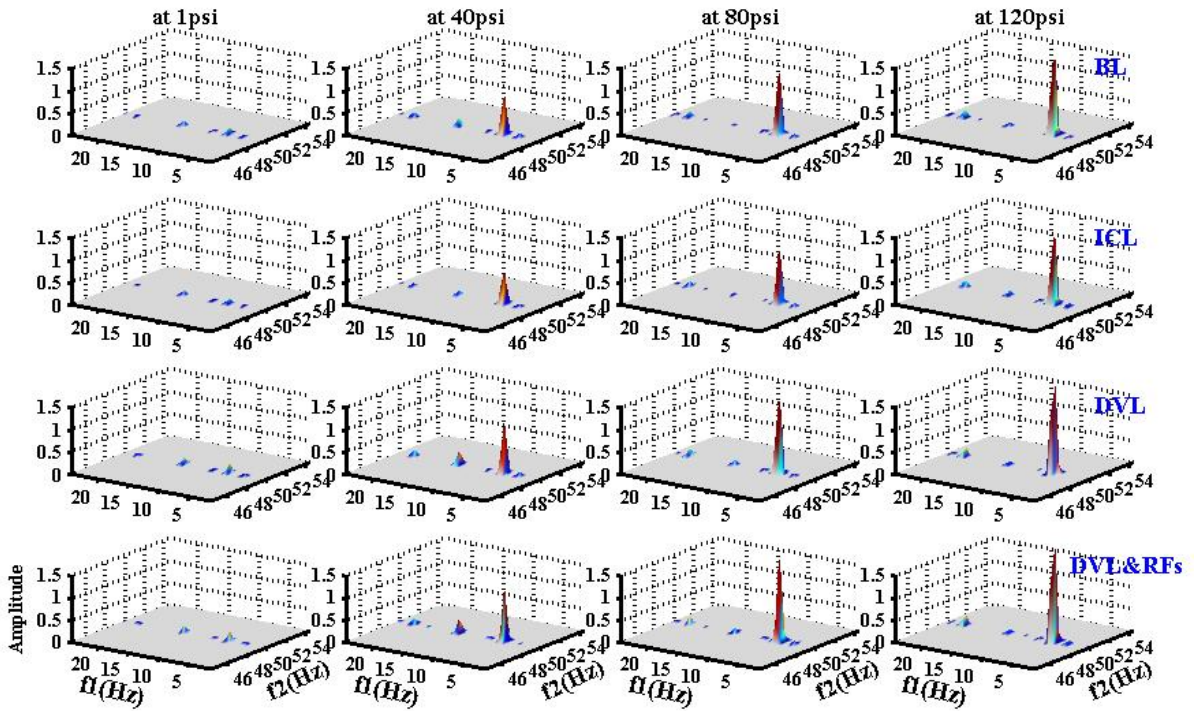


Figure 6-9 :MSB characteristics of current signals for healthy and different fault conditions under the range of operating pressures

Figure 6-10 shows a typical MSB slice at a supply frequency of 50 Hz with a peak at 7.3 Hz. It shows the increase of the sideband amplitude with the pressure increase.

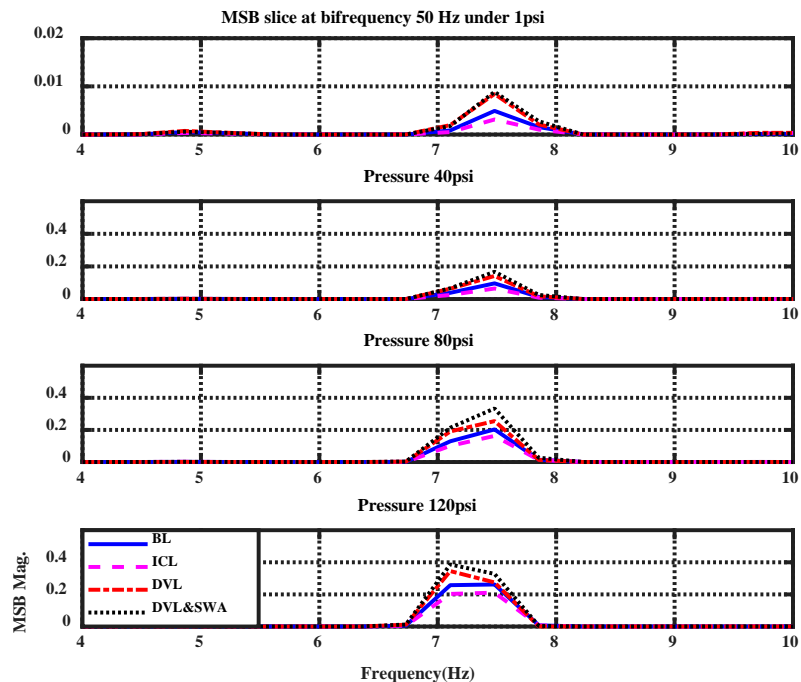


Figure 6-10: A typical MSB slice at 50.0 Hz for healthy and different fault conditions under the range of operating pressures

6.6 Comparison between Spectrum and MSB Analysis

An evaluation of different CM techniques for both a healthy system and system with seeded faults, based on the compressor stator current signals is made in Figure 6-11 which illustrates the diagnostic performance for both MSB and Spectral Analysis. It is seen that the sideband amplitudes at bifrequency (7.3, 50.0) Hz for faulty conditions differ from that of the healthy compressor. The stator winding asymmetry combined with second stage discharge valve leakage boosts the amplitude of the sideband in both the MSB and spectral results. It can be seen that the amplitude of the sideband rises as the pressure increases, with a clear separation between the combined seeded fault and healthy condition.

It can be concluded that the MSB is able to differentiate between BL, ICL, DVL and DVL+SWA. In which, the corresponding peak for the combined fault (DVL+SWA) is 35% higher than that for BL, and the peak corresponding to the DVL fault is more than 20% higher. Thus, the relative amplitude of the MSB peak at (50.0) Hz can be used directly as an important feature for the detection and diagnosis of these faults as each fault has a different amplitude compared to the healthy compressor. However, spectral analysis shows no clear difference between DVL and DVL+SWA at most of compressor discharge pressure except, 80 psi, and it is concluded that MSB gives better noise reduction and fault separation compared to spectral analysis. Generally, this experimental evaluation demonstrates that the MSB-based diagnosis performs better than the spectral analysis.

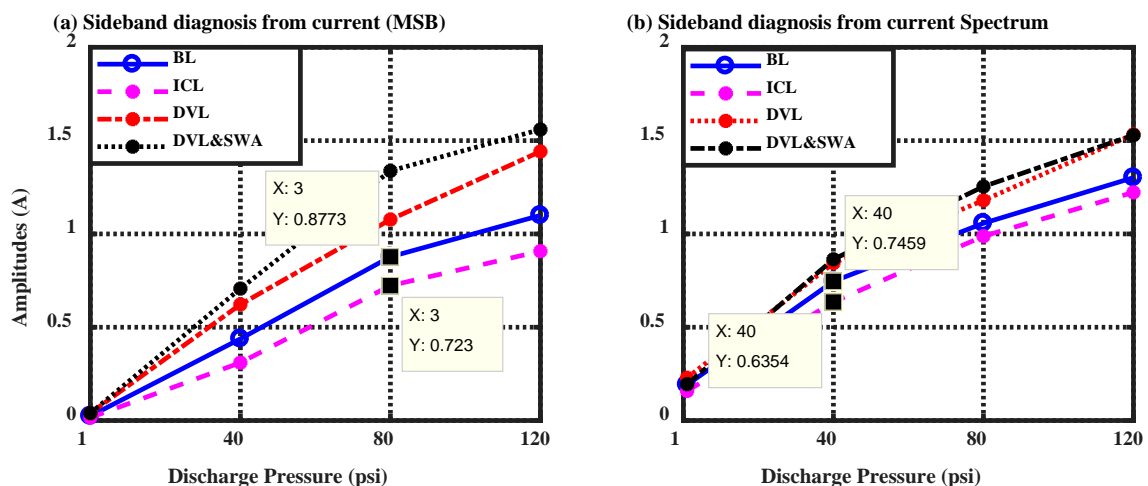


Figure 6-11: Comparison between MSB and spectral Analysis for the diagnosis of different faults

This comparative study has provided additional support for the proposal that MSB demonstrates good diagnostic performances and is able to fully differentiate between the seeded faults under different discharge pressures, and between faulty and healthy conditions.

Another way to compare the relative effectiveness of MSB and spectral analysis is to determine the percentage difference to measure the relative change in the BL level caused by the fault, according to the data presented in Figure 6-11. For example, at discharge pressure 80 psi the value for MSB sideband Figure 6-11(a), ICL and BL values are 0.7230 and 0.8773 respectively. Calculating the percentage difference between ICL and healthy condition as follows:

$$\text{PercentageDifference, \%} = [(0.7230 - 0.8773) / 0.8773] * 100 = -17.59\% \quad (6.1)$$

Another example is for spectrum sideband in Figure 6-11(b) at 40 psi, the values for ICL and BL are 0.6354 and 0.7459 respectively. The percentage difference of ICL from baseline is

$$\text{PercentageDifference, \%} = [(0.6354 - 0.7459) / 0.7459] * 100 = -14.81\% \quad (6.2)$$

Table 6-1 and Figure 6-12 present the percentage difference between the healthy compressor and compressor with seeded faults under 1, 40, 80 and 120 psi. It is very clear that the MSB analysis produces a more accurate diagnosis of the compressor condition under the full range of discharge pressures.

Table 6-1: Percentage difference between healthy compressor and compressor with seeded faults for discharge pressures 1, 40, 80 and 120 psi

Faulty Cases	Percentage Difference for MSB				Percentage Difference for Spectrum			
	1psi	40psi	80psi	120psi	1psi	40psi	80psi	120psi
ICL	-34.35%	-29.17%	-17.59%	-17.47%	-17.21%	-14.81%	-6.55%	-6.07%
DVL	65.34%	42.07%	22.76%	31.15%	19.65%	13.08%	11.60%	17.75%
DVL+SWA	65.46%	61.46%	52.48%	41.87%	1.62%	15.84%	18.61%	17.46%

From Table 6-1 slider-crank it can be seen that the MSB outperformed spectral analysis in detecting all three seeded faults. In particular, it easily separated the combined fault under

all discharge pressures, being more than 40% from baseline. On the other hand with spectral analysis, the difference was consistently less than 20%.

A clear difference can also be noted between the MSB results and spectral analysis for all seeded faults as can be seen in Figure 6-12.

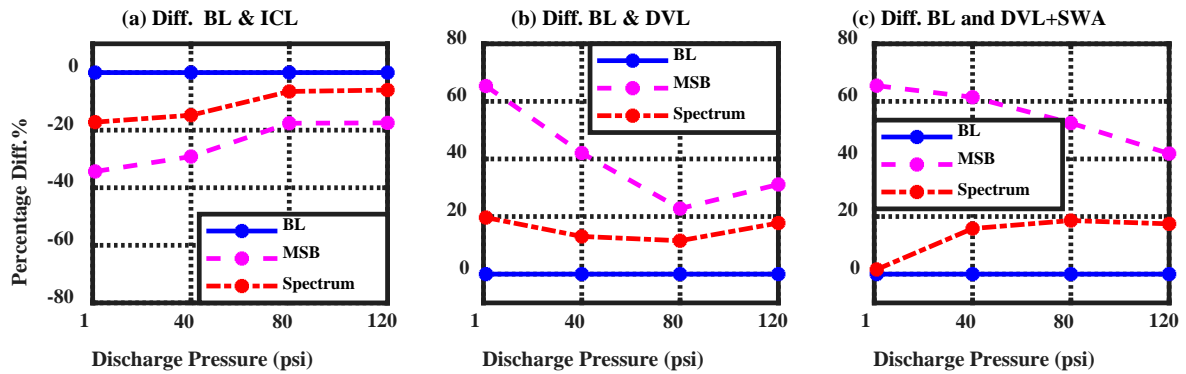


Figure 6-12: Percentage difference of BL and seeded faults under different compressor discharge pressures

6.7 Summary

The chapter has illustrated the importance of using stator current signature to study the condition of the RC and its upstream IM for early detection of various compressor faults including combined faults (stator winding asymmetry combined with discharge valve leakage) under different discharge pressures.

Figure 6-3 shows that the seeded faults had different effects on the cylinder pressure and valve opening times compared with the healthy operation. The motor current waveform exhibited a clear amplitude modulation caused by the normal load fluctuation due to the compressor pressure differences occurring naturally during a healthy working cycle. Figure 6-5 showed that the current waveform RMS values increased monotonically with discharge pressure, and with a difference between healthy and seeded faults, particularly between the healthy condition and intercooler leakage. However, it was not possible to differentiate between DVL, SWA and DVL+SWA.

The motor current spectrum Figure 6-6 also exhibited a clear AM effect in which pairs of sidebands appear around the 50 Hz carrier, the most pronounced of which was at ± 7.3 Hz (working frequency of the compressor). It has been demonstrated that the amplitude of the

sidebands increased with the increase of the compressor discharge pressure. Moreover, seeded faults cause yet another increase in the amplitude of the sideband and this increase can be seen in the current spectrum. However, spectral analysis is unable to provide a full separation for different compressor fault conditions especially between valve leakage and the combined fault as can be observed in Figure 6-7. Additionally, This chapter has demonstrated the implementation of MSB to capture the deterministic nonlinear features of modulating frequency components and effective suppression of noise to accurately detect and diagnosis incipient compressor faults under a wide range of compressor discharge pressures.

MSB provides a distinctive peak representing sideband components at bifrequency (7.3, 50.0) Hz, which increase in amplitude with the compressor discharge pressure. Also, the amplitude for the faulty conditions differs significantly from that of the healthy compressor. The combined fault (DVL+SWA) and valve leakage fault (DVL) cause further increase in the amplitude of the sideband more than 40% and 20% respectively than that of the healthy condition as can be seen in Table 6-1 and Figure 6-12.

The comparative study illustrates that the MSB based diagnosis shows very good performance in noise reduction and fault separation compared to spectral analysis. The MSB analysis of the stator current signal has significant potential to detect and diagnose the presence of compressor faults and combined motor/compressor faults, being able to provide more accurate and reliable diagnostic features under a wide range of compressor discharge pressures in comparison to conventional spectral analysis.

CHAPTER 7:

Modulation Signal Bispectrum Diagnosis of Reciprocating Compressor Faults Based on Vibration Analysis

Chapter nine studies the process of the condition monitoring of an RC, healthy and with two leakage faults; intercooler leakage and discharge valve leakage. The measured vibration signals are subject, first to the time domain, the frequency domain (envelope analysis), and finally MSB signal processing to provide a more accurate and reliable fault diagnosis. The final section reports that the MSB has produced a better performance in extracting fault features compared with spectrum analysis.

7.1 Introduction

As in the previous chapters, and for the reasons given there, the system faults considered in this chapter will be the compressor second stage discharge valve and an intercooler leak.

Different techniques have been developed and applied for the detection and diagnosis of faults in industrial machinery, see Chapter 2, Section 2.11. Vibration analysis is widely utilized as an effective monitoring approach for industrial applications such as gearboxes, induction motors and pumps [25]. However, relatively little effort has been channelled towards the application of vibration analysis for CM of RC [66, 143]. The aim of this chapter is to analyse compressor vibration as a means for monitoring and detecting common RC faults in their early stages. Here these faults will be leakage through second stage discharge valve (DVL) and through the intercooler (ICL). Detection of induction motor faults will be considered in the next chapter.

A number of signal processing methods such as that used by [21] have been used to interpret machinery vibration data to diagnose various compressor faults. The wavelet transform has been applied by [151] for compressor valve diagnosis. Yang, et al. [92] used SVMs for fault classification of butterfly valves in an RC. These have been reported in Chapter 2, Section 2.12. Most of these techniques are centred on data-driven tools and statistical learning theory from data with large bandwidth which might contain some irrelevant information affecting the detection of early faults or abnormalities.

Naturally, RC is a noisy machine which produces a high level of vibration and is prone to a range of failure modes, including deformation, fatigue and wears [36]. Because of its slider-crank mechanism, some degree of torsional vibration is involved in the operation of RCs. The signal acquired from vibration sensors attached to an RC will be a superposition of responses to impulsive events occurring during the machine cycle, e.g., valve and piston movements. The mechanical collision between valve plates and their seats generate unsteady vibration, containing non-linear characteristics, and its statistical properties change periodically with time [25]. Moreover, fluctuation of airflow also produces vibration and nonlinear transfer paths generate signal noise. However, due to the effects of the various compressor faults, the compressor vibration behaviour would be different from the healthy operation. Hence, an additional complex vibration spectrum

would be added to the healthy signal. Features obtained from the time-domain, and frequency-domain of these vibration responses, which can be measured reliably and efficiently, can be used to assess compressor condition [25]

This chapter aims to develop a monitoring condition technique based on vibration analysis which would use an effective noise removal method to study any changes associated with the compressor variation under different operating conditions. An investigation on the change in the vibration signatures was carried out using different data analysis methods, starting with common time domain waveform analysis, the spectral features in the frequency domain were obtained. After that, a HOS processing technique was applied to evaluate the periodicity of compressor structural resonances, crankshaft rotation and non-linear features of modulation components. In order to evaluate the periodic connection between compressor structural resonances and the crankshaft rotational frequency, the Modulated Signal Bispectrum (MSB) was applied on the measured surface vibration of an RC for early fault diagnosis. The MSB can extract non-stochastic, nonlinear features from the modulated components and these can provide a comprehensive characterization of the nonlinear vibration responses of the compressor, and thus enable a more accurate assessment that could pinpoint the root cause of a fault and enhance the reliability and accuracy of the diagnosis.

Leakage faults in discharge valve and intercooler were detected by monitoring the vibration resonances they caused. A better and more reliable result was achieved by using the MSB to detect incipient faults than with normal spectrum analysis.

7.2 Fault Simulation

Two common compressor faults were simulated experimentally and seeded into the test rig to study the vibration signature of each individual fault. In this chapter, DVL at the high-pressure cylinder was studied, for the reasons given in the previous chapter. The valve leakage was simulated, see Chapter 4, Section 4.3.1, by drilling a 2 mm diameter hole in the valve plate. Intercooler leakage (ICL), another common fault, was simulating by loosening the nut holding the pipe onto the second stage inlet valve, see Chapter 4, Section 4.3.2.

7.3 Test Procedure

To evaluate the vibration responses from the compressor, vibration data were sampled during the baseline tests (healthy condition) then with the two other faults separately seeded into the compressor, see Figure 7-1. Data sampling using the Cambridge Electronic CED 1401 Plus Data Acquisition Unit is described in Chapter 4. Section 4.5.1, including vibration sensors, pressure transducers and an encoder.

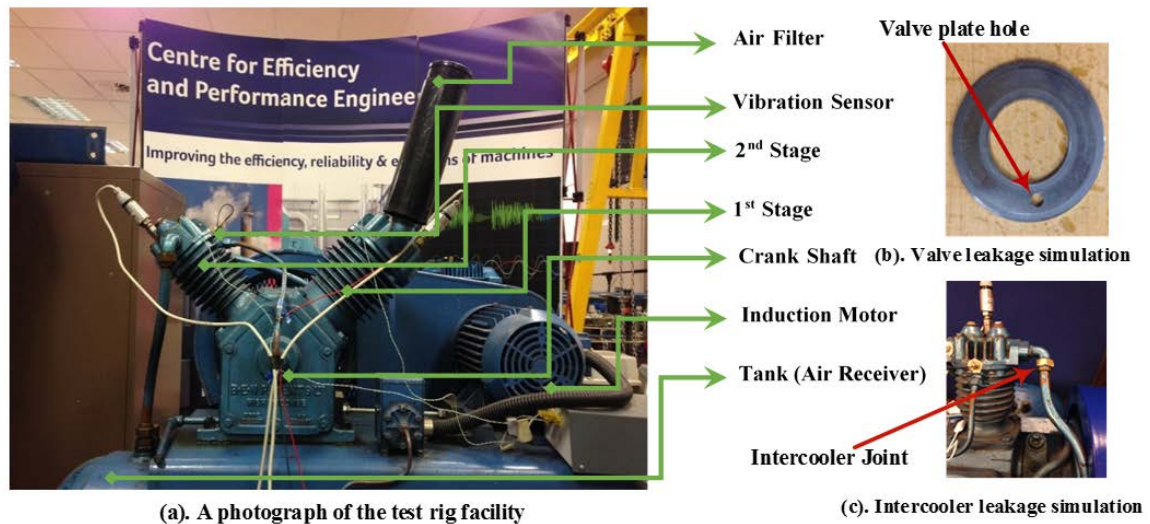


Figure 7-1: Reciprocating compressor test rig and fault simulations

7.4 Time-Domain Analysis Under Healthy Conditions

Time-domain waveform analysis was presented in Chapter 3, Section 3.2 as one of the simplest method for machine fault detection and diagnosis approaches. In this section, the change in cylinder pressure and vibration signal for a healthy RC were analysed in the time domain to study the compressor behaviour under different discharge pressures.

7.4.1 Cylinder Pressure Waveform

Figure 7-2 illustrates the waveform of the low and high in-cylinder pressures for healthy RC under discharge pressures 60, 80, 100 and 120 psi. As discussed in Chapter 6, section 6.3.1, it can be observed clearly that, both low and high stages pressures increase with the increase of the compressor discharge pressure.

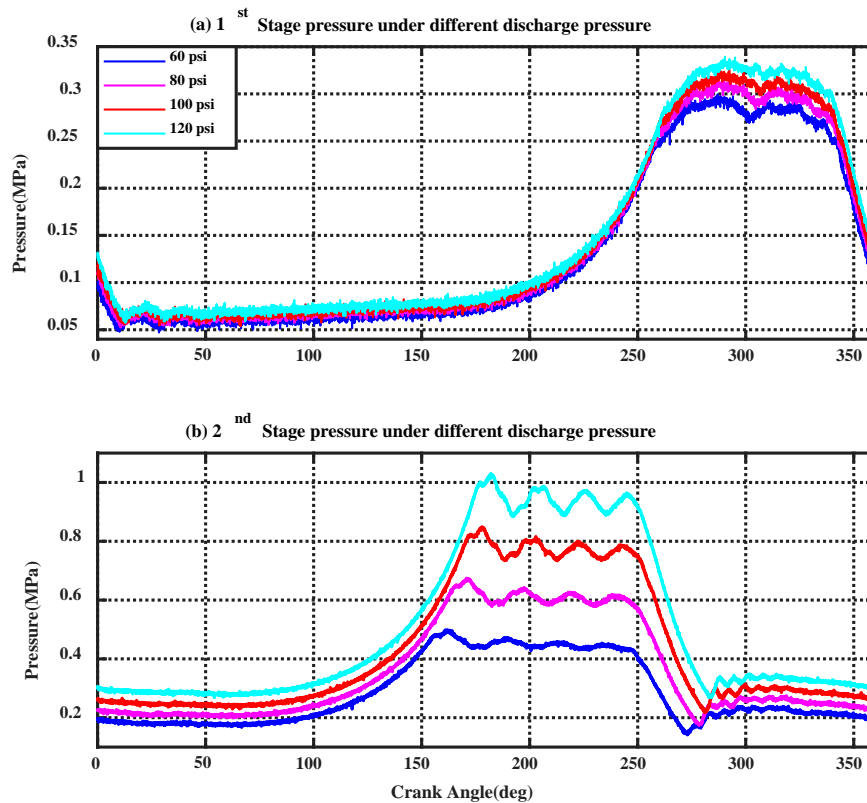


Figure 7-2: Time domain representation of (a): low stage, and (b) high stage in-cylinder pressures for a healthy condition for discharge pressures (60, 80, 100 and 120 psi)

7.4.2 Vibration Waveform Characteristics

The measured vibration signals were from an accelerometer attached to the second stage cylinder head and in-cylinder pressure signals for the healthy compressor under 100 psi discharge pressure are depicted in Figure 7-3 for one complete cycle. From the figure, it can be seen that the vibration signature shows significant transient responses for each valve action (both suction and discharge) consistent with valve impacts on their seats during valve opening and closing. As previously, the reference position of the piston was when the first stage piston was at TDC. In Figure 7-3, referring to the second stage cylinder, it is clear that the closing time of the discharge valve (DVC) produces the largest transient vibration, whereas the discharge valve opening (DVO) produces an important, but much smaller, transient peak. The suction valve opening impact (SVO) is indicated by clear transient peak, but smaller than the DVC transient. While the next transient is associated with the suction valve closing (SVC). Thus the vibration signature can be utilized to obtain useful information regards the performance of the compressor.

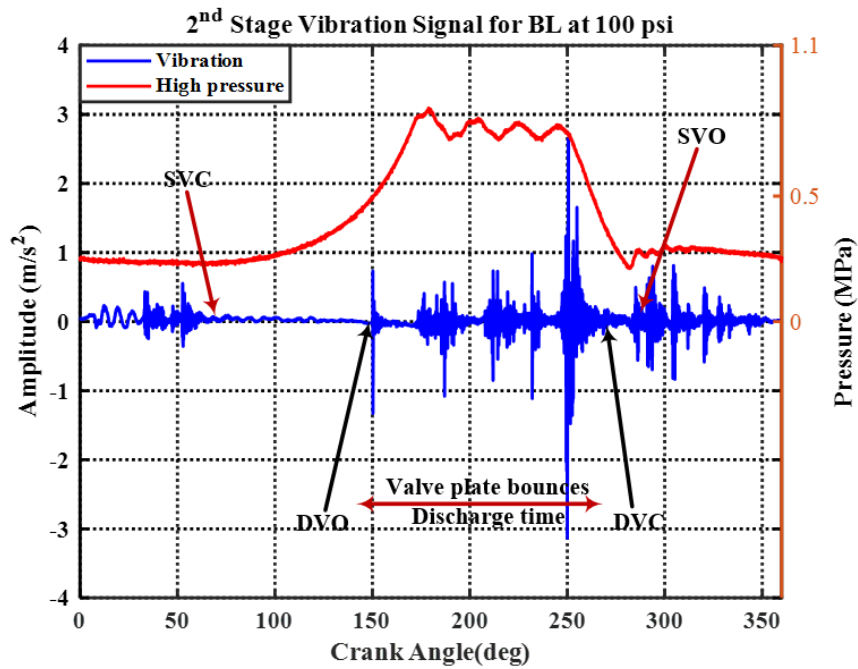


Figure 7-3: Measured vibration and pressure signals for a healthy compressor under 100 psi discharge pressure

Figure 7-4 illustrates the time domain signal from the accelerometer for the healthy compressor under different compressor discharge pressures (80, 100 and 120 psi). The pressure increase introduces a difference in vibration signals, which can be easily noted; i.e., the increase of the discharge pressure had a significant effect on the opening and closing times for both valves, especially opening times. Thus the vibration measurements confirm the description and interpretation of changes to DVL as given in Chapter 5, Section 5.10.3, confirming that any fault within the valve will have a noticeable effect on its opening and closing times.

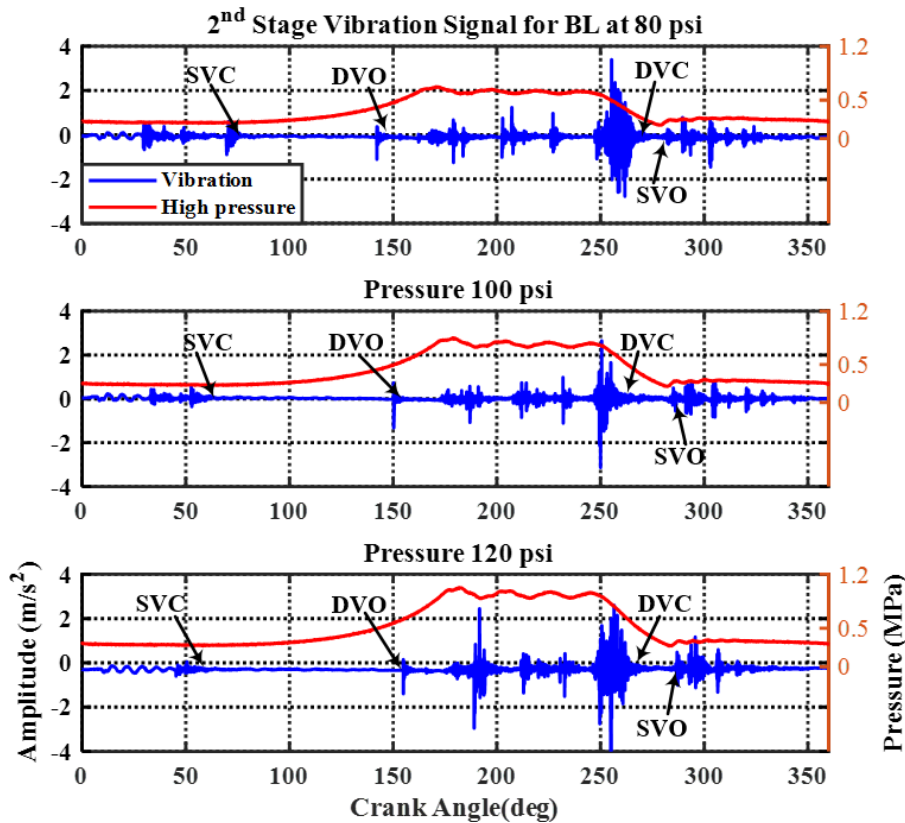


Figure 7-4: Time domain representation of a vibration signal for a healthy compressor under different discharge pressure (80, 100 and 120 psi)

7.5 Time Domain Analysis for Fault Conditions

The effect of the seeded faults, ICL and DVL, on the second stage cylinder pressure and vibration signatures are depicted in Figure 7-5, which shows vibration amplitude measured by the second stage cylinder accelerometer under healthy, ICL and DVL conditions, for a compressor discharge pressure of 100 psi. One can see immediately that the seeded faults caused noticeable changes in the measured vibration signal and compressor performance.

The leak across the second stage discharge valve permits backflow of high-pressure air from the storage tank, which leads to an increase of cylinder pressure above normal, so there is the likelihood the discharge valve opening earlier because the cylinder pressure needed to open the valve is reached earlier, see the red circle in Figure 7-5; healthy discharge valve opens at about 177°. but the leaky valve opens early at about 138°. Thus the presence of a DVL may be detected if the discharge valve is seen to open earlier than for the healthy compressor.

Figure 7-5 also shows that the seeded intercooler leakage causes a distinct decrease in pressure, lower than normal which causes a very slight delay in the opening of both valves which is not easily distinguishable from the healthy condition. However, it is clear that the vibration amplitude with the ICL fault is less than that for the healthy condition.

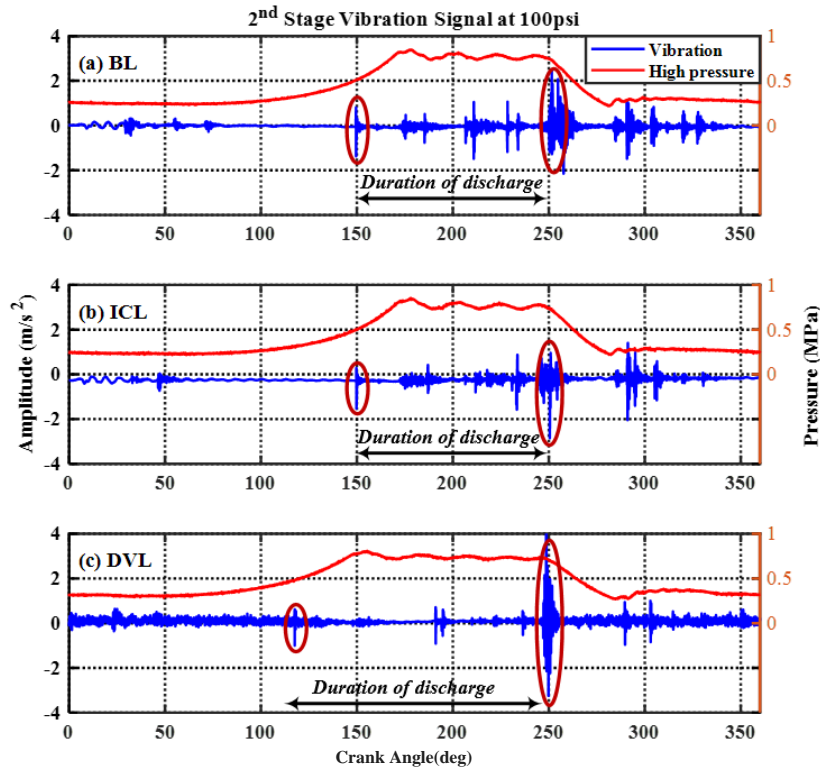


Figure 7-5: Time domain representation of vibration signal from second stage cylinder for (a) BL, (b) ICL and (c) DVL under 100 psi discharge pressure

Differences in vibration amplitudes for healthy and seeded faults are easily observed and can indicate an abnormal condition. Yet, a small change in the vibration signature may not be identified because vibration signals are the summation of multiple sources within the machine, so vibration signals from working machines are inherently contaminated with background noise. Also because some sources of vibration are impacts they can be described non-linear and possibly non-stationary. On the other hand, the vibration signals are rich in information on the condition of the machine.

Figure 7-6 illustrates the relationship between the vibration RMS and discharge pressure for the healthy condition and two seeded faults (ICL and DVL). The first observation is that the RMS value increases steadily with an increase in discharge pressure for all three conditions of the compressor. Except at the highest pressure the RMS was unable to reliably separate the seeded faults from the healthy condition.

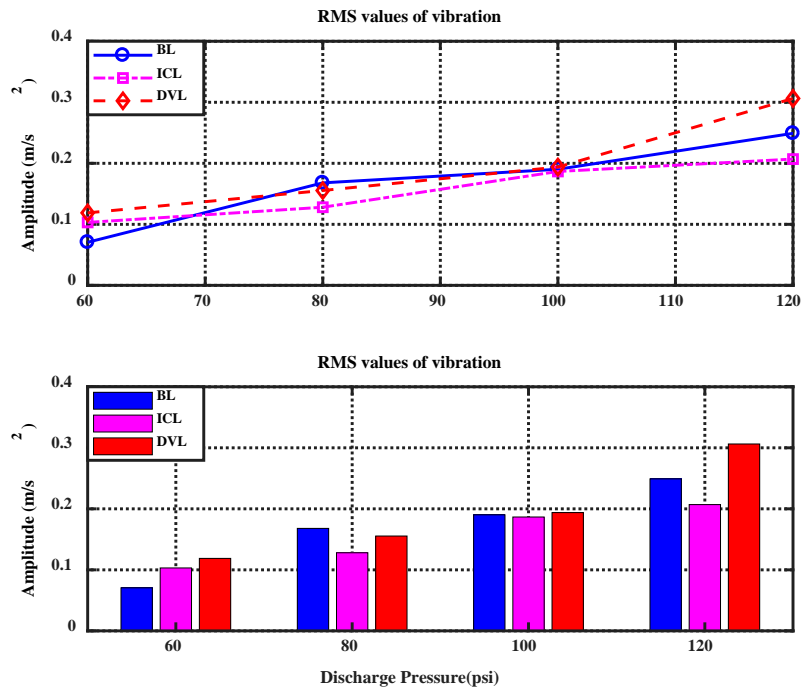


Figure 7-6: RMS values for the time-domain waveform of the second cylinder vibration for healthy condition and two seeded faults for four discharge pressures

Figure 7-7 illustrates the Kurtosis values for the healthy compressor and with ICL and DVL faults for four (60, 80, 100 and 120 psi) discharge pressures. Even though significant differences were observed in Kurtosis values between the healthy condition and seeded faults, there was no systematic differentiation between them.

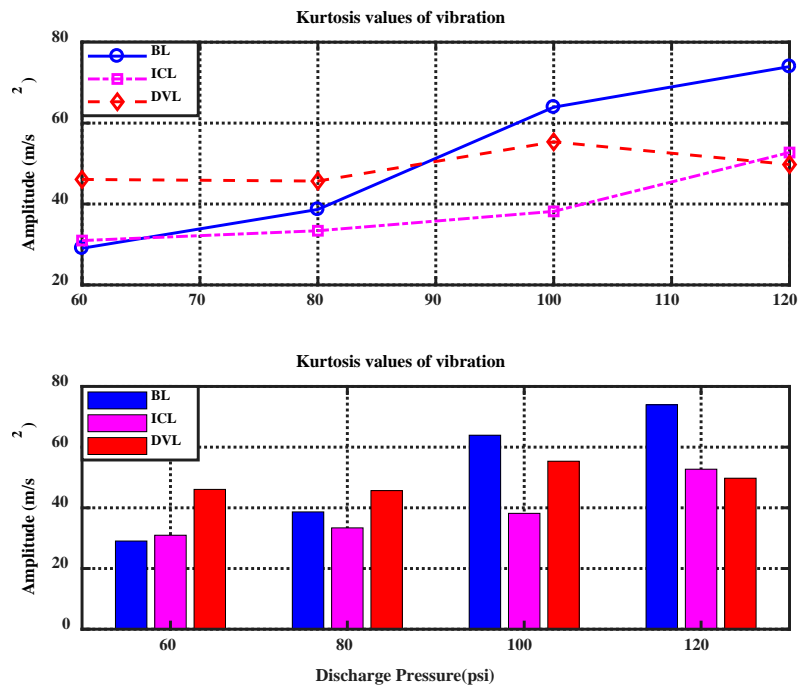


Figure 7-7: Kurtosis values for the time-domain waveform of the second cylinder vibration for healthy condition and two seeded faults for four discharge pressures

7.6 Vibration Signal Spectrum Analysis

The frequency-domain of the vibration responses often shows more useful information regards the operation of the machine being monitored than the time-domain. The presence of a fault can often be linked to a particular frequency signature in the vibration spectrum. The vibration signatures of working compressors are characterized by combinations of intermittent non-linear events as when the mechanical movement of a valve plate causes metal-to-metal impacts when they collide with their seats, which produce transient, non-linear vibrations, even shock waves [25]. The periodicity of these shocks can be related to the crankshaft rotation or to the motion of the valves. The latter is considered to be in the frequency range between 1 kHz to 10 kHz [24]. Analysing the relation between compressor speed and structural resonances permits a more comprehensive depiction of the non-linear vibration signatures.

The normal working of a compressor means the compression and expansion processes will cause a periodic variation of the load with a corresponding variation in compressor speed. Defects in an RC such as a valve leakage, shaft unbalance, loose drive belt, will cause an increase in the fluctuation of the load and, therefore, enhance amplitude modulation of the angular speed of the compressor [24]. However, other faults such as intercooler leakage may act to reduce the amplitude modulation.

The reciprocating movement of the piston normally generates periodic impacts, which will modulate the vibration signals. The frequency range of such vibrations is very broad hence their vibration spectra can be complicated [24]. If the vibration signal is subject to these modulations it will contain sidebands, primarily around the driving frequency so it would be expected that the fault features for an RC would have some degree of modulation. Consequently, demodulation analysis is a necessary part of signal processing for CM and fault diagnosis of RCs.

Figure 7-8 illustrates typical vibration spectra of the RC as measured by the accelerometer on the second stage cylinder for the low-frequency range, 2 Hz to 700 Hz. The measurements were for a healthy compressor and compressor with DVL and ICL faults for different discharge pressures (80, 100 and 120 psi). The fundamental compressor frequency ($f_r = 7.3$ Hz) is, as expected, present at all three discharge pressures, and can be seen to increase in amplitude as discharge pressure increased. The presence of the

second stage DVL caused significant variances in the amplitudes of the signals, the larger the discharge pressure the greater the difference with the healthy signal.

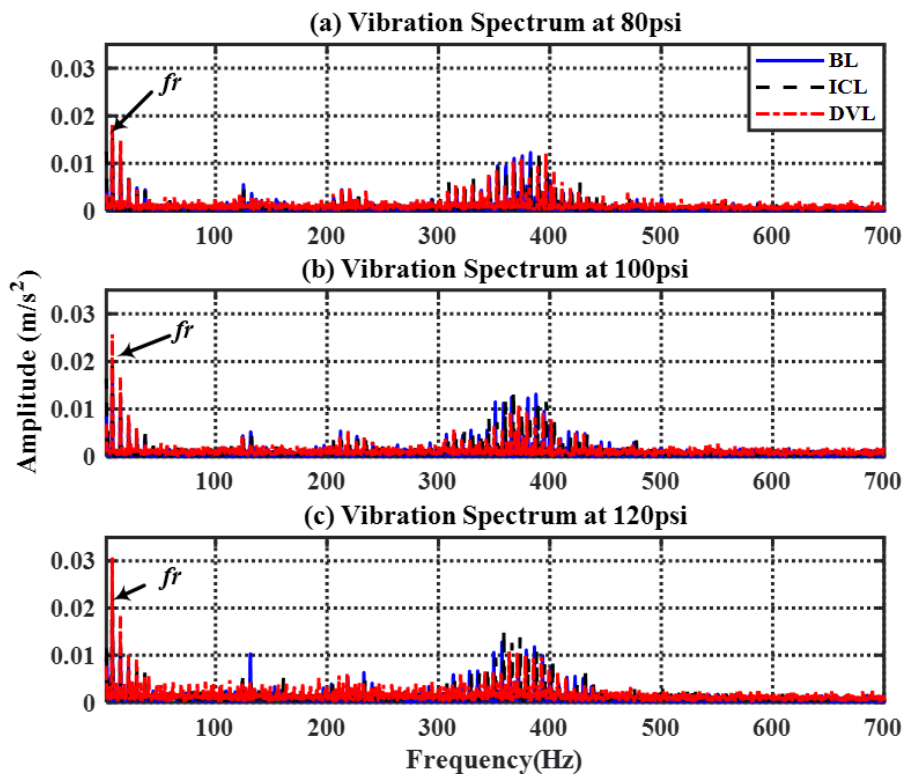


Figure 7-8: Low-frequency vibration spectra for the healthy compressor (BL) and compressor with two simulated faults (DVL and ICL) for discharge pressures 80, 100 and 120 psi

The fundamental shaft rotational frequency and its harmonics (7.3, 14.6, 21.9, 29.2 and 37.5 Hz) are clearly visible and clearly increase in magnitude with an increase in discharge pressure. However, the frequency range 300-450 Hz shows a high degree of fluctuation and the amplitude modulation could possibly be due to the effect of structural resonances. However, any structure resonance is unlikely to be affected by a change in compressor discharge pressure or the presence of faults. If this modulation effect is due to structural resonance, then demodulation analysis should be able to separate this from changes of the compressor vibration response because of the presence of seeded faults.

Demodulation (envelope) analysis is suited to machine diagnostics when the measured signal exhibits an amplitude-modulated effect [152]. Figure 7-9 depicts the envelope analysis for the high-frequency band of the measured vibration signals for healthy and simulated compressor faults. The fundamental compressor rotation frequency ($f_r = 7.3$

Hz) and its harmonics are obvious for both healthy and faulty compressors. Yet, the figure provides no clear differences between the various operating conditions. The change of amplitude is not consistent with either the change of the discharge pressure or different fault conditions.

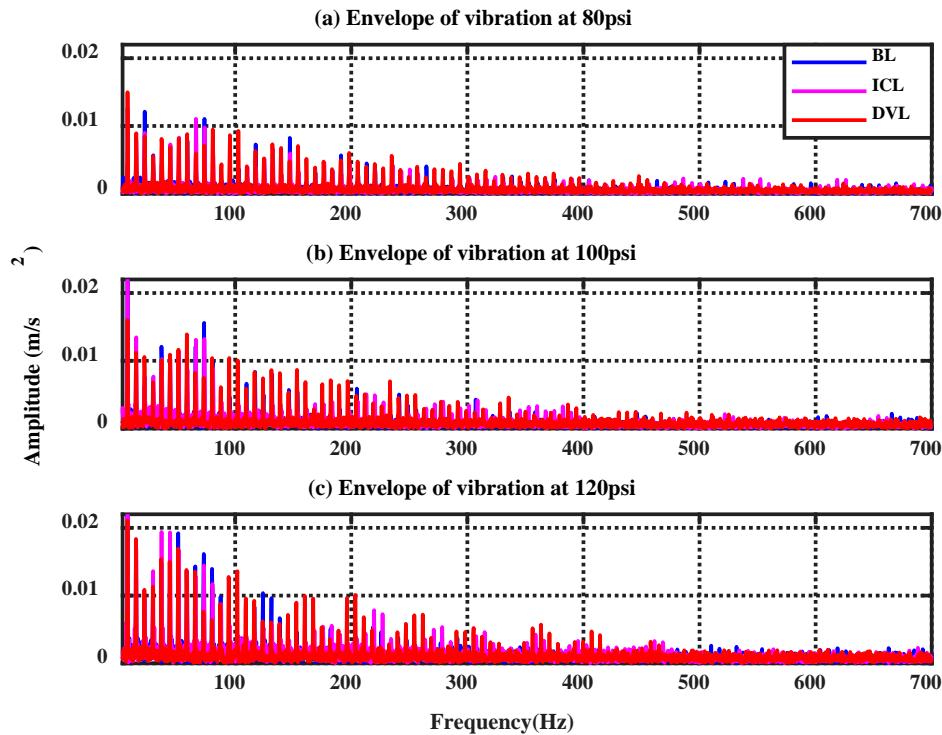


Figure 7-9: Envelope analysis of vibration signal for healthy (BL) and seeded faults (DVL and ICL) for discharge pressures 80, 100 and 120 psi

For a clearer representation of the amplitudes of the peak at f_r and its harmonics for the different compressor conditions and discharge pressures, Figure 7-10 presents the amplitudes of the first three harmonics, for healthy, DVL and ICL conditions. It is noticeable there is no clear or consistent pattern in the amplitudes of the peaks, whether for healthy or faulty conditions nor is there any clear or consistent difference between the conditions. Thus, it is not easy to separate seeded faults from the healthy operation. This means that the envelope signature is unable to clearly separate faulty and healthy cases, envelope analysis does not provide sufficient information for early diagnosis of compressor faults.

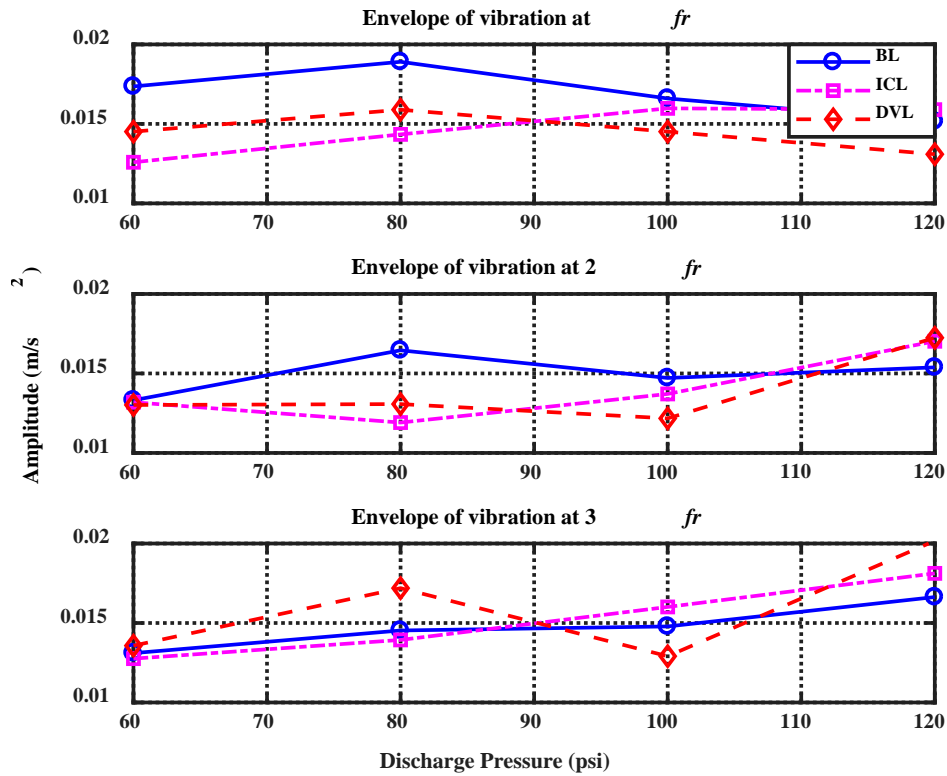


Figure 7-10: Magnitudes of the first (fr), second ($2fr$) and third harmonic ($3fr$) for healthy (BL) and seeded faults (DVL and ICL) for discharge pressures 60, 80, 100 and 120 psi.

7.7 The Implementation of MSB Analysis

As previously mentioned, the compressor normally operates with a range of discharge pressures leading to corresponding changes in crankshaft rotational speed, which causes a periodical variation in motor load. This fluctuating load can smother small changes caused by incipient faults. Consequently, advanced signal processing techniques are needed to describe the various amplitude changes and nonlinear interactions to improve the detection of minor changes in order to separate different types of compressor faults.

MSB analysis has been used to detect and diagnose the nonlinear effects of seeded faults DVL and ICL in order to depict the complex modulation. It has been described how valves impacting upon their seats generate transient vibrations and create non-linear characteristics, especially during the high-pressure stages or after a long period in service. Alwodai et al [31] have demonstrated the potential of MSB analysis to extract relevant information from modulated signals and to remove non-modulated and random

components accurately and efficiently. MSB analysis is capable of characterizing complex modulation signals, permitting easy manipulation of characteristic features and overcoming high levels of background noise.

7.8 MSB Magnitude Characteristics

In order to assess the performance capabilities of MSB analysis for RC conditions, vibration signal acquired during experimental tests were processed using MSB. In order to ensure a stable result, a frequency resolution of 0.7480 Hz through 84 averages was applied. In order to eliminate the interference of low-frequency vibration, a high-frequency range based MSB calculation was carried out. For a modulator frequency range $f_x = 0\text{Hz} \approx 30\text{Hz}$, so as to catch the crankshaft rotational frequency (7.3 Hz) up to its fourth order, the carrier signal range was, $f_c = 3.0\text{kHz} \approx 4.5\text{kHz}$.

Figure 7-11 illustrates typical MSB magnitudes of compressor vibration signals under discharge pressures 60, 80, 100 and 120 psi, for a healthy compressor and compressor with DVL and ICL. Results showing the MSB magnitudes indicate typical peak patterns through the carrier frequency which may be due to the fluctuation of airflow and/or flutter of valve plates during the suction and discharge stroke, especially for the faulty conditions. More significantly, the peak amplitudes of corresponding peaks tend to be about 30% higher for the faulty cases than the healthy cases, see discharge pressures of 100 psi and 120 psi. The higher peak amplitudes may be features to be used in the detection of faults. The shape of the MSB magnitudes tends to be more continuous along with slices through the modulator frequency at about 3 kHz and 4 kHz, and more discontinuous across the carrier frequency. Since this appears during high discharge pressure conditions, it could be an indication of the overpowering effect of valve plate impact on its seat as a result of a highly pressured air stream.

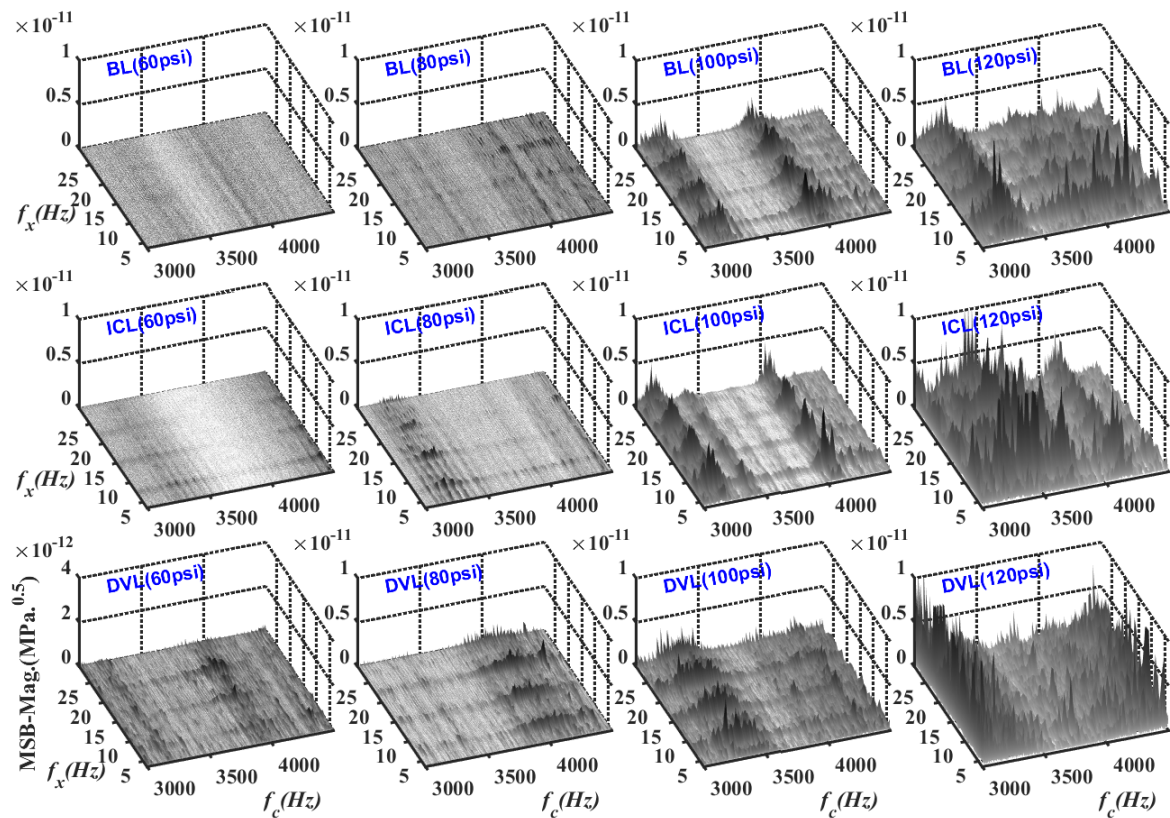


Figure 7-11: MSB magnitudes for healthy (BL) and faulty conditions (DVL and ICL) for discharge pressures 60, 80, 100 and 120 psi. Modulator frequency f_x : 0 Hz \approx 30 Hz, carrier signal f_c : 3.0 kHz \approx 4.5 kHz

7.9 Averaged MSB Magnitude Comparisons

The analysis of MSB magnitudes for the measured vibration signals can reveal unique features concerning compressor condition and compressor fault diagnostics. The diagnostic capability of the average amplitudes derived from the MSB analysis of the compressor operating at various discharge pressures under various fault conditions is illustrated in Figure 7-12. For all conditions, the amplitudes tend to increase with compressor discharge pressure and it is possible to differentiate between the three various faults (DVL, ICL and BL) based on the high-frequency band amplitude (3 - 4.5 kHz). The distinction between the three cases is clearer at higher discharge pressures because there is more fluttering of the valve plate and greater collision between the valve seat and plate thereby generating larger vibration signatures.

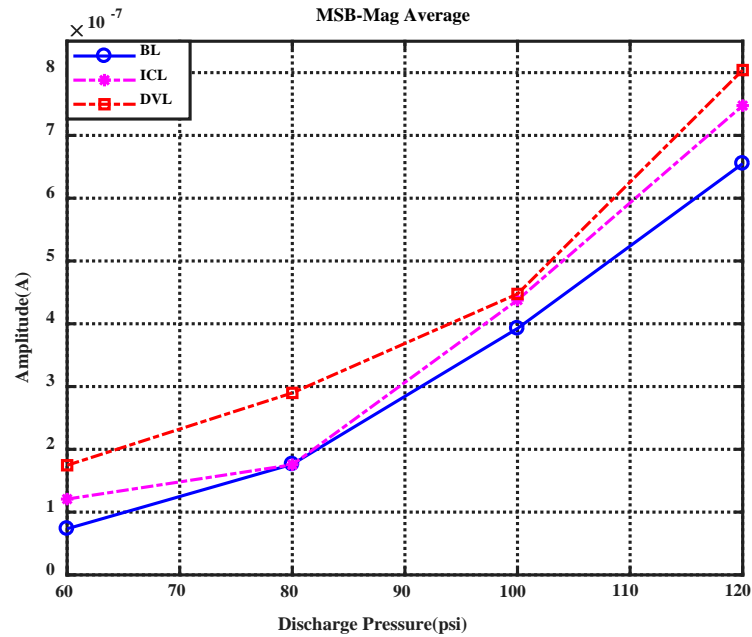


Figure 7-12: Average MSB magnitudes for healthy (BL) and faulty conditions (DVL and ICL) for discharge pressures 60, 80, 100 and 120 psi. Modulator frequency f_x : 0 Hz \approx 30 Hz, carrier signal f_c : 3.0 kHz \approx 4.5 kHz

The use of MSB to analyse the compressor vibration signals produced a successful diagnosis of two simulated faults (DVL and ICL) by characterising the nonlinear vibration responses using MSB magnitudes. The seeded DVL tended to significantly increase the MSB amplitude at every discharge pressure tested, see Figure 7-12. It can be concluded that the averaged MSB magnitude can distinguish between DVL and the healthy condition at all discharge pressures. Unfortunately, the MSB magnitudes for the ICL were only clearly different from both BL and DVL at the minimum and maximum discharge pressures. The DVL magnitudes were significantly higher than those obtained for ICL, save at 100 psi, and the ICL was significantly higher than the healthy case save at 80 psi.

7.9.1 Comparison Between Spectrum and MSB

A comparison of MSB and envelope analysis based on vibration responses for both healthy and seeded faults is depicted in Figure 7-13, which shows average peak MSB magnitudes and envelope of the vibration signal for healthy compressor, DVL and ICL at different discharge pressures (60, 80, 100 and 120 psi).

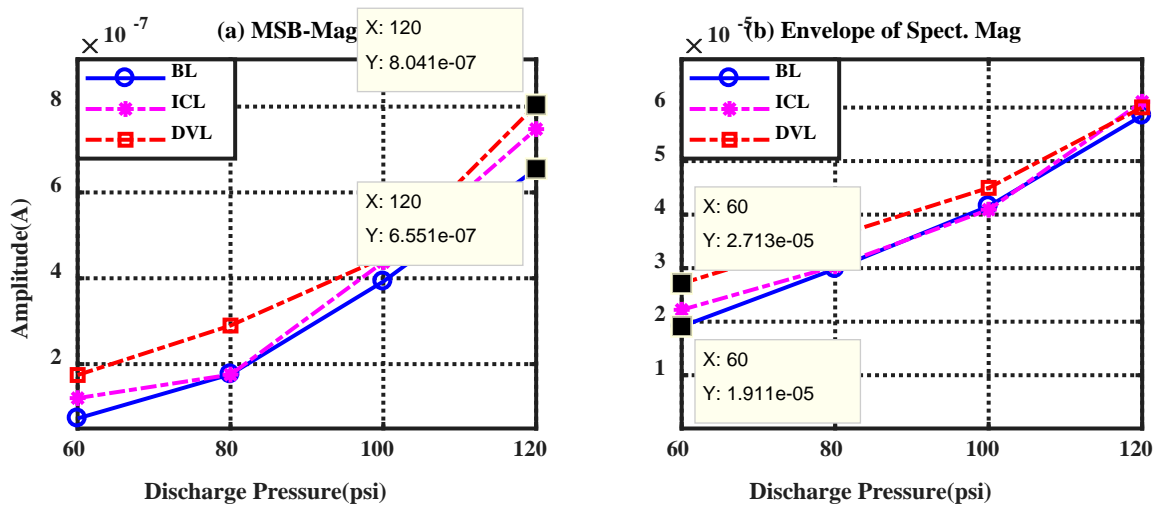


Figure 7-13: Vibration signal based diagnosis comparison between MSB and Envelope spectrum for healthy (BL) and seeded faults (DVL and ICL) at four discharge pressures

From Figure 7-13 it can be seen that the seeding of the two faults (DVL and ICL) consistently boosted the magnitude of the compressor vibration, except for a discharge pressure of 100 psi for the envelope spectrum. Similarly, the amplitude of the vibration response increased as the pressure increased. From Figure 7-13 the peak average of MSB amplitude in the high-frequency band shows that DVL can easily be separated from the healthy condition. Similarly, there is a possibility to distinguish the healthy operation from ICL faults. Additionally, the MSB showed very good performance in noise reduction compared to envelope analysis, for the same high-frequency range as illustrated in Figure 7-13 (a) and Figure 7-13(b) respectively.

The MSB results show substantial differences between different cases, whereas it is difficult to make a distinction based on the envelope analysis. It is concluded that the MSB is very effective in suppressing noise and fault separation compared to envelope analysis, particularly at the highest and lowest discharge pressures. The vibration-based diagnosis gives more support to MSB providing better diagnosis, that it separates different faulty conditions better than envelope analysis. Generally, the evaluation of this experiment demonstrates that the MSB-based diagnosis performs better than envelope analysis, giving significantly better results and clearer differentiation of the vibration signals.

As presented in Chapter 6 Section 6.6 for determining the percentage differences between level recorded for the healthy compressor and level for each seeded fault, according to the data presented in Figure 7-13.

At discharge pressure 120 psi the value for MSB sideband Figure 7-13 (a), DVL and BL values are $8.041e-07$ and $6.551e-07$ respectively. Calculating the percentage difference between DVL and healthy condition as follows:

$$\text{PercentageDifference, \%} = [(8.041e-07 - 6.551e-07) / 6.551e-07] * 100 = 22.74 \quad (7.1)$$

The spectrum sideband Figure 7-13 (b) values for DVL and BL are $2.713e-05$ and $1.911e-05$ respectively. The percentage difference of DVL from baseline is

$$\text{PercentageDifference, \%} = [(2.713e-05 - 1.911e-05) / 1.911e-05] * 100 = 42.01 \quad (7.2)$$

From Figure 7-14 and Table 7-1, it can be observed that the MSB produced more accurate results for the compressor condition under different fault cases at different compressor discharge pressures compared with envelope spectrum analysis. In particular, it easily separated the seeded faults under all discharge pressures with a clear difference between the MSB results and envelope values, as seen in Figure 7-14.

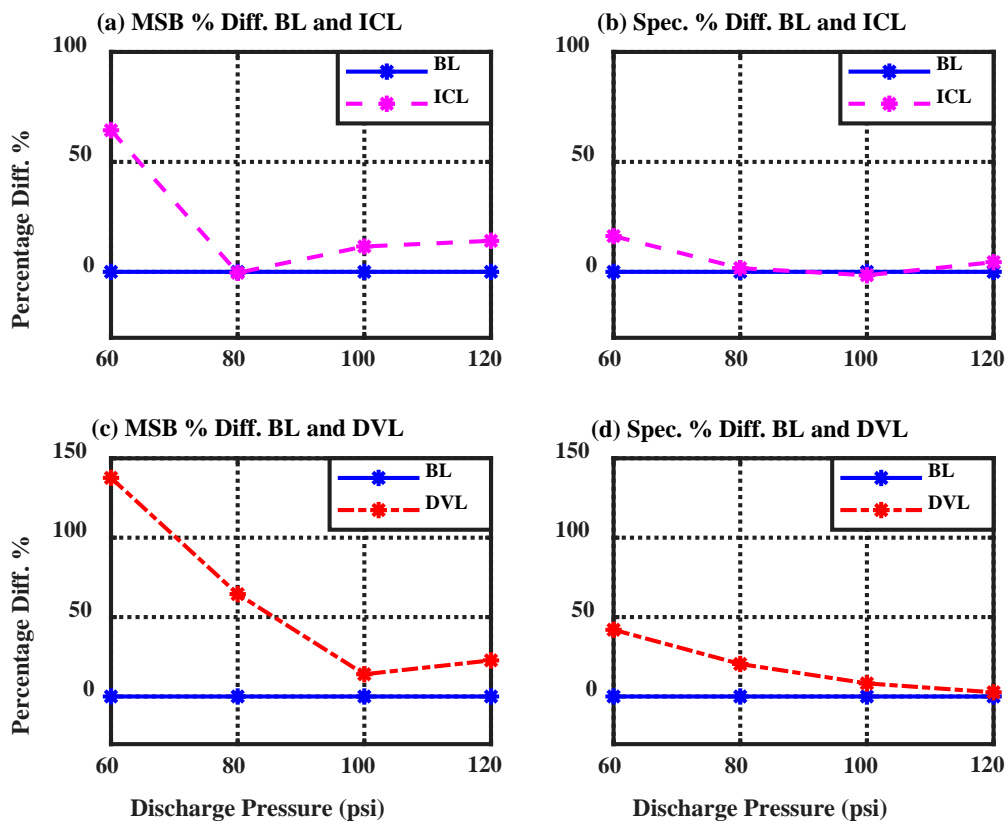


Figure 7-14: Percentage difference between DVL and MSB, and ICL and MSB for four discharge pressures

Table 7-1: Differences between BL and seeded faults

Faulty Case	Percentage Difference for MSB-mag average				Percentage Difference for Envelope Spectral-mag			
	60psi	80psi	100psi	120psi	60psi	80psi	100psi	120psi
ICL	64.38%	-0.44%	11.53%	14.11%	16.25%	1.69%	-1.57%	4.40%
DVL	137.68%	64.4%7	14.00%	22.74%	42.01%	20.46%	8.24%	2.63%

7.10 Summary

This chapter has shown the effectiveness of applying MSB to analysis the compressor vibration signature to detect valve leakage and intercooler leakage faults under different compressor discharge pressures. The vibration responses from the compressor were very complicated and contaminated with machine background noise to such an extent that simple frequency analysis was unable to characterise the abnormal compressor condition. The MSB representations were able to characterise these complicated modulations according to valve movements and airflow fluctuations and allowed easy analysis to identify characteristic features.

A key factor for machine fault detection and diagnosis is the ability to identify small changes in the sensor signal caused by abnormal conditions and extract them from a noisy and complicated vibration signal. This chapter has shown the successful implementation of the MSB to suppress random noise and enhance the periodic fault signatures to produce more accurate and reliable diagnostic results for a wide range of compressor discharge pressure in comparison with conventional spectrum analysis.

MSB was able to relate changes in the in-cylinder pressure due to the periodic couplings between structure resonances and fluctuations in speed due to change in machine loading, the mechanical impacts of valve plates, nonlinear transfer paths, and fluctuations of the airflow through the valve system leading to transient vibrations, which show different types of spectral features. The vibration signature analysis by means of the Modulation Signal Bispectrum (MSB) was used for a more detailed representation of the nonlinear vibration responses.

This work has clearly demonstrated that the MSB analysis of the compressor vibration signatures has substantial potential as a means to detect the presence of incipient faults in

RCs and thereby obtain stable and accurate features to indicate the cause of the faults. It shows that the MSB based on vibration signals provides a more reliable and accurate diagnosis of compressor faults compared with spectrum analysis as illustrated in Figure 7-13 under a wide range of compressor discharge pressures.

CHAPTER 8:

Conclusions and Suggestions for Future Work

The chapter reviews the conclusions of this study and presents its achievements based on the original objectives as mentioned in the first chapter and represented here. Next, there is a detailed summary of the contribution to knowledge made by this study. Finally, several recommendations are made for future work and improvement of reciprocating compressor condition monitoring

8.1 Objectives and Achievements

This section provides a detailed review of how this research study has met the Aim and Objectives stated in Chapter 1. The research achievements have been linked to the stated objectives of the research, Section 1.6.

With the aim to improve the performance of machine fault detection and diagnosis based on MCSA, vibration measurements, and dynamic model predictions, this study first investigated the motor current signature to assist RC condition monitoring reliability. It has been demonstrated that the current signal contains sufficient information for the detection and diagnosis of faults in compressor operation, different simulated faults to a good degree of accuracy.

Next, a comprehensive compressor model was developed and validated with experimental results and good agreement found. This enabled, effective diagnostic features of the various compressor and motor faults to be examined under various compressor discharge pressures. Focusing on MCSA, this research has developed a new procedure for fault detection of the RC based on modulation signal bi-spectrum (MSB) analysis.

The research project's key achievements corresponding to the research objectives are:

Objective 1. To gain a general knowledge on RC and associated three-phase induction motors, their working principles, operating mechanism and commonly occurring faults. To review different existing techniques for machine CM in order to evaluate the performance of these methods for early fault detection of RC.

Achievement 1. This objective is met in Chapter 2, in which, it provides a review of the compressor operation, their common constructions, types and classification. How various industries rely on RC as a useful and convenient power source for other industrial machines. The chapter also reviewed the most prevalent faults occurring in compressors and their driving motors, which include compressor leakages and stator winding asymmetry. Any failures occurring in the machine (compressor and/or motor) will alter the normal operating condition of the compressor and can lead to a total system failure. An extensive review was performed in Chapter 3 to evaluate the performance of the most common CM systems used for early and effective fault detection. It has been found that motor stator current contains

valuable information, is readily available, widely used for monitoring different industrial machinery and can be implemented remotely. Additionally, machine vibration responses are able to characterise the machine condition. Thus, the focus of this research study has been to use the motor stator current and surface vibration as reliable methods to monitor the compressor operation under different faulty conditions including combined fault.

Objective 2. To construct a compressor test facility and simulate different compressor faults in a realistic way to enable subsequent system behaviour to be characterised, then obtain experimental data to evaluate the compressor performance under these operating conditions.

Achievement 2. AN RC test facility had been constructed to investigate compressor abnormal conditions. Chapter 4 provides a full description of the RC test rig used to carry out this experimental study. It consists of, a two-stage, single action, V-shaped, two cylinders RC mounted on the top of an air tank (receiver). The compressor was run at constant speed driven by three-phase induction motor via a pulley drive belt system with a transmission ratio 3.2. A complete description of the procedure of how the simulations of different common compressor faults were seeded into the test rig to obtain experimental data was presented in this chapter.

Objective 3. To develop an extended model of compressor dynamics in a MATLAB environment to study compressor behaviour under a wide range of operating conditions including different faults. Also, to study the predicted changes in motor current signature - due to the presence of the seeded faults - on the AC induction motor, crankshaft dynamics, the mass flow rate through valves and cylinder pressure variation. To seek to establish effective and reliable diagnostic features.

Achievement 3. An extended two-stage RC mathematical model has been developed in Chapter 5 to simulate the compressor working cycle for healthy compressor and to enable the consequences of seeding different faults into the compressor to be studied. The model investigated the effect of different faults on the RC performance to demonstrate, evaluate and predict seeded faults signatures, which contributed to the compressor CM assessment. Each simulated fault had different signatures in the stator current of the motor under different loads, which also had an effect on the

pressure changes during the compressor cycle. Thus, studying these signatures can significantly improve the detection and diagnosis of the compressor faults.

Objective 4. To obtain an effective and stable analysis of the stator current signature of a two-stage RC under healthy and faulty operating conditions; in terms of both experimental tests and dynamic model responses. Also, compare experimental results and model predictions to evaluate the developed model to help implement a diagnostic approach for compressor fault feature extraction.

Achievement 4. The compressor dynamic model response has been solved numerically using MATLAB to simulate the responses of the RC under healthy and faulty conditions in Chapter 5. An evaluation of the developed model with the experimental results for a healthy compressor and compressor with different simulated faults showed a good agreement between the simulated result with the experimental findings. The model was then used to predict the signature of other compressor and motor faults occurring in isolation or combination. A number of characteristic features were obtained from the signature drawn by the stator current of the motor for each individual fault based on the analysis of the MSB peak values at different harmonics for the purpose of fault identification and diagnosis

Objective 5. Investigate the capability of the induction motor current signals to detect and diagnose compressor and motor faults (individual or combined) and apply different signal processing methods to study the possibility of using motor current for monitoring different compressor faults with a high degree of accuracy.

Achievement 5. The experimental study of the detection capabilities was carried out based on three common compressor faults and one combined fault: discharge valve leakage, intercooler leakage, stator winding asymmetry and combined fault (discharge valve leakage with stator winding asymmetry). Time domain and frequency domain were applied to the acquired data to evaluate how the motor current signatures correlated with the compressor performance under these conditions and its capacity for detecting these seeded faults. Evaluation of results in Chapter 6 shows that the motor current waveform exhibited a clear amplitude modulation caused by the load fluctuation due to the compressor pressure difference during the working cycle. The combined fault and valve leakage cause an increase

in the amplitude of the sidebands of the motor current signal, the amplitude increased as the discharge pressure increase. it showed that the motor current signals contain useful information and can give an effective indication and diagnosis of compressor faults.

Objective 6. To study modulation effects and non-linear characteristics to extract weak signatures from vibration and current signals, then compare the performance of the current and vibration techniques for the development of more efficient and reliable signal processing tools and evaluate the performance of MSB for RC condition monitoring.

Achievement 6. Chapter 6 illustrated the performance of CM of compressor faults such as stator winding asymmetry, valve leakage, intercooler leakage and combined fault. It studied the analysis of stator current signals based on MSB analysis for attaining an accurate characterisation of the modulation induced by the compressor variable loads. The experimental results based on MSB analysis are shown to achieve early detection and diagnosis of the RC conditions. The comparative study illustrated that MSB effectively suppressed noise and was able to provide better fault separation compared to spectrum analysis, as shown in Figure 6-11. The MSB analysis of the stator current signal has significant potential for the detection and diagnosis of the presence of compressor faults, thus, it is able to provide more accurate and reliable diagnostic features under a wide range of compressor discharge pressures compared with conventional spectrum analysis. In Chapter 7 the implementation of the MSB to enhance the periodic fault signatures in vibration signals from the RC. The MSB based on vibration signals gives more reliable and accurate diagnosis compared with spectrum analysis, as shown in Figure 7-13, and thereby obtain stable and accurate diagnostic features under a wide range of compressor discharge pressures.

Objective 7. To provide useful information and recommendations for future research activity relating to this field.

Achievement 7. A number of suggestions for future work compressor CM are presented in Section 8.4.

8.2 Conclusions

This research has investigated the performance of compressor CM and fault detection based on the motor current signature analysis and vibration measurements. Based on simulation and experiment, the key conclusions can be summarised as:

1. An extended comprehensive compressor dynamic model has been developed to provide a detailed simulation of motor current characteristics corresponding to changes caused by particular faults, to establish effective and reliable diagnostic features for compressor CM. A comparative study showed a good agreement between the simulated result and the experimental finding for both in-cylinder pressure and motor current signature under different compressor discharge pressures.

the was done for the same faults and under the same discharge pressure.

- 1st stage and 2nd stage cylinder pressure for both experimental and model prediction have the same basic features for each compressor cycle, see Section 5.10.2 and Figure 5-10.
 - Leakage through discharge valve caused a significant change to the cylinder pressure waveform for both stages as noted in Figure 5-16 and Figure 5-17.
 - Similar motor current behaviour (signature) for model predictions and experimental measurements Section 5.11.2 and Figure 5-18.
 - For the motor current spectrum (measured and predicted), valve leakage caused an increase in the sideband amplitude due to the high-pressure airflow back into the 2nd stage. Whereas, intercooler leakage caused a reduction in the sideband amplitude, see Section 5.11.3 and Figure 5-20 and Figure 5-21.
 - The agreement between measurement and prediction suggested that the model is precise enough to be used for further simulation research.
2. Four primary diagnostic features can be extracted for use for compressor CM based on the mathematical model, see Section 5.12, Figure 5-23.
 - Extracted feature from the speed pattern and MSB peaks at $1f_r$ and $2f_r$ for compressor simulated faults (SVL, DVL, ICL and LBT), Figure 5-24 and Figure 5-25 showed each fault produced a different signature and could be used to effectively differentiate it from other faults.

- The speed pattern and MSB peaks at $1f_r$ and at f_{brb} can be used to extract motor faults (BRB, SWA and SWA+1BRB). The BRB fault produces an obvious effect at f_{brb} .
3. The results presented in Chapter 6 showed that the motor current signal contains information, which can produce desirable results in detecting and diagnosing compressor operation under different simulated faults including the combined fault, to a good degree of accuracy.
 - It has been demonstrated that each fault causes a change to the modulated motor current signal.
 - All seeded faults can be separated for a wide range of compressor pressures.
 4. This research study also examined the diagnosis of the stator winding asymmetry combined with discharge valve leakage and other singly compressor common faults under different compressor discharge pressures (loads) based on stator current signals.
 - Both conventional spectrum analysis and MSB analysis were used to process the current signature to attain an accurate characterisation of the modulation induced by the compressor variable loads.
 - Sideband amplitude for combined fault and discharge valve leakage are significantly higher than for the baseline and intercooler leakage.
 - Spectrum analysis was able to differentiate faulty cases from the healthy condition but not fully separate the different fault conditions, see Figure 6-7.
 - MSB based diagnosis demonstrated better noise reduction and fault separation compared to spectrum analysis, see Figure 6-11.
 - MSB was able to provide diagnostic features for compressor fault detection accurately and reliably under a wide range of compressor discharge pressures compared to spectrum analysis as shown in Figure 6-12.
 5. MSB analysis of compressor vibration and motor stator current signals demonstrated the capabilities of characterising and enhances the non-linear and modulated behaviour of compressor conditions induced by a fault, in which produced better performance in extracting fault features and led to accurate and consistent fault diagnosis.
 6. The results presented in Chapter 7 demonstrated the effectiveness of using the compressor vibration signature for the detection of discharge valve leakage and intercooler leakage faults under different compressor discharge pressures. The MSB

analysis was able to produce a more accurate analysis to detect the presence of valve leakage and intercooler leakage compared to conventional spectrum analysis, as illustrated in Figure 7-13.

7. MSB analysis of compressor vibration and motor stator current signals demonstrated the capabilities of characterising and enhances the non-linear and modulated behaviour of compressor conditions induced by a fault, in which produced better performance in extracting fault features and led to accurate and consistent fault diagnosis

8.3 Contributions to the Knowledge

The research achievements have led to a number of new contributions to the knowledge in the direction of RC conditions monitoring, which can be largely highlighted in the following four aspects:

First Contribution:

The mathematical model including the simulation of electrical faults and the effect of combined compressor faults on the stator current of the induction motor has not been investigated previously to simulate and understand the stator current signatures for RC condition monitoring.

Second Contribution:

There are no previous studies in the literature of applying the advanced signal processing technique-MSB to analysing the stator currents for the diagnostics of combined mechanical and electrical faults in compressors. In particular, the author believes that the use of the MSB peaks at $1f_r$, $2f_r$ and f_{brb} for the diagnostics of compressor and motor faults is a novel contribution.

Third Contribution:

The conventional spectrum analysis, Hilbert based demodulation and MSB analysis of vibration responses have shown that MSB is more accurate in diagnosing the faults simulated. It is believed that the comparative analysis of compressor vibration is the first

one and confirmed that the MSB technique for detecting valve leakage and intercooler leakage is particularly effective.

Fourth Contribution:

No study has been found to investigate the detection and diagnosis of the stator winding asymmetry combined with discharge valve leakage and other single compressor faults using MSB analysis based on stator current signals from the induction motor. Thus, the work presented in this research is believed to be unique for providing a new technique to detect the combined faults based on MSB analysis, which leads to the establishment of more effective and reliable diagnostic features compared with conventional spectrum analysis.

8.4 Recommendations for Future Work

It has been demonstrated through the result of this research that the effectiveness of using advanced signal processing technique to analysis both numerical and experimental stator current signals for the development of more accurate detection and reliable means of diagnosis of faults in an RC and its associated three-phase motor. To further improve the compressor CM and fault diagnosis, the author of this thesis suggests a number of recommendations.

Recommendation One:

A more experimental study is needed to verify and investigate the sensitivity of the proposed method to detect incipient faults that occur in RC machines.

Recommendation Two:

A more experimental study is needed to investigate other compressor faults such as piston ring leakage, filter blockage and bearing faults with different severity levels, based on both vibration and motor current signatures.

Recommendation Three:

Improve the compressor simulation model to analyse the compressor vibration responses and include different compressor and motor faults in isolation and combined.

Recommendation Four:

The research could be extended to use different sensors such as microphones for airborne sound to monitor the compressor condition under different faults; singly and in combinations.

Recommendation Five:

In order to evaluate the performance of MCSA for its consistency and sensitivity, more investigation is needed on multi-stage RCs e.g. four-stage compressor or double-acting compressor.

Recommendation Six:

The MSB was applied to compressor vibration signal to detect and diagnose compressor faults, as demonstrated in Chapter 7. It is recommended to extend the study to examine other compressor faults such as leakage through the suction valve combined with discharge valve leakage and other combinations of faults.

Reference:

1. Britain, G., *A guide to the condition monitoring of machinery*. 1979: HM Stationery Office.
2. Davies, A., *Handbook of condition monitoring: techniques and methodology*. 2012: Springer Science & Business Media.
3. Rao, B.K.N., *Handbook of condition monitoring*. 1 ed. 1996, UK: Elsevier.
4. Kelly, A. and M. Harris, *Management of Industrial Maintenance*, Newnes. 1997, Butterworths, Oxford.
5. Mechefske, C.K., *Machine condition monitoring and fault diagnostics*, in *Vibration Monitoring, Testing, and Instrumentation*. 2007, CRC Press. p. 25-1/25-35.
6. Mobley, R.K., *An introduction to predictive maintenance*. Second ed. 2002, USA: Elsevier Science.
7. Shaeboub, A., *The Monitoring of Induction Machines Using Electrical Signals from the Variable Speed Drive*. 2018, University of Huddersfield: UK.
8. Pan, M.-C., P.-C. Li, and Y.-R. Cheng, *Remote online machine condition monitoring system*. *Measurement*, 2008. **41**(8): p. 912-921.
9. Mehala, N., *Condition monitoring and fault diagnosis of induction motor using motor current signature analysis*. A Ph. D Thesis submitted to the Electrical Engineering Department, National Institute of Technology, Kurushetra, India, 2010.
10. Zhang, Y., et al. *Condition monitoring and fault detection of a compressor using signal processing techniques*. in *American Control Conference, 2001. Proceedings of the 2001*. 2001. IEEE.
11. AlThobiani, F. and A. Ball, *An approach to fault diagnosis of reciprocating compressor valves using Teager–Kaiser energy operator and deep belief networks*. *Expert Systems with Applications*, 2014. **41**(9): p. 4113-4122.
12. Ahmed, M., et al. *Fault diagnosis of reciprocating compressors using relevance vector machines with a genetic algorithm based on vibration data*. in *Automation and Computing (ICAC), 2014 20th International Conference on*. 2014. IEEE.
13. N. A. Hussein, D.Y.M., E. M. Abdul-Baki, *3-phase Induction Motor Bearing Fault Detection and Isolation using MCSA Technique based on neural network Algorithm*. *Journal of Engineering and Development*, 2012. **16**(3): p. 15.
14. Alwodai, A., F. Gu, and A. Ball. *A comparison of different techniques for induction motor rotor fault diagnosis*. in *Journal of Physics: Conference Series*. 2012. IOP Publishing.
15. Bardou, O. and M. Sidahmed, *Early detection of leakages in the exhaust and discharge systems of reciprocating machines by vibration analysis*. *Mechanical Systems and Signal Processing*, 1994. **8**(5): p. 551-570.

16. Jardine, A.K., D. Lin, and D. Banjevic, *A review on machinery diagnostics and prognostics implementing condition-based maintenance*. Mechanical systems and signal processing, 2006. **20**(7): p. 1483-1510.
17. Márquez, F.P.G., et al., *Condition monitoring of wind turbines: Techniques and methods*. Renewable Energy, 2012. **46**: p. 169-178.
18. Li, B., et al., *Application of S transform and morphological pattern spectrum for gear fault diagnosis*. Proceedings of the Institution of Mechanical Engineers, Part C: Journal of Mechanical Engineering Science, 2011: p. 0954406211408781.
19. Cheng, H.A., R.F. Carneiro, A.L.G., *Implementation strategies and tools for condition based maintenance at nuclear power plants*. International Atomic Energy Agency, Vienna, 2007.
20. Shaeboub, A., et al. *Detection and diagnosis of compound faults in induction motors using electric signals from variable speed drives*. in *Automation and Computing (ICAC), 2016 22nd International Conference on*. 2016. IEEE.
21. Gu, F. and A. Ball, *Use of the Smoothed Pseudo-Wigner-Ville Distribution*. Maintenance & Asset Management Journal, 1995. **10**(2): p. 16-23.
22. Elhaj, M., et al., *A combined practical approach to condition monitoring of reciprocating compressors using IAS and dynamic pressure*. World Academy of Science, Engineering and Technology, 2010. **4**(3): p. 287-293.
23. Pichler, K., et al., *Fault detection in reciprocating compressor valves under varying load conditions*. Mechanical Systems and Signal Processing, 2016. **70**: p. 104-119.
24. Elhaj, M.A., *Condition monitoring of reciprocating compressor valves*, in *School of Mechanical, Aerospace and Civil Engineering*. 2005, the University of Manchester: UK.
25. Randall, R.B., *Vibration-based condition monitoring: industrial, aerospace and automotive applications*. 2011: John Wiley & Sons.
26. Thomson, W.T. and M. Fenger, *Current signature analysis to detect induction motor faults*. IEEE Industry Applications Magazine, 2001. **7**(4): p. 26-34.
27. Tandon, N., G. Yadava, and K. Ramakrishna, *A comparison of some condition monitoring techniques for the detection of defect in induction motor ball bearings*. Mechanical systems and signal processing, 2007. **21**(1): p. 244-256.
28. El Hachemi Benbouzid, M., *A review of induction motors signature analysis as a medium for faults detection*. Industrial Electronics, IEEE Transactions on, 2000. **47**(5): p. 984-993.
29. Ashari, D., et al., *Detection and Diagnosis of Broken Rotor Bar Based on the Analysis of Signals from a Variable Speed Drive*. 2014.
30. Kalaskar, C.S. and V.J. Gond, *Motor Current Signature Analysis to Detect the Fault in Induction Motor*. International Journal of Engineering Research and Applications, 2014. **4**(6): p. 58-61.
31. Alwodai, A., et al. *Modulation signal bispectrum analysis of motor current signals for stator fault diagnosis*. in *Automation and Computing (ICAC), 2012 18th International Conference on*. 2012. IEEE.

32. Gu, F., et al., *A new method of accurate broken rotor bar diagnosis based on modulation signal bispectrum analysis of motor current signals*. Mechanical Systems and Signal Processing, 2015. **50**: p. 400-413.
33. Shaeboub, A., et al., *Modulation signal bispectrum analysis of electric signals for the detection and diagnosis of compound faults in induction motors with sensorless drives*. 2017. **5**(1): p. 252-267.
34. Haynes, H. and R. Kryter, *Condition monitoring of machinery using motor current signature analysis*. 1989, Oak Ridge National Lab., TN (USA).
35. Naid, A., *Fault Detection and Diagnosis of Reciprocating Compressors using Motor Current Signature Analysis*, in *Computing and Engineering*. 2009, The University of Huddersfield: Huddersfield.
36. Bloch, H.P. and J.J. Hoefner, *Reciprocating Compressors:: Operation and Maintenance*. 1996, United States of America: Gulf Professional Publishing.
37. Brown, R.N., *Compressors: Selection and Sizing*. Third ed. 2005, United States of America: Elsevier Inc.
38. Hanlon, P.C., *Compressor handbook*. 2001, United States of America: McGraw-Hill.
39. Robison, D.H. and P.J. Beaty. *Compressor Types, Classifications, And Applications*. in *Proceedings of the 21st Turbomachinery Symposium*. 1992. Texas A&M University. Turbomachinery Laboratories.
40. Brown, R.N., *Compressors: Selection and sizing*. 1997: Gulf Professional Publishing.
41. Mobley, R.K., *Maintenance fundamentals*, ed. Second. 2004, USA: Elsevier Inc.
42. Bloch, H.P., *A practical guide to compressor technology*, ed. Second. 2006, USA: John Wiley & Sons.
43. American Society of Heating, R. and I. Air-Conditioning Engineers, *ASHRAE Handbook - Heating, Ventilating, and Air-Conditioning Systems and Equipment (I-P Edition)*. 2008, American Society of Heating, Refrigerating and Air-Conditioning Engineers, Inc.
44. Steele, A., *Advanced Plumbing Technology II*. 2015: American Society of Plumbing Engineers.
45. Gupta, A.K. and S.K. Arora, *Industrial automation and robotics*. Second ed. 2009, New Delhi: Laxmi Publications.
46. Elhaj, M., et al., *Numerical simulation and experimental study of a two-stage reciprocating compressor for condition monitoring*. Mechanical Systems and Signal Processing, 2008. **22**(2): p. 374-389.
47. Ahmed, M., et al. *Fault diagnosis of reciprocating compressors using relevance vector machines with a genetic algorithm based on vibration data*. in *Automation and Computing (ICAC), 2014 20th International Conference on*. 2014. IEEE.
48. Barnes, M., *Practical variable speed drives and power electronics*. 2003: Newnes.
49. Haba, U., et al., *Detection and Diagnosis of Compound Faults in a Reciprocating Compressor based on Motor Current Signatures*. 2016.

50. Ben Sasi, A.Y., *Exploitation of Instantaneous Angular Speed for Machinery Condition Monitoring*, in *School of Mechanical, Aerospace and Civil Engineering*. 2005, University of Manchester: UK.
51. Elson, J.P. and W. Soedel, *Criteria for the design of pressure transducer adapter systems*. 1972.
52. Payne, B.S., *Condition monitoring of electric motors for improved asset management*. 2003: University of Manchester.
53. Chapman, S.J., *Electric Machinery Fundamentals*. Fifth ed. 2004, USA: McGraw-Hill, Inc.
54. Abdelhamid, F., *Detection And Diagnosis of Electrical Faults In Induction Motors Using Instantaneous Phase Variation*. 2005, The University of Manchester.
55. Bose Bimal, K., *Modern power electronics and AC drives*. New Jersey: Prentice Hall, 2002.
56. Mustafa, M.O., *Faults detection and diagnosis for three phase induction machines*. 2012, Luleå tekniska universitet.
57. Alwodai, A., *Motor fault diagnosis using higher order statistical analysis of motor power supply parameters*. 2015, University of Huddersfield.
58. Parekh, R., *AC Induction Motor Fundamentals*. Microchip Technology Inc, 2003.
59. Thomson, W.T. and R.J. Gilmore. *Motor Current Signature Analysis To Detect Faults In Induction Motor Drives-Fundamentals, Data Interpretation, And Industrial Case Histories*. in *Proceedings of the 32nd Turbomachinery Symposium*. 2003. Texas A&M University. Turbomachinery Laboratories.
60. Naid, A., et al. *Bispectrum Analysis of Motor Current Signals for Fault Diagnosis of Reciprocating Compressors*. in *Key Engineering Materials*. 2009. Trans Tech Publ.
61. Yeh, C.-C., et al., *A reconfigurable motor for experimental emulation of stator winding interturn and broken bar faults in polyphase induction machines*. *IEEE transactions on energy conversion*, 2008. **23**(4): p. 1005-1014.
62. Bell, R., et al., *Report of large motor reliability survey of industrial and commercial installations. I*. *IEEE Transactions on Industry applications*, 1985. **21**(4): p. 853-864.
63. Bhardwaj, K. and A. Agarawal, *Fault diagnosis of three phase induction motor using fuzzy logic controller and sequence analyzer*. *MIT International Journal of Electrical and Instrumentation Engineering*, 2012. **2**(2): p. 112-118.
64. Collacott, R.A., *Mechanical fault diagnosis and condition monitoring*. 2012: Springer Science & Business Media.
65. Starr, A. and B. Rao, *Condition monitoring and diagnostic engineering management*. 2001: Elsevier.
66. Ahmed, M., et al. *Fault detection and diagnosis using principal component analysis of vibration data from a reciprocating compressor*. in *Control (CONTROL), 2012 UKACC International Conference on*. 2012. IEEE.

67. Al-Qattan, M., et al., *Instantaneous angular speed and power for the diagnosis of single-stage, double-acting reciprocating compressor*. Proceedings of the Institution of Mechanical Engineers, Part J: Journal of Engineering Tribology, 2009. **223**(1): p. 95-114.
68. Habu, U., et al. *Diagnosis of Compound Faults in Reciprocating Compressors Based on Modulation Signal Bispectrum of Current Signals*. in *Proceedings of the 2nd International Conference on Maintenance Engineering, IncoME-II 2017, (University of Manchester, 5-6 September 2017)*. 2017. University of Manchester.
69. Higgs, P.A., et al. *A survey on condition monitoring systems in industry*. in *ASME 7th Biennial Conference on Engineering Systems Design and Analysis*. 2004. American Society of Mechanical Engineers.
70. Plant, M., Resource, Center., *2002 Condition Monitoring Survey Results*. 2002 [cited 2018 22/09/2018]; Available from: <http://www.plant-maintenance.com/articles/condition-monitoring-survey-02.shtml>.
71. Weidong, L., *A study of diesel engine acoustic characteristics*, in *Department of Mechanical Engineering*. 2000, University of Manchester: UK.
72. Chandroth, G., A. Sharkey, and N. Sharkey. *Cylinder pressures and vibration in internal combustion engine condition monitoring*. in *Proceedings of Comadem*. 1999.
73. Sasi, A.B., et al. *The exploitation of instantaneous angular speed for condition monitoring of electric motors*. in *Proceedings of the 14th International Congress on Condition Monitoring and Diagnostic Engineering Management (COMADEM 2001), Manchester, UK*. 2001. MMU Cheshire.
74. Sasi, A.Y.B., et al., *A validated model for the prediction of rotor bar failure in squirrel-cage motors using instantaneous angular speed*. Mechanical Systems and Signal Processing, 2006. **20**(7): p. 1572-1589.
75. Spagnol, M. and L. Bregant, *Instantaneous angular speed: encoder-counter estimation compared with vibration data*, in *Advances in Condition Monitoring of Machinery in Non-Stationary Operations*. 2014, Springer. p. 347-354.
76. Gu, F., P. Jacob, and A. Ball, *Non-parametric models in the monitoring of engine performance and condition: Part 2: Non-intrusive estimation of diesel engine cylinder pressure and its use in fault detection*. Proceedings of the Institution of Mechanical Engineers, Part D: Journal of Automobile Engineering, 1999. **213**(2): p. 135-143.
77. Bøving, K.G., *NDE handbook: Non-destructive examination methods for condition monitoring*. 2014: Elsevier.
78. Raharjo, P., et al. *A comparative study of the monitoring of a self aligning spherical journal using surface vibration, airborne sound and acoustic emission*. in *Journal of Physics: Conference Series*. 2012. IOP Publishing.
79. Ahmaida, A., et al., *Gear wear process monitoring using acoustic signals*. 2014.
80. Lin, Y.-H., H.-C. Wu, and C.-Y. Wu, *Automated condition classification of a reciprocating compressor using time-frequency analysis and an artificial neural network*. Smart materials and structures, 2006. **15**(6): p. 1576.

81. Hassin, O., et al., *Journal bearing condition monitoring based on the modulation signal bispectrum analysis of vibrations*. 2016, Taylor & Francis.
82. Decker, H.J. and D.G. Lewicki, *Spiral bevel pinion crack detection in a helicopter gearbox*. 2003.
83. Rajendra, B.R. and S.V. Bhaskar, *Condition Monitoring of Gear Box by Using Motor Current Signature Analysis*. International Journal of Scientific and Research Publications, 2013: p. 563.
84. Ashnibha, R.A., *An investigation into current and vibration signatures of three phase induction motors*. 2012, Manchester Metropolitan University.
85. Sharifi, R. and M. Ebrahimi, *Detection of stator winding faults in induction motors using three-phase current monitoring*. ISA transactions, 2011. **50**(1): p. 14-20.
86. Gu, F., et al., *Electrical motor current signal analysis using a modified bispectrum for fault diagnosis of downstream mechanical equipment*. Mechanical Systems and Signal Processing, 2011. **25**(1): p. 360-372.
87. Benbouzid, M.E.H., M. Vieira, and C.J.I.T.o.p.e. Theys, *Induction motors' faults detection and localization using stator current advanced signal processing techniques*. 1999. **14**(1): p. 14-22.
88. Jung, J.-H., J.-J. Lee, and B.-H. Kwon, *Online diagnosis of induction motors using MCSA*. IEEE Transactions on Industrial Electronics, 2006. **53**(6): p. 1842-1852.
89. Messaoudi, M. and L. Sbita, *Multiple Faults Diagnosis in Induction Motor Using the MCSA Method*. International Journal of Signal and Image Processing 2010. **1**(3): p. 190-195.
90. Zhen, D., et al., *Fault diagnosis of motor drives using stator current signal analysis based on dynamic time warping*. 2013. **34**(1-2): p. 191-202.
91. Zhang, R., et al., *Gear wear monitoring by modulation signal bispectrum based on motor current signal analysis*. Mechanical Systems and Signal Processing, 2017. **94**: p. 202-213.
92. Yang, B.-S., et al., *Condition classification of small reciprocating compressor for refrigerators using artificial neural networks and support vector machines*. Mechanical Systems and Signal Processing, 2005. **19**(2): p. 371-390.
93. Cui, H., et al., *Research on fault diagnosis for reciprocating compressor valve using information entropy and SVM method*. Journal of loss prevention in the process industries, 2009. **22**(6): p. 864-867.
94. Pichler, K., et al. *Detecting broken reciprocating compressor valves in the PV diagram*. in *Advanced Intelligent Mechatronics (AIM), 2013 IEEE/ASME International Conference on*. 2013. IEEE.
95. Wang, Y., et al., *Fault diagnosis of reciprocating compressor valve with the method integrating acoustic emission signal and simulated valve motion*. Mechanical Systems and Signal Processing, 2015. **56**: p. 197-212.
96. Ballal, M.S., et al., *Adaptive neural fuzzy inference system for the detection of inter-turn insulation and bearing wear faults in induction motor*. Industrial Electronics, IEEE Transactions on, 2007. **54**(1): p. 250-258.

97. Garcia-Perez, A., et al., *The application of high-resolution spectral analysis for identifying multiple combined faults in induction motors*. *Industrial Electronics, IEEE Transactions on*, 2011. **58**(5): p. 2002-2010.
98. Kacani, V. *Vibration analysis in reciprocating compressors*. in *IOP Conference Series: Materials Science and Engineering*. 2017. IOP Publishing.
99. Jiang, J., B.J.J.o.V. Zhang, and Control, *Rolling element bearing vibration modeling with applications to health monitoring*. 2012. **18**(12): p. 1768-1776.
100. International Atomic Energy, A., *Implementation strategies and tools for condition based maintenance at nuclear power plants*. 2007: IAEA-TECDOC-1551.
101. Kuemlee, H., T. Gross, and J. Kolerus. *Machine vibrations and diagnostics the world of ISO*. in *Petroleum and Chemical Industry Technical Conference (PCIC), 2013 Record of Conference Papers Industry Applications Society 60th Annual IEEE*. 2013. IEEE.
102. Yang, H., J. Mathew, and L. Ma, *Vibration feature extraction techniques for fault diagnosis of rotating machinery: a literature survey*. 2003.
103. Ahmed, M., F. Gu, and A. Ball. *Fault detection of reciprocating compressors using a model from principles component analysis of vibrations*. in *Journal of Physics: Conference Series*. 2012. IOP Publishing.
104. Ahmed, M., *The Use of Advanced Soft Computing for Machinery Condition Monitoring*. 2014, University of Huddersfield.
105. Brethee, K.F., *Condition Monitoring of Helical Gear Transmissions Based on Vibration Modelling and Signal Processing*. 2018, University of Huddersfield.
106. Forrester, B.D., *Advanced vibration analysis techniques for fault detection and diagnosis in geared transmission systems*. 1996: Swinburne University of Technology Melbourne, VIC, Australia.
107. Jayaswal, P. and A. Aherwar, *Fault Detection and Diagnosis of Gear Transmission System via Vibration Analysis*. 2012.
108. Szabó, L., B. Dobai, and K.A. Biro, *Discrete Wavelet Transform based rotor faults detection method for induction machines*. 2004.
109. Al-Arbi, S.K., *Condition Monitoring of Gear Systems using Vibration Analysis*. 2012, University of Huddersfield.
110. De Silva, C.W., *Vibration and shock handbook*. 2005: CRC Press.
111. Braun, S., *Mechanical signature analysis: theory and applications*. 1986: Academic Pr.
112. Peng, Z., F.J.M.s. Chu, and s. processing, *Application of the wavelet transform in machine condition monitoring and fault diagnostics: a review with bibliography*. 2004. **18**(2): p. 199-221.
113. Edwards, S., et al., *Fault diagnosis of rotating machinery*. 1998. **30**(1): p. 4-13.
114. Lees, A., et al., *The identification of the unbalance of a flexible rotating machine from a single rundown*. 2004. **126**(2): p. 416-421.

115. Tian, X., et al., *A robust fault detection method of rolling bearings using modulation signal bispectrum analysis*. 2015.
116. Nikias, C.L. and M.R.J.P.o.t.I. Raghuvver, *Bispectrum estimation: A digital signal processing framework*. 1987. **75**(7): p. 869-891.
117. Nikias, C.L. and J.M.J.I.S.p.m. Mendel, *Signal processing with higher-order spectra*. 1993. **10**(3): p. 10-37.
118. Zhang, G., et al., *Bispectral analysis for on-line monitoring of stamping operation*. Engineering Applications of Artificial Intelligence, 2002. **15**(1): p. 97-104.
119. Li, X., et al. *Feature Extraction of Underwater Signals Based on Bispectrum Estimation*. in *Wireless Communications, Networking and Mobile Computing (WiCOM), 2011 7th International Conference on*. 2011. IEEE.
120. Sundaramoorthy, G., M. Raghuvver, and S.A. Dianat, *Bispectral reconstruction of signals in noise: Amplitude reconstruction issues*. IEEE Transactions on Acoustics, Speech, Signal Processing, 1990. **38**(7): p. 1297-1306.
121. Gu, F., et al. *Motor current signal analysis using a modified bispectrum for machine fault diagnosis*. in *Proceedings of the ICROS-SICE International Joint Conference 2009*. 2009. IEEE Xplore.
122. Wade, B., *Operating Maintenance and Parts Manual*. 1964: Bucks, England.
123. Brian, H., *Broom Wade Piston Compressor*. 2002: CompAir UK Ltd., Ref no. TS/BVH/307, Buckinghamshire, UK.
124. Sridhar, S. and K.U. Rao. *Detection of simultaneous unbalanced under-voltage and broken rotor fault in induction motor*. in *Condition Assessment Techniques in Electrical Systems (CATCON), 2013 IEEE 1st International Conference on*. 2013. Kolkata, India: IEEE.
125. Summers, R.A., *Mathematical modelling of reciprocating compressors for heat pumps*. 1988, University of Aston in Birmingham.
126. Costagliola, M., *The theory of spring-loaded valves for reciprocating compressors*. JOURNAL OF APPLIED MECHANICS-TRANSACTIONS OF THE ASME, 1950. **17**(4): p. 415-420.
127. Wambsganss, M., *MATHEMATICAL MODELING AND DESIGN EVALUATION OF HIGH-SPEED RECIPROCATING COMPRESSORS*. 1968, Purdue University: USA.
128. Singh, R., W.J.J.o.S. Soedel, and Vibration, *Mathematical modeling of multicylinder compressor discharge system interactions*. 1979. **63**(1): p. 125-143.
129. Sun, S.-Y. and T.-R. Ren, *New method of thermodynamic computation for a reciprocating compressor: computer simulation of working process*. International Journal of Mechanical Sciences, 1995. **37**(4): p. 343-353.
130. Manepatil, S., G. Yadava, and B. Nakra, *Modelling and Computer Simulation of Reciprocating Compressor with Faults*. Journal-Institution of Engineers India Part Mc Mechanical Engineering Division, 2000: p. 108-116.
131. Winandy, E., C. Saavedra, and J. Lebrun, *Simplified modelling of an open-type reciprocating compressor*. International journal of thermal sciences, 2002. **41**(2): p. 183-192.

132. Demba Ndiaye and M. Bernier, *Dynamic model of a hermetic reciprocating compressor in on-off cycling operation (Abbreviation: Compressor dynamic model)*. Applied Thermal Engineering, 2010. **30**(8–9): p. 792–799.
133. Link, R. and C.J. Deschamps, *Numerical modeling of startup and shutdown transients in reciprocating compressors*. International journal of refrigeration, 2011. **34**(6): p. 1398-1414.
134. Yang, B., C.R. Bradshaw, and E.A. Groll, *Modeling of a semi-hermetic CO2 reciprocating compressor including lubrication submodels for piston rings and bearings*. International Journal of Refrigeration, 2013. **7**(36): p. 1925-1937.
135. Dutra, T. and C.J. Deschamps, *A simulation approach for hermetic reciprocating compressors including electrical motor modeling*. International Journal of Refrigeration, 2015. **59**: p. 168-181.
136. Silva, L.R. and C.J.I.I.J.o.R. Deschamps, *Modeling of gas leakage through compressor valves*. 2015. **53**: p. 195-205.
137. Chen, S. and R. Živanović, *Modelling and simulation of stator and rotor fault conditions in induction machines for testing fault diagnostic techniques*. European Transactions on Electrical Power, 2010. **20**(5): p. 611-629.
138. Chen, S. and R. Živanović, *Modelling and simulation of stator and rotor fault conditions in induction machines for testing fault diagnostic techniques*. International Transactions on Electrical Energy Systems, 2010. **20**(5): p. 611-629.
139. Stronach, A., A. Johnston, and C. Cudworth, *Detection of Valve Faults on Reciprocating Compressors*. Pineridge Press Ltd, 1984: p. 293-304.
140. McCarthy, D.J., *Vibration-based diagnostics of reciprocating machinery*. 1994, Massachusetts Institute of Technology.
141. Ben Sasi, A.Y., *The exploitation of instantaneous angular speed for machinery condition monitoring*, in *School of Mechanical, Aerospace and Civil Engineering*. 2005, The University of Manchester (United Kingdom).
142. Sasi, A.Y.B. and A. Ball, *Exploitation of Instantaneous Angular Speed for Machinery Condition Monitoring*. 2005: University of Manchester.
143. Elhaj, M., et al., *Early detection of leakage in reciprocating compressor valves using vibration and acoustic continuous wavelet features*. 2001: p. 179-756.
144. Gu, F., A.J.M. Ball, and A.M. Journal, *Automating the diagnosis of valve faults in reciprocating compressors*. 1996. **11**(3): p. 19-22.
145. Dormand, J.R., P.J.J.J.o.c. Prince, and a. mathematics, *A family of embedded Runge-Kutta formulae*. 1980. **6**(1): p. 19-26.
146. McCarthy, D.J., *Prognostics for a reciprocating air compressor*. 1997, ASA.
147. Moore, D.J., *Condition Monitoring of Diesel Engines*. 2013, The University of Manchester: UK.
148. N. A. Hussein, D.Y.M., and I. M. Abdulbaqi, *3-phase Induction Motor Bearing Fault Detection and Isolation using MCSA Technique based on Neural Network Algorithm*. Int. J. Appl. Eng. Res., no. 5, , 2011. **6**: p. 581–591.

149. Korde, A., 2000, *Online Condition Monitoring of Motors Using Electrical Signature Analysis*. 2000(Proc. 4th Int. Conf. on Engineering and Automation, Orlando, Florida, USA).
150. Elhaj, M., *Condition monitoring of reciprocating compressor valves*. 2005, University of Manchester: Manchester.
151. Wang, Y., M. Liao, and T. Zhao, *Application of the wavelet transform to fault diagnosis in compressor valves*. *Zhongguo Jixie Gongcheng/China Mechanical Engineering*, 2003. **14**(12): p. 1046-1048.
152. Feng, G., et al. *The real-time implementation of envelope analysis for bearing fault diagnosis based on wireless sensor network*. in *Automation and Computing (ICAC), 2013 19th International Conference on*. 2013. IEEE.